DOCTOR OF PHILOSOPHY

A systems biology approach unravels the biological function of two tRNA wobble base modifications in fine-tuning translation and the response to environmental stress

Tyagi, Kshitiz

Award date:
2014

A systems biology approach unravels the biological function of two tRNA wobble base modifications in fine-tuning translation and the response to environmental stress

Kshitiz Tyagi

A thesis submitted for the degree of Doctor of Philosophy
University of Dundee

November 2014

Table of Contents

List of figures

List of tables

List of abbreviations

A-site	aminoacyl site
aaRS	aminoacyl tRNA synthetase
AdoMet	S-adenosyl methionine
ALS	amyotrophic lateral sclerosis
APM	[(N-acryloylamino)phenyl]mercuric chloride
ASL	anti-codon stem and loop
ATP	adenosine triphosphate
CID	collision induced dissociation
$cmnm^5U$	5-carboxymethylaminomethyluridine
DDA	data dependent acquisition
DIA	data independent acquisition
DNA	deoxyribonucleic acid
dPAGE	denaturing polyacrylamide gel electrophoresis
DTT	dithiothreitol
EDTA	ethylenediaminetetraacetate
ESI	electro-spray ionisation
FASP	filter aided sample preparation
FD	familial dysautonomia
FDR	false discovery rate
FWER	family wise error rate
GO-BP	gene ontology terms for biological processes
GTP	guanosine triphosphate
HAT	histone acetyl transferase
HCD	higher-energy collision induced dissociation
HEPES	4-(2-hydroxyethyl)-1-piperazineethanesulfonic acid
HPLC	high pressure liquid chromatography
IEF	iso-electric focussing
LC	liquid chromatography
MALDI	matrix-assisted laser desorption ionisation
mcm^5s^2U	5-methoxycarbonylmethyl-2-thiouridine
mcm^5U	5-methoxycarbonylmethyluridine
MERRF	myoclonic epilepsy with ragged red fibres
MIPS	Munich Information Centre for Protein Sequences
mnm^5U	5-methylaminomethyluridine
mRNA	messenger RNA
MS	mass spectrometry

mtX^{NNN}	mitochondrial tRNA for amino acid X with anti-codon NNN
NB	northern blot
ncm^5U	5-carbamoylmethyluridine
ncm^5Um	2'-*o*-methyl-5-carbamoylmethyluridine
NLS	nuclear localisation sequence
NMR	nuclear magnetic resonance
OD_{600}	optical density measured at 600 nm
P-site	peptidyl site
PAGE	polyacrylamide gel electrophoresis
PCR	polymerised chain reaction
qPCR	quantitative PCR
RCF	relative centrifugal force
RE	rolandic epilepsy
RF	random forest
RNA	ribonucleic acid
rRNA	ribosomal RNA
SAM	S-adenosyl methionine
SC-X+D	synthetic complete (with all amino acids) except X + dextrose
SC+D	synthetic complete (with all amino acids) + dextrose
SCX	strong cation exchange
SD	standard deviation
SDS	sodium dodecyl sulfate
SEM	standard error of the mean
SILAC	stable isotope labelling with amino acids in cell cultures
SSC	saline-sodium citrate
ssDNA	single stranded DNA
TAE	tris acetate EDTA
TBE	tris borate EDTA
TCA	trichloroacetic acid
TFA	trifluoroacetic acid
TPP	Trans-Proteomic Pipeline
TRIS	tris(hydroxymethyl)aminomethane
tRNA	transfer RNA
ts	temperature sensitive
tX^{NNN}	cytoplasmic tRNA for amino acid X with anti-codon NNN
UBL	ubiquitin like modifier
uHPLC	ultra-high pressure liquid chromatography
v/v	volume per volume

W-C	Watson-Crick
w/v	weight per volume
w/w	weight per weight
WB	western blot
WT	wild type
YPD	yeast-extract + peptone + dextrose
$\tau m^5 s^2 U$	5-taurinomethyl-2-thiouridine

Amino acid code

Single letter code	Three letter code	Amino acid
A	Ala	alanine
C	Cys	cysteine
D	Asp	aspartic acid
E	Glu	glutamic acid
F	Phe	phenylalanine
G	Gly	glycine
H	His	histidine
I	Ile	isoleucine
K	Lys	lysine
L	Leu	leucine
M	Met	methionine
N	Asn	asparagine
P	Pro	proline
Q	Gln	glutamine
R	Arg	arginine
S	Ser	serine
T	Thr	threonine
V	Val	valine
W	Trp	tryptophan
Y	Tyr	tyrosine

Codon table

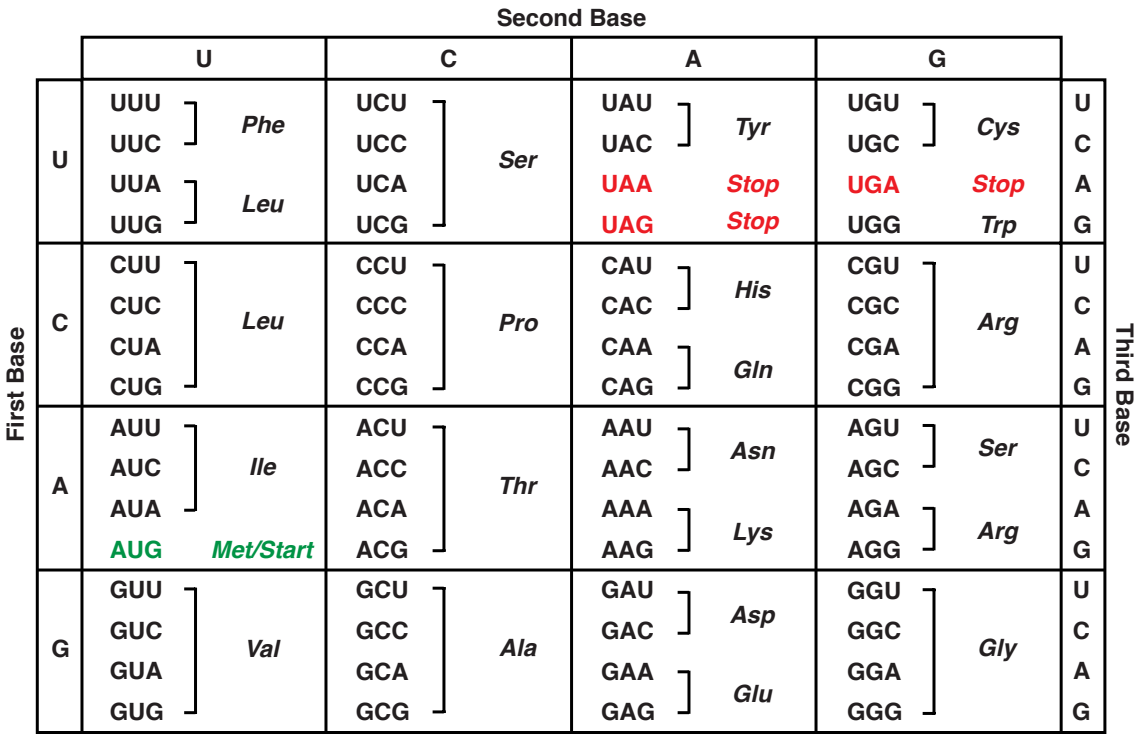
Second Base
U
C
A
G
First Base
Third Base
U
UUU Phe
UUC Phe
UUA Leu
UUG Leu
UCU Ser
UCC Ser
UCA Ser
UCG Ser
UAU Tyr
UAC Tyr
UAA Stop
UAG Stop
UGU Cys
UGC Cys
UGA Stop
UGG Trp
C
CUU Leu
CUC Leu
CUA Leu
CUG Leu
CCU Pro
CCC Pro
CCA Pro
CCG Pro
CAU His
CAC His
CAA Gln
CAG Gln
CGU Arg
CGC Arg
CGA Arg
CGG Arg
A
AUU Ile
AUC Ile
AUA Ile
AUG Met/Start
ACU Thr
ACC Thr
ACA Thr
ACG Thr
AAU Asn
AAC Asn
AAA Lys
AAG Lys
AGU Ser
AGC Ser
AGA Arg
AGG Arg
G
GUU Val
GUC Val
GUA Val
GUG Val
GCU Ala
GCC Ala
GCA Ala
GCG Ala
GAU Asp
GAC Asp
GAA Glu
GAG Glu
GGU Gly
GGC Gly
GGA Gly
GGG Gly

Acknowledgement

I express my sincere gratitude towards my supervisor, Dr. Patrick Pedrioli, for providing me with the unique opportunity to learn and conduct research in his group. Throughout my Ph.D., his valuable suggestions, supportive attitude and freedom of doing independent work, ensured an environment congenial for open discussions and learning. I am especially grateful for the efforts he put in the development of mass spectrometry and computational resources in the lab and for very patiently tutoring me in their application. At the same time, I am also thankful to the other members of the Pedrioli group for not only being always available for discussions and advise, but also for making lab a fun place to work.

I am very grateful to my thesis committee, Prof. Dario Alessi and Prof. Julian Blow, for their critical feedback and suggestions. I also thank our collaborators, the groups of Prof. Matthias Peter at the ETH Zurich and Prof. Marina Rodnina at the Max Planck Institute for Biophysical Chemistry.

There is a multitude of people without whose help my project would have been very difficult. I would like to thank the groups of Dr. Thimo Kurz and Dr. Matthias Trost for their valuable suggestions and technical support related to yeast and mass spectrometry, respectively. My special thanks goes to Dr. Deena Pedrioli for her help and suggestions in designing and conducting the qPCR experiment. I would like to thank Prof. Irwin McLean for letting me use the qPCR instrument in his lab, Prof. Julian blow for granting me access to OffGel Fractionator, which was vital for the proteomics experiments, and Prof. Mike Stark for sharing plasmids.

I would also like to acknowledge the efforts of several people for providing important services and tools for my research; Dr. Natalia Shpiro for synthesising reagents, Dr. Nicola Wood and rest of the cloning team, the DNA sequencing team, the media kitchen team and wash-up services. I also thank our lab managers, Letty Gibson and Hannah Kendall, for keeping our lab smoothly running and Angie Nicoll, Judith Hare and Rachel Naismith for the administrative support.

I am also grateful to the various funding agencies for their financial support. The work in our lab was supported by a European Regional Development Fund grant for an Innovation Pipeline for Translational Science (LUPS/ERDF/2008/2/1/0429). My stint as a Ph.D. student was financed by SCILLS Studentship, Discovery Scholarship and the College of Life Sciences Bursary. Finally, I thank the MRC and SCILLS for the amazing infrastructure and facilities and for providing a stimulating research environment, because of which my Ph.D. has been a worthwhile experience.

Last, but not the least, I am truly thankful to my family for their unconditional affection and support.

Declarations

I declare that the following thesis is based on the results of investigations conducted by myself, and that this thesis is of my own composition. Work other than my own is clearly indicated in the text by reference to the relevant researchers or their publications. This dissertation has not in whole, or in part, been previously submitted for a higher degree.

_____

Kshitiz Tyagi

I certify that Kshitiz Tyagi has spent the equivalent of at least nine terms in research work at the College of Life Sciences, University of Dundee, and that he has fulfilled the conditions of the Ordinance General No. 14 of the University of Dundee and is qualified to submit the accompanying thesis in application for the degree of Doctor of Philosophy.

_____

Dr. Patrick Pedrioli

List of publications

1. Rezgui VAN*, Tyagi K*, Ranjan N*, Konevega AL, Mittelstaet J, Rodnina MV, Peter M & Pedrioli PGA (2013) tRNA tK^{UUU}, tQ^{UUG}, and tE^{UUC} wobble position modifications fine-tune protein translation by promoting ribosome A-site binding. *Proceedings of the National Academy of Sciences* **110:** 12289–12294

   *Authors contributed equally to this work

2. Tyagi K, Pedrioli PGA (manuscript submitted) Protein degradation and dynamic tRNA modification fine-tune translation at elevated temperatures.

3. Baron Y, Pedrioli PG, Tyagi K, Johnson C, Wood NT, Fountaine D, Wightman M & Alexandru G (2014) VAPB/ALS8 interacts with FFAT-like proteins including the p97 cofactor FAF1 and the ASNA1 ATPase. *BMC biology* **12:** 39

4. Ritorto MS, Cook K, Tyagi K, Pedrioli PGA & Trost M (2013) Hydrophilic strong anion exchange (hSAX) chromatography for highly orthogonal peptide separation of complex proteomes. *J Proteome Res* **12:** 2449–2457

Summary

tRNA molecules undergo extensive post-transcriptional modifications to produce several variations of the four canonical nucleotides. Despite the huge number of nucleotide modifications that have been identified in tRNAs, to date their biological roles and regulations continue to be poorly understood. The uridines at the wobble position of the eukaryotic cytoplasmic tRNAs tK^{UUU}, tQ^{UUG} and tE^{UUC} are methoxycarbonylmethylated and thiolated to form $mcm^5s^2U_{34}$ by the *ELP*- and *URM1*-pathways, respectively. Several *in vitro* experiments have implicated these modifications in modulating wobbling capacity. Moreover, mutations in the *ELP*- and *URM1*-pathway genes have been associated with physiological defects in several organisms, including complex neurological disorders in humans. In this thesis we used a systems biology approach to study the *in vivo* functional relevance of $mcm^5s^2U_{34}$. A sensitive, robust and quantitative proteomics workflow was developed and applied to investigate differential proteome composition in budding yeast mutants deficient in U_{34} modifications.We find that, *in vivo* and under normal conditions, $mcm^5s^2U_{34}$ fine tunes proteome composition by ensuring efficient translation of mRNAs biased for AAA, CAA and GAA codons. Importantly, our results connect these tRNA modifications with various cellular stress response pathways. Follow up analyses of yeast cells subjected to environmental stresses were conducted and led to the discovery that the biosynthesis of $mcm^5s^2U_{34}$ is dynamically regulated in response to growth conditions in a *URM1*-pathway dependent fashion. We propose that this regulation allows the cells to adjust their translational capacity during unfavourable growth conditions and contributes to the management of the environmental stress response.

Overall, this thesis presents the first extensive investigation of the functional relevance of tRNA nucleotide modifications and reports one of the few known cases wherein cells regulate the levels of modified nucleotides to fine tune their metabolism in response to environmental cues. We expect that dynamic modulation of RNA modifications will prove to be a more general regulatory mechanism of cellular processes. The experimental and analytical approaches presented in this dissertation will provide a general framework for future studies in this field.

1. Introduction

1.1 RNA modifications

RNA molecules are central to several biological processes that revolve principally around gene expression and its regulation. Just like DNA, RNA monomers (ribonucloeotides) carry genetic information. In addition to this canonical role, RNAs are also required to perform specialised functions that involve making specific interactions with other macromolecules and, in some cases, exhibiting catalytic activity. The ability to fulfil multiple roles is probably a consequence of the complex 3D structures that RNAs can fold into (Helm 2006; Grosjean 2005). In this context, RNAs are somewhat similar to proteins. Nearly all RNA types carry nucleotide modifications that are produced post-transcriptionally by the action of dedicated enzymatic pathways. Nucleotide modifications act by altering the number and strength of interactions that otherwise the four conventional nucleotides can make (Nobles et al. 2002). In other words, nucleotide modifications play a fine-tuning role in modulating the RNA tertiary structure and/or altering the RNA functional sites (Jackman and Alfonzo 2012).

The first modified nucleotide from RNA was discovered in 1951, which was later identified to be the isomeric form of uridine, now known as pseudouridine (Ψ) (Cohn 1960; Cohn and Volkin 1951). To date, more than 100 RNA nucleotide modifications have been identified and enzymatic pathways responsible for many of the modifications have been discovered (Machnicka et al. 2012; Cantara et al. 2010). Despite their wide spread occurrence, the biological role of many RNA modifications remains poorly understood. RNA modifications often work in subtle and concerted manner. Furthermore, the proteins involved in the biosynthesis of a modification sometimes also perform

additional, unrelated functions. Overall, this makes it difficult to associate the phenotypes with the loss of nucleotide modification. Nevertheless, over the last few years several studies have exploited phenotypic analysis of the mutants lacking RNA modifications to give vital clues on the role of several RNA modifications.

1.2 tRNA modifications

Transfer RNAs (tRNAs) exhibit the highest diversity of modifications among all types of RNAs, with the identification of more than 90 modifications to date (Yacoubi, Bailly, and de Crécy-Lagard 2012; Phizicky and Hopper 2010). The extent of modifications on tRNAs and their importance can be guessed from the fact that cells dedicate more genomic space to tRNA modifications than the tRNAs themselves (Yacoubi, Bailly, and de Crécy-Lagard 2012). Most of the knowledge about tRNA modifications has come from research conducted in model organisms. tRNA modifications have been extensively studied in *Saccharomyces cerevisiae* where at least 37 out of 42 tRNAs have been sequenced and most of the tRNA modification genes have been identified (Phizicky and Hopper 2010; Hopper and Phizicky 2003; Yacoubi, Bailly, and de Crécy-Lagard 2012; Johansson and Byström 2005). In addition to the wealth of available information, ease of genetic manipulation makes the budding yeast a very powerful model organism for studying the role of tRNA modifications in eukaryotic cells.

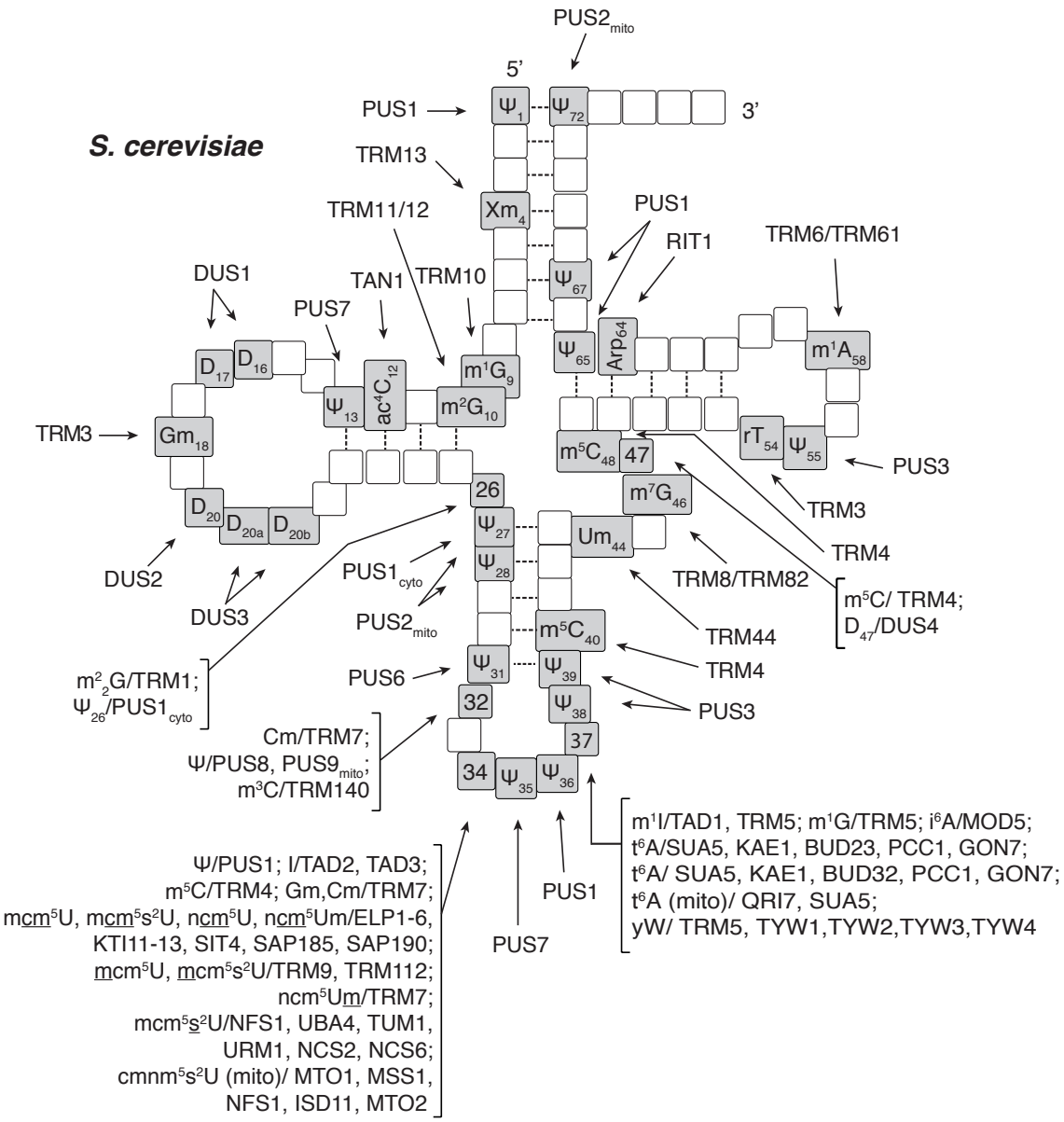

Figure 1.1: Density and diversity of tRNA modifications Schematic representation of various post transcriptional modifications found in the tRNAs of *S. cerevisiae*. Modified nucleotides are indicated along with the genes implicated in their biosynthesis. Modified from (Yacoubi, Bailly, and de Crécy-Lagard 2012).

Figure 1.1 schematically represents the various nucleotide modifications found in the tRNAs of *S. cerevisiae* along with the responsible enzymes (Yacoubi, Bailly, and de Crécy-Lagard 2012). Interestingly, most of the modifications can be classified into two categories (Helm 2006; Grosjean et al. 1996; Jackman and Alfonzo 2012). Those that have simple biosynthesis (that is, requiring two or less enzymes) and occur in and around the core of the L-shaped 3D

structure of tRNAs; and those that occur in tRNA functional sites (that is, the anti-codon stem loop (ASL) and the acceptor arm). The former, modulate tRNA folding, rigidity and flexibility (discussed in (Phizicky and Hopper 2010; Helm 2006; Yacoubi, Bailly, and de Crécy-Lagard 2012)). Interestingly, the latter modifications have complex biosynthetic processes involving the concerted action of several enzymes. Particularly, positions 34 and 37 in the ASL appear to be a hot-spot for modifications and have been implicated in affecting the primary function of tRNAs - the process of protein translation.

The functions of tRNA modifications have mainly been studied *ex vivo* or *in vitro* ((Agris 2004) and references therein). Biophysical studies using methodologies like x-ray crystallography and NMR spectroscopy, along with model building analysis, have elucidated the impact of nucleotide modifications on the structure and local conformation of tRNAs (Helm 2006). Ribosomal binding assays and protein synthesis approaches using the hypomodified artificially synthesised ASL mimics or full tRNAs have been used to assess the effect of nucleotide modifications on interactions between tRNAs and the protein translational machinery. Over the span of several years, these studies have provided important clues on the molecular contribution of these modifications. However, the overall picture of their *in vivo* functional importance is only now beginning to emerge. Importantly, there are several examples of perturbations in the functioning of tRNA modification machineries that have been implicated in complex human pathologies (for review: (Torres, Batlle, and Ribas de Pouplana 2014)).

My doctoral work focussed on two such nucleotide modifications found on the first base in the anti-codon of certain tRNAs. The following sections will introduce the two modifications in detail and summarise the state of research before this project was started.

1.3 tRNA wobble base modifications

Ribosomes are the site of cellular protein synthesis wherein genetic information carried by messenger RNAs (mRNA) is decoded and translated in to protein sequences. Even though ribosomes are themselves decorated with several poly-peptides, their main constituent and the source of their catalytic power is ribosomal RNA (rRNA). The third member of this important “all RNA club” are tRNAs that carry the relevant amino acids to be added to the polypeptide chain. The ribosomal structure and mechanism of translation have been reviewed extensively by Ramakrishnan (2002). During the elongation steps, amino-acylated tRNAs enter the aminoacyl site (A-site) of the programmed ribosomes in the form of ternary complex with elongation factor and GTP. Only after binding to their specific codons, tRNAs are released by the elongation factor thereby inducing conformational changes favourable for peptide bond formation at the peptidyltransferase centre. The specific interactions between the anti-codon nucleotides of the tRNA (position 36, 35 and 34) and the codon nucleotides of the mRNA (I, II and III respectively) (figure 1.2) lead to correct decoding of the genetic code.

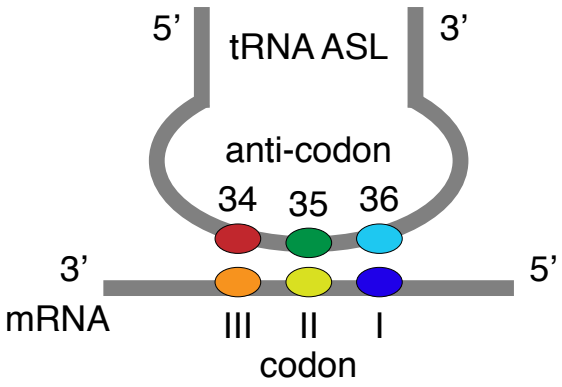

Figure 1.2: Codon anti-codon base pairing. Schematic representation of the base pairing between the tRNA anti-codon and mRNA codon trinucleotides.

The first two interactions occur by the standard Watson-Crick (WC) base pairing and are strictly monitored by the ribosomes (Ogle et al. 2001). However, in the third base pairing, some wobble or play seems to be allowed in the hydrogen bonding pattern, thereby allowing one tRNA to recognise multiple codons of the same amino acid; that is, the degeneracy of the genetic code.

The strict reading of the first two codons and wobble in the reading of the third was first proposed by Francis Crick in his wobble hypothesis (Crick 1966). The hypothesis suggests that in addition to pairing with A, it is possible for U_{34} to wobble around and make at least two direct hydrogen bonds with G, U and C (wobble pair) at the third position of the codon. However, since possibility of wobble pairing will lead to misreading of the codons in the mixed-codon families, Crick had suggested that the molecular structure is most likely to impose restriction on the wobble and that the U-G base pair is most likely to occur. Interestingly, over the subsequent years, two hypermodified forms of U were discovered at position 34. These are derivatives of 5-methyluridine (xm^5U_{34}), which sometimes contain an additional s^2 modification, and of 5-hydroxyuridine (xo^5U_{34}), respectively (figure 1.3) (Yokoyama et al. 1985). Since

their discovery, several researchers have investigated the role of these modifications with respect to the wobble hypothesis (for review see, Agris 2004; Takai and Yokoyama 2003).

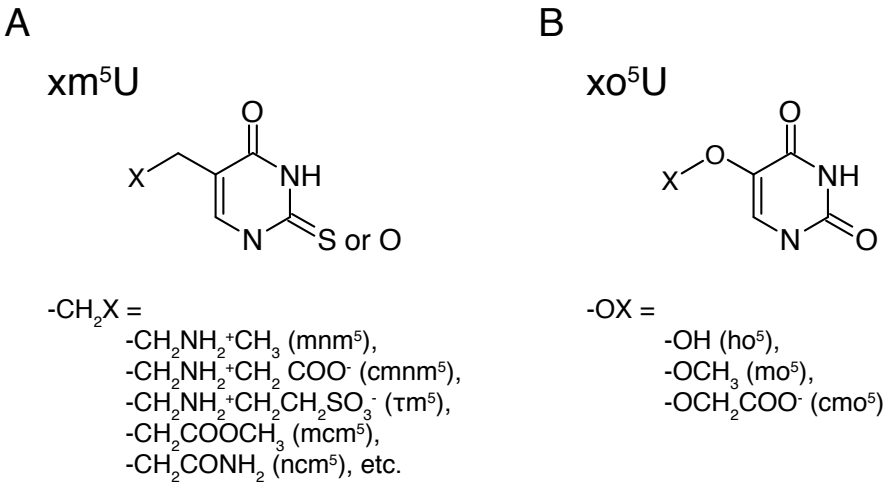

Figure 1.3: Modified wobble uridines in tRNAs. Schematic representation of (A) 5-methyluridine (xm^5U_{34}) derived and (B) 5-hydroxyuridine (xo^5U_{34}) derived modified wobble uridines. Adapted from (Takai and Yokoyama 2003).

Proton NMR analysis of the modified and unmodified uridines showed that the U_{34} modifications affect the puckering equilibrium of the ribose ring leading to different conformations of the nucleotide. xm^5 and s^2 modifications were found to restrict the uridine in the C3'-endo conformation that is more rigid and allows the formation of the standard W-C base pairs (Yokoyama et al. 1985; Agris et al. 1992) (for ribose puckering see, Harvey and Prabhakaran 1986). On the other hand, the xo^5 modification stabilises the C2'-endo conformation that allows the flexibility to form non standard base pairs like U-G and U-U that would otherwise be less favourable (Yokoyama et al. 1985). $xm^5s^2U_{34}$ is often found in the tRNAs that decode the codons for Lys, Glu and Gln (two-way degenerate mixed-codon box families) and xo^5U_{34} is generally found on the tRNAs that decode the codons of the four-way degenerate codon-box families. Summing

these two observations, it was suggested that while $xm^5s^2U_{34}$ ensures pairing with A_{III} and prevents mispairing with U_{III}, xo^5U_{34} is required for the efficient decoding of codons with A/G/U_{III}. The same study also suggested that s^2 is more important for restricting the U in C3'-endo conformation.

The speed and accuracy at which the ribosomes synthesise proteins can not be explained solely on the basis of the small energy difference between the binding of cognate and near cognate codon-anticodon pair, even when the C3'-endo or C2'-endo conformation are taken into account (Agris 2004; Takai and Yokoyama 2003). Furthermore, dissociation rates of binding between tRNA anticodon and cognate codon was found to be 10 to 100 fold higher in solution than on the ribosome (Agris 2004; Pape, Wintermeyer, and Rodnina 1998). The selection between the cognate and near-cognate tRNAs is suggested to be mediated through a two step process, wherein accurate reading of the codon in the first step is followed by the rapid accommodation of the tRNA in the ribosomal A-site. Cognate tRNAs not only show lower dissociation rate than the near cognate tRNAs but also have higher rate of GTP-activation (for hydrolysis by the elongation factor) and of accommodation at the A-site ((Pape, Wintermeyer, and Rodnina 1998) and the reviews (Rodnina and Wintermeyer 2001; Ramakrishnan 2002)). These findings suggest that in addition to the cognate anticodon, tRNAs need to have a specific conformation to facilitate accommodation at the A-site.

Thermal stability analysis of the modified and unmodified ASL oligonucleotide of the human tK^{UUU} ($tRNA_{Lys3}$) that carries $mcm^5s^2U_{34}$ in its natural form, showed that U_{34} modifications impart structure and stability to the anticodon stem loop

(Yarian et al. 2000). In the same year solution structure of the ASL of the *E.coli* tK^{UUU} that contains $mnm^5s^2U_{34}$ was solved. mnm^5 and s^2 were found to impart a canonical U-turn structure by promoting the stacking between the anticodon nucleosides. Improved stacking was also supported by the crystal structure of the modified ASL of the *E.coli* tK^{UUU} bound to the 30S ribosomal unit with the AAG codon in the A-site (F. V. Murphy et al. 2004). Moreover, ribosome binding assays and chemical probing analysis of the protected rRNA nucleosides showed that for four-way degenerate codon box families, non-modified ASL (lacking the xo^5U_{34}) were able to bind their cognate codons (Yarian et al. 2002). On the other hand, in the case of two-way degenerate codon box families, the presence of mnm^5 or s^2 was required for the binding of ASL oligonucleotides to the A-ending (cognate pair) and the G-ending (wobble pair) codons, respectively, at the ribosomal A- and P-sites (Ashraf et al. 1999; Yarian et al. 2002). Additionally, the s^2 modified ASL of tK^{UUU} did not bind to the C/U ending (non-cognate) codon (Yarian et al. 2002). These studies were supported by an *in vivo* study conducted in *E.coli* that reiterated the findings of the *in vitro* ribosome binding assays (Krüger et al. 1998). However, (Hagervall, Pomerantz, and McCloskey 1998) found that *in vivo* loss of $mnm^5s^2U_{34}$ reduced the mis-reading of Asn codons AAC/U under Asn starvation. Finally, s^2U_{34} in the ASL for tK^{UUU} was found to be sufficient and essential to restore the binding at the A-site and translocation from the A-site to the P-site of the otherwise completely unmodified ASL (Phelps et al. 2004).

It is evident from the described studies that U_{34} modifications, especially in the case of mixed-codon box families, affect the structure of the anti-codon stem loop of the tRNAs, are important for their binding at the ribosome and for the

process of translocation. However, it is important to note that the most of the described studies were conducted in *E.coli in vitro* settings. Bacteria have mnm^5U_{34} and $mnm^5s^2U_{34}$ as the derivatives of $xm^5s^2U_{34}$ modification and cmo^5U_{34} as the derivative of xmo^5 modification. On the other hand, eukaryotic cells exhibit three derivatives of $xm^5s^2U_{34}$; ncm^5U_{34}, mcm^5U_{34} and $mcm^5s^2U_{34}$, and do not have the xmo^5 type of modification. Moreover, eukaryotes code a separate tRNA for decoding the G-ending codon of the split-codon box families, thus questioning the need to use the wobble pairing (Takai and Yokoyama 2003; Marck and Grosjean 2002). This idea is supported by earlier findings in which tE^{UUC} was found to specifically translate the GAA codon (Sekiya, Takeishi, and Ukita 1969) and rabbit tK^{CUU} and modified tK^{UUU} were found to add Lys to different sites in haemoglobin synthesised in a reticulocyte translation system (Woodward and Herbert 1972). Therefore, conclusions on the importance of U_{34} modifications in the eukaryotes can not be solely based upon the results from prokaryotic systems. In the following section, more recently discovered $xm^5s^2U_{34}$ biosynthetic pathways in eukaryotic cells are summarised along with the phenotypes associated with their loss.

1.4 5-Methoxycarbonylmethyl-2-thiouridine

1.4.1 Biosynthesis of $mcm^5s^2U_{34}$

Illustrated in figure 1.4, five tRNAs tV^{UAC}, tS^{UGA}, tP^{UGG}, tT^{UGU} and tA^{UGC} have ncm^5U_{34} (5-carbamoylmethyluridine) and tL^{UAA} carries a doubly modified ncm^5Um_{34} (2'-*o*-methyl-5-carbamoylmethyluridine), two tRNAs tR^{UCU} and tG^{UCC} carry mcm^5U_{34} (5-methoxycarbonylmethyluridine) and three tRNAs tK^{UUU}, tQ^{UUG} and tE^{UUC} have a doubly modified $mcm^5s^2U_{34}$ (5-methoxycarbonylmethyl-2-thiouridine) (Johansson et al. 2008).

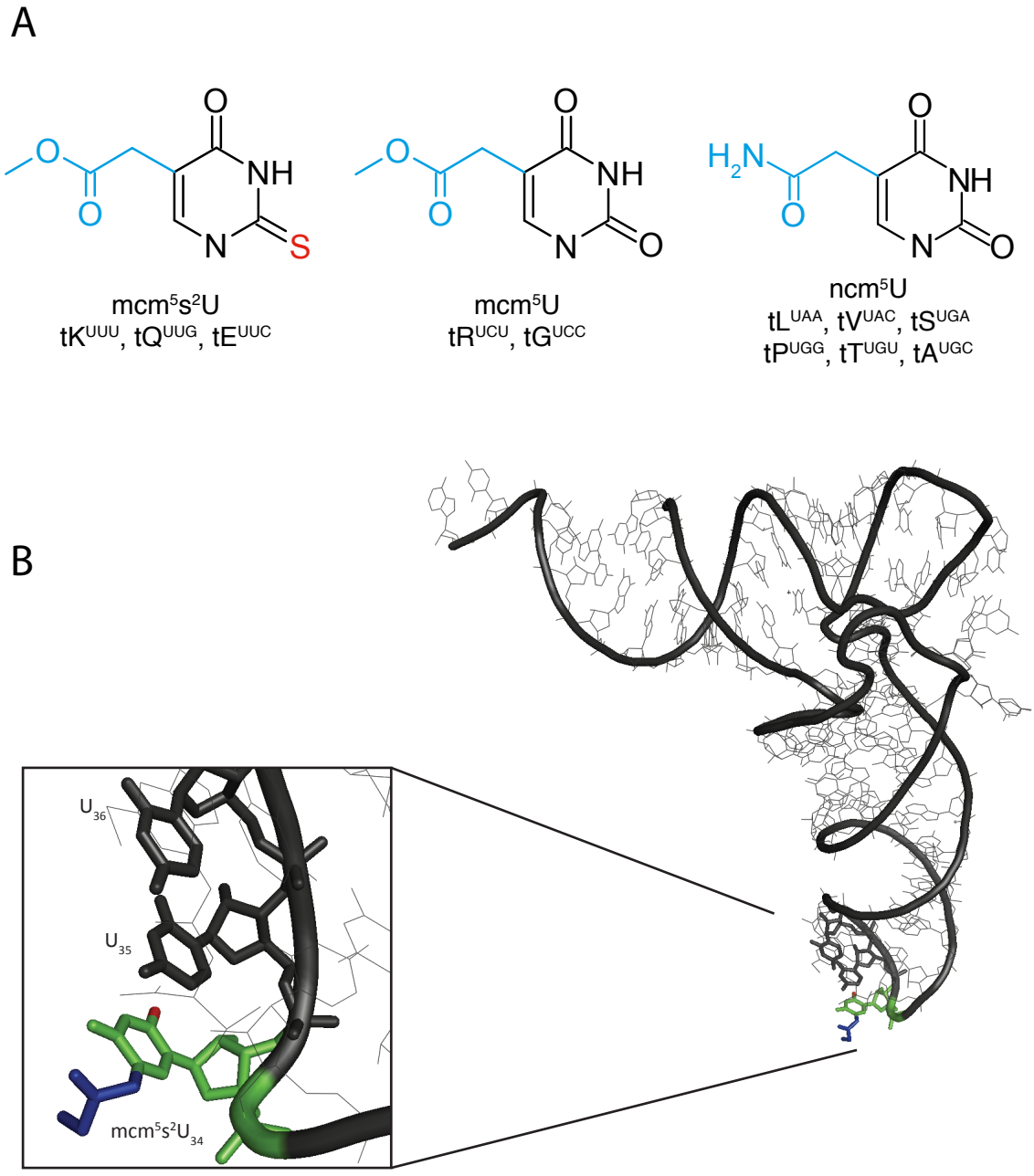

Figure 1.4: Modified wobble uridines (A) Schematic representation of the various modified forms of wobble uracil bases found in eukaryotic cytoplasmic tRNAs. (B) Cartoon representation of the 3D structure of tK^{UUU} from humans (PDB ID 1FIR). Zoomed-in region shows the three anticodon uridine residues, U_{34} is highlighted in green with the mcm^5 side chain in blue and the s^2 modification in red. mcm^5 is produced by sequential action of the ELP-complex and a methyltransferase complex comprising of Trm9p and Trm112p. s^2 is the result of Urm1p mediated sulfur transfer pathway.

Genes involved in the biosynthesis of these wobble uridine modifications have been identified in *S. cerevisiae*. A multisubunit complex consisting of six

proteins Elp1p-Elp6p, the *ELP*-complex, is required for the biosynthesis of ncm^5 and mcm^5 modifications (Huang, Lu, and Byström 2008; Huang, Johansson, and Byström 2005). The holo-*ELP*-complex was suggested to be composed of 12 polypeptide chains with two copies of each of the six *ELP* proteins and the full complex can break down into two subcomplexes (for a review on the structural organisation of the *ELP*-complex refer to Glatt and Müller (2013)). The first subcomplex is made up of three *ELP*-proteins, Elp4p-Elp6p. Crystal structure of this subcomplex showed that six polypeptide chains, two of each of Elp4p-Elp6p, are arranged into a hetero-hexameric ring (Glatt et al. 2012). The Elp4p-Elp6p subcomplex could hydrolyse ATP and bound tRNAs *in vitro*. Interestingly, the binding of tRNAs was affected by the presence of ATP in the reaction solution. The second subcomplex is made up of Elp1p-Elp3p and it has been suggested that two trimeric Elp1p-Elp3p subcomplexes bind to the Elp4p-Elp6p hexameric ring (Glatt and Müller 2013). The exact role of Elp2p in the structure and function of the *ELP*-complex is not known, but, it contains WD40 repeats and therefore has been suggested to play a scaffolding role. Elp1p, the biggest of the six Elp proteins, also has two WD40 domains and a tetratricopeptide repeat domain using which it could bind other proteins and act as scaffold. Elp1p also has a Arg/Lys rich basic region near its C-terminus that was postulated to be a nuclear localisation signal (NLS) sequence (Fichtner et al. 2003). However, a recent study has shown that Elp1p binds tRNAs *in vitro* and the C-terminal basic region is required for this binding (Di Santo, Bandau, and Stark 2014). Elp3p seems to be the catalytic core of the *ELP*-complex with its radical S-adenosylmethionine (SAM) binding domain and a histone acetyl transferase (HAT) like domain. Elp3p shows acetyltransferase activity *in vitro* (Wittschieben et al. 1999), which has been suggested to be required for the

early steps in the biosynthesis of mcm^5 and ncm^5 side chains (Huang, Johansson, and Byström 2005). In addition to the *ELP*-complex, a tRNA methylation complex made up of Trm9p and Trm112p is required for the biosynthesis of mcm^5 side chains. Interestingly, *trm9Δ* mutants were found to accumulate ncm^5U and ncm^5s^2U suggesting that ncm^5 could be the precursor for the biosynthesis of mcm^5 (C. Chen, Huang, Anderson, et al. 2011).

Additionally, mutations in several other genes affect the biosynthesis of mcm^5 and ncm^5 modifications; these include the *KTI11-KTI14*, *HRR25*, *SIT4*, *SAP185* and *SAP190* (Huang, Lu, and Byström 2008; Huang, Johansson, and Byström 2005). The exact role of these factors is not known, except, that the interplay between the kinase Hrr25p, the phosphatase Sit4p and the protein of unknown function Kti12p has been shown to modulate the phosphorylation of Elp1p. This phosphorylation affects ability of the *ELP*-complex to modify tRNAs (Huang, Lu, and Byström 2008; Mehlgarten et al. 2009; Fichtner et al. 2003). Despite these results and several studies conducted by various groups over the years, the exact steps involved in the formation of the *ELP*-complex and the biosynthesis of mcm^5 and ncm^5 modifications remain unknown.

Substitution of the oxygen at position 2 of the uridine ring (o^2U_{34}) with a sulfur, to generate s^2U_{34}, on tRNAs tK^{UUU}, tQ^{UUG} and tE^{UUC} requires an intricate sulfur relay pathway involving the ubiquitin related modifier 1 protein (Urm1p) and hence referred to as the *URM1*-pathway. Urm1p bears sequence and structural resemblance with ubiquitin and ubiquitin like modifier (Ubl) proteins, such as the C-terminal GlyGly motif and the β-grasp-fold structural motif (figure 1.5B)

(Pedrioli, Leidel, and Hofmann 2008; Furukawa et al. 2000). Originally, it was found to covalently conjugate with the yeast thioredoxin protein Ahp1p (Goehring, Rivers, and Sprague 2003). This conjugation, termed as urmylation, was found to be dependent upon the activity of Uba4p that resembles the E1 (activating) proteins of the Ubl systems (Goehring, Rivers, and Sprague 2003). Even though the corresponding E2 and E3 enzymes have not been found, Urm1p was proposed to be a canonical Ubl conjugating to the Lys side chains of the target proteins via its C-terminal GlyGly motif. Since then, at least one more study has reported urmylation in cells treated with oxidising agents (Van der Veen et al. 2011). However, the functional relevance of urmylation remains unknown. Interestingly, sequence homology studies show that Urm1p is closely related to the bacterial sulfur transfer proteins ThiS and MoaD (figure 1.5A) (Pedrioli, Leidel, and Hofmann 2008) that are involved in the biosynthesis of thiamine and molybdopterin (Webb et al. 2007). Prokaryotic sulfur carrier proteins carry the same GlyGly C-terminal motif, exhibit the β-grasp-fold (figure 1.5B) and, mechanistically, require the activating enzymes ThiF and MoeB that resemble the E1 proteins of the Ubl system (Xi et al. 2001; Schmitz et al. 2008). Owing to these similarities, it has been suggested that Ubls have evolved from the prokaryotic sulfur transfer proteins and that Urm1p is the evolutionary link between the two systems (Xu et al. 2006). Subsequently, several groups independently identified sulfur carrier function of Urm1p, responsible for thiolation of the wobble uridines in the the cytoplasmic tRNAs tK^{UUU}, tQ^{UUG} and tE^{UUC}, as well as the other members of the sulfur relay pathway (Leidel et al. 2009; Y. Nakai, Nakai, and Hayashi 2008; Noma, Sakaguchi, and Suzuki 2009; Dewez et al. 2008; Schlieker et al. 2008).

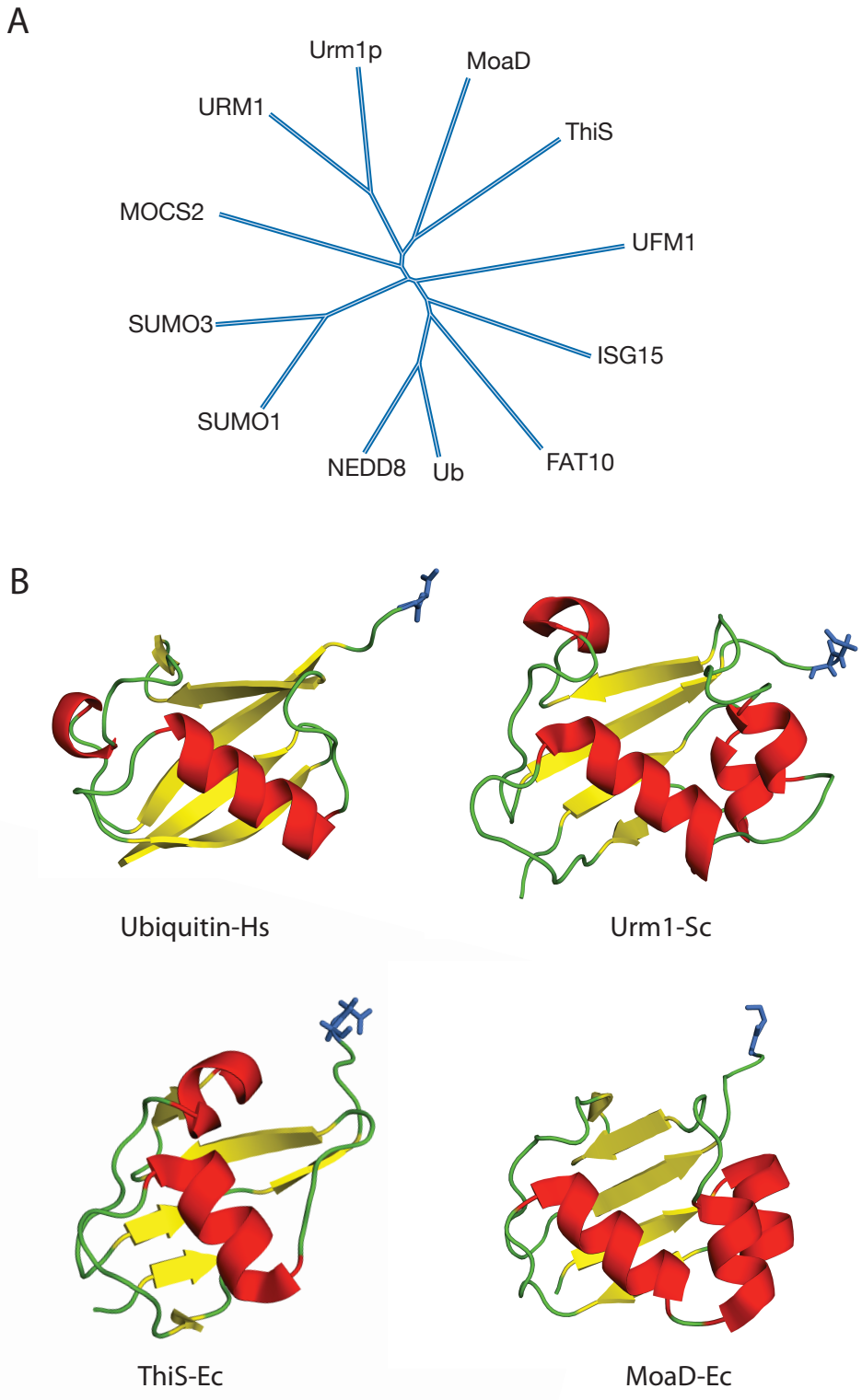

Figure 1.5: *URM1*-linking eukaryotic ubiquitin and bacterial sulfur transfer proteins (A) Neighbour joining dendrogram based on the sequence homology between ubiquitin, ubiquitin like proteins and bacterial sulfur transfer proteins (obtained from Pedrioli, Leidel, and Hofmann (2008)). (B) Cartoon representation of the 3D structure of Ubiquitin from humans (PDB ID 1UBQ), Urm1p from *S. cerevisiae* (PDB ID 2AX5), ThiS from *E.coli* (PDB ID 1FOZ) and MoaD from *E.coli* (chain D of PDB ID 1FMA). The cartoons have been coloured according to secondary structure elements. A β-sheet made up of four β-strands grasp an α-helix, making the β-grasp fold (Burroughs et al. 2007). The C-terminal GlyGly motif has been shown in blue with sticks.

The sulfur relay (Leidel et al. 2009; Noma, Sakaguchi, and Suzuki 2009), illustrated in figure 1.6, has been suggested to start from the mitochnodrially localised cysteine desulfurase protein Nfs1p. Sulfur is then passed onto Uba4p possibly with the help of Tum1p. Both Tum1p and Uba4p have rhodanese-homology domains (RHD) that are found in the proteins involved in sulfur transfer. Uba4 RHD contains a Cys (C397) at the active site, which could be responsible for carrying the modifying sulfur in the form of a persulfide. Additionally, it has a nucleotide binding domain (NBD) using which it activates Urm1p at its C-terminus by adenylation. The activated C-terminus of Urm1p is then converted to a thiocarboxylate via an acyl-disulfide intermediate by another Cys residue (C225) of Uba4p. The remaining two proteins of the *URM1* pathway are Ncs2p and Ncs6p, which belong to PP-loop family of ATPases that bind tRNAs and activate the target residues by adenylation. Ncs6p, at least, has been shown to bind tRNAs *in vitro* and adenylate them (Leidel et al. 2009).

Taken together, the action of the *ELP*- and *URM1*-pathways leads to the $mcm^5s^2U_{34}$ on the eukaryotic cytoplasmic tRNAs tK^{UUU}, tQ^{UUG} and tE^{UUC}.

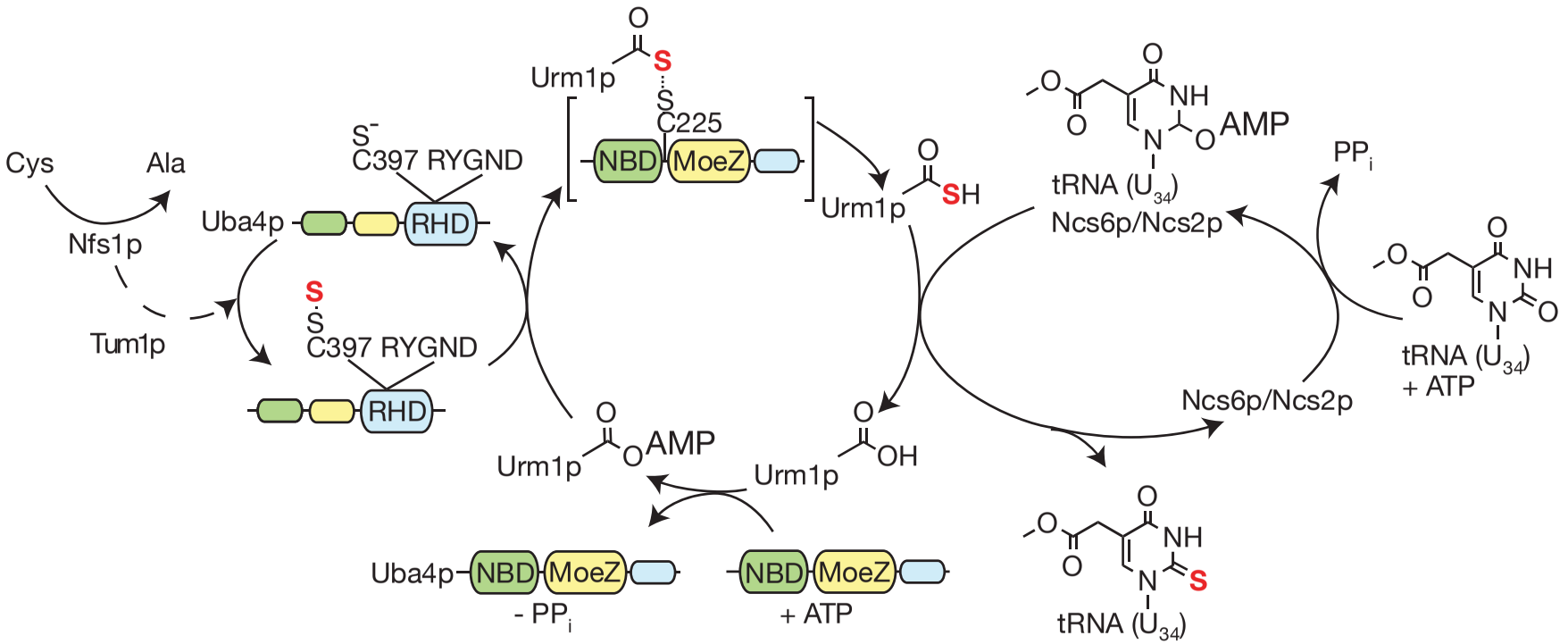

Figure 1.6: *URM1*-pathway Schematic representation of the likely sulfur relay across the *URM1*-pathway resulting in thiolation of wobble uridine of certain tRNAs (modified from (Leidel et al. 2009)).

1.4.2 Phenotypes in the absence of $mcm^5s^2U_{34}$

The discovery of the *ELP*- and *URM1*-pathways facilitated the investigations into the importance of tRNA wobble uridine modifications in eukaryotes. Member genes of the two pathways were mutated and the effect of hypomodified tRNAs was studied in *S. cerevisiae*. Disruption of the *URM1*-pathway (henceforth referred to as *urmΔ* mutants) was found to cause the complete removal of thiolation from the wobble uridines; the only exception was the *tum1* deletion that drastically reduced the levels of tRNA thiolation but did not abrogate it completely (Leidel et al. 2009). Deletion of *elp*-genes (henceforth referred to as *elpΔ*) caused complete lack of ncm^5 and mcm^5 modifications (Huang, Johansson, and Byström 2005; Huang, Lu, and Byström 2008) and a drastic reduction in the levels of U_{34} thiolation, suggesting the existence of a crosstalk between the two U_{34} modification pathways (Leidel et al. 2009). Interestingly, absence of ncm^5 and mcm^5 or s^2 modifications did not affect the steady state levels of total tRNAs nor their aminoacylation (Johansson et al. 2008). This is contrary to prokaryotic tRNAs wherein modified anticodon bases were required for recognition by the amino-acyl tRNA synthetases (aaRS) (Rodriguez-Hernandez et al. 2013; Sylvers et al. 1993; Madore et al. 1999).

Johansson and colleagues (Johansson et al. 2008) have exploited the mutants of the two pathways to investigate the decoding properties of the hypomodified tRNAs. In their study, viability of yeast strains carrying only the tRNA genes with anti-codons complementary to A-ending codons of an amino acid was investigated in the presence or absence of wobble uridine modifications. For example, to investigate the role of mcm^5, tR^{UCC} or tG^{CCC} were deleted from wild-type, *elp3Δ* and *urm1Δ* strains and the viability of the resulting strains was

tested. From these experiments, mcm^5 was found to promote binding of tR^{UCU} and tG^{UCC} to the codons AGG and GGG, respectively. Similarly, ncm^5 was also found to improve the binding of tRNAs tV^{UAC}, tS^{UGA} and tT^{UGU} to the G-ending codons GUG, UCG and ACG; with the catch that tS^{UGA} and tT^{UGU} decoded G-ending codons only when over-expressed. Interestingly, the strains carrying tP^{UGG} as the only tRNA for Pro were viable with or without *elp3Δ*, thereby implying that tP^{UGG} can read all the codons of Pro irrespective of the modification on its wobble uridine. Lastly, strains lacking tQ^{CUG} and tE^{CUC} were not viable. However, over-expression of the fully modified tQ^{UUG} restored viability in the former, suggesting that normally $mcm^5s^2U_{34}$ carrying tRNAs play only a minor role in decoding the G-ending codons. These results indicate that the effect of similar modifications differs for different codon anti-codon combinations and that no general rule can be postulated. Importantly, they also suggest that the abundance of a tRNA affects its decoding properties.

Phenotypic characterisation of the *elpΔ* and *urmΔ* mutants provides important clues on the physiological importance of tRNA wobble base modifications. Combined disruption of the two pathways (for example, the double mutant *elp3Δ urm1Δ*) causes lethality in *S. cerevisiae*. On the other hand, cells lacking functional *URM1* or *ELP*-pathways are viable but show pleiotropic phenotypes (Esberg et al. 2006; Leidel et al. 2009; C. Chen, Huang, Eliasson, et al. 2011; Pedrioli, Leidel, and Hofmann 2008 and papers therein). Interestingly, the majority of *elpΔ* phenotypes overlaps with the phenotypes of *urmΔ* cells. These include, defects in histone acetylation, reduced telomeric gene silencing, defects in exocytosis due to mislocalisation of Sec2p, slow growth, increased sensitivity to stress caused by high temperature, rapamycin (inhibitor of TOR

complex), caffeine (effect similar to rapamycin: Kuranda et al. 2006) and diamide (oxidises glutathione reversibly), cell wall damage caused by calcofluor white (fluorochrome that binds cell wall: Roncero et al. 1988; Arias et al. 1997) and replication stress caused by hydroxyurea. Additionally, *elpΔ* or *urmΔ* mutants take longer to adapt to alternative carbon sources and exhibit insensitivity to *Kluvveromyces lactis* γ-toxin - a tRNA endonuclease (Esberg et al. 2006 and papers therein). Interestingly, over-expression of the hypomodified tRNAs tK^{UUU}, tQ^{UUG} and tE^{UUC} was found to suppress all of the tested phenotypes (Esberg et al. 2006; Leidel et al. 2009), including the synthetic lethality of the double mutants (*urmΔ elpΔ*) (Bjork et al. 2007). These results establish that the phenotypes of *urmΔ* or *elpΔ* cells are caused by their inability to modify their tRNAs and not by the loss of other functions with which the *ELP*- and *URM1*-pathways have been associated. Additionally, in yeast, these phenotypes functionally link the two tRNA wobble base modifications to cellular processes involved in sensing and responding to nutrients and stress conditions.

Beside yeast, $mcm^5s^2U_{34}$ and homologs of *ELP* genes and *URM1*-pathway members are found in all the higher eukaryotes investigated so far, which include plants, worms, fruit flies, mice and humans (Pedrioli, Leidel, and Hofmann 2008; Mehlgarten et al. 2010; C. Chen, Tuck, and Byström 2009; J. C. Chan et al. 1982). In Plants (*Arbidopsis thaliana*), mutations in *ELP* genes cause reduced rate of cell proliferation leading to narrow leaves and poor root growth (Nelissen et al. 2005). In worms (*Caenorhabditis elegans*), loss of $mcm^5s^2U_{34}$ causes neurological and developmental defects (Dewez et al. 2008; C. Chen, Tuck, and Byström 2009), while in mice it is embryonically lethal (Veen

2011; Y.-T. Chen et al. 2009). Similar defects were found in fruit flies (*Drosophila melanogaster*) with dysfunctional *ELP*-complex (Walker et al. 2011; Singh et al. 2010). In humans, mutations in the homolog of *ELP1* affects the development and survival of sensory and autonomic neurones, resulting in a hereditary sensory and autonomic neuropathy called as Familial Dysautonomia (FD) (Shohat and Halpern 2010; Slaugenhaupt and Gusella 2002; Y.-T. Chen et al. 2009). Additionally, variations in human *ELP3* and *ELP4* have been associated with amyotrophic lateral sclerosis (ALS) and rolandic epilepsy (RE), respectively (Strug et al. 2009; Simpson et al. 2009), and SNPs in human *ELP1* were found to be associated with increased risk of bronchial asthama (Takeoka et al. 2001), a chronic inflammatory disease. Interestingly, human mitochondrial tRNA mtK^{UUU} carries a 5-taurinomethyl-2-thiouridine (τm^5s^2U) at the wobble position of the anti-codon and inability to synthesise it results in myoclonic epilepsy with ragged red fibres (MERRF), a rare maternally inherited disease characterised by mitochondrial dysfunction caused by impaired mitochondrial protein synthesis (DiMauro and Hirano 2009; Yasukawa et al. 2000).

The available literature indicates that post transcriptional modifications of tRNA wobble uridines affect its decoding properties and the interactions that tRNAs make with the protein translational machinery. Furthermore, characterised phenotypes of the organisms with impaired biosynthesis of $mcm^5s^2U_{34}$ and its association with several human pathologies give important clues about the importance of mcm^5 and s^2 modifications for the proper functioning of certain cellular processes. However, several important questions remain unanswered. For instance, it is unclear if the absence of mcm^5s^2U can result in differential translation. Additionally, it is not known whether the whole proteome or only a

subset of proteins is affected and whether differential translation can explain the known phenotypes. Another obvious question is that of whether and how the levels of mcm^5s^2U are regulated. In the present doctoral work, a system wide approach was used to target these questions using mass spectrometry based quantitative proteomics, which allows quantitative estimation of many proteins in a high throughput and sensitive manner. The next section briefly discusses mass spectrometry based proteomics and merits and demerits of different approaches to quantitative proteomics.

1.5 Mass spectrometry based quantitative proteomics with SILAC

Mass spectrometry (MS) is a very sensitive technique that involves assessing the mass of charged analytes by measuring their response to electric and magnetic fields inside a mass spectrometer. Since these measurements take place in gaseous phase under vacuum, an ion-source that ionises and converts analytes into gas phase is an integral part of a mass spectrometry set-up. Matrix-assisted laser desorption ionisation (MALDI) and electro-spray ionisation (ESI) are two of the most widely used techniques that ionise and volatise analytes of biological interest, like proteins and peptides, with little to no decomposition of the analyte (for detailed review see Mann, Hendrickson, and Pandey (2001)). MALDI, as the name suggests, uses laser pulses targeted upon dried up mixture of sample with a suitable matrix that transfers energy from the laser to analyte molecules leading to their desorption and ionisation. ESI, on the other hand, works by spraying sample in liquid solutions through a porous needle maintained at high voltage, thereby leading to atomisation and ionisation of the sample. Due its ability to work with liquid samples, ESI is more suitable for complex samples, such as the protein extracts from whole cells, because it can be coupled to analyte separation techniques such as reversed phase liquid chromatography.

In a typical workflow for MS analysis of proteins (figure 1.7A), samples are first digested by site-specific proteases, such as trypsin, to generate peptides that are then analysed by tandem MS measurements. The first round of these measurements, called MS^1 or survey scan, involves measuring the mass to charge ratio (m/z) of all the ions injected into a mass spectrometer. In the subsequent measurements, selected ions are fragmented and the m/z ratios of

the product ions measured, this is called an MS^2 scan. Selection of ions for MS^2 follows the order of intensity observed in the MS^1 scan (figure 1.7B). Due to this semi random nature of selection, this format of proteomics analysis by MS is termed shotgun proteomics. MS measurements are often presented as spectra of ions with their m/z values on the x-axis and intensity on the y-axis. After acquisition of the data, MS^1 and MS^2 spectra are matched against the theoretical spectra predicted from a protein sequence database by dedicated software packages, called database search engines (for example SEQUEST: Eng, McCormack, and Yates 1994), to identify the peptides and consequently the proteins present in the sample. Since the match between theoretical and observed spectra is often partial, search engines give a score to every match. This score, along with other observed parameters, is used by sophisticated statistical packages to assign probabilities of successful matches, followed by computation of false discovery rates to control the number of false positives when several thousand spectra are searched (for a comprehensive review of statistical packages, refer to Choi and Nesvizhskii (2008)). Some of the most widely used software packages for the proteomics analysis are available in the form a collection known as the Trans Proteomics Pipeline (TPP) (Deutsch et al. 2010; Pedrioli 2010; Keller et al. 2005).

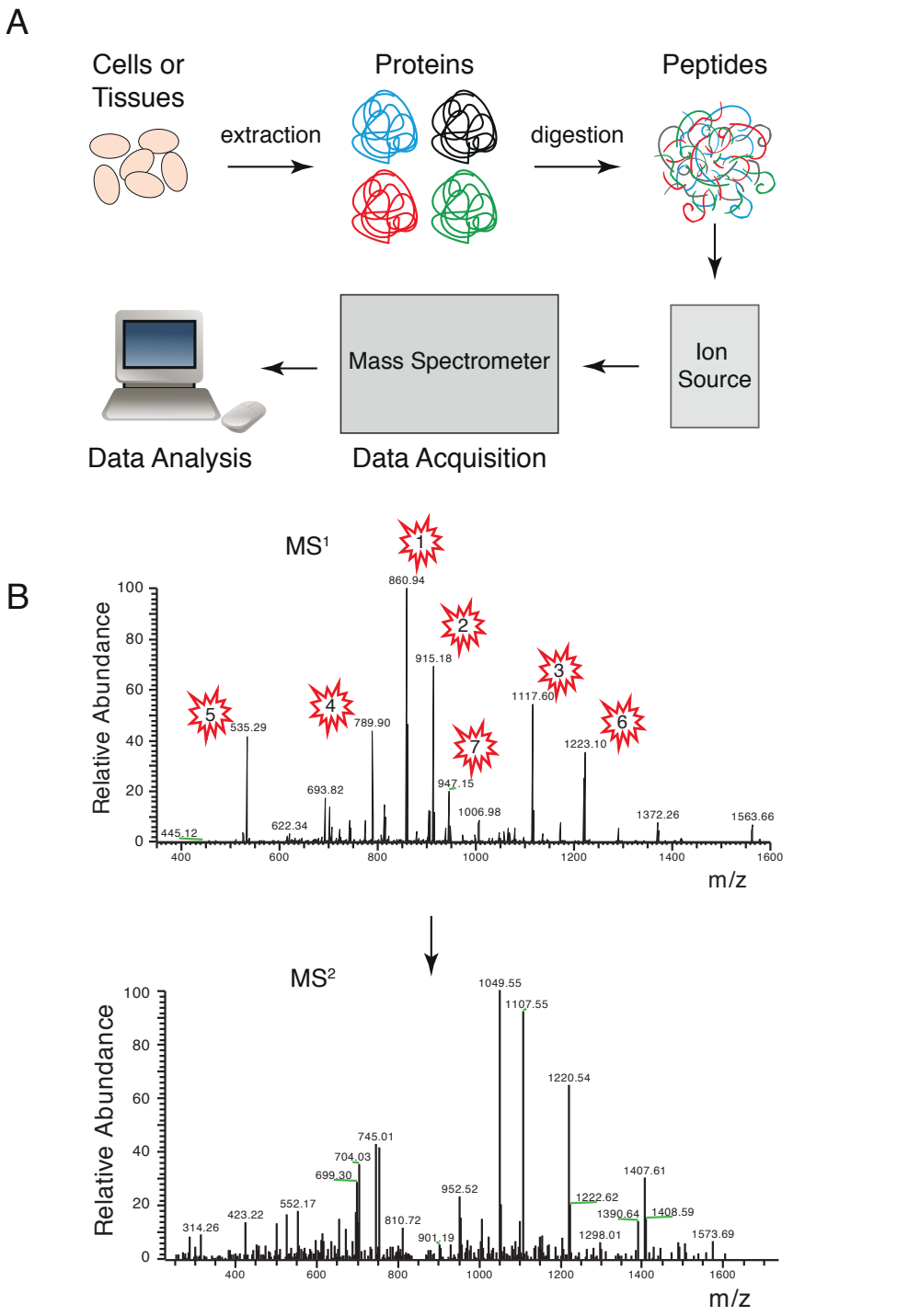

Figure 1.7: Proteomics with mass spectrometry (A) A typical workflow for mass spectrometry based proteomics. Proteins are extracted from cells or tissues followed by their digestion to peptides. Peptides are then ionised and converted to gas phase by a suitable ion-source (usually ESI or MALDI) and injected into a mass spectrometer. Data obtained from the mass spectrometer is analysed to obtain identification of peptides and proteins in the sample. (B) Shotgun proteomics: Ions are selected for fragmentation and MS^2 analysis in decreasing order of their intensity measured in MS^1 scans. Shown on the top is an example MS^1 scan from an LC-MS run of yeast protein extracts, digested by Trypsin, separated by reverse phase LC and electrosprayed into an LTQ-Orbitrap-Velos mass spectrometer. The red flash symbols indicate fragmentation events in the order of the number indicated. Shown at the bottom is the MS^2 scan obtained after the fragmentation of the most abundant precursor from the MS^1 scan on the top (i.e. m/z = 860.94).

Quantitative proteomics with mass spectrometry combines qualitative (identification) analysis of the proteins in a sample with their quantification as an additional dimension (Aebersold and Mann 2003). LC-ESI-MS is particularly well suited for quantitative mass spectrometry. Peptides eluting from the LC setup are volatilised and ionised by ESI and analysed by MS. The area of the signal intensity vs. time profile of an eluting peptide is termed as its ion current and under given experimental conditions it is directly proportional to the peptide's abundance (Ong and Mann 2005; Mann M, Hendrickson, and Pandey 2001). For the biological relevance of this type of estimation, it is often useful to compare it with another sample representing a different physiological state. There are two popular strategies for measuring relative changes in protein abundances. In the first strategy, samples representing two or more biologically relevant states are subjected to LC-MS analysis in a sequential manner and elution profiles of every peptide are recorded. Subsequently, MS raw data is analysed to identify the peptides from their MS^2 spectra and their abundances are estimated by extracting their ion chromatograms from MS^1 spectra. Even though this strategy is straight forward in application, it is very prone to incorporation of unwanted noise and differences due to fluctuation between different LC-MS runs. Additionally, since MS analysis requires extensive sample preperation, this approach suffers from the risk of introduction of errors due to differential handling of samples (Mueller et al. 2008).

The second strategy involves analysing the samples to be compared simultaneously. In this approach, samples are differentially labeled with stable isotopes. This allows for the samples to be mixed before their analysis while

retaining the ability to differentiate them in a mass spectrometer. As a result, MS measurements are more robust and not affected by fluctuations between the runs (Ong and Mann 2005; Mann 2006). After the LC-MS analysis, ion chromatograms of the co-eluting, isotopically labeled peptide pairs can be extracted on the basis of their isotopic mass shift in the MS spectrum (bottom panel in figure 1.8). There are multiple ways of introducing isotopic labels in the protein samples that can be broadly classified into (1) by enzymatic reactions, (2) by chemical modifications and (3) by metabolic incorporation of isotopes within the cell cultures (figure 1.8) (Mann 2006; Aebersold and Mann 2003). In the first two methods, samples to be compared are processed and labeled separately before they can be combined for analysis. Therefore, they are prone to technical errors. The third method involves growing two populations of the cells, one in a normal medium and the other in a medium containing heavy ^{15}N-salts or one or more heavy amino acids (like $^{13}C_6{}^{15}N_2$Lys, $^{13}C_6{}^{15}N_6$Arg). This way, as the two cultures grow, all the proteins in the two populations of cells get differentially labeled. Post labelling, cultures can be combined and processed to extract proteins, thus allowing the identical treatment of the samples. The approach involving labeled amino acids is called stable-isotope labelling by amino acids in cell culture (SILAC) (Mann 2006) and allows more control on labelling as compared to using ^{15}N-salts. More importantly, the exact mass difference between the SILAC labelled peptides is known before hand, thereby simplifying their identification and quantitation.

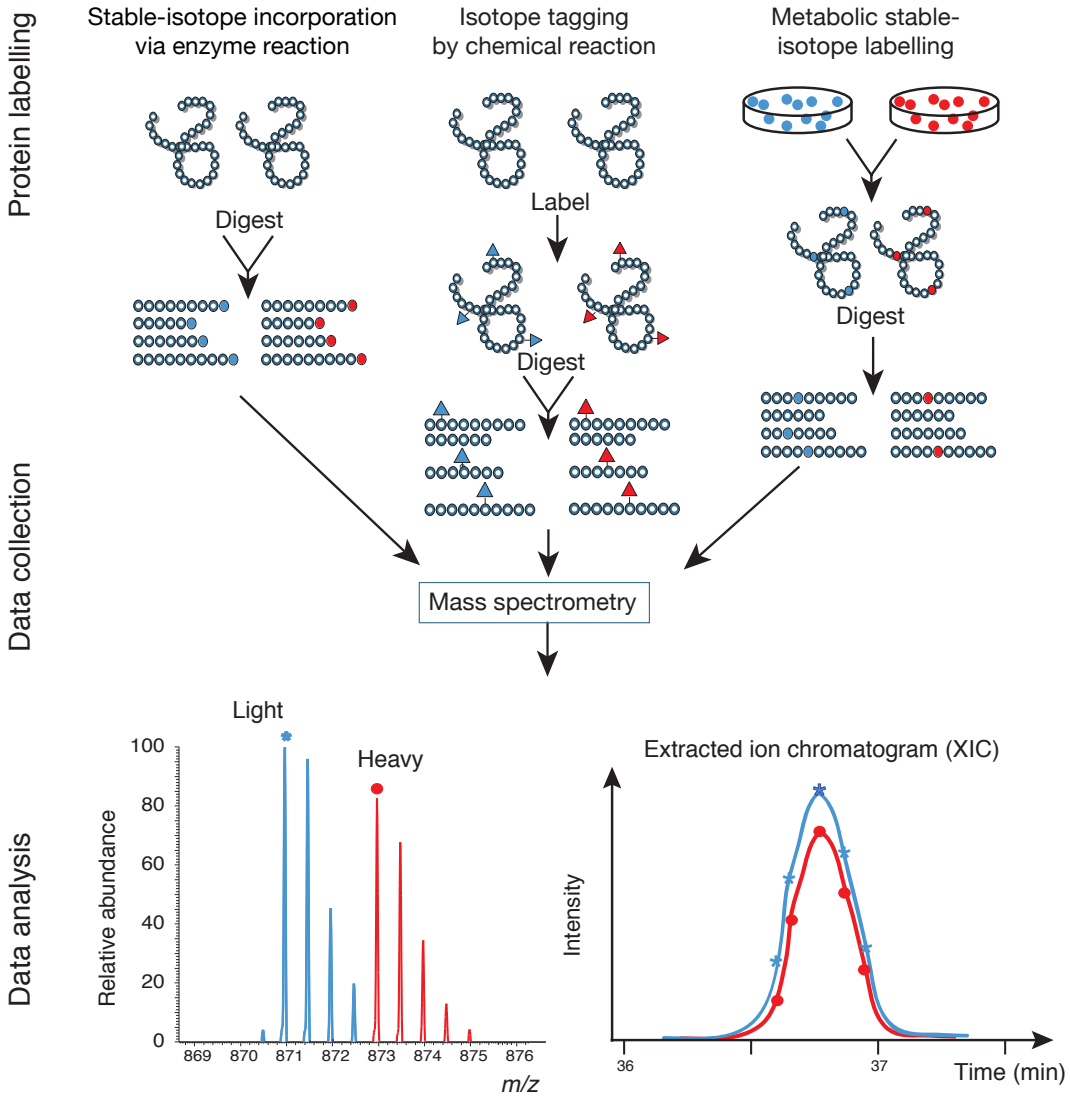

Figure 1.8: Quantitative mass spectrometry with isotopically labelled samples. Schematic representation of the methods used to differentially label protein samples with stable isotopes. Chemical isotope labelling (in the middle) can be done both at the protein or peptide level. During the MS analysis, each peptide co-elutes with its isotopically labeled partner, which can be easily identified based on the mass shift cause by the isotopes. Bottom panels show isotopically labelled peptide pair and their quantitation. Modified from Ong and Mann (2005); Aebersold and Mann (2003).

In principle, SILAC can be used to label and compare several samples in one MS run. However, in practice sample complexity restricts the number of samples that can be compared. As previously described, the semi-random nature of shotgun proteomics selects peptides for fragmentation in decreasing order of their abundance. In the analysis of complex samples, such as whole cell/ tissue extracts, the number of peptides fragmented in a duty-cycle (gap

between two MS^1 scans) is generally smaller than the number of peptides eluting from the LC. As a result, lower abundance peptides escape fragmentation and consequently, identification. High abundance proteins give several high abundance peptides. Consequently, shotgun proteomics is biased for the identification of high abundance proteins while lower abundance proteins are under-sampled. With SILAC, or any other type of stable isotope labelling, complexity increases and under-sampling worsens with the addition of each differentially labeled sample. Fortunately, there are ways to circumvent this problem to a certain extent, such as sample fractionation (Breci et al. 2005). A complex sample can be divided into smaller less complex sub-samples on the basis of differences in the physical and chemical properties of proteins or peptides; such as size, ionisation, iso-electric point, hydrophobicity, etc. The methods that exploit the mentioned properties include SDS-PAGE (Breci et al. 2005), strong cation exchange (SCX) (Slebos et al. 2008), strong anion exchange (SAX) (Ritorto et al. 2013), OffGel electrophoresis (Chenau et al. 2008; Ros et al. 2002) and reverse phase chromatography (Nakamura, Kuromitsu, and Oda 2008), respectively. In combination with sample fractionation, SILAC becomes a very robust and sensitive approach to do quantitative proteomics with mass spectrometry.

1.6 Goal of the study

The main goal of the presented doctoral project was to understand the *in vivo* functional relevance of wobble uridine modifications found on the eukaryotic cytoplasmic tRNAs tK^{UUU}, tQ^{UUG} and tE^{UUC}. Since tRNAs play a central role in protein synthesis, SILAC based quantitative proteomics was employed to measure and compare protein abundances in presence and absence of $mcm^5s^2U_{34}$. *S. cerevisiae* was chosen as the model organism because of its malleability to genetic manipulation and SILAC labelling. As the first objective of the project, a robust and sensitive quantitative proteomics workflow was established and statistically significant changes in protein abundances were measure in the mutant yeast cells unable to modify their tRNAs relative to wild-type cells. Subsequently, the objective was to investigate whether and how the hypomodification of tK^{UUU}, tQ^{UUG} and tE^{UUC} leads to differential translation. An unbiased data-driven approach was used to identify the codon signatures of the mRNAs whose translation might be affected by the loss of $mcm^5s^2U_{34}$. Results from the computational analysis were supported by conventional biochemical experiments. Additionally, we collaborated with the groups of Prof. Matthias Peter (ETH Zurich, Switzerland) and Prof. Marina Rodnina (Max Planck Institute for Biophysical Chemistry, Göttingen) for some of the supporting biochemical experiments and importantly, to investigate the contribution of mcm^5 and s^2 modifications at the molecular level. All together, results from this section are described and discusses in **chapter 3** of the thesis.

The next focus of the project was to identify whether cells alter the levels of these modifications in response to changes in their standard growth conditions. To start in this direction, we picked a stress condition based on the results of the

proteomics analysis of cells lacking $mcm^5s^2U_{34}$ and measured the protein level response of wild-type cells to the stress condition by quantitative proteomics. This led to the revelation that *URM1*-pathway activity and consequently the cellular levels of $mcm^5s^2U_{34}$ are modulated in response to stress. Subsequently, we aimed to investigate the mechanism behind this regulation and how it aids the cells in coping against the stress. This is presented in **chapter 4**.

2. Material and Methods

2.1 Yeast culture media

Yeast YPD media was composed of 10 g/L Bacto Yeast Extract (Becton Dickinson, USA), 20 g/L Bacto Peptone (Becton Dickinson, USA) and 2% (w/v) D-glucose. Yeast synthetic complete (SC+D) media was composed of 1.7 g/L Difco Yeast Nitrogen Base without amino acids and $(NH_4)_2SO_4$ (Becton Dickinson, USA), 5.0 g/L $(NH_4)_2SO_4$ (Sigma), 0.03 g/L isoleucine, 0.15 g/L valine, 0.04 g/L adenine, 0.02 g/L histidine, 0.1 g/L leucine, 0.02 g/L methionine, 0.05 g/L phenylalanine, 0.2 g/L threonine, 0.04 g/L tryptophan, 0.03 g/L tyrosine, 0.02 g/L uracil, 0.1 g/L glutamic acid, 0.1 g/L aspartic acid, 0.02 mg/mL arginine, 0.03 mg/mL lysine (all amino acids were bought from Sigma), 2% (w/v) Glucose). For the experiments described in chapter 4, liquid culture media was always sterilised by filtration.

2.2 SILAC labelling

SILAC strains were exponentially grown in SC-K-R + D supplemented with 0.2 g/L Proline and 0.02 mg/mL Arg, 0.03 mg/mL Lys (referred to as light amino acids) or 0.02mg/mL $^{13}C_6$,$^{15}N_4$-Arg (Sigma) and 0.03 mg/mL $^{13}C_6$,$^{15}N_2$-Lys (Sigma) (referred to as heavy amino acids). Equal ODs of light and heavy culture were mixed and subsequently processed together. To ensure complete labelling, even the pre-cultures were done in the respective SILAC labelled medium and during the main culture, cells were allowed to grow for at least 4 doublings.

2.3 Protein extraction and digestion for MS

Harvested yeast cells were lysed by treating with 1.85 M NaOH, 7.6% (v/v) β-mercaptoethanol for 10 min on ice followed by protein precipitation with equal volume of 50% (w/v) trichloroacetic acid (CCl_3COOH) for 20 min on ice. The

precipitated protein pellet was washed three times with acetone and the protein pellet was air-dried.

For experiments in chapter 3, the protein pellets were resolubilised in 8 M urea, 0.5% (w/v) RapiGest (Waters), 100 mM Tris pH 8.0. Protein concentration was measured using the BCA protein assay kit (Pierce). Subsequently, proteins were reduced with 10 mM DTT at 56 °C for 30 min and carboxyamidomethylated with 25 mM iodoacetamide at room temperature in the dark for 30 min. For digestion, protein samples were diluted 10x with 50 mM NH_4HCO_3 and trypsin (V5113, Promega) was added at an enzyme:substrate ratio of 1:100 and incubated overnight at 37 °C.

For Chapter 4, the protein pellets were resuspended in an SDS-buffer (5% SDS, 50 mM NH_4HCO_3) by shaking at 37 °C for 30 min and at 65 °C for 10 min Protein concentration was measured using the BCA protein assay kit (Pierce). Subsequently, the required amount of proteins were reduced with 10 mM DTT at 56 °C for 30 min and carboxyamidomethylated with 25 mM iodoacetamide at room temperature in the dark for 30 min Proteins were then digested using the FASP method (Wiśniewski et al. 2009). Briefly, 50–150 μg of proteins were mixed with 8 M urea, 100 mM Tris pH 8.0 solution such that the volume of the urea solution was at least twice of the protein solution in SDS buffer (This step is crucial because concentrated urea solution reduces the size of SDS micelles, which will otherwise block the filter membrane. Also, before loading the sample mixed with the urea solution, filter cartridges were checked for damage by adding 200 μL of 8 M urea, 100 mM Tris pH 8.0 and spinning for 1-2 min at 10,000 rcf. Undamaged filter would allow very little flowthrough.) The samples were then added into the Vivacon 500 filter cartridges (VN01H22ETO, sartorius

stedium biotech) and spun at 10,000 rcf at room temp for ~10 min or until all the fluid had flown through. Only up to 400 μL of sample could be loaded in the filter cartridge in one go. Therefore, loading was repeated until all the sample was loaded. Next, immobilised sample was washed at least thrice with 400 μL of 8 M urea, 100 mM Tris pH 8.0 and twice with 400 μL of either 50 mM Tris pH 8.0 or 50 mM NH_4HCO_3. For digestion, filter cartridges were placed in new collection tubes and 200 μL of 50mM Tris pH 8.0 or 50 mM NH_4HCO_3 was added. Trypsin (V5113, Promega) was added and mixed by pipetting up-down gently. Samples were left overnight on a thermomixer at 37 °C. Wet paper towels were added for humidity control and to prevent drying. Next morning, samples were recovered by spinning 15 min at 10,000 rcf and rinsing the cartridges twice with 200 μl of 0.5 M NaCl.

Note: urea and iodoacetamide solutions were always freshly prepared. Water used for the MS samples was of MS / HPLC grade purity.

2.4 Peptide clean-up and desalting

C18 micro- or macro-spin columns (Nest Group) were used. Columns were washed once with CH_3CN and once with 50% (v/v) CH_3CN. After washing, columns were equilibrated twice with with 0.1% (v/v) CF_3COOH (TFA). Peptide samples were acidified with 1% (v/v) TFA to pH 3.0 or lower. For larger volumes of sample or for highly buffered samples 100% CH_3COOH (FA) was used, but only after adding some 1% TFA. TFA being an ion-pair agent, helps in binding the peptides to C18 resin. (Note: If RapiGest was used in the samples, after acidification samples were incubate at 37 °C for 30 min and spun down at max. speed for 10-15 min). Acidified peptides were loaded onto the equilibrated C18 cartridges and washed 3-4 times with 0.1% (v/v) TFA. Finally, cleaned peptides

were eluted twice with 60% (v/v) CH_3CN, 0.1% (v/v) TFA and dried in a vacuum drier.

2.5 Peptide fractionation by isoelectric focussing (OffGel)

C18 purified peptides were fractionated by iso-electric focusing on the OffGel Fractionator (G3100AA, Agilent) according to the manual of the High Res Kit, pH 3–10 (Agilent, 5188-6424), except the strips were exchanged by pH 3-11 NL, 13 cm (17-6003-75, GE Healthcare) or pH 3-11 NL, 24 cm (45-000-406, GE Healthcare) and ampholytes were substituted by 2% IPG Buffer pH 3-11 NL (17-6004-40, GE Healthcare). After the completion of focussing, fractions were acidified with 1% (v/v) CF_3COOH, purified on C18 MicroSpin columns (The Nest Group) and dried in a vacuum dryer.

2.6 Peptide fractionation by strong cation exchange (SCX)

Microspin PolySULFOETHYL Aspartamide columns (The Nest Group) were used for the SCX fractionation. The procedure was performed essentially as per the manufacturer's instructions. SCX columns were first wetted with 100% CH_3OH or 100% CH_3CN and then rinsed twice with a strong buffer (0.2 M NaH_2PO_4, 0.3 M CH_3COONa, pH 3-6.5). Then, the columns were conditioned for at least one hour before use at room temperature by allowing them to sit in the strong buffer. Next, they were equilibrated 3 times with 100 μL of equilibration buffer (20% CH_3CN, 5 mM NaH_2PO_4, pH 3.0). C18 purified peptides were resuspended in buffer of very low salt concentration (5-15 mM) and loaded on to the columns, washed twice with 100 μL of wash buffer(20% (v/v) CH_3CN, 5 mM NaH_2PO_4, pH 3.0). For step wise elution into fractions, 50 μL of water followed by 100 μL of elution buffer (20% CH_3CN, 5mM NaH_2PO_4, pH 3.0 plus the required NaCl concentration) were used. The eluate was collected

and elution was repeated with a different NaCl concentration. In total, peptides were eluted with a six-step NaCl fractionation (50 mM,100 mM, 150 mM, 200 mM, 400 mM and 800 mM). Flowthrough was also kept as a fraction. All the fractions were dried in a vacuum drier prior to the cleanup on C18 MicroSpin columns (The Nest Group).

2.7 LC-MS-MS/MS

Dried peptides were resuspended in 0.1% CF_3COOH for the LC-MS-MS/MS analysis. A split-free Easy-nLC (Proxeon) HPLC system was used for the analyses in chapter 3 and an UltiMate 3000 uHPLC system (Dionex, Thermo Scientific) was used for chapter 4, for the online reverse phase (C18 silica) liquid chromatography. Coated-tip fused silica columns, 25 cm for WT vs. *urm1Δ* analysis and 50 cm thereafter, (PicoFrit columns, PF-360-75-10-CE-5, New Objective) were packed with C18 silica beads (Magic C18, 200 Å, 3 μm, Michrom Bioresources). A gradient of buffer B (0.1 % (v/v) HCOOH, 90 % (v/v) CH_3CN) in buffer A (0.1 % (v/v) HCOOH, 2 % (v/v) CH_3CN) ranging from 2% to 35% was used to resolve peptides. For analyses in chapter 4, buffer A and buffer B also contained 3% (v/v) DMSO. Length of the gradient was 170 min for the WT vs. *urm1Δ* and WT vs. *urm1Δ* + ptKQE analyses, 240 min for the 30 °C vs. 37 °C analysis and 360 min for the rest. The chromatography setup was directly coupled to an LTQ-Orbitrap Velos Pro mass spectrometer (Thermo Finnigan) configured for the top-15 data dependent acquisition (DDA) by collision-induced fragmentation (CID) or top-8 DDA by higher-energy collision-activated dissociation (HCD). When CID was used, MS^1 scans were done in profile mode at an FT-MS resolution of 60,000 and MS/MS scans were done in centroid mode with the IT rapid scan rate . For HCD, MS^1 scans were done in profile mode at an FT-MS resolution of 30,000 and MS^2 scans were done at an

FT-MS resolution of 7,500. Precursor intensity threshold for triggering fragmentation was kept at 10,000 units for analyses in chapter 3 and thereafter lowered to 500 units.

2.8 Protein identification and quantitation

MS data was processed and analysed as explained in Pedrioli (2010). Briefly, RAW data files were converted to the mzXML format (Pedrioli et al. 2004) and searched against the Saccharomyces Genome Database protein database. For experiments presented in Chapter 3, X!Tandem (Craig and Beavis 2004) with the K-score plug-in (MacLean et al. 2006), OMSSA (Geer et al. 2004), Mascot (Matrix Science) and UW SEQUEST were used for MS/MS searches. For chapter 4, Comet search engine (Eng, Jahan, and Hoopmann 2012) was used. Search parameters used were carboxyamidomethylation (57.022 Da) of Cys as static modification, $^{13}C_6$,$^{15}N_2$-Lys (8.01419892 Da), $^{13}C_6$,$^{15}N_4$-Arg (10.008252778 Da) and oxidation of Met (15.99491463 Da) as variable modifications, semitryptic digestion with the maximum of two missed cleavages, 25 ppm and 0.4 Da error tolerances for MS and MS/MS, respectively. Peptide probabilities were evaluated with PeptideProphet (Keller et al. 2002) and ProteinProphet (Nesvizhskii et al. 2003) was used to estimate protein probabilities. Protein abundance ratios were computed as L/H (light/heavy) ratios using XPRESS (Han et al. 2001). Finally proteins were filtered at a ProteinProphet calculated 1% FDR.

2.9 Data normalization and statistical analysis of differential abundance

Protein ratios were stored into an in-house developed database (manuscript in preparation). From there, protein abundance ratios were imported into R

(version 'Frisbee Sailing' 3.0.2 (2013-09-25)) for further analysis (Team 2009). Protein ratios were median normalised and statistical analysis of the differential abundance of proteins was done with the empirical bayes moderated t-test (Smyth 2004) using the LIMMA package of the Bioconductor project (Smyth 2005) and the obtained *p*-values were adjusted with Benjamini & Hochberg correction to control for false discovery rate (FDR). Protein ratios were filtered at an FDR threshold of 1% (or adjusted p-value = 0.01).

2.10 Random Forest analysis for codon importance

Significantly changing proteins were split into two classes and the abundance of codons that best predicted class membership was extracted by machine learning in R using the random forest implementation of the party package (v0.9- 99992). The abundance of all codons, minus the stop codons in each gene was used as variables. The overall number of trees in the forest was set to 1,000 and the number of randomly preselected predictor variables for each split was set to the square root of the variables. Random seeds were varied to check the robustness of the prediction.

2.11 GO terms and MIPS functional classes enrichment analysis

Analysis for over-represented GO terms and MIPS functional classes was done using the FunSpec tool available online (http://funspec.med.utoronto.ca). A *p*-value of 0.01 was used as the threshold for statistical significance. The wordcloud package from R was used to display GO terms for biological processes with p-values < 0.001.

2.12 Quantitative PCR

Total RNA was extracted from the exponentially growing yeast cells using the Ribo-pure yeast kit (AM1926, Life Technologies) and converted to cDNA using

the High Capacity cDNA Reverse Transcription Kit with RNase Inhibitor (4374966, Life Technologies) according to the manufacturer's instructions. qPCR was performed using predesigned TaqMan gene expression assays (table 2.2) on an Applied Biosystems 7900HT Fast Real-Time PCR System strictly following the manufacturer's protocol.

2.13 Immunoblotting

Exponentially growing yeast cells were harvested by centrifugation and lysed by treatment with 1.85 M NaOH, 7.6% β-mercaptoethanol for 10 min on ice followed by protein precipitation with 50% (w/v) TCA for 15 min on ice. Precipitated proteins were washed twice with acetone and the protein pellet was air-dried to remove residual acetone. Next, it was resolubilised in 10% (w/v) SDS, 1.0 M unbuffered Tris and subsequently, reduced with 0.2 M DTT, 30 % (v/v) Glycerol, 0.002% (w/v) Bromophenol blue for 30 min at 65 °C. Denatured protein samples were separated by poly-acrylamide gel electrophoresis, transferred onto a nitrocellulose membrane and probed with specific antibodies (mouse-anti-HA antibody (HA.11 Clone 16B12; MMS-101R, Covance), PAP (P1291, Sigma), mouse-anti-Actin antibody (ab8224, Abcam) and goat-anti-mouse IgG, IgA, IgM (H+L) horseradish peroxidase conjugate (A-10668, Invitrogen)) using standard procedures.

2.14 Extraction of total RNA and enrichment for bulk tRNA

For small scale extraction, 25 mL of exponentially growing yeast culture was harvested by centrifugation and resuspended in 0.5 mL 150 mM NaCl solution. Cells were lysed by beating with ~750 μL of glass beads in 750 μL of saturated phenol for 7 min Subsequently, 75 μL of chloroform were added and mixture was vortexed for another minute. The aqueous phase was separated from the

organic phase by centrifugation and transferred to a new tube where phenol chloroform extraction was repeated with 500 μL of saturated phenol and 50 μL chloroform. Tubes with organic phases were re-extracted for RNA with 2 mL of 150 mM NaCl. Bulk tRNA were enriched over the Nuclebond AX20 anion exchange columns (Macherey-Nagel, 740511). Prior to sample loading, columns were equilibrated with 3.0 mL column buffer (10 mM Tris pH 6.8, 15% (v/v) Ethanol, 200 mM KCl). When needed, flow of liquid through the columns was assisted by spinning in a suitable centrifuge at the lowest rpm setting. Bound RNAs were washed with 6 mL of column buffer and total tRNAs were eluted with 1.5 mL elution buffer (10mM Tris pH 6.5, 15% Ethanol, 650 mM KCl). Subsequently, tRNA were concentrated by precipitating overnight with 2.5 volumes of ethanol at –20 °C. Next morning, the tRNA pellets were washed extensively by 80% (v/v) ice-cold ethanol, air-dried and resuspended in nuclease free water (Applied Biosystems, AM9930). For large scale applications, 1 litre of yeast culture was grown and volumes of reagents/ buffers used were scaled proportionally. Nucleobond AX500 columns were used for the enrichment of bulk tRNA. Importantly, for this procedure, phenol:chloroform ratio, salt concentration, temperature and pH of buffers were carefully controlled according to the procedure as they affect the yield of tRNA and contamination with other RNAs.

2.15 Purification of specific tRNAs

3’ biotinylated DNA oligonucleotide probes specific for the amino-acyl arm of the tRNAs were purchased from Invitrogen. Streptavidin-sepharose resin (17-5113-01, GE Healthcare) was used in an approximate ratio of 1 nmole of probe to 10 μL of the resin slurry. Prior to coupling, the streptavidin slurry was extensively washed at room temp to remove all traces of nucleases that might

be present; first in the coupling buffer (5 mM Tris-HCL (pH 7.5), 1 mM EDTA (pH 8.0), 1 M NaCl) for 10 min, then twice in solution-A (0.1 M NaOH, 0.05 M NaCl) for 2 min each, then once in solution-B (0.1 M NaCl) for 2 min and finally, twice in coupling buffer for 5 min each. Following washes, the probe was added to the resin in coupling buffer and incubated for 45 min at 37 °C on a thermo-mixer. Next, the resin was washed once with coupling buffer and 4 times with the tRNA binding buffer (30 mM HEPES-KOH (pH 7.5), 15 mM EDTA (pH 8.0) , 1.2 M NaCl).

To the resin with immobilised probe, about 400 µg of bulk tRNA in tRNA binding buffer was added and the mixture was incubated at 65 °C for 15-20 min to partially denature the tRNAs. Then, the mixture was moved to a rotating-wheel for 1 h at room temperature to allow annealing of the tRNAs with the immobilised probes by gradual cooling. Subsequently, the resin was washed 5 times with tRNA wash buffer (100 mM NaCl, 2.5 mM HEPES-KOH (pH 7.5), 1.25 mM EDTA (pH 8.0)) at 37 °C for 5 min each. Finally, the tRNAs were eluted twice with the elution buffer (20 mM NaCl, 0.5 mM HEPES-KOH (pH 7.5), 0.25 mM EDTA (pH 8.0)) at 70 °C for 15 min each (elution with 70 °C resulted in inactivation of streptavidin and possibly leaching of the immobilised probes. Therefore, 65 °C can also be tried to reduce contamination with probes). Eluted tRNAs were precipitated over-night at –20 °C with 0.1 volumes of 20% (w/v) NaOAc and 2.5 volumes of Ethanol.

Importantly, temperature, concentration of salts and pH were carefully controlled as they affect annealing (Tm) of nucleic acids. The probes used were; 5’-CTCCGATACGGGGAGTCGAACCCCGGTCTC-3’ for Sc-tE^{UUC}, 5’-

AGGTCCTACCCGGATTCGAACCGGGGTTGT-3' for Sc-tQ^{UUG} and 5'-CACTCACGATGGGGGTCGAACCCATAATCT-3' for Sc-tR^{UCU}.

2.16 RNA MS analysis

10 µg of a specific tRNA were digested and dephosphorylated in a 50 μL reaction volume with 2 U of Nuclease P1 (N7000-USB, Stratech), 300 U of bacterial alkaline phosphatase (18011-015, Life Technologies) in presence of 0.9 mM $ZnSO_4$ at 37 °C for 90-120 min. To the above mixture, 15 μL of 0.5 M NH_4HCO_3 were added and incubated at 37 °C for 90-120 min to complete dephosphorylation to individual nucleosides. The reaction mixture was then acidified using HCOOH, the nucleosides were purified over graphite TopTips (Glygen Corp.) and dried in a vacuum dryer.

For the mass spectrometric analysis, nucleosides were resuspended in water and separated by liquid chromatography over a Hypercarb graphite column (35005-100065, Thermo Scientific) connected to an UltiMate 3000 uHPLC system (Dionex) running a 1.0 μL/min gradient of buffer-B (0.1% (v/v) HCOOH, 90% (v/v) CH_3CN) in buffer A (0.1% (v/v) HCOOH, 2% (v/v) CH_3CN) ranging from 1% to 37% over 45 min and at a column-oven temperature of 65 °C. A fused silica emitter (PicoFrit columns, PF360-75-10-N-5, New Objective) was used to spray eluting nucleosides into an LTQ-Orbitrap Velos Pro mass spectrometer (Thermo Finnigan) operating at a source voltage of 1.8 kV. MS^1 scans were acquired in profile mode at an FT-MS resolution of 100,000. Nucleosides were fragmented in data-independent acquisition mode (DIA) by collision-induced fragmentation (CID) with isolation width set at 2.0 m/z and normalised collision energy of 35.0. MS/MS spectra were acquired in centroid

mode with the IT normal scan rate. Settings used for targeting the nucleosides for fragmentations were empirically determined and indicated in the table below.

MS m/z	RT start (min)	RT end (min)	Name
113.03455	24.16	34.16	U (BH^+)
185.05567	36.89	46.89	mcm^5U (BH^+)
201.03283	52.68	62.68	mcm^5s^2U (BH^+)
245.0768	24.16	34.16	U (MH^+)
317.09793	36.89	46.89	mcm^5U (MH^+)
333.07508	52.68	62.68	mcm^5s^2U (MH^+)

For data analysis, MS raw files were converted to mzXML format (Pedrioli et al. 2004) and analysed by an in-house developed software (AYB) to identify and quantify the nucleosides. Identification was validated by matching the obtained MS/MS spectra with the ones that have been previously reported (Bullinger et al. 2008; Leidel et al. 2009).

2.17 APM supplemented denaturing PAGE

0.5 to1.0 µg of bulk tRNA was mixed 1:1 with 2x loading buffer (AM8547, LifeTechnologies) and electrophoresed through 10% acrylamide gel containing 7 M urea, 0.5X TBE and 50 µg/mL [(N- acryloylamino)phenyl] mercuric chloride (APM: synthesised in house according to the procedure described in Igloi (1988) at 200 V for 60-90 min (until the dye front ran-out). Gels were pre-run without any sample for 15 minutes at 200V and each well was washed by pipetting the electrophoresis buffer multiple times to get rid of the urea diffusing out from the gel, which would otherwise interfere with the loading of samples. After electrophoresis gels were stained with SYBR Gold (Invitrogen) diluted 1:10,000 in 0.5X TBE for 5 min before imaging.

2.18 tRNA northern blot analysis

Electrophoretically separated tRNAs were transferred to a positively charged nylon membrane (Hybond-N+, GE Healthcare) using the semi-dry blotter (Fastblot, biometra) at a constant current of 400 mA for 40 min in 0.5X TBE transfer buffer. Membrane and gel were imaged after the transfer to assess the efficiency of transfer. Transferred tRNAs were cross linked using a UV cross linker (C-1000, UVP) at an energy setting of 1,200 J for 30 sec, when the membrane was still moist. Subsequently, the membrane was prehybridised using 5 mL (2.7 mL in 15 mL centrifugation tube) of PerfectHyb Plus (Sigma) buffer with 1x ProtectRNA RNAse inhibitor (R7397, Sigma Aldrich) and 0.1 ug/ μL ssDNA (D9156-1ML, Sigma Aldrich) for 2 h in a 50 mL centrifugation tube. 10 pmol of DNA oligonucleotide probe were labelled with 10 U of T4 Polynucleotide Kinase (M0201S, New England Biolabs) and 5 μL of 3000 Ci/ mmol 10 μCi/μL [Y-^{32}P] ATP (PerkinElmer) at 37 °C for 60 min. Labelling was quenched by 1 μL of 0.5 M EDTA and incubating at 65 °C for 20 min Labeled probes were cleaned using the illustra MicroSpin G-25 Columns (27-5325-01, GE Healthcare). After pre-hybridisation, labeled probes were added directly to the tube and incubated overnight at 55 °C in a hybridisation oven. 100x Denhardt's reagent was prepared with 1.0 g BSA, 1.0 g PVP (P5288-100G, Sigma Aldrich) and 1.0 g Ficoll (F2637-5G, Sigma Aldrich) in 50 mL of molecular biology grade water (W4502-1L, Sigma Aldrich).

Next morning, hybridisation buffer containing the residual radioactively labelled probe was carefully discarded according to the site's protocols and membrane was washed twice for 10 min each and again twice for 30 min each at 55 °C using 10 mL wash buffer (3x SSC (S8015-1L, Sigma Aldrich), 25 mM NaH_2PO_4 pH 7.5 , 5% SDS , 10x Denhardt's reagent) prewarmed to 37 °C. Finally,

membrane was washed for 8 min in high stringency buffer (1x SSC , 10% SDS) prewarmed to 37 °C and exposed on an X-Ray Film.

Probes used were; 5'-CTCCTCATAGGGGGCTCGAACCC-3' for Sc-tK^{UUU}, 5'-AGGTCCTACCCGGATTCGAACCGG-3' for Sc-tQ^{UUG}, 5'-CGCCCAAACAGGGACTTGAACCC-3' for Hs-tK^{UUU}, 5'-GGTCCCACCGAGATTTGAACTCGG-3' for Hs-tQ^{UUG}, 5'-CGACTCTGGTGGGATTCGAACCC-3' for Hs-tR^{UCU} and 5'-TGCGTTGGCCGGGAATCGAACCCG-3' for $_{Hs}$tG^{UCC}.

2.19 Yeast strains

Table 2.1: List of yeast strains

Code	Description	Mat.	Reference
CHAPTER 3			
yKT68 (BY4741)	*his3Δ1 leu2Δ0 met15Δ0 ura3Δ0*	A	Brachmann et al. 1998
yKT1 (SILAC WT)	BY4741 *trp-, CAN1+, lys1Δ::KAN, lys2Δ::KAN, arg4Δ::KAN*	A	This study
yKT2 (SILAC *urm1Δ*)	BY4741 *trp-, CAN1+, lys1Δ::KAN, lys2Δ::KAN, arg4Δ::KAN*, *urm1Δ::NATMX6*	A	This study
yKT193 (SILAC *elp3Δ*)	BY4741 *trp-, CAN1+, lys1Δ::KAN, lys2Δ::KAN, arg4Δ::KAN*, *elp3Δ::HIS3MX6*	A	This study
yKT71	BY4741 *DEF1-TAP::HIS3MX6*	A	Ghaemmaghami et al. 2003
yKT73	BY4741 *FPR4-TAP::HIS3MX6*	A	Ghaemmaghami et al. 2003
yKT14	BY4741 *CMS1-TAP::HIS3MX6*	A	Ghaemmaghami et al. 2003
yKT84	BY4741 *BFR1-TAP::HIS3MX6*	A	Ghaemmaghami et al. 2003
yKT85	BY4741 *MCM1-TAP::HIS3MX6*	A	Ghaemmaghami et al. 2003

Code	Description	Mat.	Reference
yKT111	BY4741 *CMS1-TAP::HIS3MX6, urm1Δ::NATMX6*	A	This study
yKT101	BY4741 *MCM1-TAP::HIS3MX6, urm1Δ::NATMX6*	A	This study
yKT103	BY4741 *BFR1-TAP::HIS3MX6, urm1Δ::NATMX6*	A	This study
yKT100	BY4741 *FPR4-TAP::HIS3MX6, urm1Δ::NATMX6*	A	This study
yKT102	BY4741 *DEF1-TAP::HIS3MX6, urm1Δ::NATMX6*	A	This study
yKT133	SILAC WT + pRS425 (*AMP^r, LEU2*)	A	This study
yKT136	SILAC *urm1Δ::NATMX6* +pRS425-tK^{UUU}-tQ^{UUG}-tE^{UUC} (*AMP^r, LEU2*)	A	Leidel et al. 2009
yKT137	SILAC *urm1Δ::NATMX6* +pRS425-tK^{UUU} (*AMP^r, LEU2*)	A	Leidel et al. 2009
yKT138	SILAC *urm1Δ::NATMX6* +pRS425-tQ^{UUG} (*AMP^r, LEU2*)	A	Leidel et al. 2009
yKT139	SILAC *urm1Δ::NATMX6* +pRS425-tE^{UUC} (*AMP^r, LEU2*)	A	Leidel et al. 2009
CHAPTER 4			
yKT68 (BY4741)	*his3Δ1 leu2Δ0 met15Δ0 ura3Δ0*	A	Brachmann et al. 1998
yKT224 (SILAC WT)	BY4741 *trp-, CAN1+, lys1Δ::KAN, lys2Δ::KAN, arg4Δ::KAN, MET17+*	A	This study
yKT220 (*urm1Δ*)	BY4741 *MET17+*, *urm1Δ::NATMX6*	A	This study
yKT226 (WT)	BY4741 *MET17+*	A	This study
yKT244	BY4741 *MET17+, NCS2-3HA::His3MX6*	A	This study
yKT245	BY4741 *MET17+, NCS6-3HA::HIS3MX6*	A	This study
yKT242	BY4741 *MET17+*, *npr2Δ::KANMX6*	A	This study
yKT120	W303 *Cim3-1*	-na-	Ghislain et al. 1993
yKT122	W303 *Cim5-1*	-na-	Ghislain et al. 1993
yKT287	BY4741 MET17+, *ncs2Δ::NATMX6* +pRS413 EV (*AMP^r, HIS3*)	A	This study
yKT288	BY4741 MET17+, *ncs2Δ::NATMX6* +pRS413-*prom.$_{ADH1}$-3HA-NCS2-term$_{CYC1}$* (*AMP^r, HIS3*)	A	This study

Code	Description	Mat.	Reference
yKT289	BY4741 MET17+, *ncs2Δ::NATMX6* +pRS413-*prom.$_{ADH1}$-3HA-ncs2A212T-term$_{CYC1}$* (*AMP^r, HIS3*)	A	This study

2.20 TaqMan gene expression assays used for quantitative real time PCR

Table 2.2: List of TaqMan gene expression assays used for quantitative real time PCR. These predesigned probes were ordered from Applied Biosystems and were tested by the manufacturer for the specificity and efficiency of the amplification. Procedure used is described in section 2.12.

Gene name	Catalog no.	Assay ID	Dye combo	Primer limited	Assay location	Amplicon length
ACT1	4448892	Sc04120488_s1	VIC/MGB	Yes	1045	86
IPP1	4448892	Sc04100229_s1	VIC/MGB	Yes	745	65
18S rRNA	4333760T	--	FAM/MGB	No	NA	187
ALD4	4448892	Sc04169425_s1	FAM/MGB	No	1451	70
BFR1	4448892	Sc04167147_s1	FAM/MGB	No	1254	94
DEF1	4448892	Sc04140418_s1	FAM/MGB	No	1954	71
FPR4	4448892	Sc04150889_s1	FAM/MGB	No	951	106
MCM1	4448892	Sc04153357_s1	FAM/MGB	No	648	62
NCS2	4448892	Sc04158644_s1	FAM/MGB	No	1247	73
NCS6	4448892	Sc04110578_s1	FAM/MGB	No	948	73
PRB1	4448892	Sc04117095_s1	FAM/MGB	No	1746	71
PRE5	4448892	Sc04157135_s1	FAM/MGB	No	652	98
TUM1	4448892	Sc04167754_s1	FAM/MGB	No	849	71
UBA4	4448892	Sc04130538_s1	FAM/MGB	No	1248	86
URM1	4448892	Sc04132030_s1	FAM/MGB	No	252	77

3. tRNA tK^{UUU}, tQ^{UUG}, and tE^{UUC} wobble position modifications fine-tune protein translation by promoting ribosome A-site binding

3.1 Introduction

The uridines at position 34 of tRNAs tK^{UUU}, tE^{UUC} and tQ^{UUG} are universally modified to 5-methyl-2-thio derivatives. In the cytoplasm of yeast and higher eukaryotes, these tRNAs carry a 5-methoxycarbonylmethyl-2-thiouridine at position 34 ($mcm^5s^2U_{34}$). Several *in vitro* studies have suggested that modification of U_{34} regulate its wobbling potential and influence the interactions between the tRNA and protein translation machinery (discussed in detail in sections 1.3 and 1.4). However, many factors that ensure accurate protein translation *in vivo*, such as the correct charging by the aminoacyl-tRNA synthetases (Beuning and Musier-Forsyth 1999), the tRNA gene copy numbers, various tRNA post-transcriptional modificiations (Novoa et al. 2012), and the ratio of free to translating ribosomes (Shah et al. 2013) cannot be reproduced *in vitro*. To address this, we devised and applied a methodology to measure the relevance of tRNA modifications *in vivo*.

In yeast, $mcm^5s^2U_{34}$ relies on the URM1-pathway for the s^2 and on the *ELP* pathway for the mcm^5 addition (described in detail in section 1.4). Yeast cells lacking functional *URM1* and *ELP*-pathways are not viable and disrupting either of the pathways causes increased sensitivity to a wide range of drugs and stress conditions. Interestingly, these phenotypes can be rescued by the over-expression of the hypomodified substrate tRNAs, suggesting a regulatory role of these modifications in translation under stress conditions. Moreover, perturbations in the wobble uridine modifications have been linked with physiological defects in higher eukaryotes (Dewez et al. 2008; C. Chen, Tuck, and Byström 2009; Veen 2011; Y.-T. Chen et al. 2009; Walker et al. 2011; Singh et al. 2010) and several diseases in humans (Torres, Batlle, and Ribas de

Pouplana 2014). However, the connection between the loss of $mcm^5s^2U_{34}$ and these defects is poorly understood.

This chapter presents work that was undertaken to understand the function of tRNA thiolation and methoxycarbonylmethylation at the cellular and molecular levels. Specifically, proteome wide analyses of the changes in protein abundances caused by the absence of $mcm^5s^2U_{34}$ revealed that, *in vivo* and under normal growth conditions, tRNA wobble uridine modifications are not required for general translation. Instead, bio-informatics analysis of the differentially expressed genes showed that $mcm^5s^2U_{34}$ modulates the translation of mainly AAA, CAA, and GAA rich genes. Furthermore, biochemical analyses using purified components revealed that U_{34} modifications promote ribosomal A-site binding and peptide bond formation *in vitro*.

Work presented in this chapter was done in collaboration with the groups of Prof. Matthias Peter (ETH Zurich, Switzerland) and Prof. Marina Rodnina (Max Planck Institute for Biophysical Chemistry, Göttingen). Experiments conducted in collaboration or by other researchers are marked and acknowledged.

3.2 Results

3.2.1 Lack of *URM1* affects only a small subset of the proteome

Proteins are the final readout of the tightly regulated gene expression programs and the main effectors of biological processes inside a cell. Therefore, impact of a perturbation on cellular processes can be inferred by measuring the induced changes in protein abundances. In order to understand the functional importance of tRNA wobble base modifications, SILAC based quantitative proteomics was employed to measure protein abundance changes in yeast cells unable to thiolate wobble uridines. To facilitate efficient labelling of proteins, a yeast strain with a genetic background compatible with SILAC labelling was used. This strain is auxotrophic for the amino acids Lys and Arg (henceforth referred to as SILAC-WT). The gene encoding for Urm1p was deleted from SILAC-WT and the resulting SILAC-*urm1Δ* strain was further characterised.

First, tRNAs from these cells were analysed for the presence or absence of thiolation. Bulk tRNA was isolated from the SILAC-*urm1Δ* cells and analysed by APM ([(N- acryloylamino)phenyl] mercuric chloride) supplemented denaturing polyacrylamide gel electrophoresis (APM-dPAGE). APM is a sulfur interacting molecule that polymerises with acrylamide and bis-acrylamide to form a thio-affinity gel that retards the mobility of sulfur containing tRNAs. As shown in figure 3.1A, only a fraction of the tRNA from wild-type cells, but not from the mutant cells, is shifted. Next, SILAC-*urm1Δ* was tested for two of the known *urm1Δ* phenotypes. As expected, SILAC-*urm1Δ* was more sensitive to rapamycin and caffeine than the SILAC-WT cells, similar to the increased sensitivity of the *urm1Δ* cells relative to WT cells (figure 3.1B). These

observations confirmed that SILAC-*urm1Δ* lack tRNA thiolation and is, therefore, suitable for further analysis.

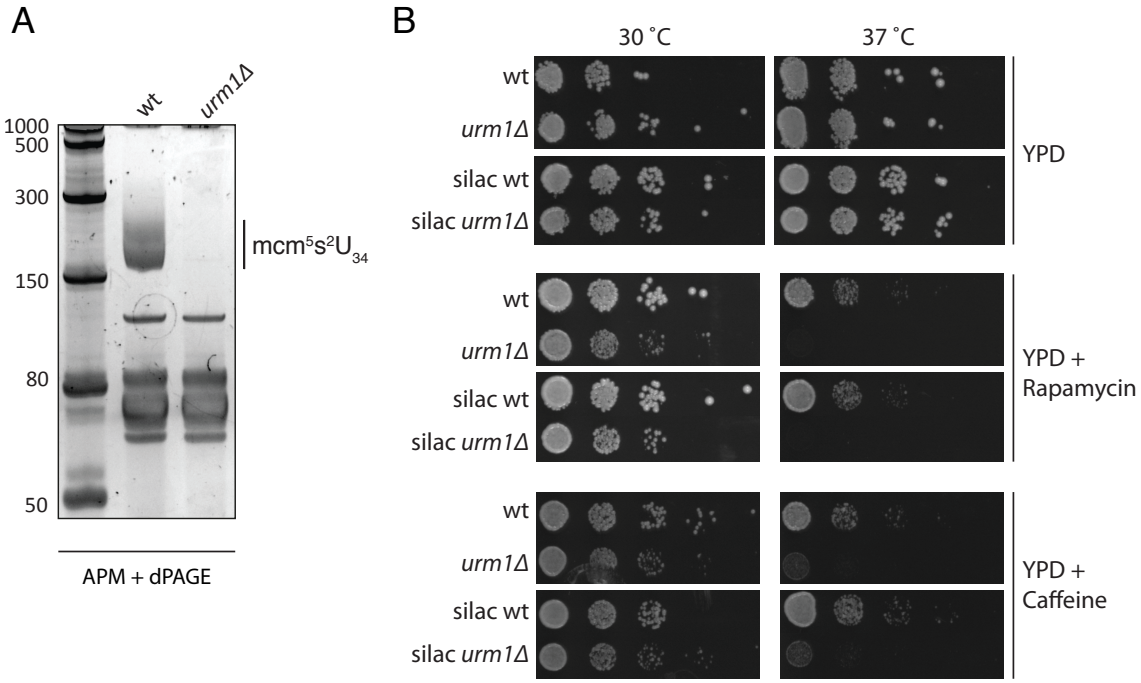

Figure 3.1: Validation of the SILAC-*urm1Δ* strain. (A) Electropherogram of bulk tRNA isolated from SILAC-WT and SILAC-*urm1Δ* cells and analysed by APM supplemented dPAGE. (B) Yeast cultures normalised to an OD_{600} of 1.0 were serially diluted 10 folds and 6 *µ*l were spotted on nutrient agar plates with or without drugs. 37 °C was used to aggravate the drug sensitivity phenotype.

Subsequently, SILAC-*urm1Δ* mutant cells were grown in medium containing [$^{13}C_6$,$^{15}N_4$]Arg and [$^{13}C_6$,$^{15}N_2$]Lys (hereafter referred to as heavy amino acids), while wild-type cells were grown with the natural (light) forms of Arg and Lys. After harvesting, an equal number of cells (based on OD_{600}) were mixed and processed as a single sample to obtain peptides. Mixing of the two differentially labelled samples at an early stage is one of the main advantages of SILAC and limits the incorporation of technical errors due to differential treatment of samples. To improve the proteome coverage, peptides were fractionated by strong cation exchange fractionation (SCX) on the first dimension followed by

reverse phase chromatography and mass spectrometry analysis. Relative protein abundance ratios between wild-type and *urm1Δ* cells were obtained and plotted as a kernel density estimation (figure 3.2). Only a small fraction of the proteome was found to be differentially expressed and that too with small changes in abundance.

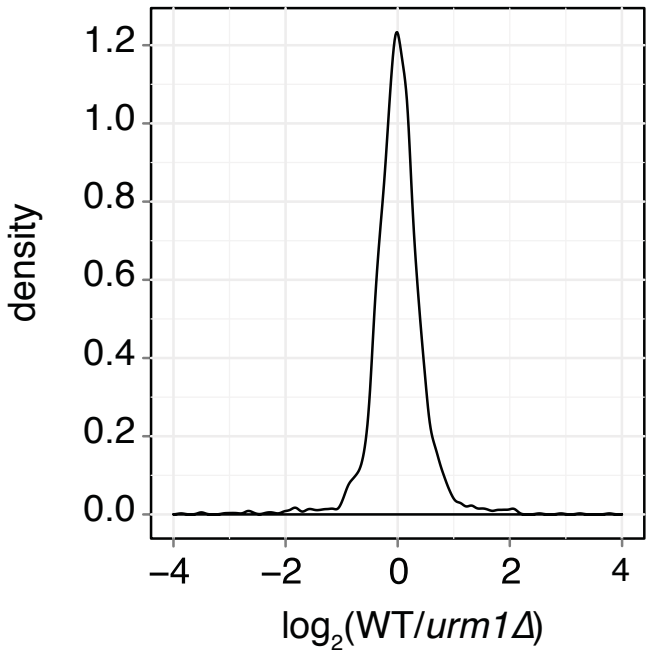

Figure 3.2: Loss of U_{34} thiolation does not affect the majority of the proteome. Curve representing the kernel density estimation of the $\log_2$ of the protein abundance ratios (WT/*urm1*Δ) obtained by SILAC-based comparison of the two strains.

Similar observations were made by our collaborators in the group of Prof. M. Peter using ^{35}S pulse-chase labelling and polysome profiling (figure 3.3).

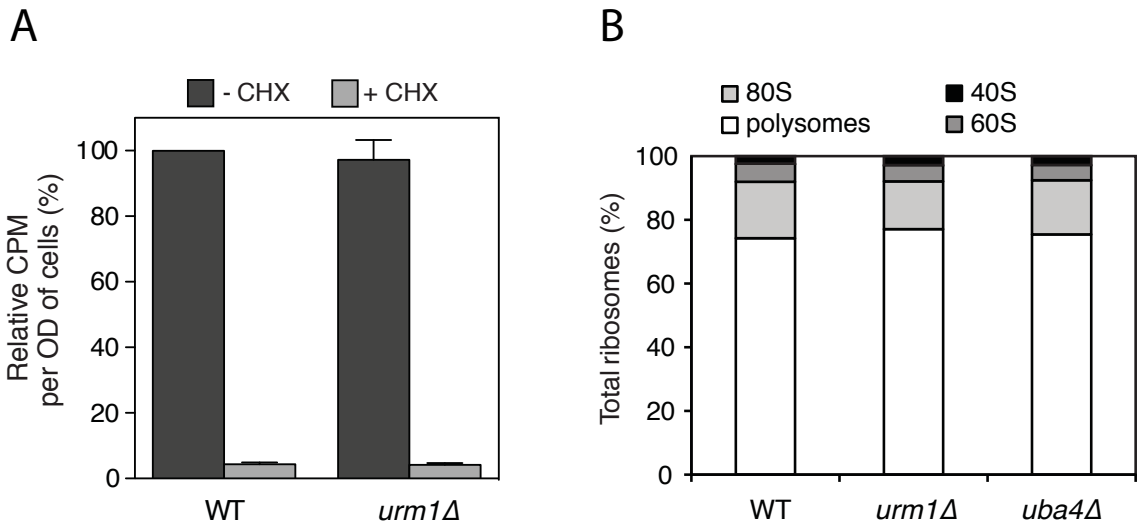

Figure 3.3: General translation in the absence of tRNA thiolation. (A) WT and *urm1Δ* cells were pulsed with [^{35}S]Met and [^{35}S]Cys in the presence (+) or absence (-) of cycloheximide (CHX). [^{35}S] incorporation into proteins was quantified by liquid scintillation counting. Counts per minute (CPM) were normalised to the WT value. Data show mean ± SEM of three independent experiments. (B) Quantification of the polysome profiles from WT, *urm1Δ*, and *uba4Δ* cells separated on a 6-45% sucrose gradient showing the distribution of 40S, 60S, 80S particles and polysomes as percentage of total ribosomes from the average of three independent experiments. These experiments were conducted by V. A. N. Rezgui in the group of Prof. M. Peter (Inst. of Biochem., ETH Zurich).

3.2.2 Comprehensive proteomics analyses of cells deficient in tRNA wobble uridine modifications

Results from the preliminary WT vs. *urm1Δ* analysis suggested that a proteomics workflow was required that could maximise proteome coverage and sensitivity. To start with, we carried out a power analysis for one sample *t*-test with a significance cutoff of 0.01, standard deviations that were typically observed in proteomics experiments in our lab and different number of replicates (figure 3.4). Results suggested that the number of replicates typically used in proteomics or transcriptomics analyses, like 3-4 replicates, would not be sufficient to have the statistical power required to identify low level changes in protein abundances (a fold change of around 1.5).

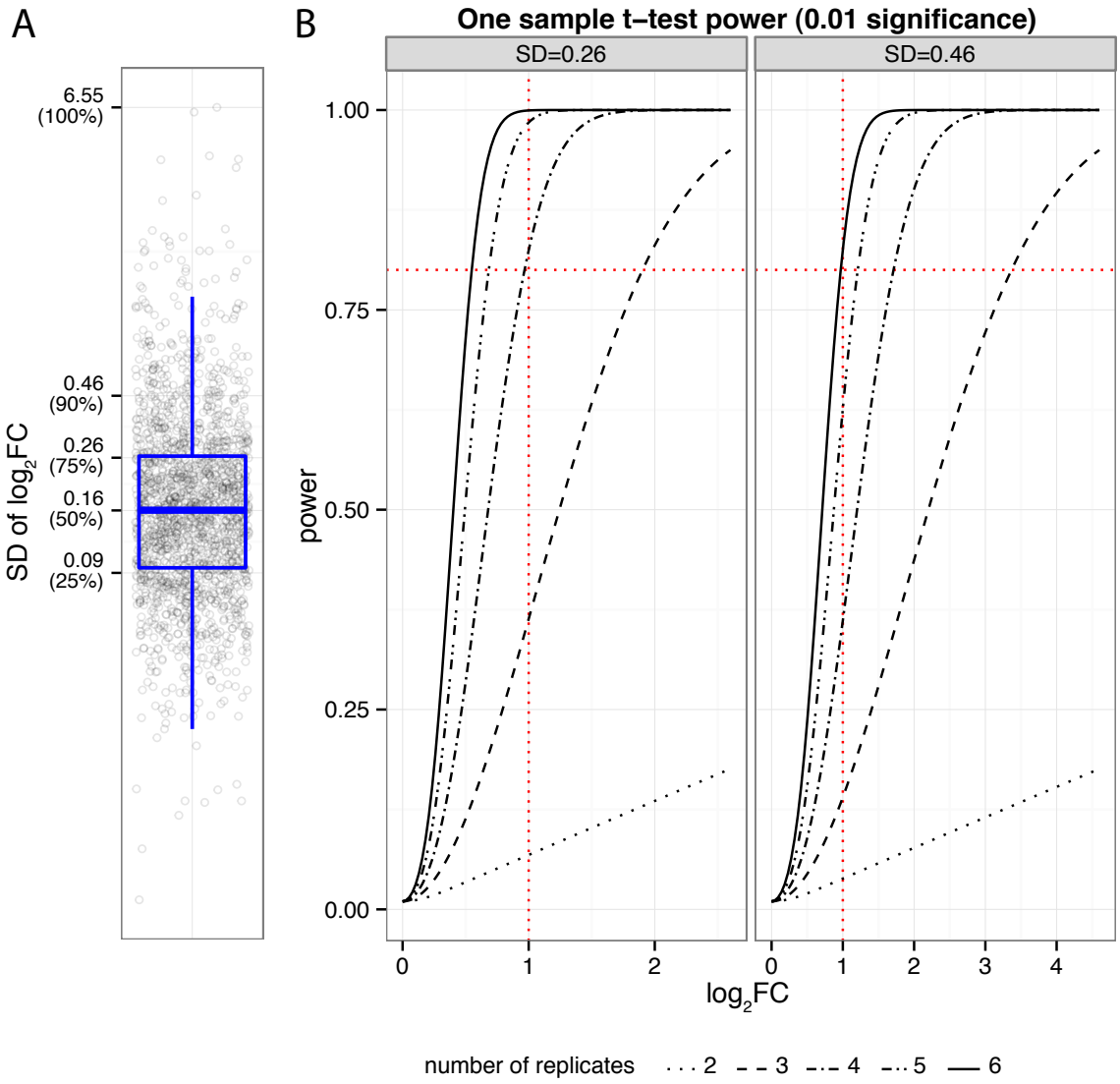

Figure 3.4: Statistical power vs. number of replicates. (A) Box and whisker plot of standard deviations (SD) of $\log_2$ protein fold changes, observed in a representative example of SILAC based quantitative proteomics, plotted on log-scale. Box represents the inter-quartile range representing 50% of the data (25% to 75%). The thick-horizontal line in the box represents median and whiskers extend two standard deviations from the median. On the y-axis, SD values corresponding to various percentiles are indicated. (B) Plots showing changes in the statistical power with the number of replicates. Power analysis was done for one sample *t*-test with a significance cutoff of 0.01, using the SD values of 0.26 and 0.46 representing the 75th and 90th percentiles, respectively, from the representative SILAC dataset. Horizontal (y = 0.8) red dotted line represents a power of 80% and the vertical (x = 1) red dotted line represents a protein fold change of 1.

Therefore, we designed a SILAC-based experimental workflow with six biological replicates to confidently identify the small changes in protein abundances in the absence of a functional *URM1*-pathway (figure 3.5). SILAC labelling for two of the replicates was swapped to minimise measurement errors

due to incomplete incorporation of heavy amino acids, degradation and conversion to other amino acids (like Arg to Pro), extreme ratios due to false positive peptide match and bias caused by an overlapping noise-signal in one channel (Wang et al. 2001; Park et al. 2012). To maximise proteome coverage, samples were extensively fractionated. In addition to SCX, that was used in the

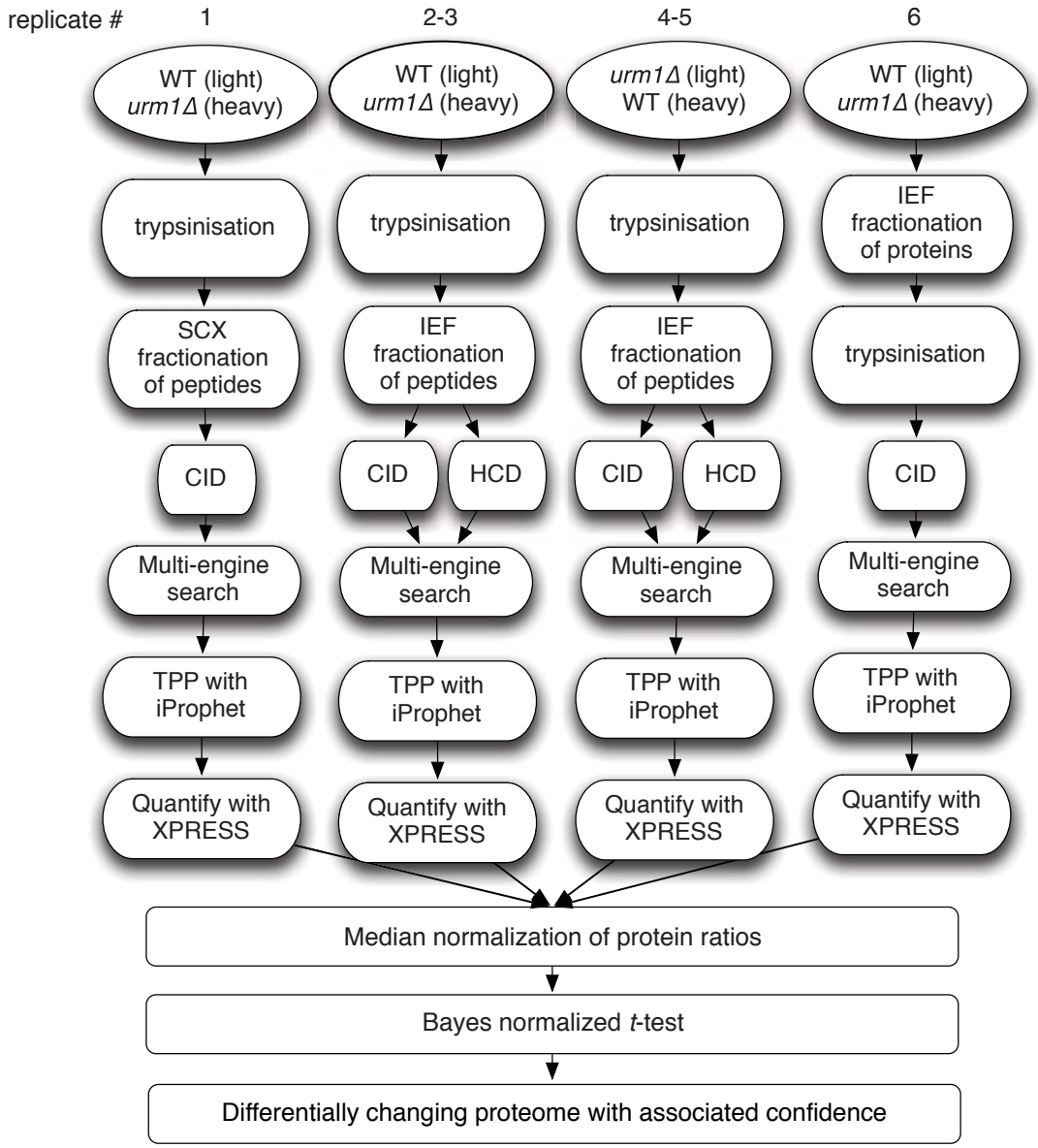

Figure 3.5: SILAC-based proteomics workflow. Schematic representation of the SILAC-based quantitative proteomics workflow that was undertaken to identify differentially expressed proteins in *urm1Δ* cells. Note that SILAC labelling was swapped for replicates numbered 4 and 5. SCX: strong cation exchange; IEF:iso-electric focussing; TPP:trans-proteomics pipeline; CID: collision induced dissociation; HCD: higher-energy collisional dissociation; XPRESS: Quantitation software available withiin the TPP

last section, fractionation based on isoelectric focussing with OffGel electrophoresis was used. Samples were then analysed by LC-MS-MS/MS.

Identification of peptides from MS measurements is achieved by matching the fragmentation spectrum or the MS/MS spectrum of a peptide observed in the instrument with the one theoretically obtained from sequence databases. Therefore, it is dependent upon sensitivity and resolution of the instrument, type of fragmentation technique and computational packages used. The LTQ Orbitrap Velos hybrid mass spectrometer (Thermo Finnigan) that combines the high sensitivity of a dual pressure linear ion trap (LTQ Velos) with the greater mass resolution of an Orbitrap was used for the mass spectrometric measurements (Olsen et al. 2009). Collision induced dissociation (CID) and higher-energy collisional dissociation (HCD) were used for peptide fragmentation to combine the potential advantages of the two techniques . For the identification of the peptides from the MS/MS spectra, four popular peptide search engines, X!Tandem, Mascot, Sequest and OMSSA, were used. Different peptide search engines use different algorithms for peptide identification and their scoring. Therefore, each search engine identifies overlapping peptides (or intersection peptides) and few unique peptides (or complementary peptides) (figure 3.6A and B). The partial overlap between the results of multiple search engines can be used to increase the proteome coverage without any extra effort in sample preparation and MS measurement (figure 3.6 C and D) (Searle, Turner, and Nesvizhskii 2008; Shteynberg et al. 2011).

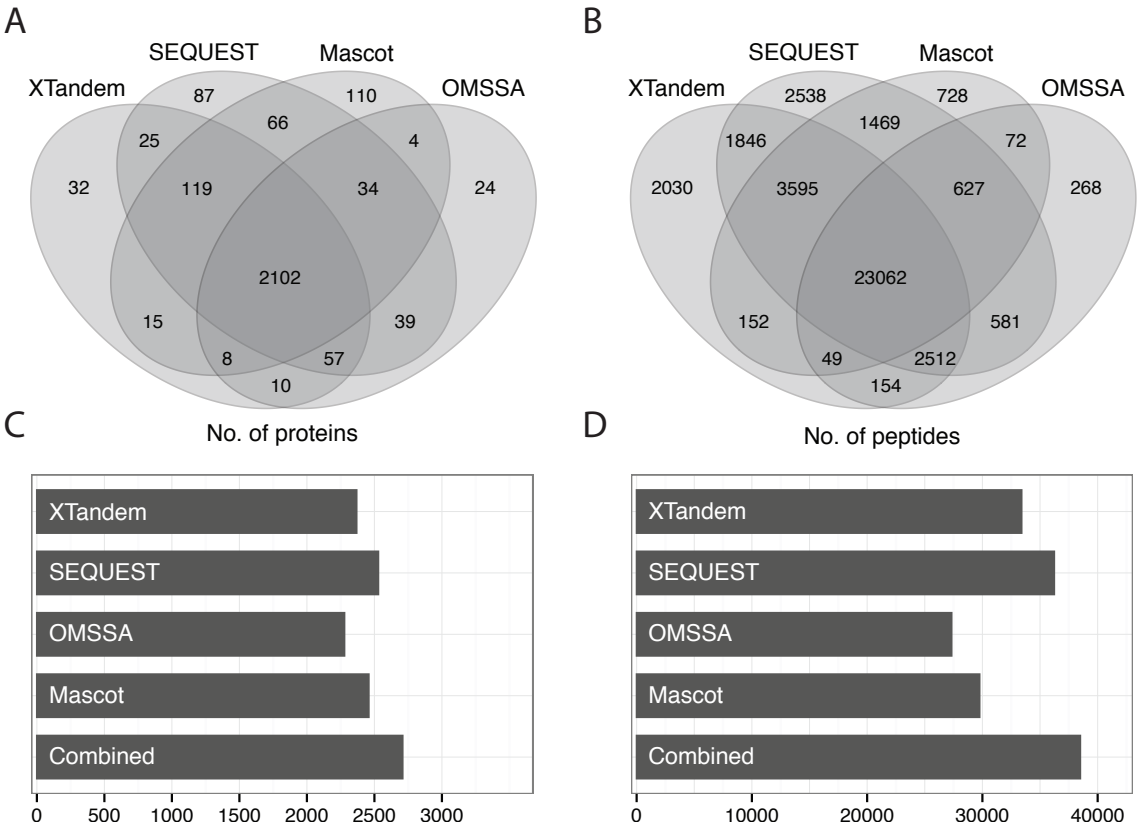

Figure 3.6: Search engine overlap. Data from the MS analysis of replicate no. 2 was searched with multiple search engines. The protein and peptide identifications were filtered at an FDR of 1% at the protein and peptide level, respectively. (A) and (B) Venn diagrams illustrating the partial overlap between the proteins and peptides identified by different peptide search engines. (C) and (D) Bar plot representation of the number of proteins and peptides identified by different search engines and with the combination of all four. Increase in the number of protein and peptide identifications in the combined dataset was 7.1% and 6.2%, respectively, relative to the highest number from an individual search engine (SEQUEST).

Overall, 3,818 proteins were identified, corresponding to 57% of the predicted yeast proteome, at a threshold of 1% false discovery rate (FDR) at the protein level. The obtained data were then processed and analysed for statistical significance of differential protein abundance as explained in the following paragraph.

As discussed under the introduction (section 1.5), the SILAC approach to quantitative proteomics is relatively robust to experimental errors. However,

several limitations and sources of error associated with design and conduct of proteomics experiments remain. These include intra-sample variations due to unequal pooling of the SILAC labelled samples, inter-sample variations due to differential handling of replicates and the cellular abundance of proteins biasing their quantitation (Ting et al. 2009). Fortunately, some of these problems are not unique to proteomics and several computational approaches have been developed to check and correct for these possible sources of error in the micro-array based transcriptomics field (Ting et al. 2009). Data generated from two-label microarray experiments (used for relative gene expression analysis) has been suggested to be similar to isotope-labelling based proteomics studies (used for relative protein abundance analysis). Therefore, many tools that have been designed for the transcriptomics field can also be used in proteomics (Ting et al. 2009).

First, we preprocessed the data by filtering out the proteins that were quantified in only one of the replicates because their quantitation is expected to be less accurate and therefore, can potentially skew the subsequent steps of the data analysis. Next, data were transformed by calculating the $\log_2$ of protein ratios. Small variations in the distribution of protein ratios across the biological replicates were normalised using median normalisation. Box and whisker plots (figure 3.7A) were used to detect inter-sample variance and ascertain the effectiveness of the normalisation procedure used. The plots showed that the samples were very similar without any strong skew (medians close to 0), even before normalisation; as would be expected from equal pooling of samples and SILAC based quantitation (refer to figure legend for a detailed description). MA plots (figure 3.7B) showed that the data did not show any trend in protein ratios

vs. number of peptide pairs (number of quantitations) before or after normalisation as suggested by Ting et al. (Ting et al. 2009). The number of quantitations was used a proxy for the abundance of a protein as an abundant protein is expected to get quantified more frequently.

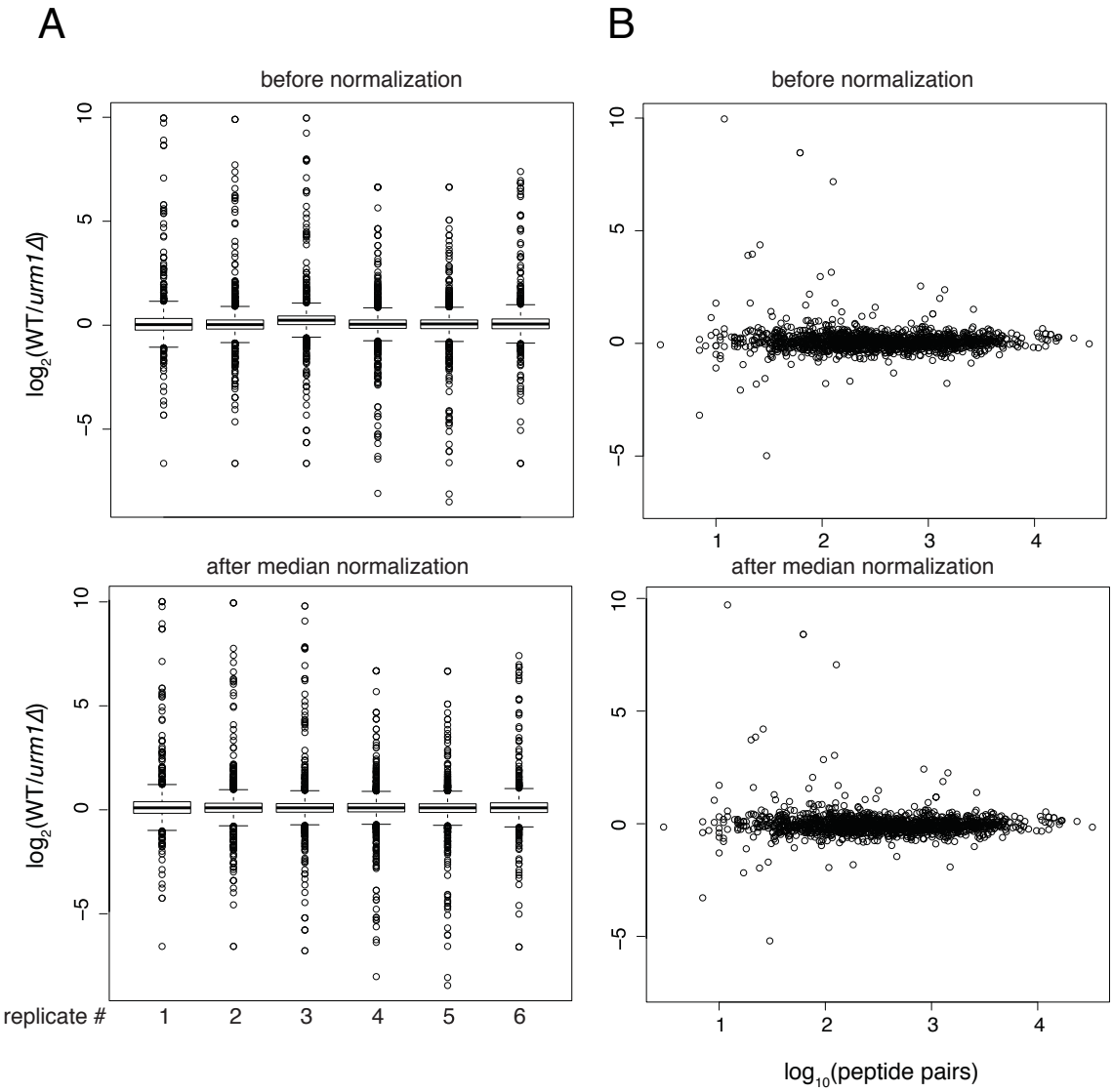

Figure 3.7: Box and whisker plots and MA plots of protein ratios. (A) The median ratio is shown as a thick black line surrounded by a box representing the inter quartile range containing 50% of the data. Whiskers extend up to two SDs from the median. Before normalisation; box and whiskers are symmetric as would be expected for a log-normal distribution, medians for the six samples are close to each other suggesting absence of any major inter-sample bias. After normalisation; intra and inter sample variances, even though small, were removed. (B) The simple mean of ratios for each protein across the six samples was calculated and its $\log_2$ was plotted against the $\log_{10}$ of the number of SILAC pairs used for quantitation of each protein. A linear distribution centred at the line Y=0 means no or very low levels of bias.

Finally, an empirical Bayes moderated *t*-test was used for the statistical analysis of the differentially abundant proteins. The bayes moderated *t*-test has been suggested to perform better than the unmoderated *t*-test and to be more appropriate for the statistical analysis of data from proteomics like studies (Ting et al. 2009). In MS based proteomics, very large numbers of observations are made with very few replicates, and proteins often have missing observations between the samples. This can cause underestimation of variance due to reduced degrees of freedom. In such situations, Bayes moderated *t*-test has been suggested to be powerful in detecting the significance, but, at the same time staying conservative on its estimation (Ting et al. 2009). For the present analysis, the implementation of the Bayes moderated *t*-test in R (LIMMA package) was used (Smyth 2005). The estimated significance values (*p*-values) were adjusted by Benjamini-Hochberg FDR correction to correct for increased probability of type-I errors caused by multiple hypothesis testing. Figure 3.8 shows the 'Volcano Plot' representation of the distribution of the protein ratios (WT/*urm1Δ*) and the associated significance (adj. *p*-values). An FDR value of 5% (adj. *p*-value of 0.05) was used as the threshold for statistical significance. In total, 553 proteins were found to have significantly altered expression in *urm1Δ* cells. Out of these, 286 were up-regulated and 267 proteins were down-regulated in *urm1Δ* (see appendix 1 table A1.1). As expected, Urm1p was in the list of significantly down-regulated proteins, indicating that our methodology is free from any major problem and sensitive enough to quantify a low abundance protein of *ca.* 1,200 copies/cell (Ghaemmaghami et al. 2003).

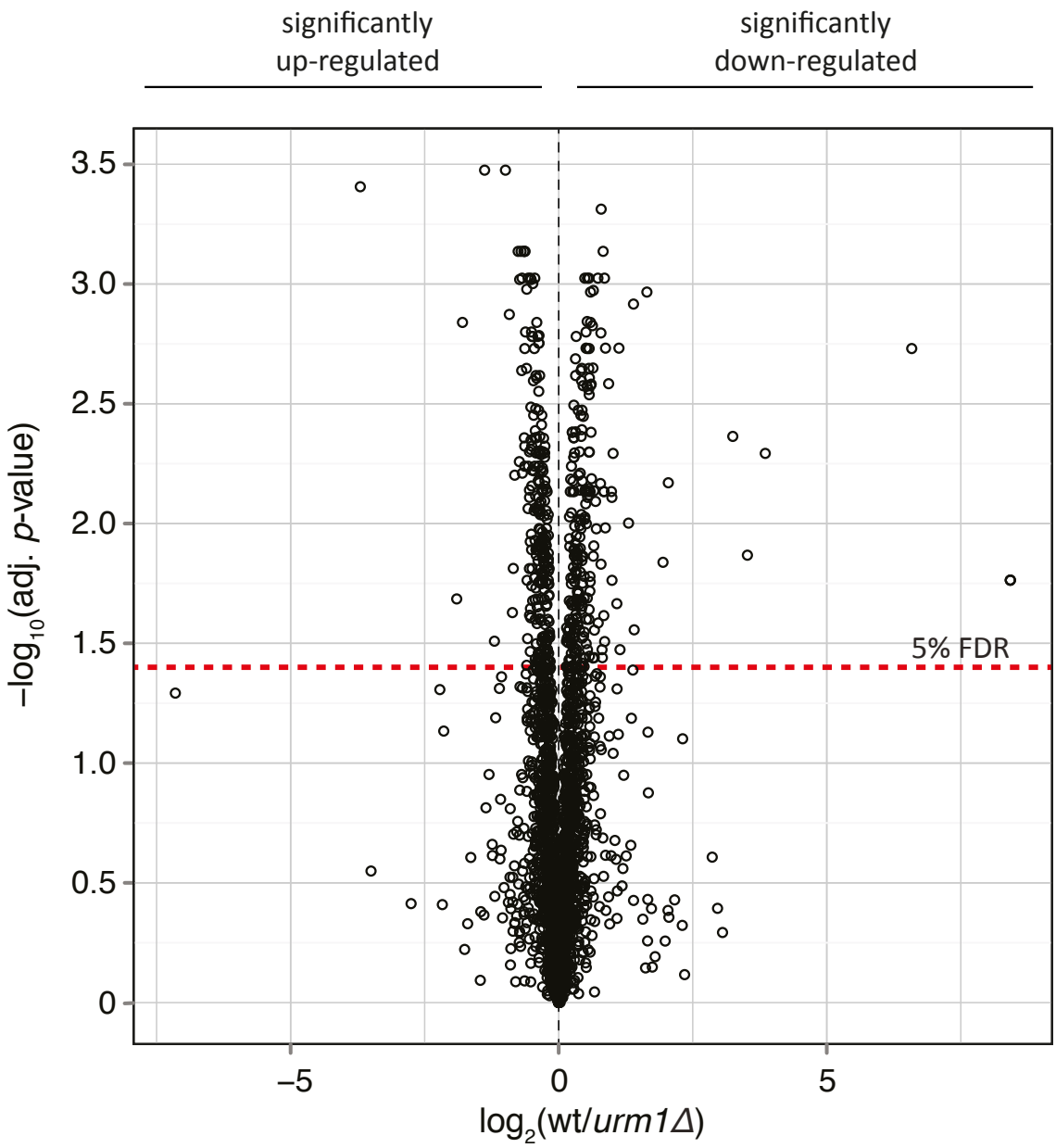

Figure 3.8: Differentially expressed proteins in *urm1Δ*. (A) Volcano plot of protein abundance ratios vs their Bayes normalized t-test calculated confidence. Results shown are from six biological replicates. Red dotted line represents 5% false discovery rate (FDR) that was chosen as the threshold for statistical significance.

Differentially expressed (up- or down-regulated) proteins were analysed for the enrichment of Gene Ontology terms for Biological Processes (GO-BP) and MIPS Functional Classes. GO terms and MIPS Functional Classes are a set of controlled vocabularies associated with different genes and gene products, provided and maintained by GO Consortium (The Gene Ontology Consortium 2007) and Munich Information Centre for Protein Sequences (Mewes et al.

2008) respectively, that can be used to indicate the various biological roles played by genes and their products. The web based FunSpec tool (Robinson et al. 2002) was used for the enrichment analysis with a *p*-value of 0.01 as the threshold for statistical significance of the over-representation of a GO term or Functional Class (appendix 1 tables A1.2 and A1.3). The most significantly over-represented GO terms (*p*-values less than 0.001) are represented in the form of wordclouds in figure 3.9. Down-regulated proteins were enriched for anabolic processes such as rRNA processing, ribosome biogenesis and export, translation initiation and elongation. Interestingly, proteins involved in the primary glucose metabolism and metabolism of sulfur containing amino acids were also in the down-regulated set. On the other hand, up-regulated proteins were enriched for catabolic processes such as proteasome mediated degradation. Unexpectedly, response to oxidative stress and temperature were also among the enriched categories from the up-regulated proteins. Overall, these results suggest that in absence of tRNA thiolation cells down regulate growth and up regulate stress response pathways.

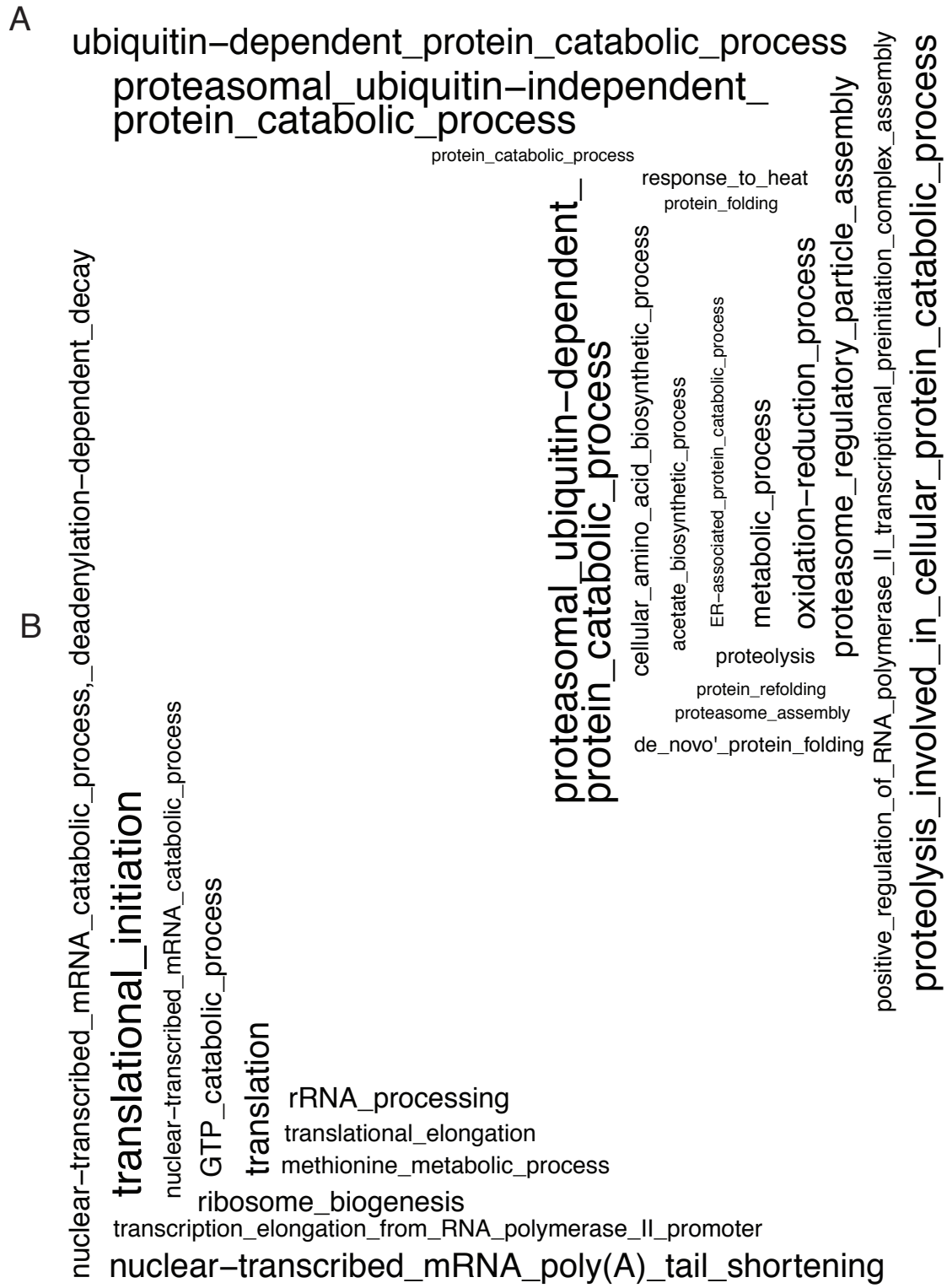

Figure 3.9: Biological processes perturbed in *urm1Δ*. Most significantly over-represented GO terms for biological processes (having *p*-values less than 0.001) from (A) significantly up- and (B) down-regulated proteins. For the full list with significantly enriched GO terms and MIPS Functional Classes see appendix 1 tables A1.2 and A1.3.

In addition to s^2, wobble uridine of tRNAs tK^{UUU}, tE^{UUC} and tQ^{UUG} also carry mcm^5 modification. Available literature has shown several similarities between the two modifications (discussed in detail under the general introduction (section 1.5)). Importantly, disruption in the biosynthesis of mcm^5, by deleting *ELP*-genes, also results in pleiotropic phenotypes, most of which overlap with the phenotypes of *urm1Δ*. Moreover, similar to *urm1Δ* phenotypes, over expression of tK^{UUU} and tQ^{UUG} is sufficient to rescue the *elp3Δ* phenotypes (Esberg et al. 2006). Given the intimate link between the two pathways, we performed a second proteomics analysis, *elp3Δ* vs. *urm1Δ*, to study the differences and similarities between the role of two pathways. The SILAC-based workflow used for this analysis involved four biological replicate samples of *elp3Δ* vs. *urm1Δ* that were not fractionated. Sample fractionation, even though it helps in reducing the sample complexity and improving the proteome coverage, increases the machine and analysis time required by many folds. Therefore, instead of fractionation, gradient and column lengths of the reverse phase LC step were increased to 6 h and 50 cm, respectively.

A total of 2,720 proteins at 1% FDR were identified, which is about 71% of the number of proteins identified in the *urm1Δ* vs. wild-type analysis in about one-tenth of the analysis time. Therefore, a good compromise between proteome coverage and time was obtained. Importantly, 243 proteins (85%) from the significantly up-regulated and 199 proteins (74.5%) from the significantly down-regulated comparison of wild-type vs. *urm1Δ* were also quantified in the *elp3Δ* vs. *urm1Δ* comparison. Remarkably, the levels of all these proteins were comparable in *urm1Δ* and *elp3Δ* cells (table 3.1), implying that the *URM1*- and *ELP*-pathways impact an overlapping set of target proteins. Surprisingly, only 12

proteins in total were significantly changing in the *elp3Δ* vs. *urm1Δ* analysis (table 3.1). Two of these were Elp3p and His3p (the auxotrophic marker that was used to delete *ELP3*), thus validating the analysis. Of the remaining 10, three proteins, namely; Ald5p, Asn1p, and Ygp1p, were already significantly different in the *urm1Δ* vs. wild-type. In the *elp3Δ* vs. *urm1Δ* analysis, they were different only in the magnitude of the change, but not in its direction (in other words, the indicated 3 proteins were just more up- or down-regulated in *elp3Δ* than *urm1Δ*). This left seven proteins, out of which 6 were significantly down-regulated in *elp3* mutants, whereas 1 was significantly up-regulated.

Table 3.1: Significant changes in *elp3Δ* vs. *urm1Δ*. List of proteins that were found to have statistically significant differential abundance between the *elp3Δ* and *urm1Δ* cells. Protein ratios were obtained using the SILAC based quantitative proteomics from four biological replicates and were median normalised prior to statistical analysis by Bayes moderated *t*-test. An adjusted *p*-value of 0.05 (that corresponds to 5% FDR) was chosen as the threshold for statistical significance. Highlighted with yellow are the proteins that were found to be significantly changing only in the *elp3Δ* vs. *urm1Δ* and do not include either Elp3p or the auxotrophic marker used for deletion.

Systematic name	$\log_2$(*elp3Δ*/*urm1Δ*)	adj.P.Val	Protein name
YPL086C	-3.89	0.031	Elp3p
R0040C	-1.73	0.002	Rep2p
YNL160W	-1.31	0.049	Ygp1p
YMR120C	-1.01	0.012	Ade17p
YHR087W	-0.61	0.049	Rtc3p
YBR214W	-0.55	0.049	Sds24p
YFR053C	-0.48	0.049	Hxk1p
YLR058C	-0.40	0.049	Shm2p
YPR145W	0.40	0.049	Asn1p
YER073W	0.43	0.049	Ald5p
YLR348C	0.58	0.045	Dic1p
YOR202W	6.80	0.051	His3p

3.2.3 Lack of s^2 and mcm^5 impairs the expression of AAA, CAA and GAA rich mRNAs

After identifying the significant protein abundance changes in the tRNA hypomodifying mutants in the previous section, we decided to analyse the codon content of the genes coding for proteins that were differentially abundant in *urm1Δ* cells. For this purpose, an unsupervised machine learning approach, based on the Random Forest (RF) algorithm, was used. Random Forest is an ensemble learning algorithm based on decision trees that are built upon randomly selected subsets of the input data (X. Chen and Ishwaran 2012; Touw et al. 2012). Each tree is grown by recursive partitioning such that the resulting partitions (daughter nodes) have improved homogeneity (order or purity) compared to the parent node. At each node of every tree, a subset of variables is chosen randomly from all the variables and the ability of each variable is then evaluated in splitting the node to improve homogeneity. Partitioning is repeated until homogenous (pure) terminal nodes are obtained, thereby growing the tree to the full extent. Based on this algorithm, a forest of random trees is generated that can be used to rank the variables in the order of their ability (variable importance) in classifying the data. In the present case, the Random Forest approach was used to rank the codons in their ability to separate the genes into significantly up- or down-regulated sets. A bar plot of variable importance (figure 3.10A) shows that the codons AAA, CAA, AAG, GGG and GAA, in decreasing order of their importance, were the best at classifying the data in up- or down-regulated sets. Interestingly, wobble uridines of the tRNAs with anti-codons complementary to the codons AAA, CAA and GAA are the substrates of the *URM1*-pathway's sulfur transfer activity and AAG codes for the same amino acid as AAA, which is Lys.

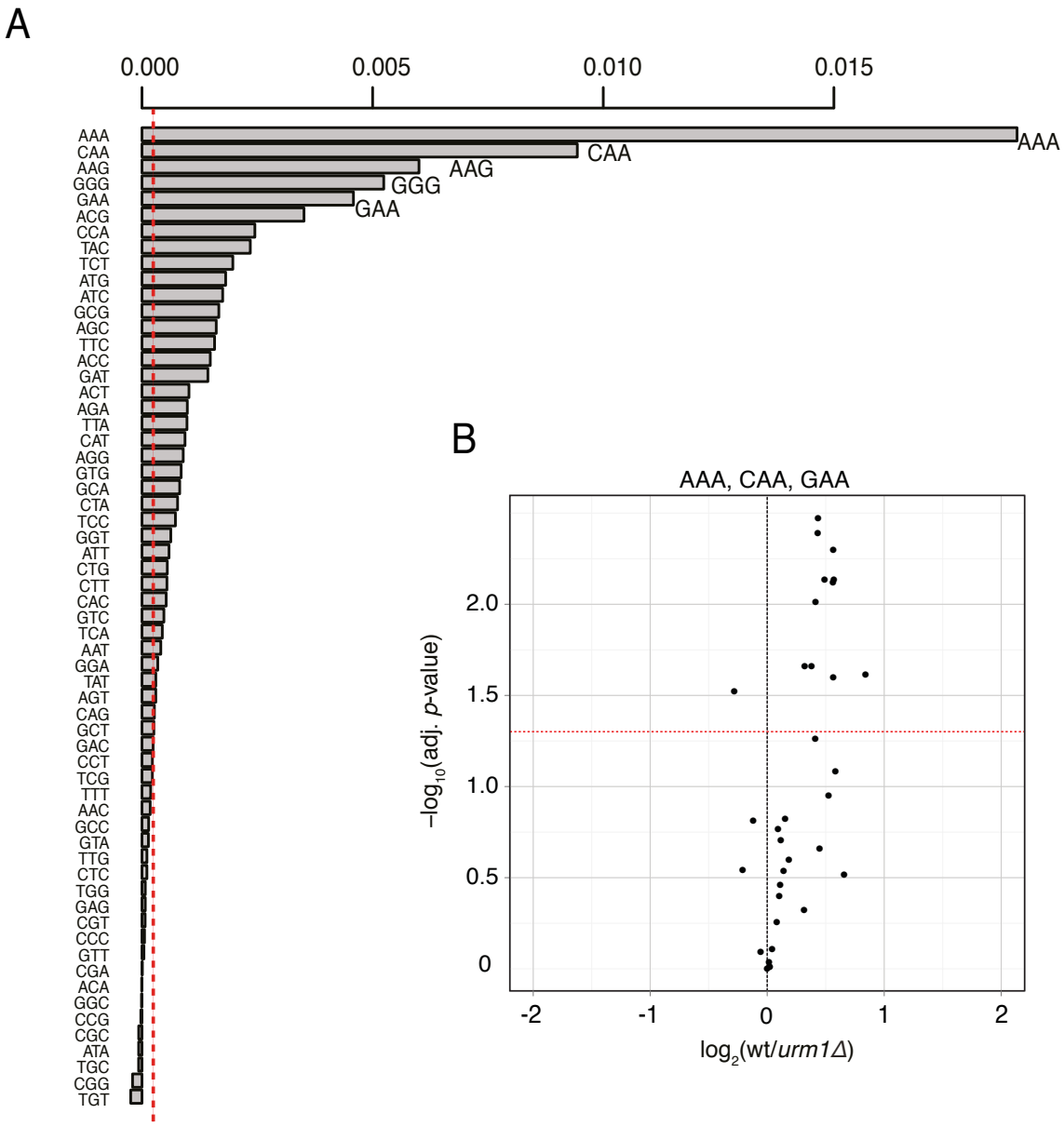

Figure 3.10: Codon bias in differentially expressed genes. (A) Bar-plot representation of the variable importance learned by a random forest algorithm used to estimate the ability of the abundance of different codons in classifying proteins in significantly up- and down-regulated sets. Dotted red line indicates absolute value of the lowest predictor. (B) Proteins with the corresponding highest frequency (1% of the genome) of AAA, CAA, GAA codons are represented in the volcano plot from figure 3.8. Red dotted line represents 5% FDR.

RF based analysis suggested that in absence of tRNA thiolation, content of certain codons is an important determinant for the classification of proteins into up- and down-regulated classes. However, it did not indicate whether an important codon is associated with up- or down-regulated proteins. To find this

association, the frequency of each codon and of codons AAA, CAA and GAA (NAA) together was calculated for every gene of the *S. cerevisiae* genome. Subsequently, protein abundance ratios (WT/*urm1Δ*) of the top 1% yeast genes with the highest frequency of each codon and the three NAA codons together were plotted against their significance value to give a volcano plot representation of the genes with the most anomalous content of different codons. Figure 3.10B and appendix 1 figure A1.1, suggested that codons AAA, CAA and GAA , and to a lesser extent AAG, were significantly enriched in the down-regulated dataset. On the other hand, GGG was enriched in the up-regulated dataset. Intuitively, perturbations in translation caused by hypomodification of tRNAs are more likely to result in down-regulation of proteins instead of their up-regulation. To rule our the role of tRNA thiolation in differential translation of GGG codons, three genes (*ALD4*, *PRE5* and *PRB1*) rich in GGG codon and significantly up-regulated in *urm1Δ* cells were selected and their mRNA levels were estimated in *urm1Δ* cells relative to wild-type cells by using quantitative real-time PCR (figure 3.11). As expected, mRNA levels of these genes were found to be elevated in *urm1Δ* cells suggesting that GGG rich genes are up-regulated due to differential transcription indirectly resulting from absence of tRNA thiolation.

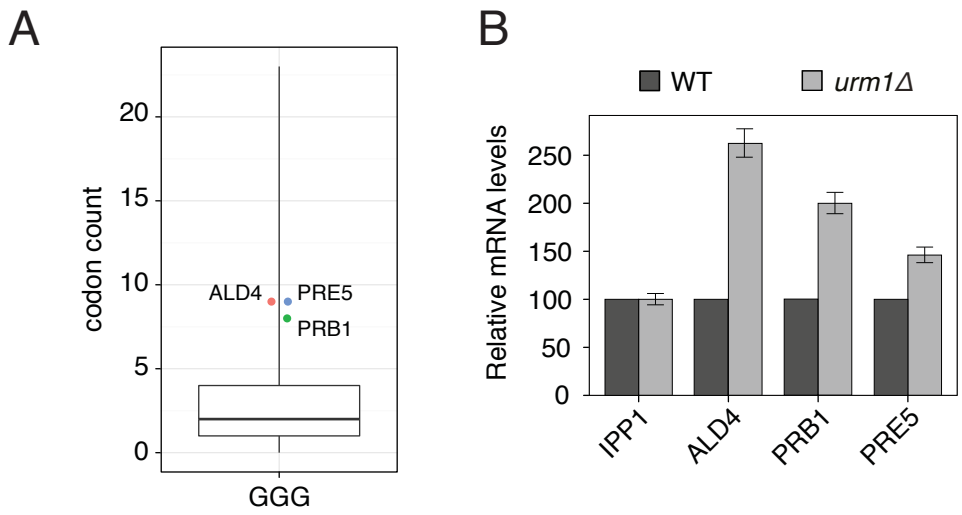

Figure 3.11: Analysis of GGG rich genes. (A) Box and whisker plot representation of the distribution of GGG codons across the yeast genome. The thick black line inside the box indicates median of the distribution, while the box represents the inter quartile range containing 50% of the data. Whiskers represent the minimum and maximum count of GGG codon. Highlighted are three genes that were significantly up-regulated in the *urm1Δ* vs. wild-type quantitative proteomics analysis. (B) The mRNA levels of the three genes highlighted in panel A were measured in *urm1Δ* cells relative to wild-type cells by quantitative real-time PCR. *IPP1* was used as a negative control. Data show the mean ± SEM from three experiments

As previously mentioned, over-expressing the three tRNAs rescues the phenotypes associated with the mutants of *URM1-* or *ELP*-pathway, including the synthetic lethality of the double mutants like *urm1Δ elp3Δ* (Leidel et al. 2009; Esberg et al. 2006). Based on these reports and to validate the predictions made by the RF analysis, the ability of individual tRNAs to rescue differential protein abundances in *urm1Δ* cells was assessed. To start with, a pilot analysis was done in which a multi-copy yeast plasmid (2*μ* plasmid) harbouring the genes of tK^{UUU}, tE^{UUC} and tQ^{UUG} was introduced into the *urm1Δ* cells (to give *urm1Δ* + ptKQE) and they were compared with the wild-type cells transformed with the empty-vector using the SILAC-based proteomics. Shown in the figure 3.12A is the scatter plot of the statistically significant protein ratios from the earlier wild-type vs. *urm1Δ* analysis (x-axis) against the ratios of same proteins after the over-expression of tRNAs (WT/*urm1Δ* + tKQE on the y-axis).

Histograms on the margins of the scatter plot show the distribution of protein ratios before (blue) and after (red) the tRNA over-expression. The plots show that after the over-expression of tKQE, distribution of protein abundance ratios changes from bimodal, resulting from the up- and down-regulated proteins, to zero-centred unimodal. In other words, over-expression of all three tRNA species reverts most of the differentially expressed proteins back to wild-type levels. This indicates that the loss of *URM1*-pathway's tRNA thiolation function is mainly responsible for the observed differential protein abundance in *urm1Δ* cells.

Encouraged by the results of this preliminary analysis, similar proteomics analyses were done to compare *urm1Δ* cells over-expressing individual tRNAs one at a time (tK, tQ or tE) vs. the wild-type cells carrying an empty-vector. Protein abundance ratios from different tRNA over-expression analyses were then compared with each other in the form of a heat-map (figure 3.12B). Columns of the heat-map represent ratios from the indicated comparisons and were clustered based on euclidean distances. The middle column represents the protein abundance ratios of the significantly changing proteins from the *urm1Δ* vs. wild-type analysis, which is ordered from the up-regulated (in orange) to down-regulated (in green). As expected, column representing ratios from the over-expression of all three tRNAs (tKQE) was clustered farthest from the column without over-expression. Interestingly, over-expression of just tK^{UUU} (tK) was clustered closest to tKQE and the over-expression of tE^{UUC} was closest to no over-expression. This suggested that over-expression of tK^{UUU} , followed by tQ^{UUG} and tE^{UUC}, was the most effective in rescuing differential protein abundance in absence tRNA thiolation. Overall, these findings recapitulated and

validated the relative importance of different codons predicted by the random forest analysis.

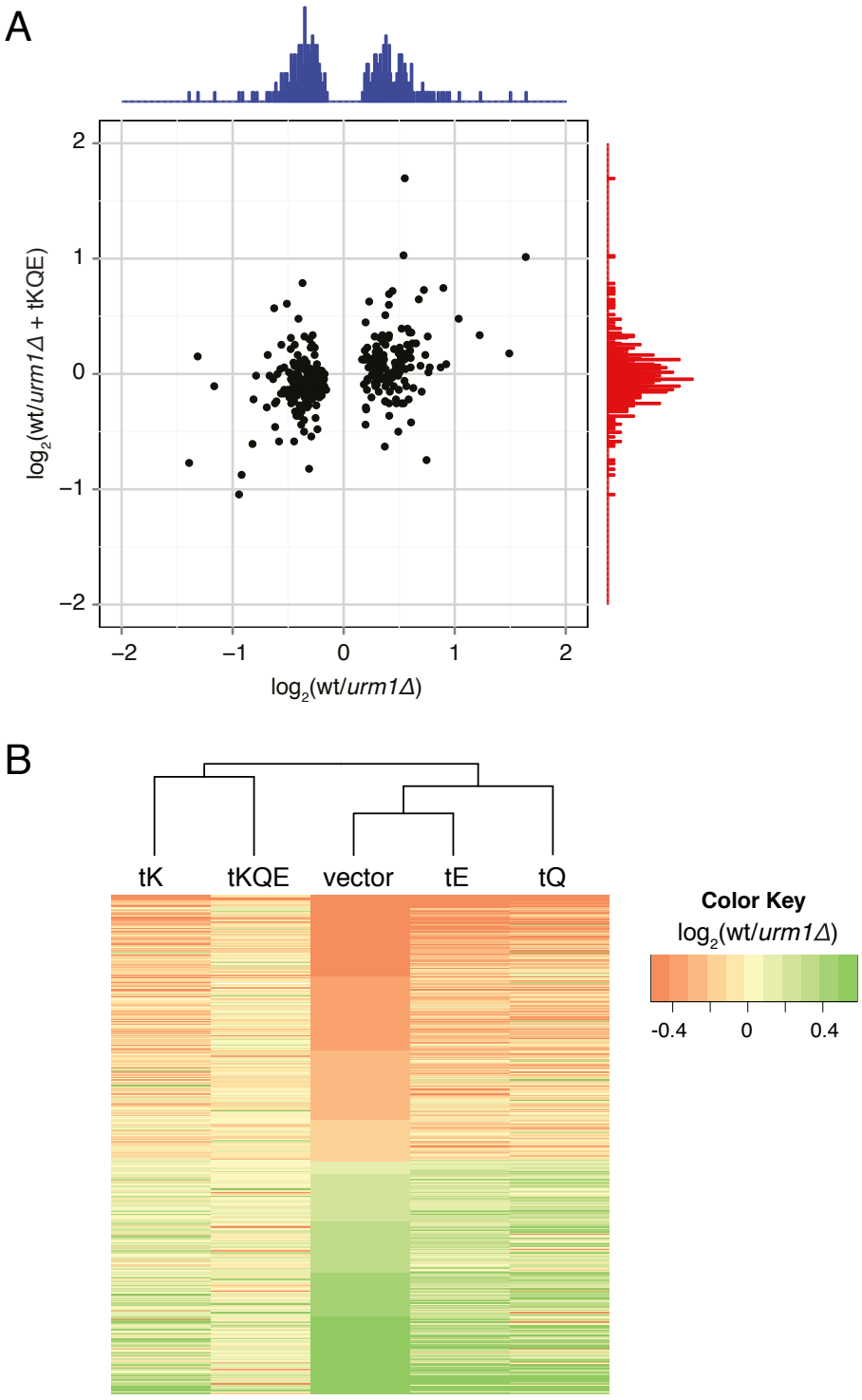

Figure 3.12: Effect of tRNA over-expression on differential protein expression. (A) Scatter plot of protein abundance ratios of the proteins found to be significantly changing in the *urm1Δ* vs. wild-type analysis on the x-axis versus the abundance ratios of the same proteins after combined over-expression of tK^{UUU}, tQ^{UUG}, tE^{UUC} on the y-axis. Marginal histograms show the distribution of the ratios plotted in the scatter plot. (B) Heatmap of $\log_2$(WT/*urm1Δ*) protein abundance ratios of the significantly up- and

down-regulated proteins from figure 3.8 in cells over-expressing tK^{UUU}, tQ^{UUG}, tE^{UUC} individually, or in combination compared to cells without plasmid. Columns are clustered based on euclidean distances.

Following the validation of results from the bioinformatics analysis, the next logical step in the investigation was to identify the cause behind the down-regulation of proteins whose genes are rich in the codons AAA, CAA and GAA. For this, six candidates were selected that were found to be down regulated in the *urm1Δ* vs. wild-type analysis (figure 3.8) and also exhibited a significant codon bias. The candidates were *CMS1*, *YPL199C*, *BFR1*, *DEF1*, *FPR4* and *MCM1* with protein ratios (WT/*urm1Δ*), estimated by SILAC based approach, equal to 2.02, 1.83, 1.48, 1.33, 1.38 and 1.48, respectively. First, strains with the tap-tagged versions of the candidates were obtained (from the TAP-tagged yeast ORF library), *urm1* was deleted and abundance of the candidates was compared between the *urm1Δ* and wild-type cells by immunoblotting for the TAP-tag. As shown in the figure 3.13, immunoblotting analysis corroborated the results obtained from the SILAC-based proteomics analysis. Subsequently, quantitative real-time PCR was used to assess mRNA levels of the candidate genes in *urm1Δ* relative to the wild-type cells. Except *BFR1*, mRNA levels of all the candidates were found to be comparable in wild-type and *urm1Δ* cells, implying that changes at mRNA level were not responsible for the reduced expression of proteins with codon bias.

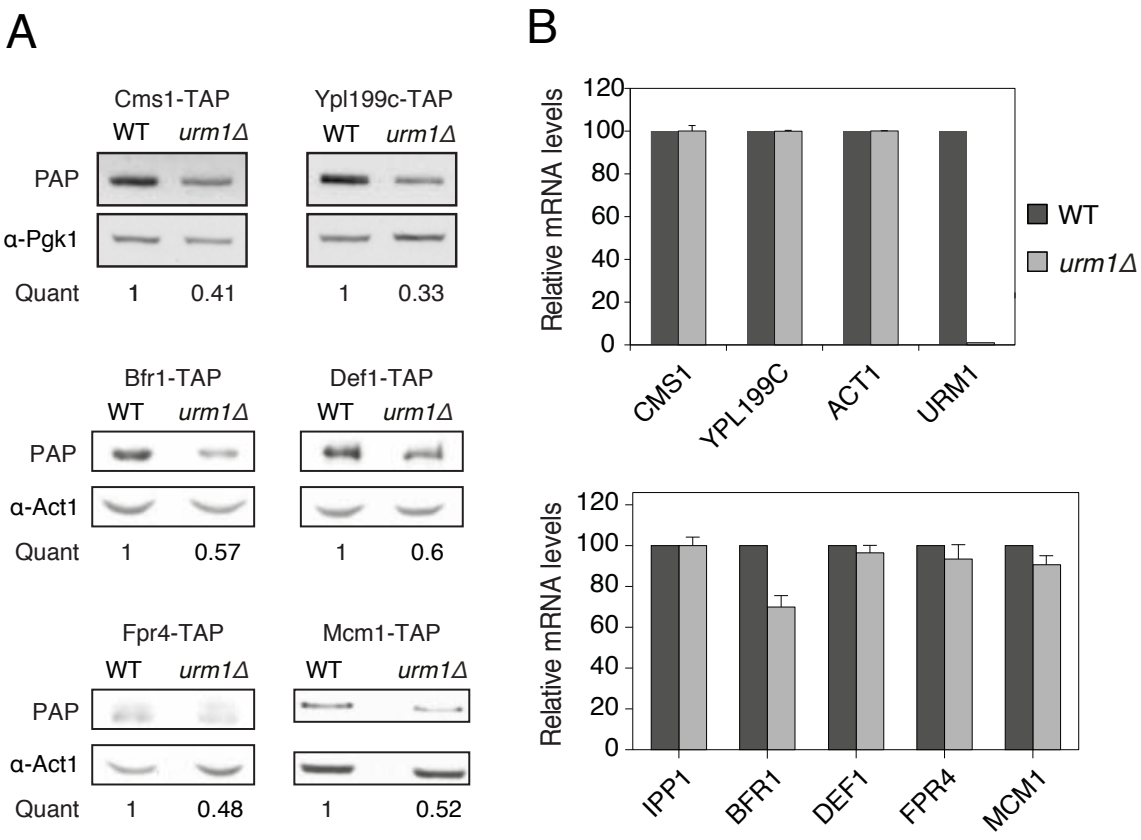

Figure 3.13: Down-regulation of codon biased genes is not caused by reduced mRNA. Down-regulated candidates exhibiting a significant codon-bias were selected. (A) Reduced protein abundance of the candidates was confirmed by immunoblotting for the Tap-tagged proteins from wild-type (WT) and *urm1Δ* cells using PAP antibodies. Pgk1p and Act1p were used as loading control. Quantifications indicate *urm1Δ* /WT protein abundance ratios averaged from three independent experiments. (B) Bar plot of mRNA levels of the same candidates that were assessed by qRT-PCR and indicated relative to wild-type levels. Error bars represent SEM from three independent experiments. Note: Analysis of CMS1 and YPL199C was done by V. A. N. Rezgui in the group of Prof. M. Peter (Inst. of Biochem., ETH Zurich)

Having assessed the mRNA levels, protein stability analysis was conducted to rule out protein degradation as the cause for the reduced abundance of proteins (these experiments were performed by V. Rezgui from the group of Prof. M. Peter). Abundance of the TAP-tagged versions of Cms1p and Ypl199cp was monitored by immunoblotting after blocking translation by cycloheximide treatment in wild-type and *urm1Δ* cells (figure 3.14). Both protein were found to be getting degraded with similar half-lives of approximately 60 and 70 minutes, respectively, in wild-type and *urm1Δ* cells. This implied that the observed

reduction in the levels of proteins was not due to degradation, but it was caused by reduced translation in *urm1Δ* cells.

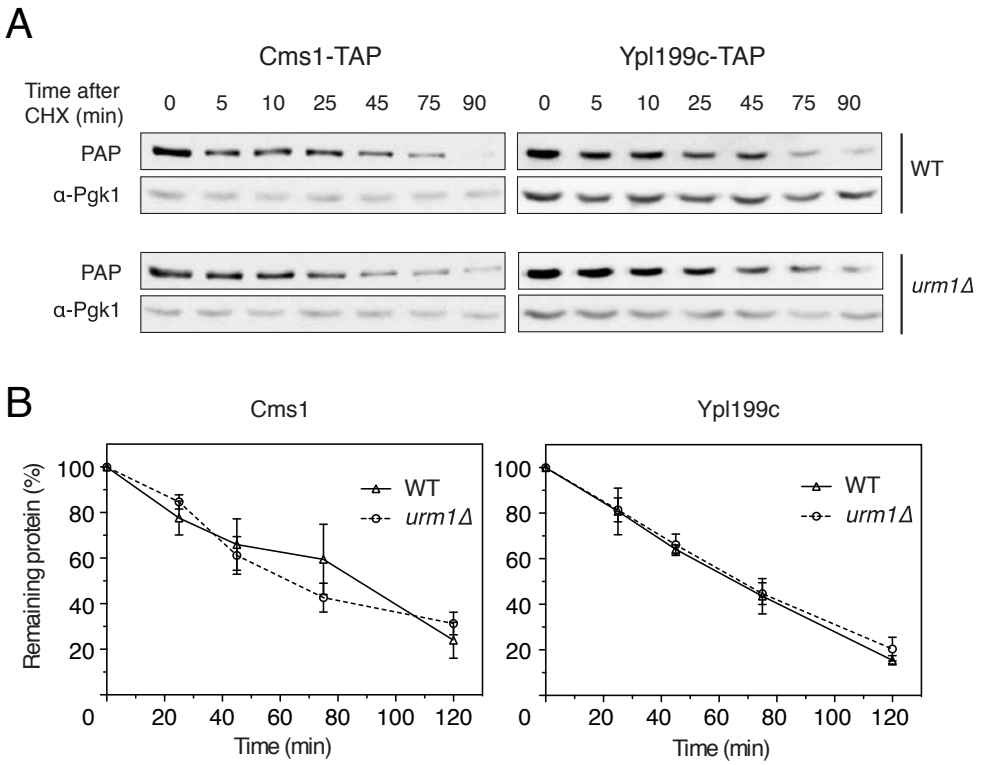

Figure 3.14: Protein degradation is not responsible for down-regulation of codon biased genes. A) The protein stability of TAP-tagged Cms1p and Ypl199cp in WT and *urm1Δ* cells was determined by immunoblotting the protein extracts, prepared at the indicated time (min) after treatment with 200 *μ*g/*μ*l of cycloheximide (CHX), with PAP antibodies or anti-Pgk1p antibody. Equal volumes of culture was harvested at the indicated time points. Pgk1p was used as a loading control (B) Protein amount over time were compared to amount at time zero. Data show the mean ± SEM of three independent experiments. Note: Protein stability analysis of CMS1 and YPL199C was done by V. A. N. Rezgui in the group of Prof. M. Peter (Inst. of Biochem., ETH Zurich).

Taken together, the results from the bioinformatics analysis were supported by proteomics analysis of tRNA over-expression, assessment of mRNA levels and protein stability, which suggested that translation of mRNA molecules rich in AAA, CAA, GAA and AAG codons is reduced in the absence of tRNA thiolation caused by the lack of a functional *URM1*-pathway. Since, almost no significant differences were found between the *urm1Δ* and *elp3Δ* cells, similar conclusion

can be drawn about the translation of AAA, CAA, GAA and AAG rich mRNAs with respect to the *ELP*-pathway dependent mcm^5 modification.

3.2.4 U_{34} modifications enhance ribosomal A-site binding and dipeptide formation rates *in vitro*

So far, our experiments had focussed on understanding the importance of modifications found on the wobble uridine of tRNAs tK^{UUU}, tE^{UUC} and tQ^{UUG} at the systems level. Next, we wanted to investigate how s^2 and mcm^5 promote efficient translation of the cognate codons at the molecular level. In this regard, binding of native and hypomodified tRNAs to the ribosomal A-site and rates of dipeptide formation were compared *in vitro*. These experiments were done by N. Ranjan from the group of Prof. M. Peter in collaboration with the group of Prof. M. Rodnina. Figure 3.15A illustrates the early steps of translation elongation. Briefly, after successful initiation, ribosomes exist in an initiation complex loaded with the mRNA and acylated initiator tRNA in the P-site, while the A-site is empty and ready to receive aminoacylated-tRNA for elongation. Incoming tRNAs are presented in the form of a ternary complex with an elongation factor (EF-Tu or eEF-1A) and GTP. After the correct recognition of a codon anti-codon interaction, resulting conformational changes trigger hydrolysis of GTP and leads to the release of initiation factor now bound with GDP. Subsequently, with its amino-acyl arm free, A-site tRNA swings into the peptidyl transferase site of the ribosome, called accommodation, and peptide bond formation takes place by deacylation of the tRNA at the P-site and transfer of the growing peptidyl chain to the one in the A-site. Next, translocation takes place after which deacylated tRNA occupies the E-site and the peptidyl tRNA moves to P-site leaving the A-site empty for another round of elongation.

tRNAs isolated from wild-type, *urm1Δ* or *elp3Δ* yeast cells were amino acylated (aa) with [^{14}C]Lys using the recombinantly expressed Lysyl-tRNA synthetase. Charged tRNAs were incubated with EF-Tu·GTP to form the ternary complex [^{14}C]Lys-tRNA^{Lys}, which was then mixed with the 70S initiation complex comprising of ribosomes from *E. coli* that were loaded with f[^{3}H]Met-tRNA^{fMet} and mRNA containing an AAA codon following AUG, the initiation codon. Subsequently, the amount of tRNAs bound to ribosomes was estimated by nitro-cellulose filtration assays. Interestingly, A-site binding of aa-tRNA^{Lys} from *urm1Δ* was decreased by 60% compared to wild-type controls (figure 3.15B). A similar effect was observed with tRNAs extracted from *elp3Δ* cells that lack the mcm^5 modification (figure 3.15B), suggesting that both modifications enhance A-site binding. As a control, binding of [^{14}C]Phe-tRNA^{Phe} ternary complex to the 70S initiation complex was estimated. In this case 70S initiation complex was loaded with f[^{3}H]Met-tRNA^{fMet} and mRNA containing an UUC codon following the AUG initiation codon. As expected, the A-site binding of [^{14}C]Phe-tRNA^{Phe} from wild-type, *urm1Δ* or *elp3Δ* cells was not significantly different (figure 3.15C), demonstrating that the observed binding defects of [^{14}C]Lys-tRNA^{Lys} are indeed caused by the missing U_{34} modifications.

To determine the kinetic parameters of ribosomal A-site binding, ribosomal pre-translocation complexes bearing fMet[^{14}C]Lys-tRNA^{Lys} were prepared and peptidyl-tRNA dissociation was followed by nitrocellulose binding assay. The equilibrium dissociation constant, K_d, and the rate constant of tRNA dissociation (k_{off}) from and association (k_{on}) with the A-site were calculated from the apparent dissociation rates and the final level of the reaction. Strikingly, the k_{on}

for peptidyl-tRNA^{Lys} from *urm1Δ* cells and *elp3Δ* cells were about three times lower than for tRNAs from wild-type cells. On the other hand, k_{off} was higher with tRNA^{Lys} from *urm1Δ* cells and *elp3Δ* cells compared to tRNALys from wild-type controls (figure 3.15D).

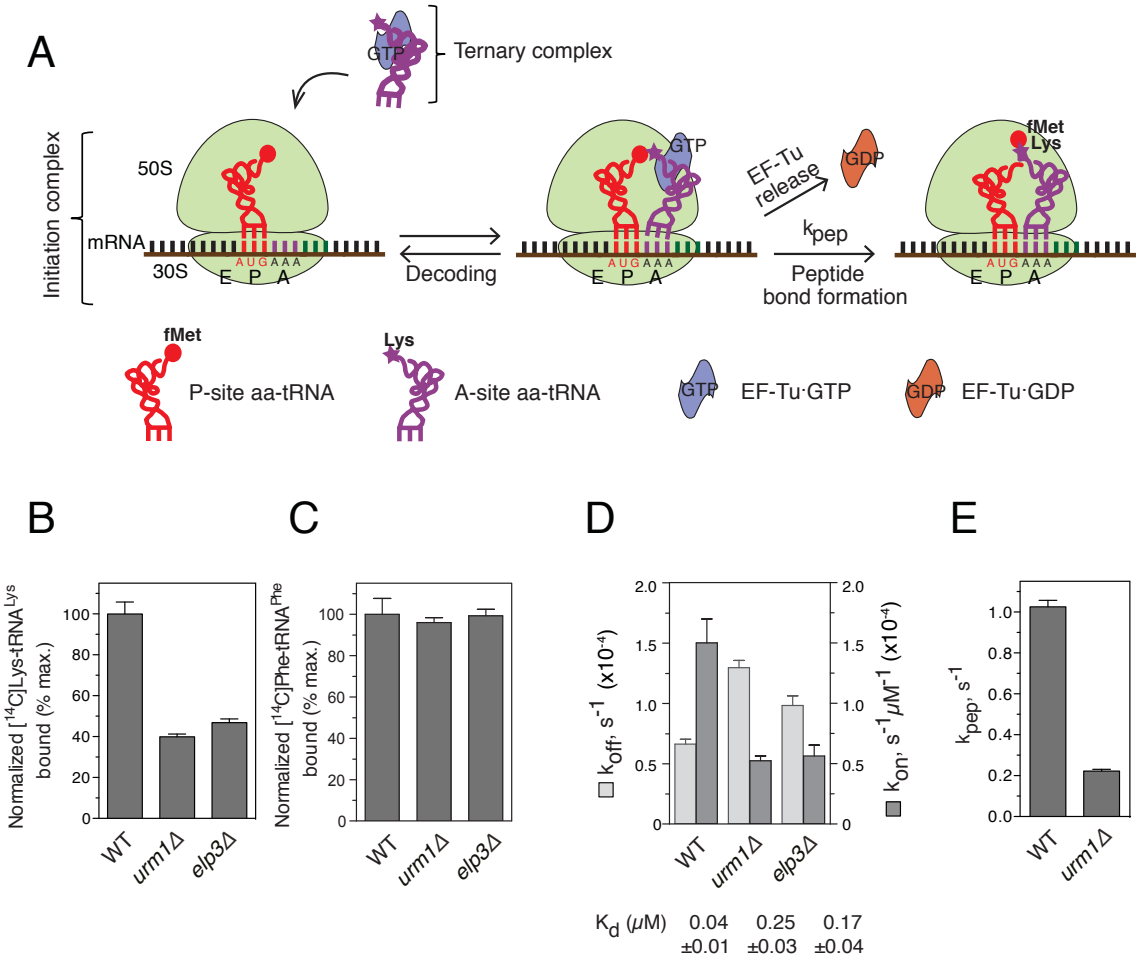

Figure 3.15: mcm^{5}s^{2}U promotes ribosomal A-site binding and peptide bond synthesis. (A) Schematic illustration of the early steps of elongation cycle. (B and C) Ribosomal A-site binding of [^{14}C]Lys-tRNA^{Lys} (B) or of control [^{14}C]Phe-tRNA^{Phe} (C) isolated from either wild-type (WT) or *urm1Δ* or *elp3Δ* cells was measured after incubation of initiation complex with ternary complex. Data show the mean [^{14}C] signal ± SEM of three independent experiments plotted as percentage (%) of WT. (D) The rate constants of tRNA dissociation (k_{off}) and tRNA association (k_{on}) of peptidyl-tRNALys prepared from WT, *urm1Δ* or *elp3Δ* cells. The equilibrium dissociation constant (Kd) ± SEM is shown below the graph. (E) The rate of dipeptide formation (K_{pep}) using tRNALys isolated from WT and *urm1Δ* cells.

The final step in decoding results in peptide bond formation. Therefore, the rate of ribosome-catalysed formation of f[^{3}H]Met[^{14}C]Lys-tRNA^{Lys} dipeptides (k_{pep}) was measured using quench-flow analysis with rapid mixing of an excess of initiation complex with ternary complex (EF-Tu·GTP·[^{14}C]Lys-tRNA^{Lys}). Dipeptide formation was found to be five times slower with aa-tRNA^{Lys} tRNA from *urm1Δ* cells compared to wild-type with apparent rate constants (figure 3.15E). Together, these *in vitro* experiments demonstrate that wobble position modifications stabilise cognate codon-anticodon interactions at the ribosome, and thereby enhances the efficiency of translation.

3.3 Discussion

3.3.1 U_{34} modifications stabilise binding of cognate tRNAs to the A site and promote peptide-bond formation

Previous *in vitro* studies have shown that an artificially synthesised ASL fragment of human LYS3 tRNA ($hASL_{Lys}^{UUU}$) lacking the $mcm^5s^2U_{34}$ and $t6A_{37}$ modifications was unable to bind to AAA and AAG codons at the ribosomal A site (Vendeix et al. 2012). Furthermore, X-ray crystallography explained that while both mnm^5 and s^2 improve stacking of U_{34}-A_3 base pair with U_{35}-A_2 base pair, mnm^5 (the prokaryotic analog of mcm^5) also allowed the conformation required for U_{34}-G_3 base pairing (F. V. Murphy et al. 2004). In the present study, results from *in vitro* ribosome binding assays using full length native tRNAs show that hypomodified tRNA tK^{UUU}, carrying either mcm^5U_{34} or s^2U_{34}, have reduced binding at the ribosomal A-site. Consequently, the rate of peptide bond formation was drastically reduced. This suggests that mcm^5 and s^2 stabilise the binding of tRNAs to their cognate codons. The fact that over-expression of tRNAs masks the phenotypes caused by their hypomodification supports these results, because increased abundance of tRNAs can compensate for the lower binding. A recent study reported similar observations from ribosome foot-print analysis of wild-type and *urmΔ* or *elpΔ* mutant cells (Zinshteyn and Gilbert 2013). The authors found that relative to wild-type cells, dwell-time of ribosomes when the codons AAA, CAA and GAA were in the A-site was increased in the mutants lacking mcm^5 or s^2. Additionally, Trm9p that is involved in the biosynthesis of mcm^5 was recently shown to contribute towards correct coding of codons AGA and GGA (Patil et al. 2012). Taken together, it seems that modifications at and near the anti-codon loop are generally required to enhance efficiency and fidelity of translation.

3.3.2 U_{34} thiolation and methoxycarbonylmethylation control efficient translation of specific mRNAs *in vivo*.

Our, and other, *in vitro* studies have shown that $mcm^5s^2U_{34}$ ensures efficient translation by promoting binding of tRNAs to their cognate codons at the ribosomal A-site. Moreover, translational defects caused by the loss of these modifications lead to several phenotypes stressing the importance of $mcm^5s^2U_{34}$ for the proper functioning of cellular processes. However, the link between molecular defects in translation and the observed phenotypes has been missing. Therefore, to better understand the *in vivo* biological relevance of tRNA wobble uridine modifications, an unbiased data driven approach was used to analyse the differential proteome of wild-type and *urm1Δ* cells. Early experiments showed that the majority of the proteome and general translation is not affected in *urm1Δ* cells. Furthermore, even the differentially expressed proteins showed a very small magnitude of abundance change. Therefore, a robust statistical quantitative proteomics workflow was developed to confidently detect small changes in protein abundances. Bioinformatics analysis of the differentially regulated proteins revealed that in the absence of tRNA wobble base thiolation, genes rich in the cognate AAA, CAA and GAA codons showed reduced expression. Further biochemical evidences indicated differential translation to be the reason behind reduced expression.

Previous *in vitro* and structural studies have implicated thiolation in the efficient recognition of G-ending codons (Vendeix et al. 2012; F. V. Murphy et al. 2004; Sen and Ghosh 1976). Interestingly, in the present study, bioinformatics analysis of the differentially regulated proteins in *urm1Δ* cells also highlighted differential translation of mRNAs rich in AAG but not CAG or GAG codons. *In*

vivo, there are non-thiolated tRNAs with C_{34} to recognise G-ending codons. Therefore, there is no obvious need for the cells to use U_{34} containing tRNAs to decode G-ending codons. Consistent with this notion, Johansson et al. (Johansson et al. 2008) have shown that yeast cells lacking tQ^{CUG} or tE^{CUC} are non viable. Over-expression of tQ^{UUG}, only in the presence of functional *ELP*- and *URM1*-pathways, was able to rescue the lethality of cells lacking tQ^{CUG}, albeit with very poor growth, suggesting that the fully modified tQ^{UUG} and tE^{UUC} cannot efficiently recognise CAG and GAG codons (Johansson et al. 2008). However, it is important to note that between the A- and G-ending codons for the amino acids Lys, Gln and Glu, AAG, CAA and GAA are preferentially used codons in the highly expressed proteins in the budding yeast (Hiraoka et al. 2009). This raises the possibility that tK^{UUU} might be required to supplement the translational capacity for these AAG-rich proteins. Nevertheless, Zinshteyn and Gilbert showed in their study (Zinshteyn and Gilbert 2013) that ribosomal dwell times were not increased in *urmΔ* or *elpΔ* cells when AAG was in the A-site, suggesting that the role playes by thiolated tK^{UUU} in the recognition of highly AAG biased genes is only marginal. Along the same lines, even though AAA, CAA and GAA constitute 11.4% of the coding genome of *S. cerevisiae*, only the mRNAs strongly biased in these codons were translated with reduced efficiency in *urm1Δ* cells. This is to be somewhat expected since initiation is the rate limiting step in translation under non limiting conditions, while elongation proceeds very fast (Milon et al. 2008; Kudla et al. 2009).

The wild-type vs. *urm1Δ* proteomics screen presented in this study was complemented by *urm1Δ* vs. *elp3Δ* analysis to understand the importance of mcm^5 modification. Absence of a functional *ELP*-complex leads to complete

lack of mcm^5 and ncm^5 modifications from eight tRNAs in addition to the three tRNAs that are substrates of the *URM1*-pathway (in total 11 substrates). Therefore, *urm1Δ* vs. *elp3Δ* proteomics analysis should have highlighted the importance of U_{34} modifications of these eight tRNAs. Surprisingly, there were very few significant differences (in total 10, besides Elp3p and His3p) between the proteomes of *urm1Δ* and *elp3Δ* cells, suggesting that under standard growth conditions the same set of mRNAs are differentially translated in *urm1Δ* and *elp3Δ* cells. This conclusion is supported by the overlap between the phenotypes of *urmΔ* and *elpΔ* cells and their rescue by the over-expression of unmodified tK^{UUU} and tQ^{UUG} (Esberg et al. 2006). However, it is important to stress that a role of *ELP*-pathway catalysed modifications on other tRNAs can not be ruled out. It is, for instance, possible that under different growth conditions a similar analysis might identify more significant differences. Taken together, the results of this study, and of previous reports, indicate that *in vivo* and under standard growth conditions, mcm^5 and s^2 modifications of tRNAs tK^{UUU}, tQ^{UUG} and tE^{UUC} U_{34} cooperatively ensure efficient translation of mRNAs rich in AAA, CAA, GAA and possibly AAG.

3.3.3 Phenotypes link to stress response pathways

Cells lacking the functional *URM1*- and *ELP*-pathways show increased sensitivity to stress induced by elevated temperature, chemicals such as rapamycin, caffeine and diamide and are slower to adapt to changes in environmental conditions such as alternative carbon sources (Esberg et al. 2006). However, under nutrient-rich, standard growth conditions, lack of $mcm^5s^2U_{34}$ does not cause obvious phenotypes, except slow growth. Consistent with these observations, proteomics analysis of the *urm1Δ* cells

grown in nutrient-rich standard growth conditions found quite small changes in protein abundances in the mutant cells. Nevertheless, under challenging conditions these small changes could become biologically relevant. For instance cells carrying mutations in *URM1*- and *ELP*-pathways as well as cells lacking CMS1, whose translation is reduced in absence of U_{34} thiolation, show increased sensitivity to quinine when compared to the wild-type yeast cells (Santos and Sa-Correia 2011). Similarly, in the fission yeast, reduced translation of the AAA codon rich transcription factors, ATF1 and PCR1, in the absence of $mcm^5s^2U_{34}$ was associated with increased sensitivity to oxidative stress caused by H_2O_2 (Fernández-Vázquez et al. 2013). Therefore, the impact that mcm^5 and s^2 modifications have on the process of translation affects how cells respond to challenging conditions and could perhaps have a regulatory role in the management of cellular homeostasis.

Over-represented GO terms for biological processes and MIPS functional classes from the down-regulated proteins in *urm1Δ* cells indicate that in the absence of $mcm^5s^2U_{34}$ cells down-regulate growth by turning down the production of the translational machinery. This is one of the hallmarks of the environmental stress response in the budding yeast (Gasch 2002). Similarly, proteins involved in response to oxidative stress, heat shock and temperature perception were up-regulated. These results hint at the possibility that cells could up- and down-regulate the mentioned processes by modulating the levels of mcm^5 and/or s^2 on their tRNAs. Dedon and Begley have argued in their recent article (Dedon and Begley 2014) that for a tRNA modification to play a regulatory role their presence or absence must change the decoding properties of the tRNAs and that the levels of modifications must change depending on the

cellular state. In the present study we have shown that mcm^5 and s^2 modifications of tRNA U_{34} affect the efficient recognition of cognate codons. Additionally, a previously reported analysis found that the levels of mcm^5s^2U, among other tRNA modifications, change after exposure to stress (C. T. Y. Chan et al. 2010); therefore, strongly supporting a regulatory role of these modifications. The next chapter of this thesis addresses this question by analysing the response of budding yeast to heat stress and the role played by $mcm^5s^2U_{34}$ in its management.

4. Protein degradation and dynamic tRNA modifications fine tune translation at elevated temperatures

4.1 Introduction

Robust and rapid response to ever changing environmental conditions is a prerequisite for the survival of all life forms. In *S. cerevisiae* a common gene expression program is triggered to balance growth in response to a variety of extracellular perturbations (Gasch 2002). The idea of a common gene expression program was supported by several early observations. Exposure to a mild stress condition provided yeast cells with cross-protection against higher levels of other stresses (Lewis, Learmonth, and Watson 1995; Wieser et al. 1991). Additionally, it was found that the expression of heat shock proteins (HSPs), otherwise traditionally attributed to heat shock, was also induced under several other stress conditions (Werner-Washburne et al. 1989; Kobayashi and McEntee 1990). Subsequently, over the span of several years, a set of approximately 900 genes was identified that makes up what is now the called environmental stress response (ESR) (Causton et al. 2001; Gasch et al. 2000). Even though the genes constituting the ESR are common to several stress conditions, the mechanism, timing and intensity of their expression is tied to the nature and severity of the stress (Gasch 2002). In addition to this common theme, specific expression of several genes makes up the response to a particular stress.

It is clear that the regulation of gene expression is an important aspect of the stress response mechanisms. In addition to the transcriptional regulation that makes up the ESR, the role of protein modifications and degradation has also been studied, albeit in less extensive detail. Protein post-translational modifications, including the ubiquitin proteasome system, is an integral part of the stress response pathways. They play important roles in the process from

directly sensing the stress, transducing signals to finally affecting the gene expression program (Flick K and Kaiser P 2012; Leach and Brown 2012; Kaiser et al. 2006; Solé et al. 2011). In recent years, regulation of protein translation has emerged as another layer of the modulation of gene expression. Splicing of *HAC1* mRNA and translation of *GCN4* mRNA, are two of the well studied cases where important regulators of stress related genes are specifically translated in the presence of stress (Hinnebusch 2005; Kuhn et al. 2001; Back et al. 2005). Cells also regulate the abundance of ribosomes and tRNAs under stressful conditions to slow-down general translation (Mayer and Grummt 2005; Causton et al. 2001; Gasch et al. 2000). Additionally, proteins such as the translation initiation factors and ribosomal structural proteins are post-translationally modified to regulate their activity (Kaufman 1999; Meyuhas 2008; Ruvinsky and Meyuhas 2006). However, the role of post-transcriptional modifications found on RNA, the main constituent of the translational apparatus of a cell, is somewhat not clear (Machnicka et al. 2012; Cantara et al. 2010; Crain and McCloskey 1997). RNA nucleotide modifications increase the repertoire of otherwise limited inter- and intra-molecular interactions that the four canonical nucleotides can make (Grosjean 2005). Among all the types of RNAs, tRNAs exhibit the maximum diversity of modified nucleotides with more than 90 documented modifications (Yacoubi, Bailly, and de Crécy-Lagard 2012; Phizicky and Hopper 2010). Even though the structure and biosynthesis for the majority of the tRNA nucleotide modifications have been characterised (Grosjean 2005; Johansson and Byström 2005), their role and regulation is still poorly understood. It is likely that several of these nucleotide modifications are important for the functioning of RNAs and can be used to regulate their activity. Recently, it was reported that in *S. cerevisiae* exposure to chemicals causing oxidative and/or DNA-damage

stress changes the levels of several tRNA modifications (C. T. Y. Chan et al. 2010).

The wobble uridines of the three eukaryotic cytoplasmic tRNAs tK^{UUU}, tQ^{UUG} and tE^{UUC} are doubly modified to 5-methoxycarbonylmethyl-2-thiouridine ($mcm^5s^2U_{34}$) (Esberg et al. 2006; Johansson and Byström 2005). In *S. cerevisiae,* s^2 is the end product of the sulfur transfer along the *URM1*-pathway involving Urm1p, Uba4p, Ncs2p, Ncs6p and Tum1p. Biosynthesis of mcm^5 requires the *ELP*-pathway that is composed of the proteins Elp1p-Elp6p, Trm112p and Trm9p (Johansson and Byström 2005; Huang, Johansson, and Byström 2005; Leidel et al. 2009). Double loss of mcm^5 and s^2 is lethal in *S. cerevisiae* and *C. elegans*. Loss of either of the modifications causes overlapping and pleiotropic phenotypes in budding yeast that include sensitivity to stress induced by elevated growth temperature, oxidising agents like diamide, growth inhibitor rapamycin, and caffeine (Pedrioli, Leidel, and Hofmann 2008; Leidel et al. 2009). Mutations in the *ELP*-pathway genes cause neurological defects in *C. elegans* (C. Chen, Tuck, and Byström 2009) and in humans problems in the biosynthesis of $mcm^5s^2U_{34}$ have been associated with neurological diseases (Nguyen et al. 2010) such as familial dysautonomia (Close et al. 2006; Anderson et al. 2001; Slaugenhaupt et al. 2001), rolandic epilepsy (Strug et al. 2009) and amyotrophic lateral sclerosis (Simpson et al. 2009). In the previous chapter, it was shown that *in vitro* mcm^5 and s^2 modifications promote ribosomal A-site binding of tK^{UUU} and *in vivo* they were found to be important for the efficient translation of mRNAs biased in the content of codons AAA, CAA, GAA and AAG (Rezgui et al. 2013). Additionally, protein abundance changes, in yeast cells lacking $mcm^5s^2U_{34}$, indicated

activation of stress response pathways. These included down-regulation of the translational machinery and up-regulation of proteins involved in stress responses such as heat and oxidative stress. These observations plus the phenotypes of yeast cells lacking $mcm^5s^2U_{34}$ suggest a close association between these tRNA modifications and cellular stress response pathways. To better understand this connection, the response of yeast cells exposed to a mild, but continuous heat stress of 37 °C was investigated and is described in this chapter.

4.2 Results

4.2.1 Proteomics analysis of yeast grown at elevated temperature

SILAC based quantitative proteomics was used to study the proteome level response of yeast cell to continuous heat stress. The proteomics workflow used was similar to the one employed in the previous wild-type vs. *urm1Δ* comparison. Briefly, as illustrated in figure 4.1, yeast cells were differentially labelled by growing them in SILAC media at either 30 °C or 37 °C. In total three biological replicates were analysed and the labelling design was switched in one of them. Peptides from each sample were fractionated using isoelectric focussing with the OffGel electrophoresis to increase proteome coverage. Subsequently, peptides were subjected to LC-MS-MS/MS analysis with few important changes to the analysis conditions and parameters, compared to the previous wild-type vs. *urm1Δ* analysis. First, dimethylsulfoxide (DMSO) was used as an additive in the LC solvent to exploit its ability to cause charge state coalescence (Meyer and A Komives 2012) and thereby improve the identification of peptides (Hahne et al. 2013). Second, a Dionex ultra-high

pressure LC system with heated column compartment was used that allowed the use of long (~50 cm) reverse phase (C18) chromatography columns for improved chromatographic separation of peptides (Thakur et al. 2011). Finally, a lower MS^1 intensity threshold (500 units) for the fragmentation and MS^2 analysis of precursor peptides was used to improve sensitivity.

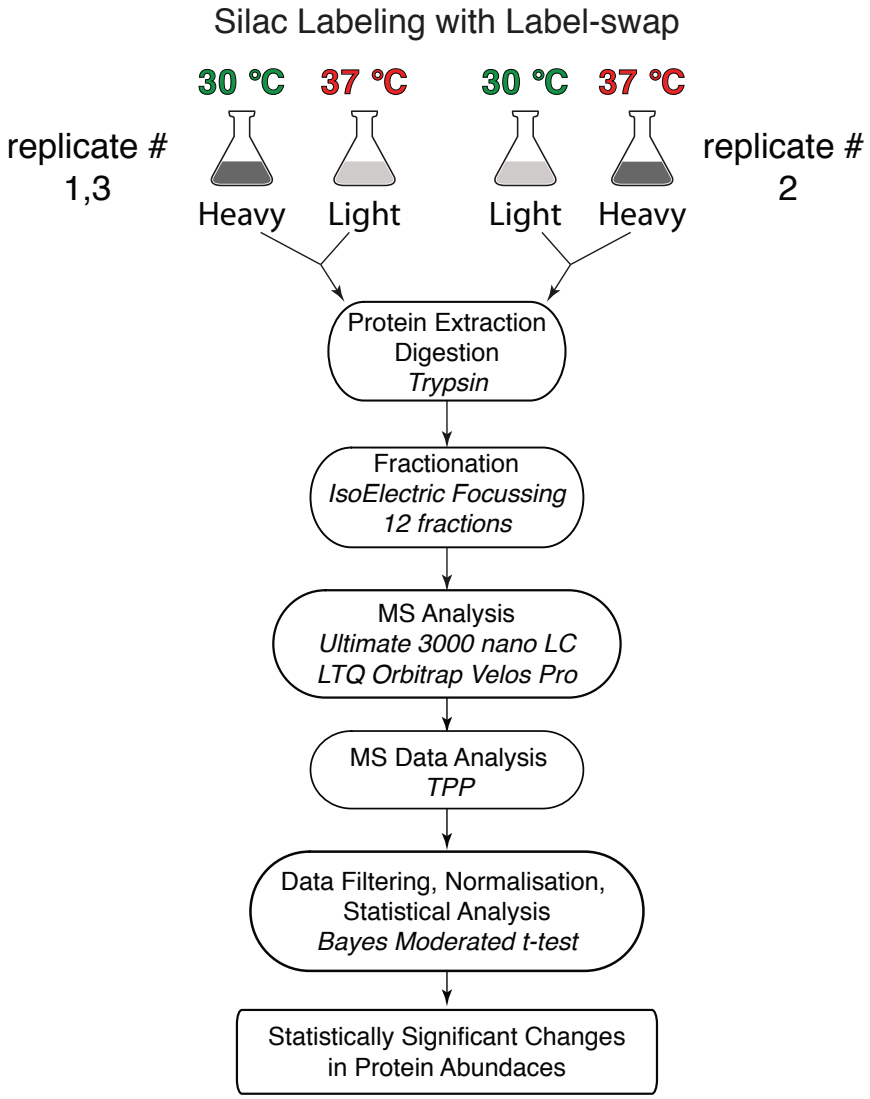

Figure 4.1: 30 °C vs. 37 °C proteomics workflow. Schematic representation of the SILAC-based quantitative proteomics workflow that was used to identify significant changes in protein abundances in response to continuous heat stress at 37 °C. In total, 3 biological replicates were used and SILAC labelling was switched for replicate number 2. After digestion, peptides were fractionated with OffGel electrophoresis. MS data were analysed with the software packages available within the Trans Proteomics Pipeline (TPP). Resulting protein ratio data was filtered to remove noise and improve the quality of data, followed by statistical analysis with Bayes moderated *t*-test.

After the MS analysis, raw data was processed and analysed for the identification and quantitation of proteins. This led to the identification of 4,663 proteins at 1% FDR (calculated by ProteinProphet: Nesvizhskii et al. 2003). Out of these, 4,612 proteins were quantified with at least one high-confidence peptide (that is, meeting the PeptideProphet calculated 1% FDR at the peptide level (Keller et al. 2002)). This number corresponds to more than 68% of the predicted yeast proteome and is an increase of about 21% from the number of proteins identified in the previous wild-type vs. *urm1Δ* analysis. Highlighted in table 4.1 and figure 4.2, proteome coverage compared positively with two other large scale proteomics studies of the budding yeast. Interestingly, even combining the three lists covers only 78.4% of the predicted proteome indicating that the remaining fraction of proteins are either expressed under specific growth conditions or are expressed below the detectable levels.

Table 4.1: Number of quantified proteins in 30 °C vs. 37 °C SILAC analysis. Comparison of the number of proteins quantified in the present study against the number of proteins from the Saccharomyces Genome Database, number of proteins analysed by the tag based proteomics (Ghaemmaghami et al. 2003) and the list of proteins available in the Peptide Atlas repository (canonical & possibly distinguished proteins, build 2013-03 for yeast). The number of proteins, indicated here, from the Tag-based studies is 13 less than the number indicated in the original study because these protein entries have either been deleted from SGD or merged into existing ORFs.

	SGD	MS based This study (% of SGD)	Tag based Ghaemmaghami et al. 2003	MS based PepAtlas King et al. 2006
total	6717	4612 (68.66)	4504	4668
verified	4939	4198 (85)	4048	4197
uncharacterised	853	401 (47.01)	409	402
dubious	810	4 (0.49)	41	11
transposable element	89	4 (4.49)	3	55
pseudogene	26	5 (19.23)	3	3

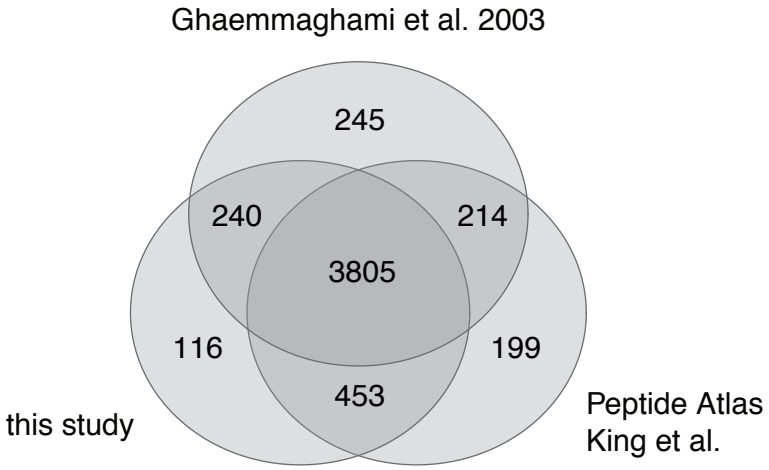

Figure 4.2: Venn diagram of proteome coverage. Venn diagram showing the overlap of the quantified proteins in this study with those studied by GFP- and TAP-tag based approaches (Ghaemmaghami et al. 2003) and list of proteins available from the Peptide Atlas repository (canonical & possibly distinguished proteins, build 2013-03 for yeast).

The list of quantified proteins was analysed further to assess the performance of the proteomics analysis (figure 4.3). Comparison with copies per cell data (obtained from (Ghaemmaghami et al. 2003)) showed that the quantified proteins spanned a wide range of abundances, from as low as 41 copies to 1.26 million copies per cell. This corresponds to a dynamic range of five orders of magnitude. Protein sequence coverage was found to correlate positively ($r = 0.56$) with the $\log_{10}$ of copies per cell. The average coverage per protein was 42.64%. Lastly, the number of high-confidence quantified peptides was found to generally increase with percent sequence coverage or with copies per cell. On average each protein was quantified with 21 high-confidence peptides. Overall, this suggests that the obtained proteomics data should facilitate a comprehensive analysis of the heat stress response of the budding yeast.

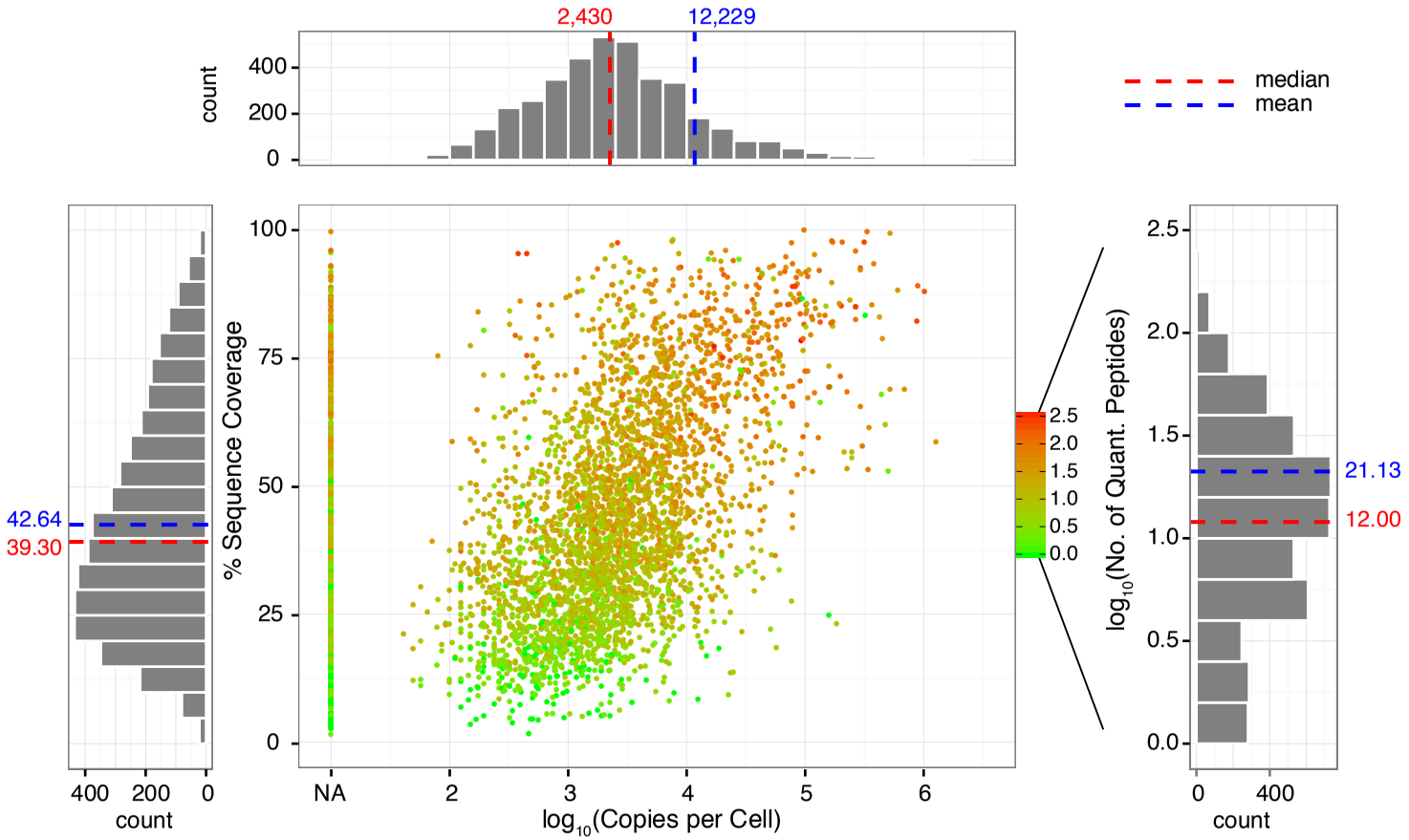

Figure 4.3: Graphical assessment of the performance of the proteomics analysis. The scatter plot in the middle shows the relationship between percent sequence coverage of the proteins quantified in the present study with $\log_{10}$ of their copies per cell (obtained from (Ghaemmaghami et al. 2003)). The colour of the points represents $\log_{10}$ of the number of high confidence quantified peptides for that protein. The histograms along the margins represent the distribution of the dimensions plotted in the scatter plot. On the left is the histogram for percent sequence coverage, on the right that for the $\log_{10}$ of high confidence quantified peptides per protein and on the top that for $\log_{10}$ of copies per cell (NA values are not plotted). The blue and red dashed lines represent the median and mean in the linear scale, respectively.

After the initial assessment, proteomics data were stringently filtered by a novel procedure we developed to improve the quality of SILAC based quantitative proteomics. This filter exploits the SILAC label-switch design at the peptide level, wherein a true peptide SILAC ratio is expected to get inverted upon switching the SILAC labels. For this procedure, first, proteins not quantified by at least two high-confidence peptides were removed. Next, proteins not identified in both SILAC label switch designs (that is, 30 °C_{light} vs. 37 °C_{heavy} and 30 °C_{heavy} vs. 37 °C_{light}) were also removed. Finally, only peptides that were quantified consistently across label switch conditions (that is, $\left|\log_2(R_1)-\log_2(R_{-1})\right| < 0.56$, where R_1 and R_{-1} are the mean SILAC ratios of a peptide in the two label switch designs) were used for the final calculation of the relative protein abundances across samples. Figure 4.4 shows the distribution of peptide ratios in the two SILAC label switch conditions before and after the application of the filter.

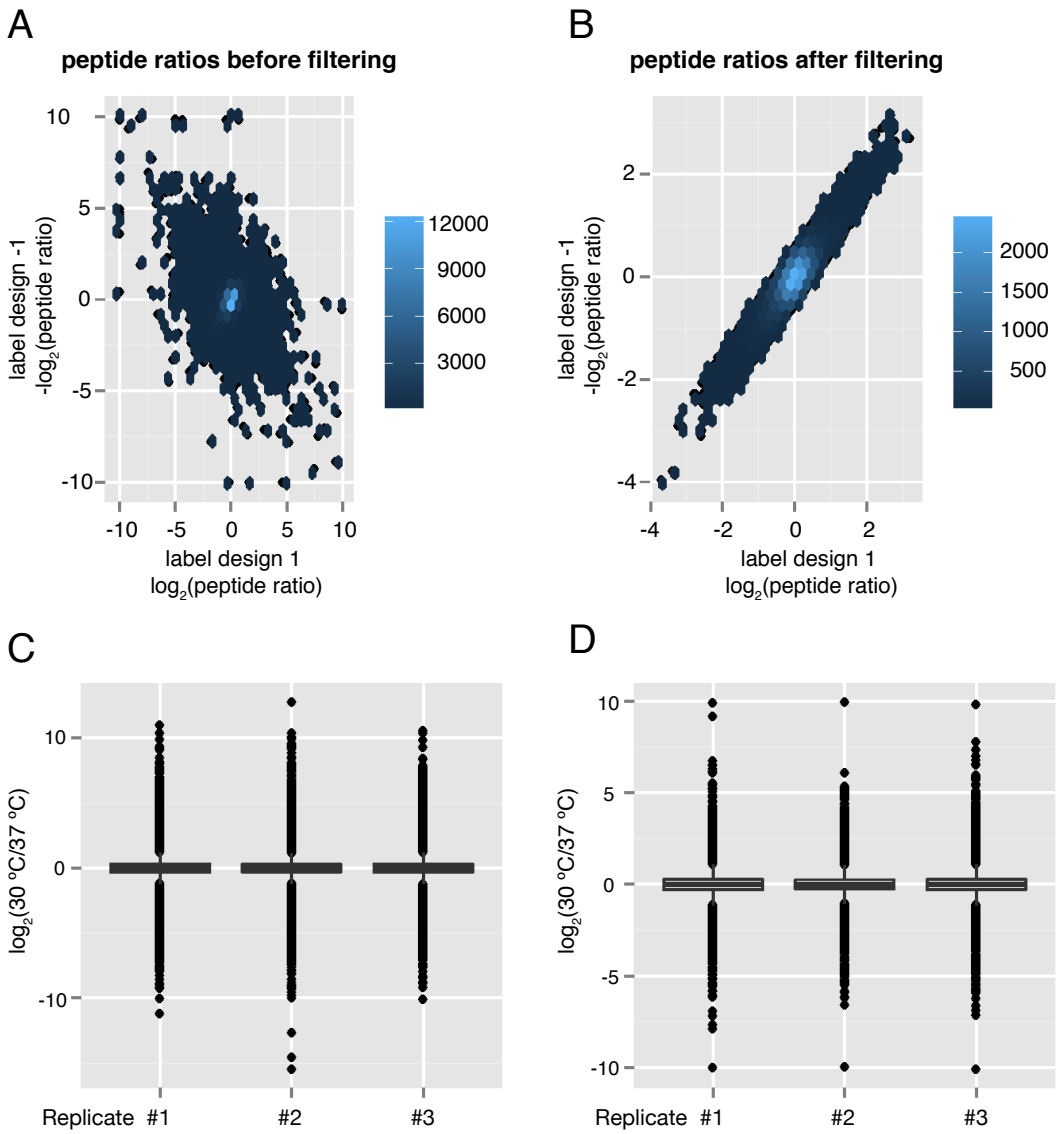

Figure 4.4: SILAC label switch filter. Switched SILAC labelling is denoted by the label design -1. (A) and (B) represent the distribution of peptide ratios before and after label switch filter, respectively, in the form of a scatter plot of binned hexagonal tiles. Colour of tiles represents number of peptides binned into each tile and serves to indicate the density of data in a given range of ratios. (C) and (D) Box and whisker plots of the protein ratios from the three biological replicates before and after peptide label switch filter, respectively. The box represents the inter quartile range (50% of the data) with the solid-line in the centre of the box representing the median of the peptide ratios.

After the stringent label switch filter, the histogram of copies per cell of the filtered proteins was plotted to confirm good coverage of the dynamic range of protein expression (figure 4.5).

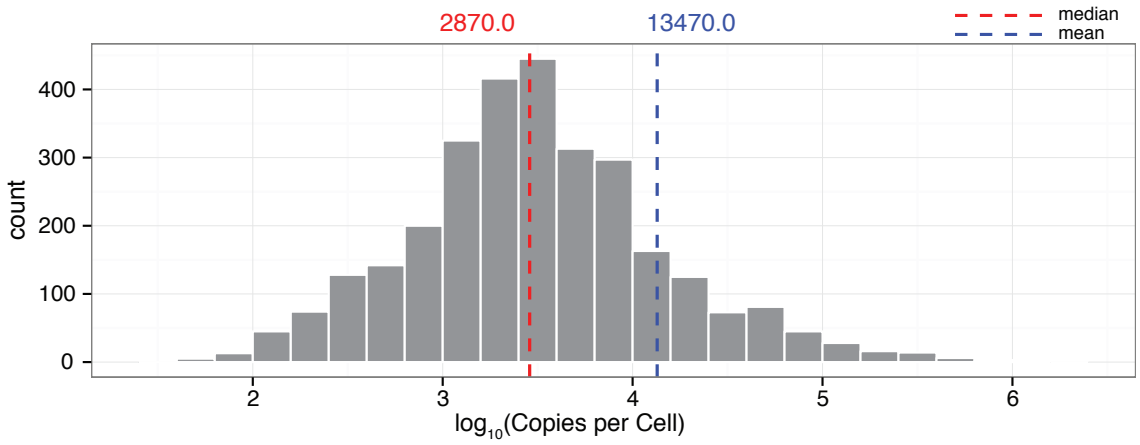

Figure 4.5: Post filter copy per cell coverage. Histogram highlighting the distribution of expression levels (log_{10} copies per cell) of the proteins passing the labels switch filter. The blue and red dashed lines represent the median and mean in linear space, respectively**.**

Protein ratios were then median normalised to remove small variations between the replicates. Box and whisker plots and MA plots were used, as described in the previous chapter and in Ting et al. (2009), to ascertain the effectiveness of the normalisation procedure and to rule out any bias between protein ratios vs. number of peptides used for their computation (figure 4.6). Finally, protein ratios were tested for their statistical significance.

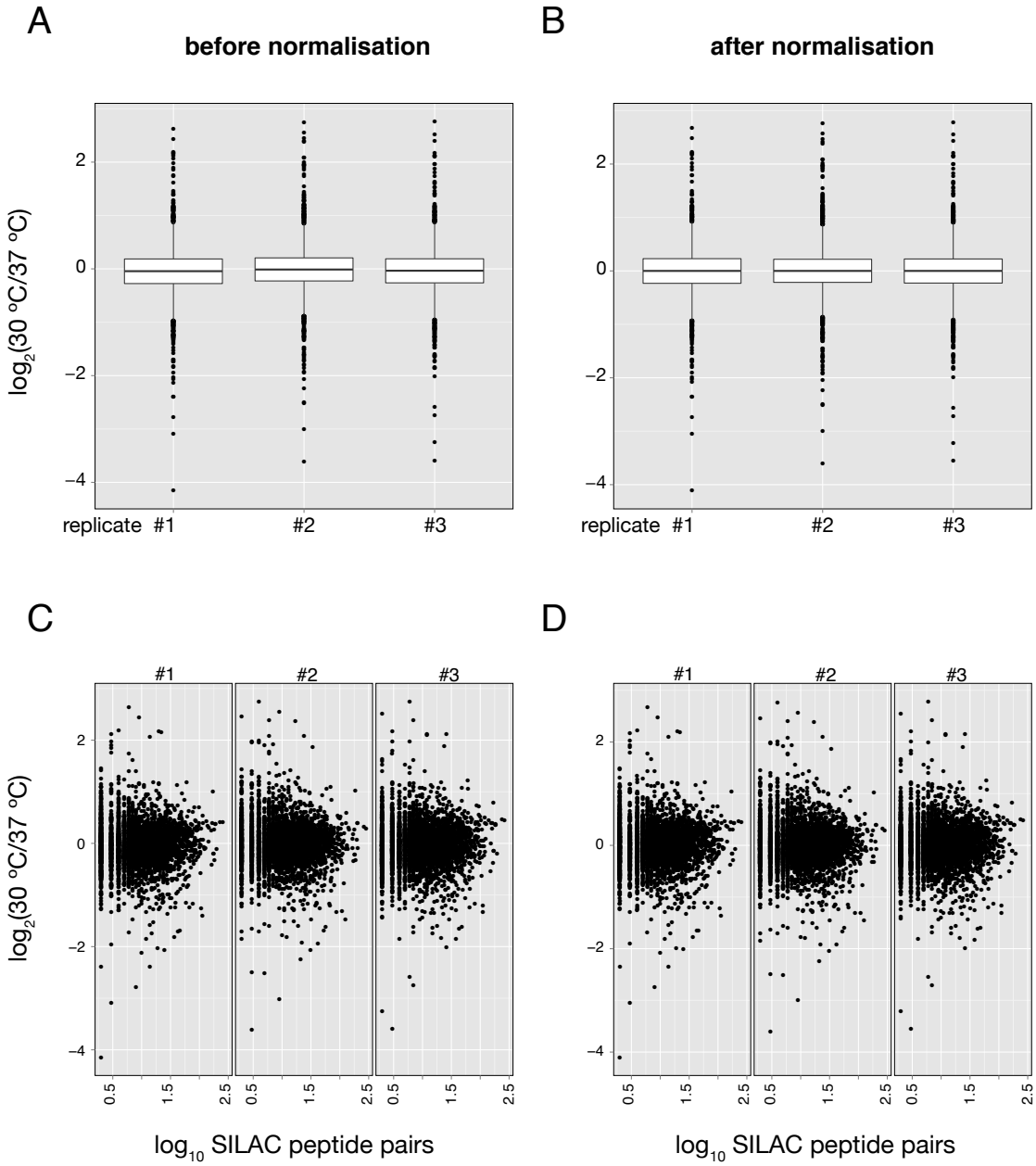

Figure 4.6: 30 °C vs 37 °C proteomics data quality check and normalisation. Systematic inter-sample variances were checked and subsequently removed using median normalisation. (A) and (B) Box and whisker plots of the protein ratios from the three biological replicates before and after normalisation, respectively. The box represents the inter quartile range (50% of the data) with the solid-line in the centre of the box representing the median of the distribution of protein ratios. (C) and (D) MA plots of protein-abundance ratios before and after median normalisation, respectively. For each protein the mean 30 °C/37 °C ratio from each of the three replicates was calculated and plotted as $\log_2$(30 °C/37 °C) against $\log_{10}$ of the number of SILAC pairs used for the quantification of that protein.

4.2.2 Proteome-wide changes in response to prolonged heat stress

Empirical Bayes moderated *t*-test was used to test for the statistical significance of the protein abundance ratios (Ting et al. 2009) and the resulting *p*-values were adjusted to correct for multiple hypothesis testing by Benjamini & Hochberg FDR correction. Figure 4.7 shows the protein abundance ratios against their adjusted *p*-values. 1% FDR (adjusted p-values of 0.01) was chosen as the threshold for statistical significance. In total 1,007 proteins were found to have significantly altered abundance, with 488 and 519 proteins up- and down-regulated respectively, in the cells grown at 37 °C (appendix 2 table A2.1).

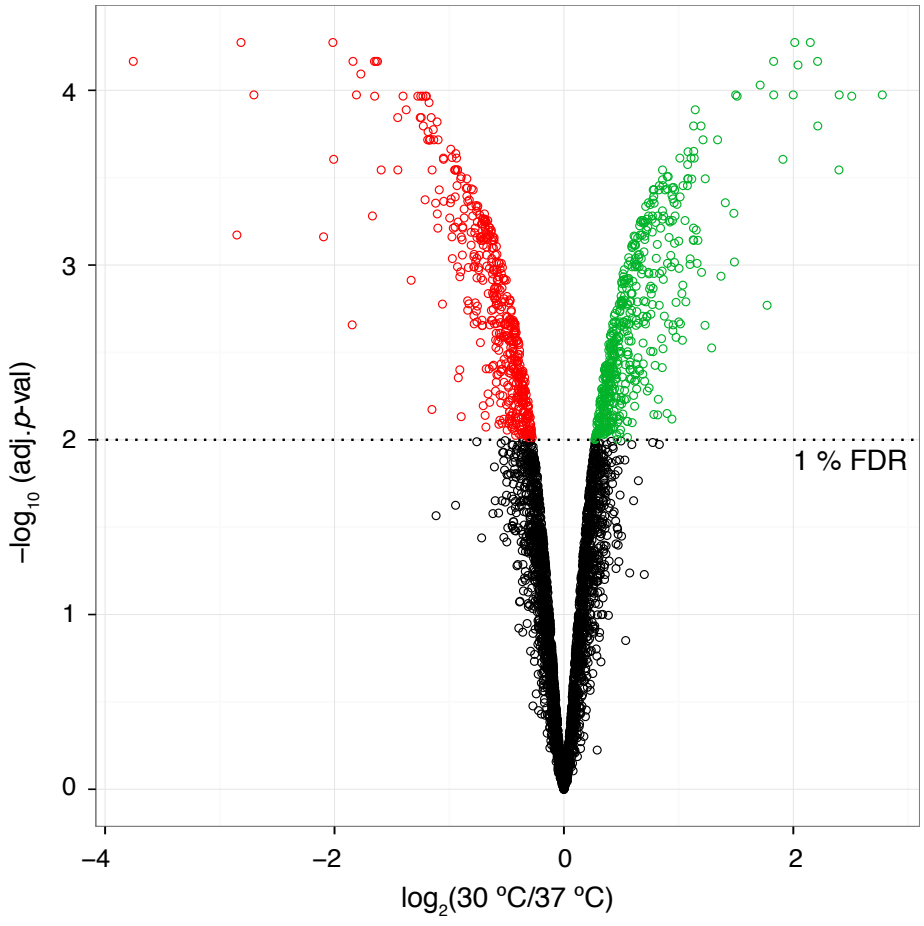

Figure 4.7: 30 °C vs. 37 °C volcano plot. Volcano plot of protein fold change vs. their significance value calculated by Bayes normalised *t* test and adjusted to control for the false discovery rate (FDR) using the Benjamini–Hochberg correction. The horizontal (y=2) dotted line represents an FDR of 1% chosen as the threshold for statistical significance. Circles in red and green highlight the significantly up- and down-regulated proteins, respectively, in the cells grown at 37 °C.

To validate the proteomics data, these results were first compared with those of the proteomics and transcriptomics analyses presented in Nagaraj et al. (2012) and Gasch et al. (2000), respectively. Nagaraj *et al.* had found that after a heat shock of 30 min at 37 °C a total of 234 proteins showed statistically significant altered abundance. Out of these, 115 were in common with the significant changes from the present analysis and 83.5% of these were positively correlated (figure 4.8A). In the transcriptomics study of Gasch et al. (2000), several stress conditions were analysed including heat shocks of various intensities and durations. However, statistical analysis to identify significant changes in mRNA levels was not done. Therefore, in order to perform a similar comparison with the transcriptomics data, three micro-array experiments matching closely in their conditions were treated as biological replicates and significant changes in mRNA levels were determined using a Bayes moderated *t*-test. Figure 4.8B shows the comparison of the significant protein ratios from the present study against the significant mRNA ratios from Gasch et al. (2000) in the form a heat-map. The majority of the changes (89.5%) were positively correlated between the two studies.

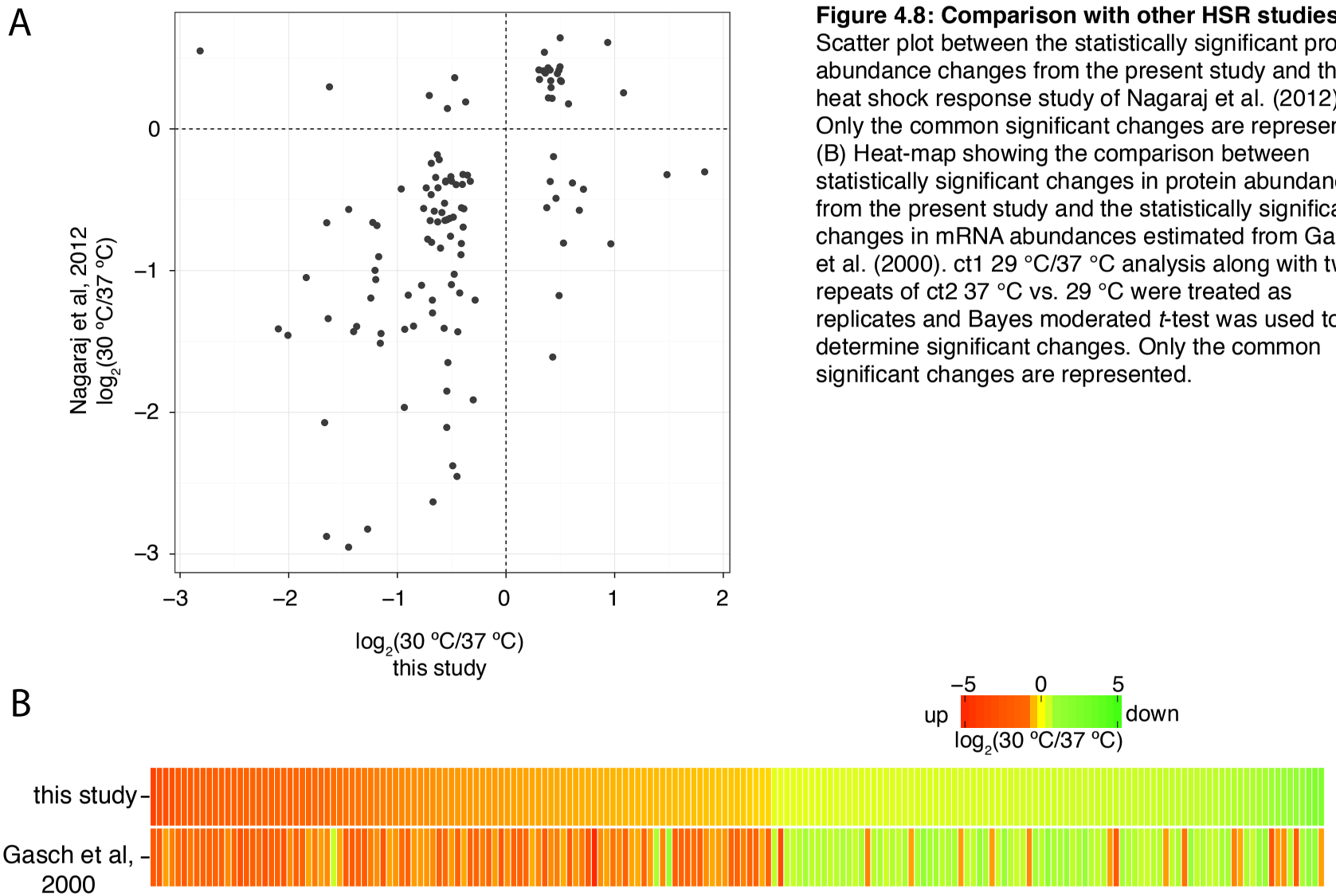

Figure 4.8: Comparison with other HSR studies. (A) Scatter plot between the statistically significant protein abundance changes from the present study and the heat shock response study of Nagaraj et al. (2012). Only the common significant changes are represented. (B) Heat-map showing the comparison between statistically significant changes in protein abundances from the present study and the statistically significant changes in mRNA abundances estimated from Gasch et al. (2000). ct1 29 °C/37 °C analysis along with two repeats of ct2 37 °C vs. 29 °C were treated as replicates and Bayes moderated *t*-test was used to determine significant changes. Only the common significant changes are represented.

Subsequently, several proteins that are known to be regulated in response heat shock were manually selected and their abundance changes were validated (figures 4.9 and 4.10). Exposure to heat shock causes increased expression of many protective factors, altered sugar and energy metabolism and reduced translation capacity (Morano, Grant, and Moye-Rowley 2012; Verghese et al. 2012). Along these lines, the abundance of proteins Ssa1-4p from the Hsp70 family of chaperones along with their cofactors Sse1-2p from the Hsp110 subfamily and Apj1p, Mdj1p, Sis1p and Ydj1p from the Hsp40/DnaJ family of cochaperones was increased in the cells grown at 37 °C. Hsp70s are the principal chaperones in eukaryotes that promiscuously bind hydrophobic patches in the unfolded or partially folded proteins and aid in their folding. Protein folding activity of Hsp70s is coupled to the energy released by ATP hydrolysis and consequently, they depend on nucleotide exchange factors such as the Hsp110s. Hsp40/DnaJ proteins interact with Hsp70s through their J-domains and enhance Hsp70 function by facilitating substrate binding and accelerating its otherwise weak nascent ATPase activity. Similarly, Hsp90 chaperons Hsp82p and Hsc82p, which selectively aid in the final steps of maturation of substrate proteins were also up-regulated. Like the Hsp70 system, Hsp90s also rely on ATP hydrolysis for their chaperone activity and are therefore regulated by cochaperones. Hsp90 cochaperones such as Sti1p, Aha1p, Cpr6p and Cpr7p had elevated expression. Contrary to this theme, phosphatase Ppt1p, whose deletion leaves Hsp90 hyperphosphorylated reducing its efficiency (Soroka et al. 2012; Wandinger et al. 2006), was down-regulated. Interestingly, even though heat stress caused by 37 °C is not believed to cause much protein denaturation (Nathan, Vos, and Lindquist 1997), proteins involved in the disaggregation of denatured proteins, Hsp104, and

prevention of unfolded protein aggregation such as the oligomeric chaperones Hsp26p and Hsp42p were also up-regulated. In addition to the mentioned cytosolic chaperone system, a number of mitochondrial and ER chaperones and cochaperones showed increased protein abundance in the cells grown at 37 °C.

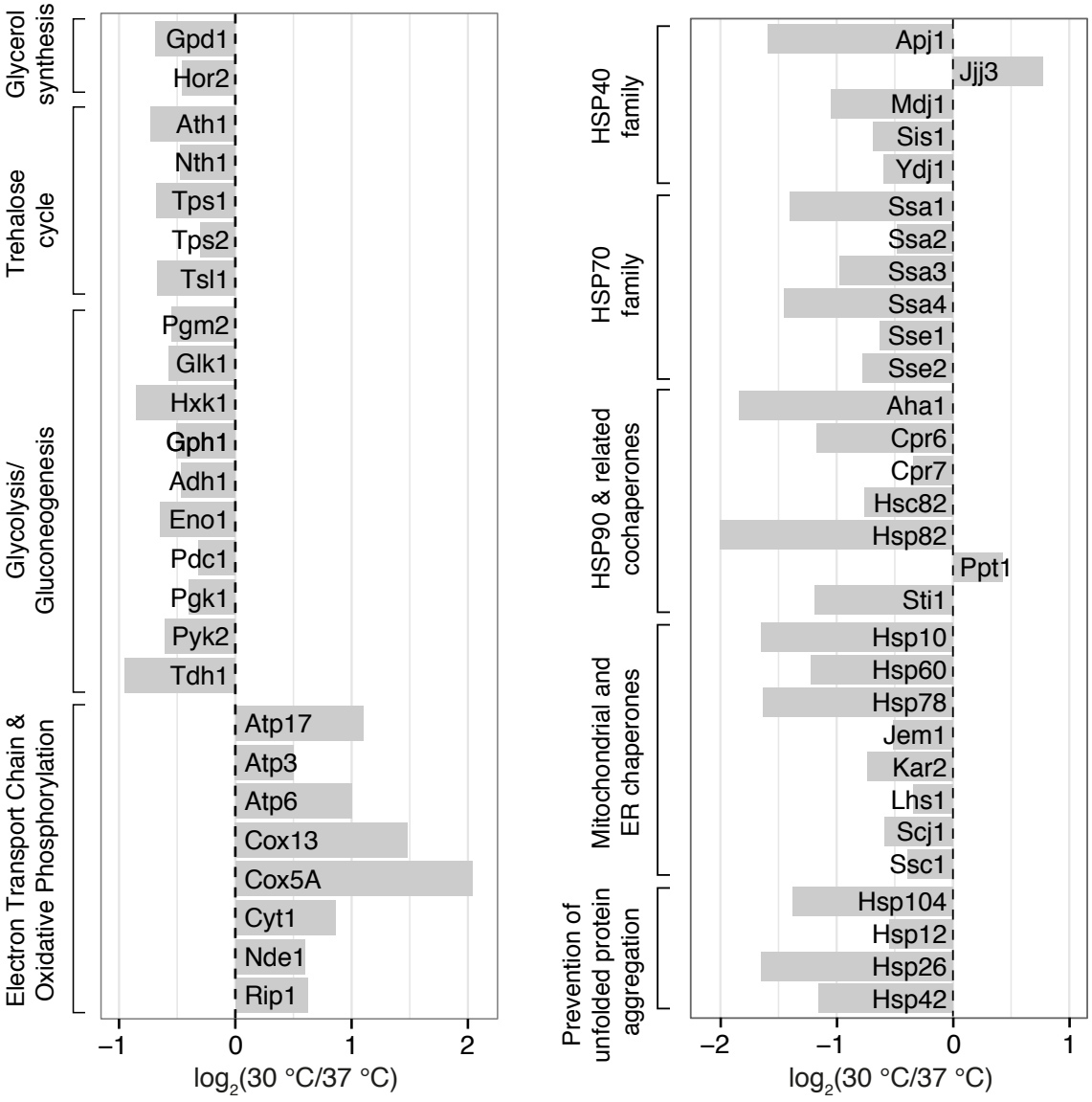

Figure 4.9: Key-players of heat shock response under prolonged heat stress. Bar plots showing abundance change of proteins known to play important roles in HSR.

Stress caused by elevated temperature also alters the sugar and energy metabolism (figure 4.9). Most prominent of these changes is the increased

intracellular levels of the protective sugar trehalose (figures 4.9) that stabilises unfolded proteins and prevents their aggregation. As previously reported (Gasch et al. 2000), levels of the proteins involved in the trehalose cycle were up-regulated in the cells grown at 37 °C. These included, trehalose synthase proteins Tps1p, Tps2p and Tsl1p, trehalases Nth1p and Ath1p, and glucose metabolism enzymes Hxk1p, Pgm2p and Gph1 that are required for the synthesis of trehalose precursors. In addition to these, the proteomics data showed elevated levels of Pfk26p, Adh1p, Eno1p, Pdc1p, Pgk1p, Pyk2p and Tdh1p suggesting up-regulation of the glycolytic and gluconeogenesis pathways. On the other hand, proteins involved in the utilisation of NADH for energy production (Nde1p), mitochondrial electron transport chain and ATP synthase were significantly down-regulated. Up-regulation of the glycolytic pathway is consistent with previous reports (Gasch et al. 2000; Gasch 2002). Down-regulation of respiration and oxidative phosphorylation could help in reducing damage caused by oxidative stress resulting from dysfunction of the electron-transport chain at elevated temperatures (Davidson et al. 1996; Davidson and Schiestl 2001). Furthermore, deletion of *NDE1* or *NDE2* is known to block the effect of dysfunctional electron-transport chain (Davidson and Schiestl 2001). Interestingly, levels of glycerol synthesising enzymes Gpd1p and Hor2p were also up-regulated.

Lastly, many proteins that are involved in the process of translation were among the significantly down-regulated proteins. These included proteins involved in the synthesis, processing and maturation of rRNA and tRNA, aminoacyl-tRNA synthetases, ribosomal proteins and factors regulating different steps of translation. Down-regulation of the protein translational machinery is a well

known component of the common environmental stress response (Gasch and Werner-Washburne 2002; Gasch 2002).

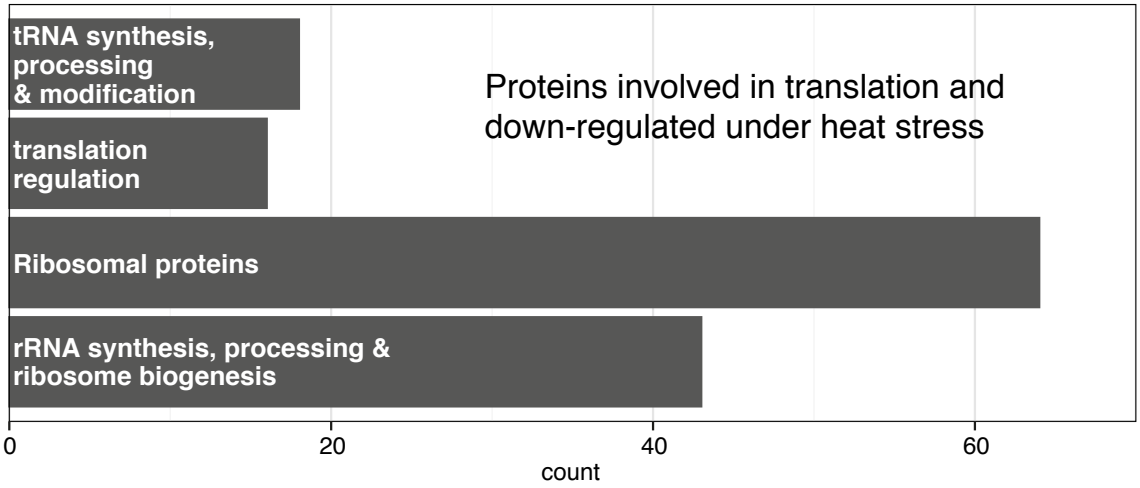

Figure 4.10: Down-regulation of protein synthesis. Histogram representing the major categories of proteins involved in translation that were significantly down-regulated in the cells grown at 37 °C

Overall, significantly changing proteins were analysed for enrichment of GO terms and MIPS functional classes, to highlight the various biological processes that are involved in the response to the prolonged heat stress (appendix 2 tables A2.2 and A2.3). Word-clouds in figure 4.11 show the most significantly over-represented (*p*-values less than 0.001) GO terms. As expected, the results indicate that, during heat stress, yeast cells down-regulate proteins involved in oxidative phosphorylation, translation and biosynthesis of translational machinery. On the other hand, proteins involved in various stress responses and proteolysis were up-regulated. Interestingly, GO analysis also showed down-regulation of methionine biosynthesis and up-regulation of arginine biosynthesis. Down-regulation of Met biosynthesis has previously been associated with oxidative stress (C.-Y. Wu et al. 2009). The Met biosynthetic pathway includes reduction of sulfate to sulfite and its utilisation in the biosynthesis of methionine (Met) and S-adenosylmethionine (AdoMet). This

pathway requires large amounts of NADPH, whose supply could become crucial in presence of heat stress induced oxidative stress.

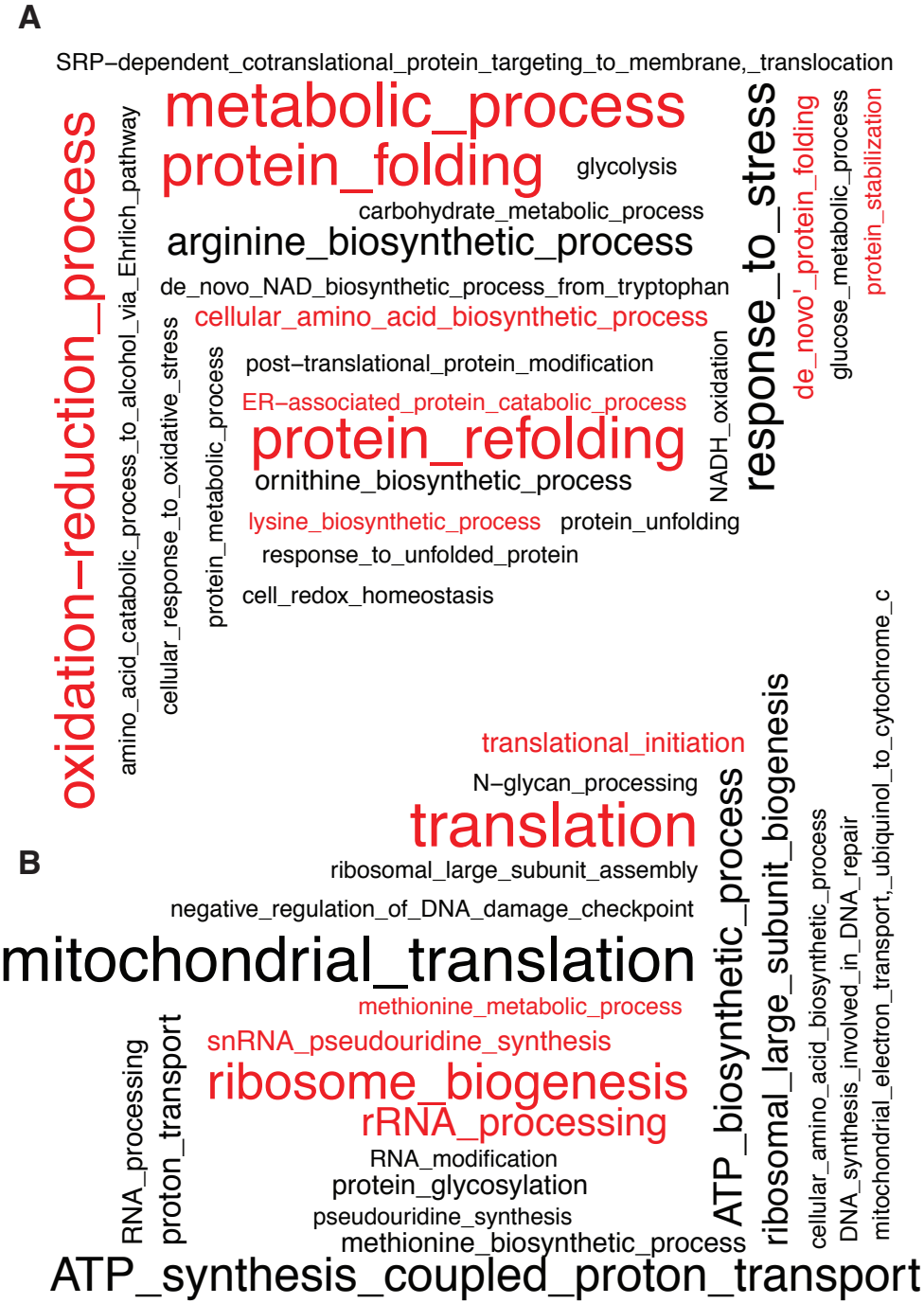

Figure 4.11: Biological processes responding to prolonged heat stress of 37 °C. Most significantly over-represented GO terms for biological processes (having *p*-values less than 0.001) from (A) significantly up- and (B) down-regulated proteins in the cells grown at 37 °C. For the full list of significantly enriched GO terms and MIPS Functional Classes see appendix 2 table A2.2 and A2.3. GO terms that were in common with the GO terms significantly over-represented in wild-type vs. *urm1Δ* analysis are shown in red.

Similarly, up-regulation of Arg biosynthesis under heat stress is consistent with previous reports (Kitagaki and Takagi 2014; Nishimura et al. 2010; Domitrovic et al. 2003), wherein elevated Arg levels were found to confer resistance to a variety of stress conditions including heat stress. The exact mechanism of this cytoprotective function of Arg is not known, but it has been suggested that Arg is used to produce nitric oxide (NO) in a Tah18p dependent manner (Nishimura, Kawahara, and Takagi 2013).

4.2.3 Down regulation of *URM1*-pathway and tRNA thiolation

GO terms and MIPS functional classes enrichment analysis revealed that several of the biological processes modulated in response to heat stress were also affected by the absence of tRNA thiolation in *urm1Δ* cells. Highlighted in red in figure 4.11 are the common up- and down-regulated biological processes from the two analyses. This suggested that the *URM1*-pathway activity is perturbed under heat stress. Indeed, closer inspection of the significantly changing proteins revealed that the levels of *URM1*-pathway proteins were also affected by heat stress. Urm1p itself was not in the list of proteins because it was quantified by only one high confidence peptide and therefore, it was filtered out before the statistical analysis. Manual inspection of the pre-filter MS data showed that although the single Urm1p peptide was identified in all three replicates, it was not significantly changing (figure 4.12).

A

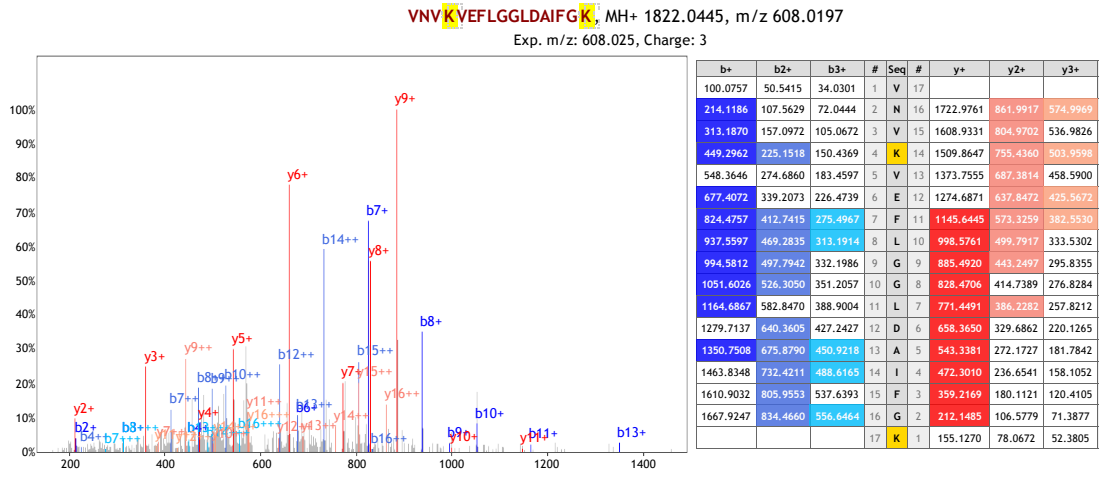

b+	b2+	b3+	#	Seq	#	y+	y2+	y3+
100.0757	50.5415	34.0301	1	V	17			
214.1186	107.5629	72.0444	2	N	16	1722.9761	861.9917	574.9969
313.1870	157.0972	105.0672	3	V	15	1608.9331	804.9702	536.9826
449.2962	225.1518	150.4369	4	K	14	1509.8647	755.4360	503.9598
548.3646	274.6860	183.4597	5	V	13	1373.7555	687.3814	458.5900
677.4072	339.2073	226.4739	6	E	12	1274.6871	637.8472	425.5672
824.4757	412.7415	275.4967	7	F	11	1145.6445	573.3259	382.5530
937.5597	469.2835	313.1914	8	L	10	998.5761	499.7917	333.5302
994.5812	497.7942	332.1986	9	G	9	885.4920	443.2497	295.8355
1051.6026	526.3050	351.2057	10	G	8	828.4706	414.7389	276.8284
1164.6867	582.8470	388.9004	11	L	7	771.4491	386.2282	257.8212
1279.7137	640.3605	427.2427	12	D	6	658.3650	329.6862	220.1265
1350.7508	675.8790	450.9218	13	A	5	543.3381	272.1727	181.7842
1463.8348	732.4211	488.6165	14	I	4	472.3010	236.6541	158.1052
1610.9032	805.9553	537.6393	15	F	3	359.2169	180.1121	120.4105
1667.9247	834.4660	556.6464	16	G	2	212.1485	106.5779	71.3877
			17	K	1	155.1270	78.0672	52.3805

B

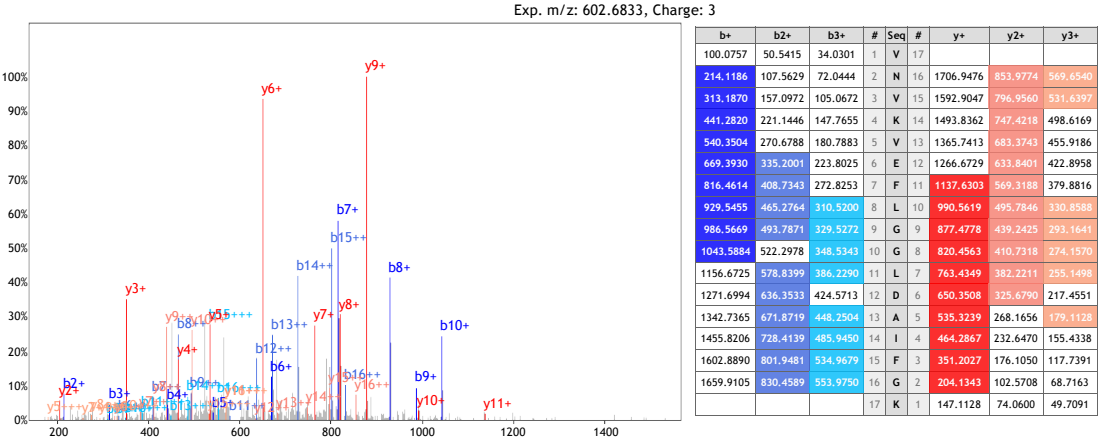

b+	b2+	b3+	#	Seq	#	y+	y2+	y3+
100.0757	50.5415	34.0301	1	V	17			
214.1186	107.5629	72.0444	2	N	16	1706.9476	853.9774	569.6540
313.1870	157.0972	105.0672	3	V	15	1592.9047	796.9560	531.6397
441.2820	221.1446	147.7655	4	K	14	1493.8362	747.4218	498.6169
540.3504	270.6788	180.7883	5	V	13	1365.7413	683.3743	455.9186
669.3930	335.2001	223.8025	6	E	12	1266.6729	633.8401	422.8958
816.4614	408.7343	272.8253	7	F	11	1137.6303	569.3188	379.8816
929.5455	465.2764	310.5200	8	L	10	990.5619	495.7846	330.8588
986.5669	493.7871	329.5272	9	G	9	877.4778	439.2425	293.1641
1043.5884	522.2978	348.5343	10	G	8	820.4563	410.7318	274.1570
1156.6725	578.8399	386.2290	11	L	7	763.4349	382.2211	255.1498
1271.6994	636.3533	424.5713	12	D	6	650.3508	325.6790	217.4551
1342.7365	671.8719	448.2504	13	A	5	535.3239	268.1656	179.1128
1455.8206	728.4139	485.9450	14	I	4	464.2867	232.6470	155.4338
1602.8890	801.9481	534.9679	15	F	3	351.2027	176.1050	117.7391
1659.9105	830.4589	553.9750	16	G	2	204.1343	102.5708	68.7163
			17	K	1	147.1128	74.0600	49.7091

C

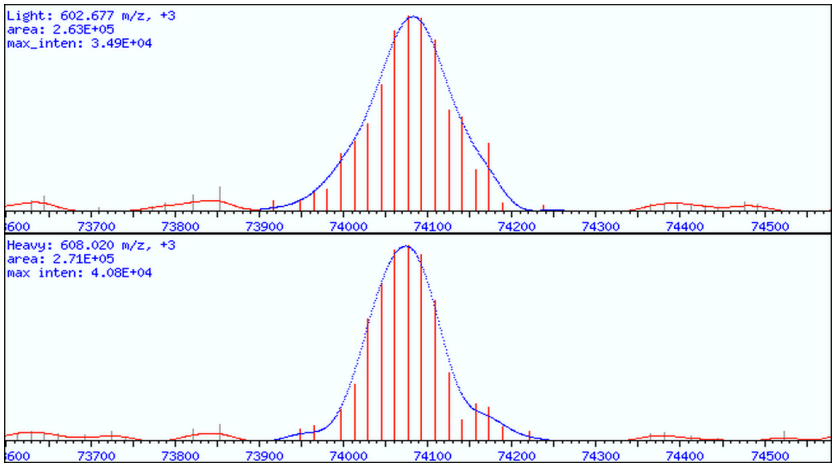

Figure 4.12: Manual validation of Urm1p identification and quantitation. (A) and (B) are the annotated ms/ms spectra of the heavy and light versions of the only peptide of Urm1p identified and quantified in the wt 30 °C/37 °C proteomics analysis. Annotated spectra were obtained from the Lorikeet Spectrum Viewer for Comet (available as part of the TPP). (C) shows the extracted ion chromatograms of the light and heavy peptide pair obtained from XPRESS. Protein ratios based on the single peptide across the three replicates were tested by simple one-sample *t*-test and were not found to be statistically significant (*p*-value = 0.39)

Besides Urm1p, all other members of the pathway were quantified with more than one high confidence peptides and passed the stringent filters. The abundance of Tum1p was not significantly altered, Uba4p was significantly up-regulated by 1.49 folds and Ncs2p and Ncs6p were significantly down-regulated by 1.61 and 4.04 fold respectively (table 4.2). Down-regulation of Ncs2p and Ncs6p was confirmed by immunoblotting for the HA-tagged versions of the two proteins (figure 4.13). Overall, these observations suggested that tRNA wobble uridine thiolation is down-regulated in cells grown under heat stress.

Table 4.2: Heat stress affects the *URM1*-pathway. Table showing the protein abundance ratios of the *URM1*-pathway members in the cells grown at 30 °C and 37 °C. Indicated adjusted *p*-values were calculated by Bayes moderated *t*-test and adjusted by Benjamini & Hochberg correction. Urm1p was not present in the stringently filtered dataset because it was quantified by only 1 high confidence peptide (and the filtering criteria required a minimum of 2 high confidence peptides).

Protein name	$\log_2$(30 °C/37 °C)	adj. *p*-value
Tum1p	-0.03	0.7328
Uba4p	-0.58	0.0012
Ncs2p	0.69	0.0020
Ncs6p	2.01	0.0001
Urm1p	NA	NA

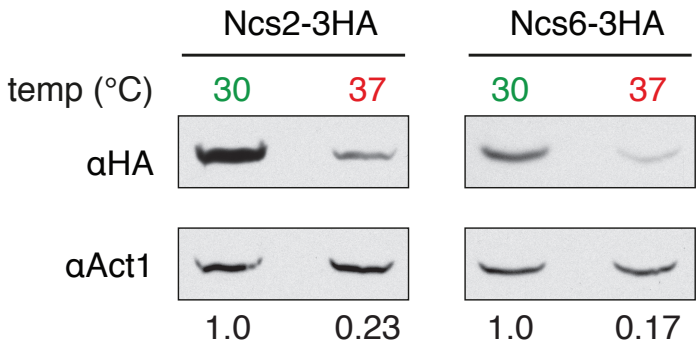

Figure 4.13: Western blot analysis of Ncs2p and Ncs6p. Down-regulation of Ncs2p and Ncs6p was verified by immunobloting for the 3HA-tagged versions of the proteins extracted from the yeast cells grown at 30 °C or 37 °C. Act1p was used as the loading control.

To test this hypothesis, thiolation levels in tRNAs extracted from the yeast cells grown at 30 °C or 37 °C were compared using APM-dPAGE and northern blot (NB) analysis. The 30 °C vs. 37 °C analysis, as mentioned earlier, showed that the proteins involved in the biosynthesis of methionine (Met) were down-regulated at 37 °C. The Met biosynthetic pathway, linked to cysteine (Cys) and S-adenosylmethionine (AdoMet) biosynthesis could be the source of s^2 and mcm^5 modifications on tRNAs. Considering the obvious importance of the sulfur metabolic pathways, starvation for sulfur containing amino acids and sulfate salts were also tested in addition to heat stress for their effect on tRNA thiolation. APM-dPAGE electropherogram (figure 4.14) showed that tRNAs isolated from cells grown at 37 °C or in the absence of sulfur containing amino acids were drastically hypothiolated. Northern blot analysis using ^{32}P labelled DNA oligonucleotide probes complementary to tQ^{UUG} or tK^{UUU} also confirmed the reduction in tRNA thiolation.

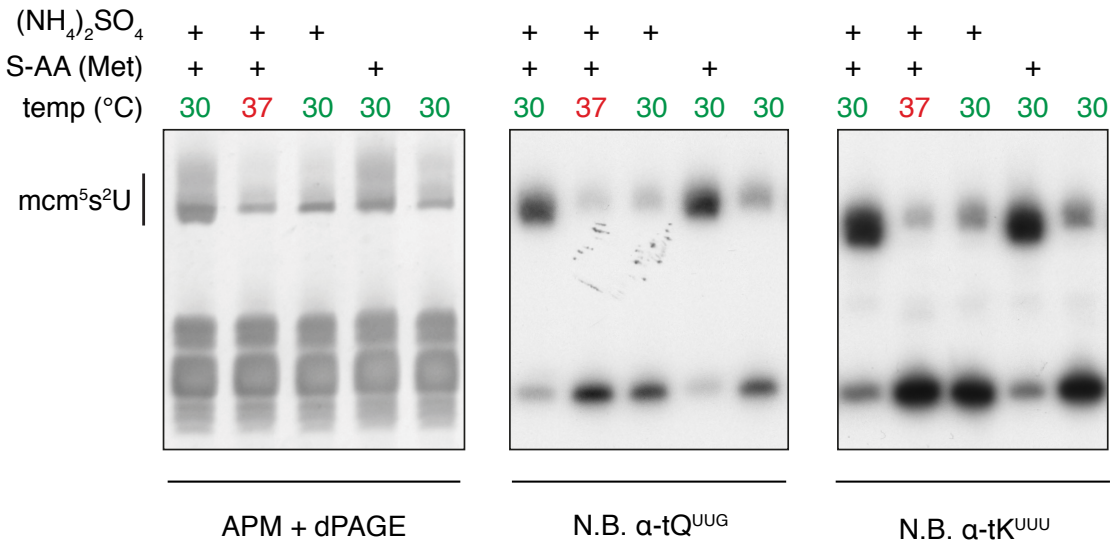

Figure 4.14: Modulation of tRNA thiolation. Bulk tRNA isolated from wild-type yeast cells grown under the indicated conditions was separated by APM supplemented dPAGE and either directly imaged or after transfer to a nylon membrane, probed with ^{32}P labelled DNA oligonucleotide probes complementary to tRNAs tQ^{UUG} or tK^{UUU}. S-AA is used to denote the presence/absence of sulfur containing amino acids in the growth medium, + indicates presence of Met in standard concentration. Similarly, presence or absence of $(NH_4)_2SO_4$ was tested to check if inorganic sulfur sources can compensate for S-AA.

It has been previously reported that deletion of *ELP*-complex genes causes a drastic reduction in the levels of tRNA thiolation in addition to the loss of the mcm^5 modification (Leidel et al. 2009). Therefore, reduction in the tRNA thiolation levels can indirectly be caused by decrease in the levels of the mcm^5 modifications. To rule out this possibility and to definitively validate the down-regulation of *URM1*-pathway activity, the levels of mcm^5s^2U and mcm^5U in tRNAs tE^{UUC}, tQ^{UUG}, and tR^{UCU} were compared by mass spectrometry (RNA-MS) analysis. U_{34} in tE^{UUC} and tQ^{UUG} is doubly modified to $mcm^5s^2U_{34}$, whereas in tR^{UCU} it is singly modified to mcm^5U_{34}. Using immobilised DNA oligonucleotide probes, the three tRNAs were purified from cells grown either in standard nutrient rich media at 30 °C or 37 °C or in absence of sulfur containing amino acids at 30 °C. After their purification, each tRNA was digested and dephosphorylated to individual nucleosides that were then analysed by LC-MS-MS/MS. The identity of nucleosides was established based on two criteria. The first criterion was the overlapping elution profiles of the nucleoside and the nucleobase resulting from the cleavage of the N-glycosidic bond during electropspray ionisation (Leidel et al. 2009). Figure 4.15 shows, as examples, the overlapping elution profiles of nucleosides and nucleobases resulting from mcm^5s^2U and mcm^5U.

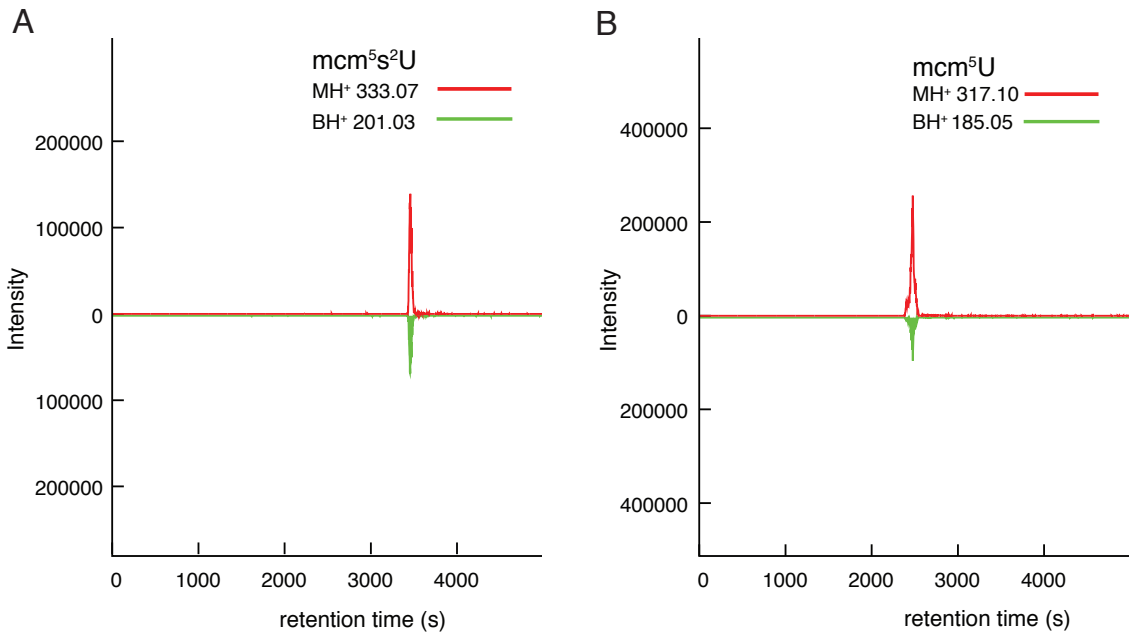

Figure 4.15: Nucleoside and nucleobase overlap. After elution from the chromatography column, a fraction of nucleosides undergo cleavage of the N-glycosidic bond resulting in the appearance of a “co-eluting” nucleobase. Shown here are the extracted ion chromatograms (XICs) for the m/z values corresponding to the protonated nucleoside (MH^+) and the protonated nucleobase (BH^+) for mcm^5s^2U and mcm^5U.

Secondly, MS^2 spectra of the nucleosides and nucleobases obtained after fragmentation by CID were compared with the MS^2 scans available in the literature. Figure 4.16 shows the MS^2 spectra of the nucleobases from mcm^5s^2U and mcm^5U annotated based on the fragmentation ions described in Bullinger et al. (2008) and Leidel et al. (2009).

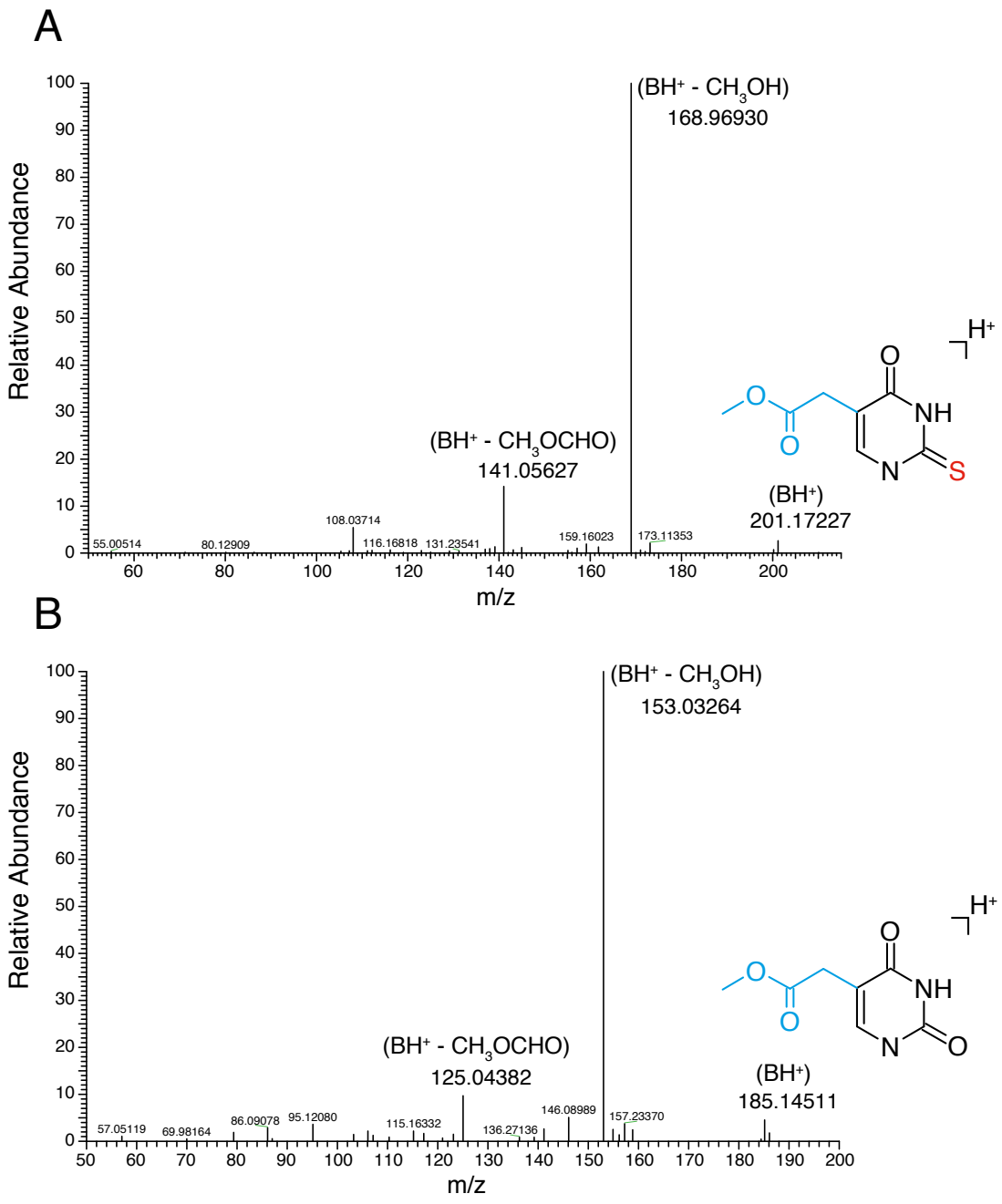

Figure 4.16: Fragmentation of modified uridines. MS^2 spectra of mcm^{5}s^{2}U and mcm^{5}U nucleobases obtained after CID based fragmentation. Spectra were annotated by matching against the published fragmentation products of the modified uridines (Bullinger et al. 2008; Leidel et al. 2009).

Levels of mcm^{5}s^{2}U and mcm^{5}U were estimated based on the area under their extracted ion chromatograms (appendix 2 figures A2.1, A2.2 and A2.3). Adenosine levels were used as the loading control. Figure 4.17 summarises the changes in the levels of mcm^{5}s^{2}U and mcm^{5}U at 37 °C or in the absence of sulfur amino acids relative to standard growth conditions (30 °C and nutrient rich medium). tRNAs tE^{UUC} and

tQ^{UUG} isolated from cells grown at 37 °C or starved for sulfur amino acids showed reduced levels of mcm^5s^2U and increased levels of mcm^5U. On the other hand, mcm^5s^2U was not detected from tR^{UCU}, as has been previously shown (Leidel et al. 2009). Levels of tR^{UCU} mcm^5U were unchanged in either of the stress conditions. These results not only confirmed the results from the APM-dPAGE and northern blot analysis, but also showed that the activity of the *ELP*-pathway and mcm^5 biosynthesis are not affected by the tested stress conditions.The apparent increase in the levels of mcm^5U in tE^{UUC} and tQ^{UUG} can be explained by the accumulation of an intermediate product in the biosynthesis of mcm^5s^2U, similar to the reported accumulation of mcm^5U in *urm1Δ* mutants (Huang, Lu, and Byström 2008; Leidel et al. 2009).

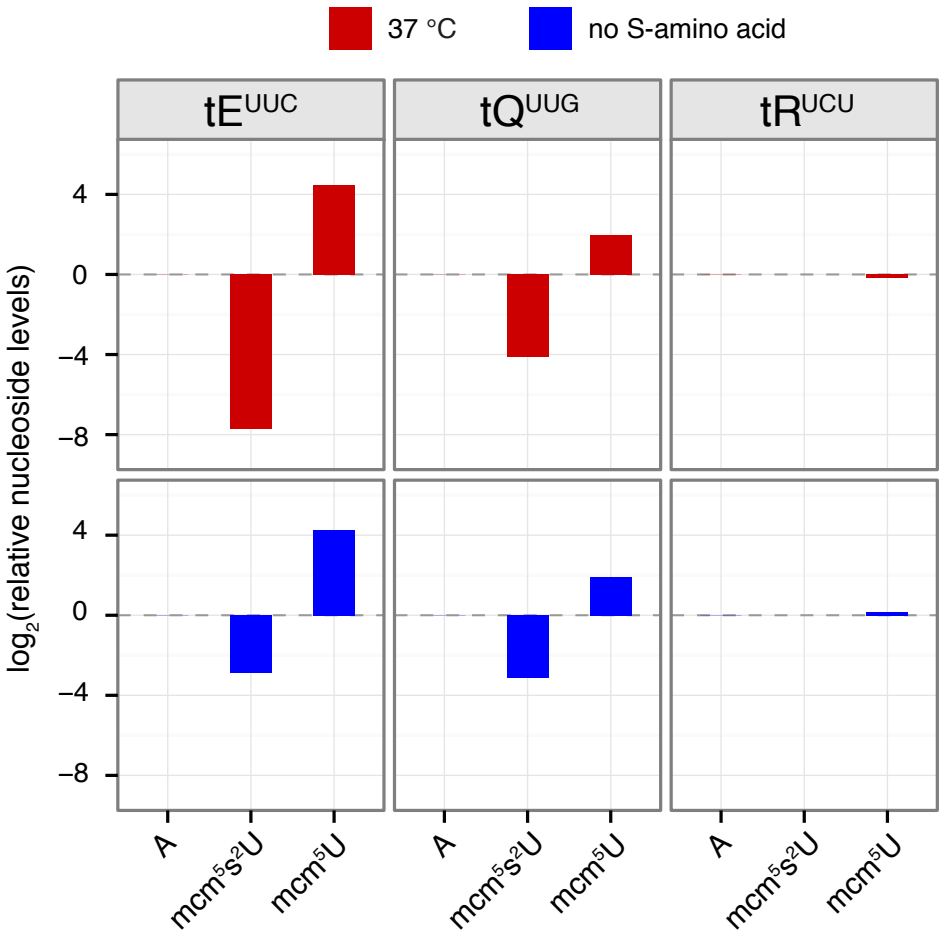

Figure 4.17: MS based quantitation of modified uridines. Bar-plots showing changes in the levels of mcm^5s^2U and mcm^5U in the tRNAs tE^{UUC}, tQ^{UUG}, and tR^{UCU} isolated from cells grown at 37 °C or without sulfur amino acids relative to the cells grown at 30 °C in amino acid rich medium. Adenosine (A) levels were used to normalise for differences in loading. Also refer to (appendix 2 figures A2.1, A2.2 and A2.3).

4.2.4 Diverse mechanisms regulate tRNA thiolation by the *URM1*-pathway

Results presented in the previous sections have shown that cells grown at 37 °C down-regulate methionine biosynthesis and hypothiolate their tRNAs. Additionally, hypothiolation was also found in cells starved for sulfur amino acids. It is possible that prolonged heat stress could cause a reduction in the cellular levels of sulfur containing amino acids or metabolites, thereby indirectly causing tRNA hypothiolation. To test for this possibility, wild-type yeast cells were grown at 37 °C in synthetic complete media (SC+D) supplemented with extra Met or in complex rich media (YPD) and thiolation of their tRNAs was compared. As shown in figure 4.18A, extra methionine or YPD media could not rescue tRNA hypothiolation caused by elevated temperature, suggesting that heat stress and sulfur amino acid starvation affect tRNA thiolation by independent mechanisms.

Recently, Laxman *et al.* also reported the hypothiolation of tRNAs in response to sulfur amino acid starvation (Laxman et al. 2013). Additionally, they found that the disruption of the Iml1p-complex, composed of Npr2p, Npr3p and Iml1p, rescues tRNA thiolation levels in cells starved for sulfur amino acids. To check if the Iml1p-complex was also involved in the regulation of tRNA thiolation in response to heat stress, *npr2Δ* cells were grown at 30 °C or 37 °C and thiolation levels of their tRNAs were measured. The APM-dPAGE electropherogram in figure 4.18B shows that while *npr2Δ* cells grown at 30 °C with or without sulfur amino acids had comparable levels of thiolated tRNAs, *npr2Δ* and wild-type cells grown at 37 °C exhibited a similar reduction in tRNA thiolation. This clearly indicates that heat stress induced tRNA hypothiolation does not require the Iml1p-complex.

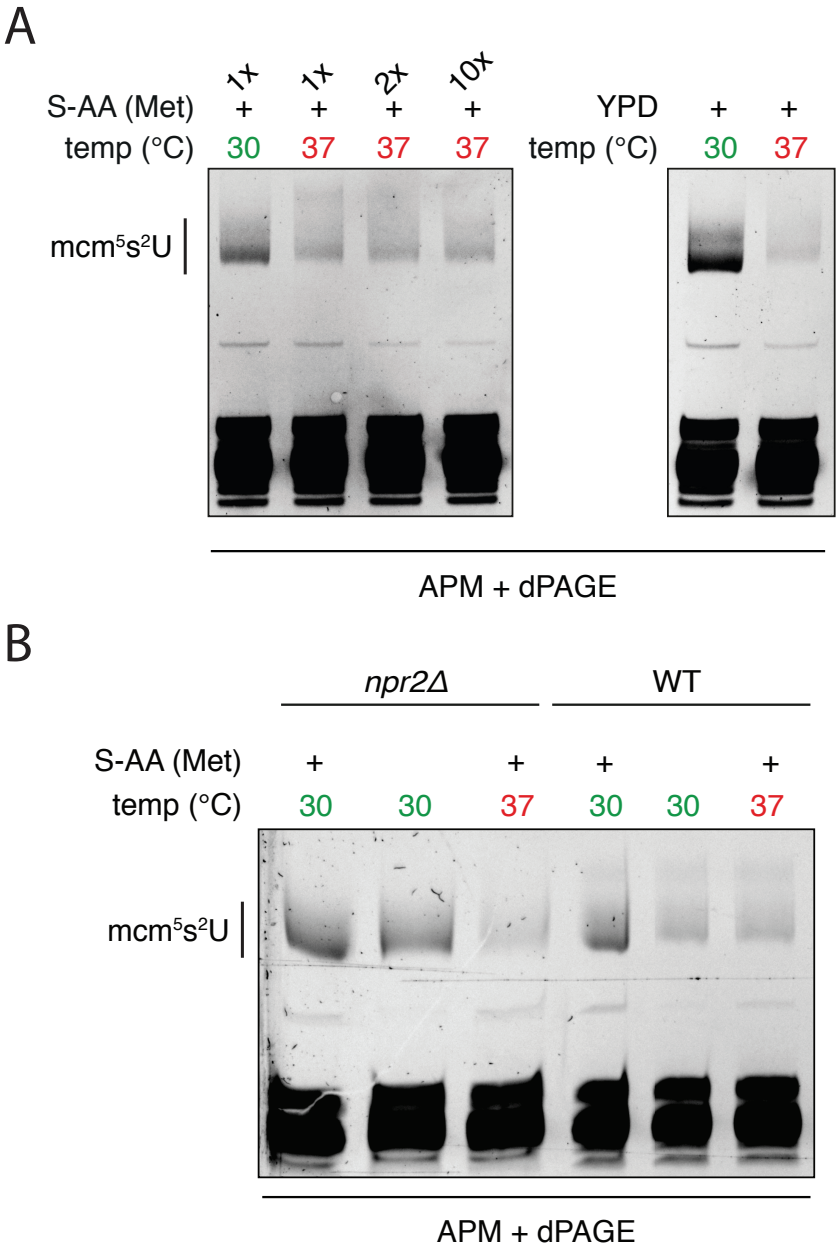

Figure 4.18: Independent mechanisms regulate tRNA thiolation. (A) Hypothiolation at elevated temperatures is not rescued by supplementation with extra methionine or nutrient rich media. Thiolation levels of tRNAs extracted from wild-type yeast cells grown at 30 °C or 37 °C in synthetic complete media (SC+D) with different amounts of methionine or in complex rich media (YP+D) were checked by APM+dPAGE. (B) Electropherogram shows that *npr2Δ* cells hypothiolate tRNAs at 37 °C.

To further understand the regulation of the *URM1*-pathway under heat stress, quantitative real time PCR analysis was used to measure changes in the mRNA levels of *URM1*-pathway genes at elevated temperatures. This showed (figure 4.19A) that the mRNA levels of *URM1*-pathway genes were not down-regulated at 37 °C, suggesting that the down-regulation of the *URM1*-pathway is not transcriptionally controlled.

Subsequently, the involvement of the proteasome in regulating tRNA thiolation was investigated using the temperature sensitive (ts) mutant strains of the proteasome regulatory particle ATPases Cim5p and Cim3p, *cim5-1* and *cim3-1* (Ghislain, Udvardy, and Mann 1993). Yeast strains carrying *cim5-1* or *cim3-1* instead of the wild-type copies of these genes show drastically reduced proteasomal activity at the restrictive temperature of 37 °C (Ghislain, Udvardy, and Mann 1993). Figure 4.19B shows that in comparison to wild-type cells, *cim5-1* or *cim3-1* strains exhibited a much less severe reduction in tRNA thiolation at 37 °C. This indicates that proteasomal activity is required for the down-regulation of tRNA thiolation at elevated temperatures.

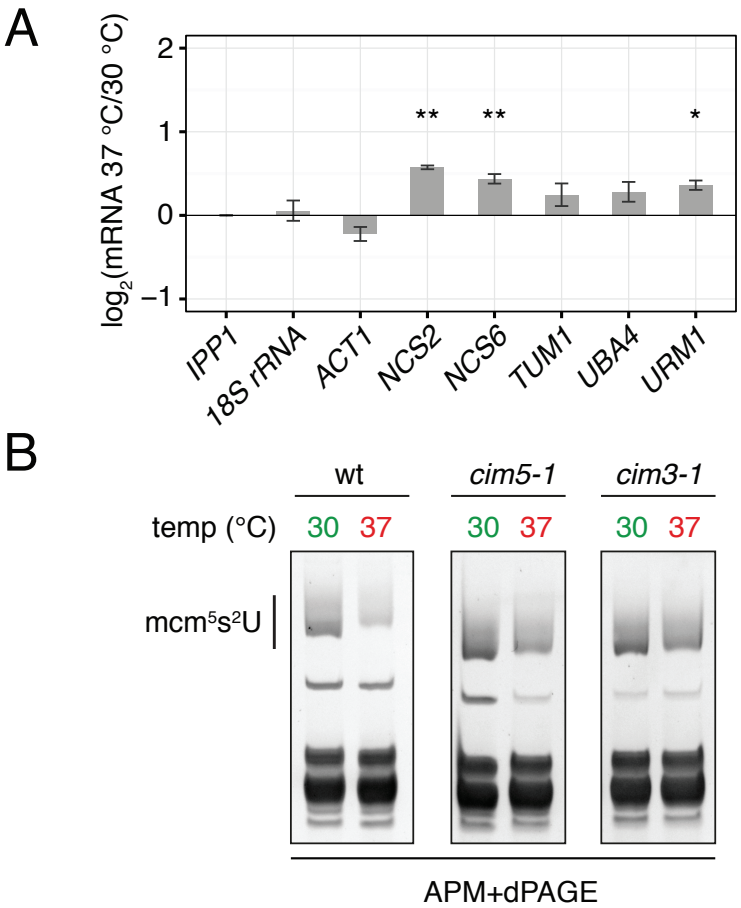

Figure 4.19: Post-transcriptional mechanisms regulate tRNA thiolation. (A) Bar-plot showing changes in the mRNA levels of URM1-pathway genes at 37 °C relative to 30 °C, determined by TaqMan based quantitative real time PCR analysis. Mean ΔCt values (equivalent to log2 mRNA levels) were tested by a two sample t-test for their statistical significance. (*) and (**) indicate p-values of less than 0.05 and 0.01, respectively. *18S rRNA* and *ACT1* were used as negative controls and *IPP1* mRNA levels were used for normalisation. (B) wild-type, *cim5-1* and *cim3-1* yeast cells were grown at 30 °C or 37 °C, their tRNAs extracted and analysed by APM-dPAGE to measure tRNA thiolation levels. Shown here is the electropherogram of the analysis.

Previously, an infectious strain of *S. cerevisiae*, isolated from the ascites fluid of a patient, was found to have an allelic variant of *NCS2* (Sinha et al. 2008). This allele differed in one nucleotide (A212T that translates to H71L), which conferred the yeast strain with the ability to grow at higher temperatures. Since Ncs2p is essential for tRNA thiolation in yeast and its levels were down-regulated at 37 °C, we speculated that the ncs2pH71L variant could affect the regulation of tRNA wobble uridine thiolation. To test for this hypothesis, an *ncs2Δ* strain was transformed with a low copy yeast plasmid either with no added gene (empty-vector), with the wild-type *NCS2* or with the *ncs2_A212T* allele. The resulting strains were then subjected to heat stress or starvation for sulfur-amino acids and their tRNAs analysed by APM-dPAGE. As shown in figure 4.20, *ncs2Δ* cells transformed with the wild-type *NCS2* showed reduced thiolation at 37 °C or in the absence of sulfur amino acids similarly to wild-type cells (compare lanes 5-7 with 2-4).

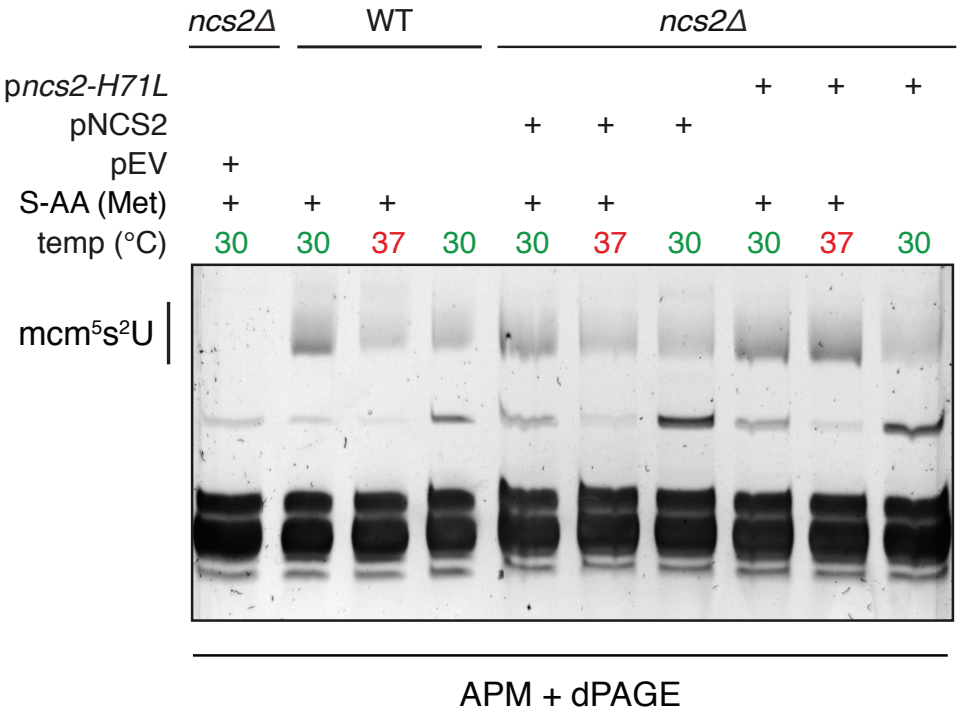

Figure 4.20: An Ncs2 mutant deregulates tRNA thiolation. Electropherogram from the APM-dPAGE analysis of bulk tRNA isolated from wild-type (WT) or *ncs2Δ* cells transformed with either an empty plasmid (pEV), a plasmid with wild-type *NCS2* (p*NCS2*) or a plasmid with *ncs2_A212T* (p*ncs2_A212T*) and grown under the indicated conditions.

Conversely, in the *ncs2Δ* cells transformed with *ncs2_A212T*, tRNA thiolation levels at 37 °C were comparable to the levels at 30 °C (compare lanes 8-9 with 5-6 and 2-3). Interestingly, cells with the mutant *ncs2_A212T* still reduced tRNA thiolation in response to sulfur amino acid starvation (lane 10). These results once again indicate that multiple mechanisms regulate the URM1-pathway activity in response to stress.

4.2.5 Altered tRNA thiolation causes differential translation

In the previous chapter, using an unbiased bioinformatics analysis we had found that the absence of tRNA thiolation causes reduced translation of mRNAs rich in codons AAA, CAA, GAA and AAG. Here we undertook a similar analysis to understand if the heat stress induced reduction in tRNA thiolation affects proteome composition. Specifically, a random forest based unsupervised machine learning analysis was used to rank the codons in the order of their importance in predicting the up- or down-regulation of proteins at elevated growth temperature. Figure 4.21A shows the predicted importance of each codon. Codons AAA and GAA, whose corresponding tRNAs are thiolated by the *URM1*-pathway, were among the three-most important codons. The top 2% of the genes with the highest frequency of each codon were represented in volcano plots derived from the 30 °C vs. 37 °C proteomics analysis. The plots for AAA and GAA rich genes showed that the high abundance of these codons was associated with reduced protein expression (figure 4.21B and appendix 2 figure A2.4).

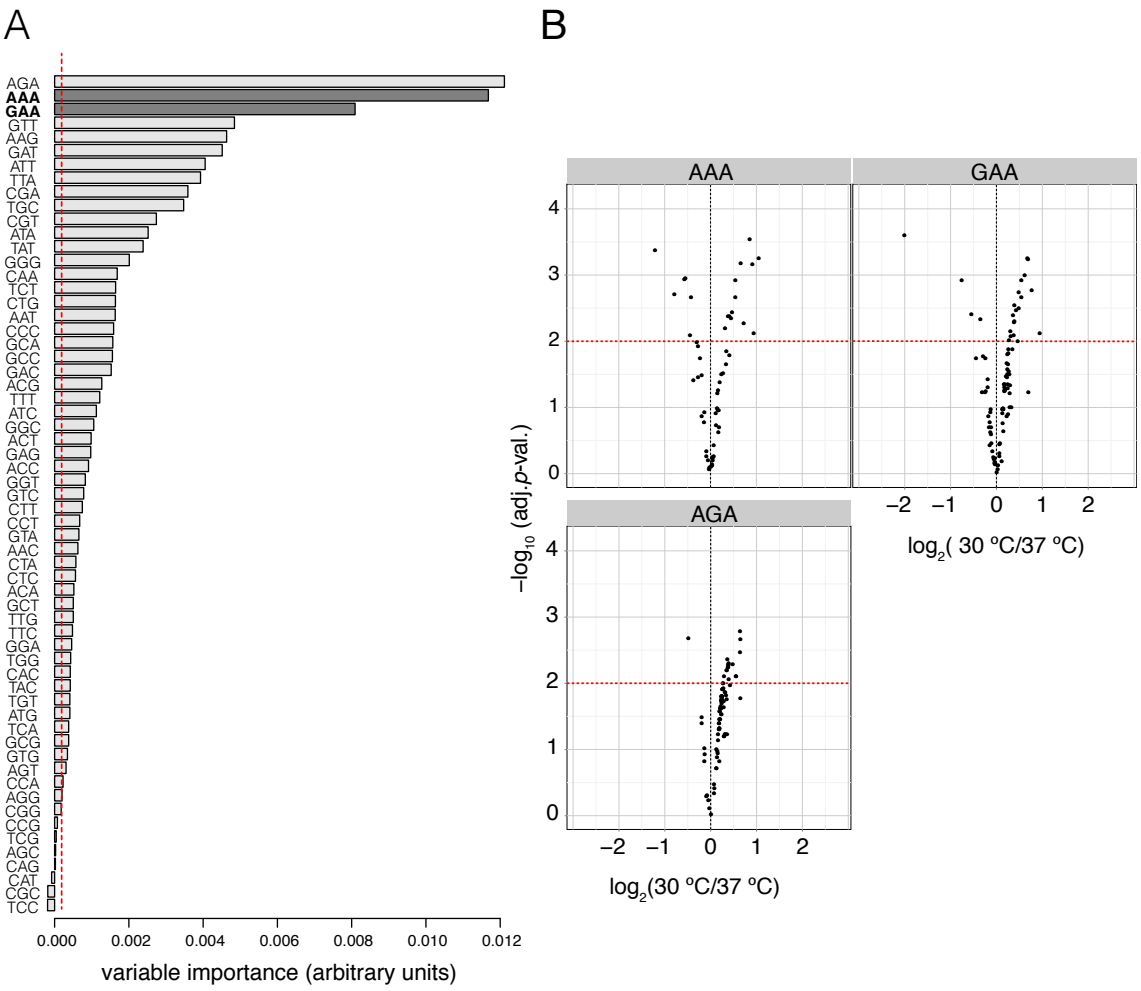

Figure 4.21: Codon bias in genes differentially expressed under heat stress. (A) Bar-plot representing the importance of each codon as learned by the random forest algorithm based analysis of the genes that code for the significantly changing proteins from the 30 °C vs. 37 °C analysis. Highlighted in bold and dark-grey are the codons for which the corresponding tRNAs are thiolated by the *URM1*-pathway. Dotted red line indicates absolute value of the lowest predictor. (B) Proteins with the corresponding highest frequency (top 2% of the genome) of AAA, GAA or AGA are represented in the volcano plot from figure 4.7. Horizontal red dotted line represents 1% FDR and vertical black dotted line represents a protein abundance ratio of 1:1.

Unexpectedly, the content of the AGA codon was also identified as an important factor associated with down-regulated proteins (figure 4.22A). The wobble uridine of tRNA tR^{UCU} is not thiolated in *S. cerevisiae* (Leidel et al. 2009) (figure 4.22A and B). Since at 37 °C the levels of mcm^5U_{34} in tR^{UCU} were unaffected (figure 4.17), the reasons behind the reduced expression of genes rich in AGA codons are not clear. Interestingly, it has been reported that the wobble uridine

of bovine tR^{UCU} is thiolated (Keith 1984). Northern blot analysis of bulk tRNA isolated from HEK293 cells confirmed that tR^{UCU} is also thiolated in human cells (figure 4.22C) suggesting that in higher eukaryotes altered tRNA thiolation can result in differential translation of AGA biased genes.

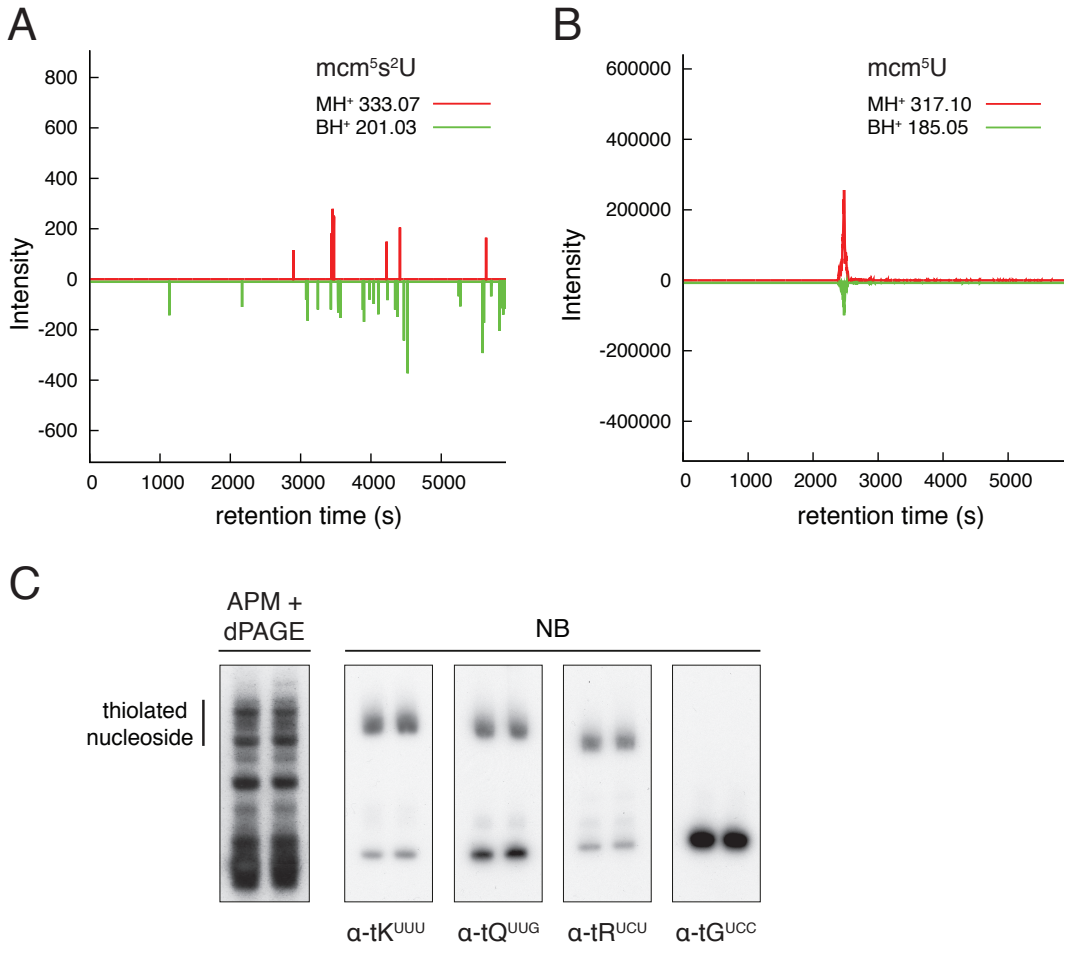

Figure 4.22: Thiolation status of tR^{UCU}. (A) and (B) Extracted ion chromatograms (XICs) for nucleosides (red) and nucleobases (green) of mcm^{5}s^{2}U and mcm^{5}U, respectively, from the RNA-MS analysis of the nucleosides obtained from tR^{UCU} purified from *S. cerevisiae*. (C) Analysis of tR^{UCU} thiolation in higher eukaryotes. Bulk tRNA isolated from HEK293 was separated by APM-dPAGE and analysed by northern blots for tK^{UUU}, tQ^{UUG}, tR^{UCU} and tG^{UCC}.

Over-expression of hypomodified tRNAs tK^{UUU}, tQ^{UUG} and tE^{UUC} is known to rescue the phenotypes associated with *URM1*- and *ELP*-pathway mutants. We have also shown that this was sufficient to rescue the differential protein abundance caused in *urm1Δ* cells (section 3.6.3). Hence we decided to test the effect of tRNA over-expression on differential protein abundance at 37 °C. Yeast cells over-expressing the tRNAs (ptKQE) were grown at 37 °C and compared to cells carrying an empty plasmid and grown at 30 °C by a SILAC based proteomics workflow similar to the one used in the original 30 °C vs. 37 °C analysis (figure 4.23). Three biological replicates were used with SILAC label switch, but the samples were not fractionated prior to the MS analysis. Instead each sample was run using a 6 h long gradient. The MS data were processed and filtered with the same stringency criteria previously described (figure 4.24), which resulted in 1,957 proteins quantified with at least two high confidence peptides. Protein ratios were then median normalised and their distribution was checked with box and whisker plots before and after normalisation (figure 4.25). Finally, protein abundance ratios were tested by the empirical Bayes moderated *t*-test to estimate their statistical significance (volcano plot in figure 4.26) and compared with the original 30 °C vs. 37 °C dataset. Since the two datasets identified different subsets of proteins, which could result in a biased comparison, only proteins commonly identified in the two datasets were compared.

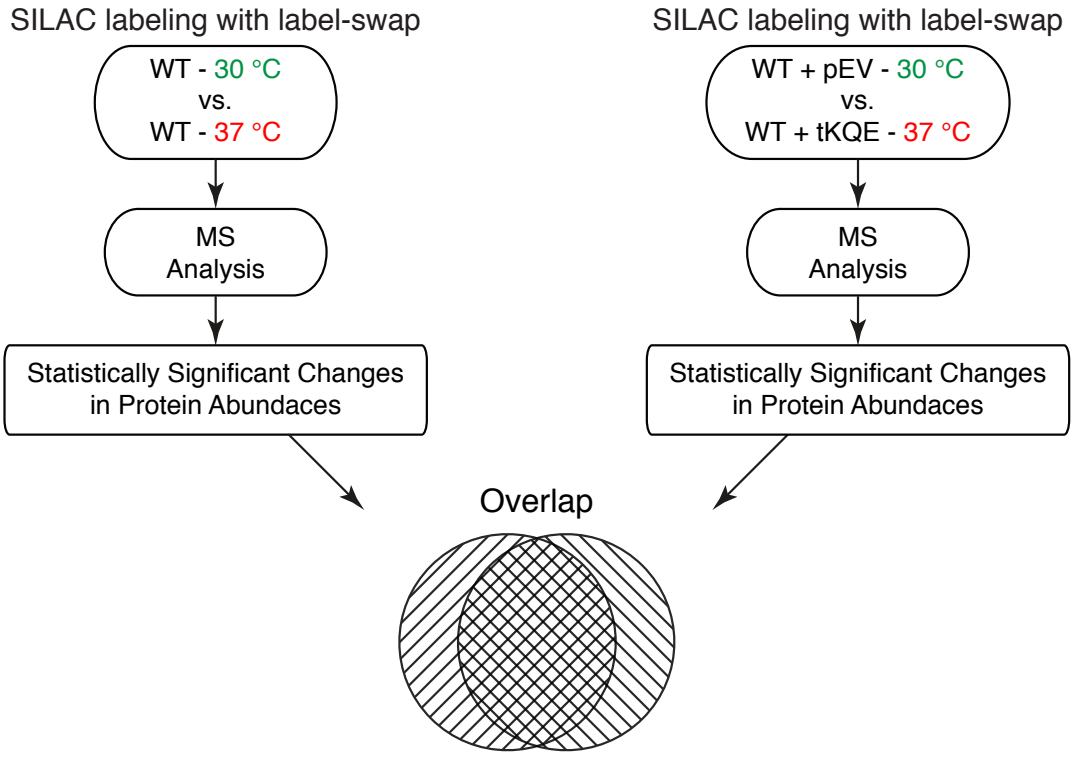

Figure 4.23: Proteomics & analysis workflow for tRNA over-expression combined with heat stress. Schematic representation of the proteomics workflow to analyse the effect of tRNA over-expression on the response to heat stress. Flowchart on the left is a simplified depiction of the 30 °C vs. 37 °C analysis workflow (refer to figure 4.1). The flowchart on the right depicts the proteomics analysis undertaken to compare the wild-type yeast cells carrying a multi-copy plasmid containing tRNA tK^{UUU}, tQ^{UUG} and tE^{UUC} genes (ptKQE) and grown at 37 °C versus wild-type yeast cells carrying the empty-vector (pEV) and grown at 30 °C. To rule out biases resulting from the comparison of unequal number of identifications from the two datasets, only the commonly identified proteins were compared.

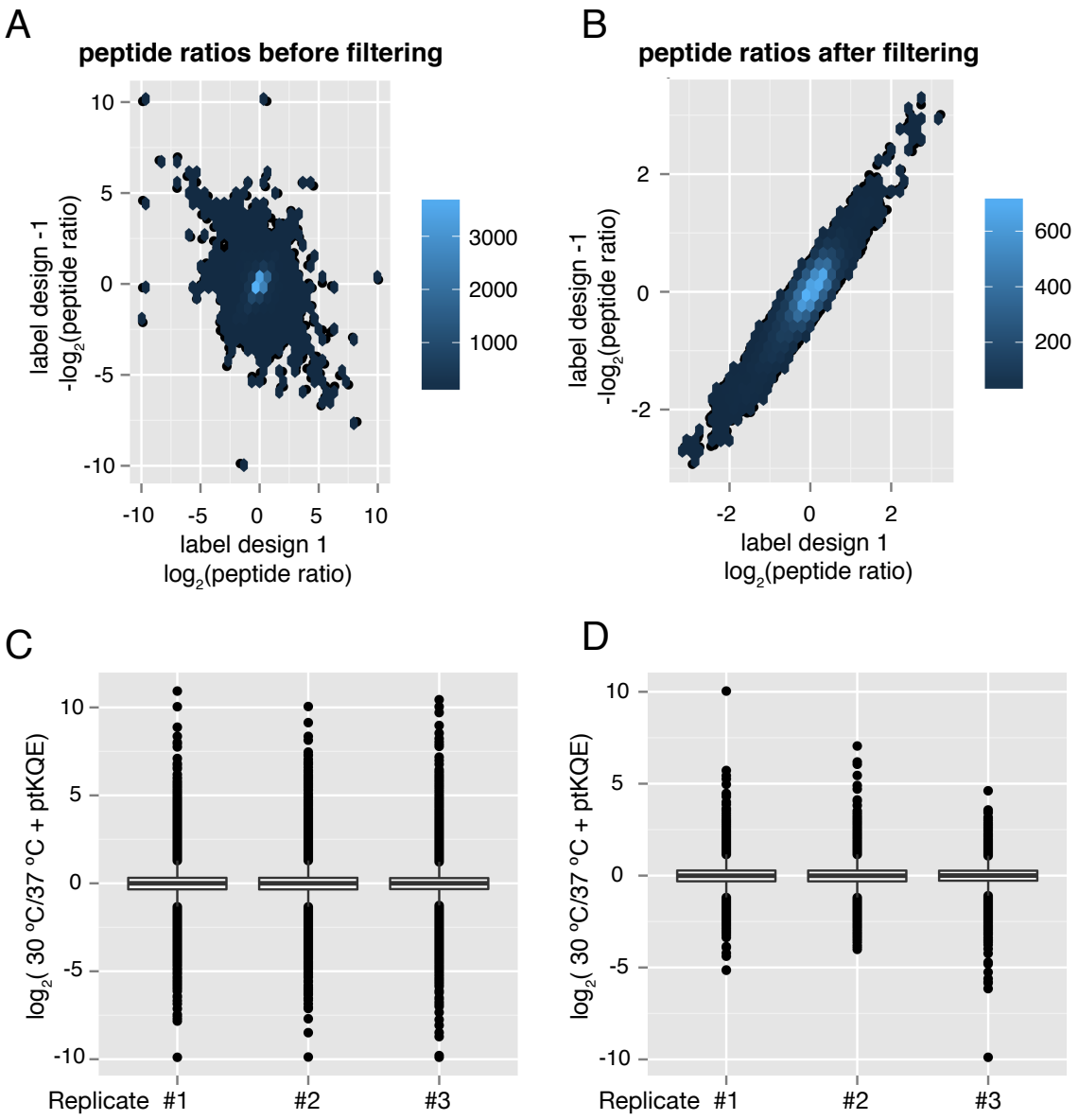

Figure 4.24: 30 °C vs 37 °C combined with tRNA over-expression proteomics label switch filter. SILAC labelling design for replicate number 2, was switched (denoted by label design -1) and the means of $\log_2$ of ratios of each peptide from the two designs were compared. The peptides that were not consistently quantified across the label switch conditions were filtered out. (A) and (B) represent the distribution of peptide ratios before and after label switch filter, respectively, in the form of a scatter plot of binned hexagonal tiles. The colour of the tiles represents the number of peptides binned into each tile and serves to indicate the density of the data in a given range of ratios. (C) and (D) Box and whisker plots of the protein ratios from the three biological replicates before and after peptide label switch filter. The box represents the inter quartile range (50% of the data) with the solid-line in the centre of the box representing the median of the peptide ratios.

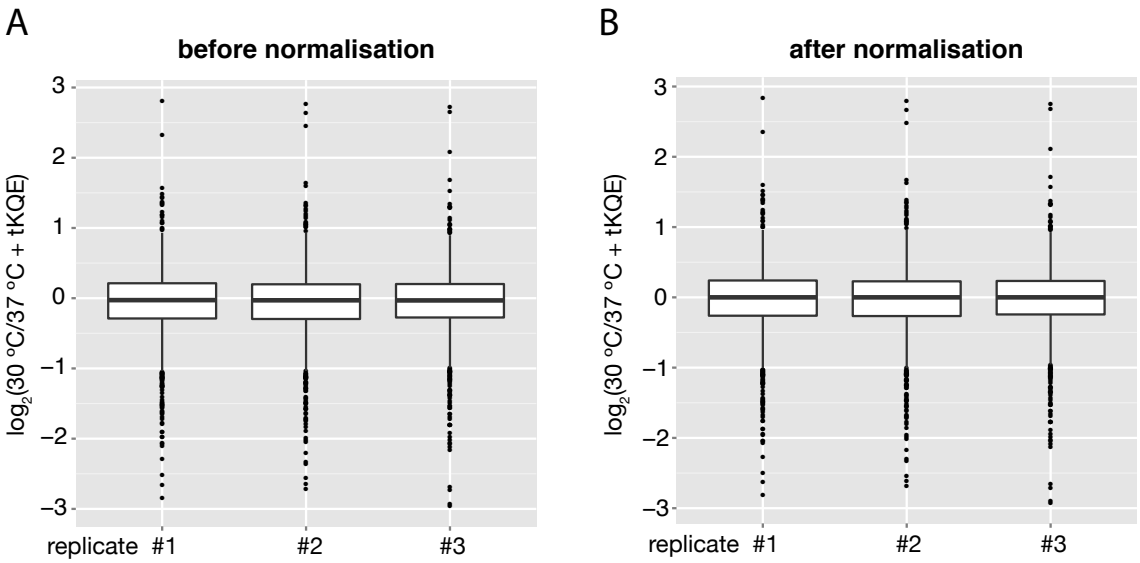

Figure 4.25: 30 °C vs 37 °C combined with tRNA over-expression proteomics data quality check and normalisation. Systematic inter-sample variances were checked and removed using median normalisation. (A) and (B) Box and whisker plots of the protein ratios from the three biological replicates before and after normalisation, respectively. The box represents the inter quartile range (50% of the data) with the solid-line in the centre of the box representing the median of the distribution of protein ratios.

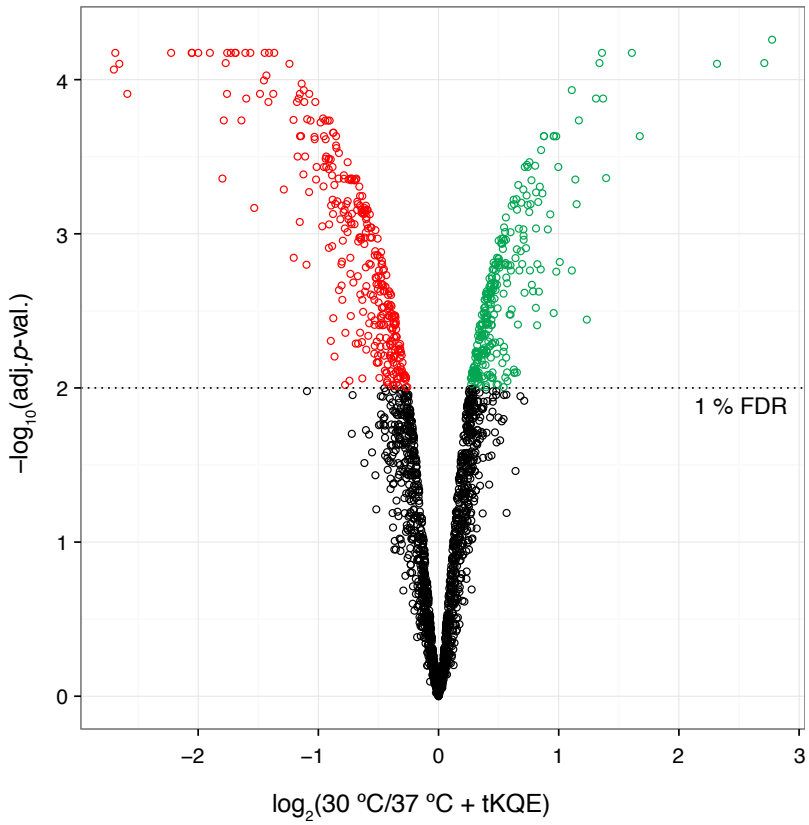

Figure 4.26: Volcano plot of tRNA over-expression proteomics analysis. Proteomes of wild-type (pEV) cells grown at 30 °C were compared with the wild-type cells over-expressing tRNA tK^{UUU}, tQ^{UUG} and tE^{UUC} (tKQE) and grown at 37 °C.

Relative protein abundance ratios were measure by the SILAC approach from three biological replicates and their statistical significance was calculated by Bayes normalised *t*-test and adjusted to control for the false discovery rate (FDR) using the Benjamini–Hochberg correction. The horizontal dotted line represents an FDR of 1% that was chosen as the threshold for statistical significance. Circles in red and green highlight the significantly up- and down-regulated proteins, respectively, in the ptKQE cells grown at 37 °C.

The common subset consisted of 1,881 proteins, out of which 547 proteins were significantly changing in the normal 30 °C vs. 37 °C dataset with 274 up- and 273 down-regulated. On the other hand, 611 of these proteins were of significantly different abundance in the 30 °C vs. ptKQE+37 °C dataset with 322 up- and 289 down-regulated proteins. A straightforward comparison of the significant protein abundance ratios from the two datasets showed high level of correlation (r = 0.86). However, comparing the results from the random forest analyses highlighted important differences between the two dataset. As shown in figure 4.27A, even in the subset of proteins common between the two datasets, the content of codons AAA and GAA was still important for classifying the proteins into up- or down-regulated classes. Over-expression of tRNAs tK^{UUU}, tQ^{UUG} and tE^{UUC} reduced the importance of AAA and GAA codons suggesting that the content of these two codons was no longer detrimental for translation. In other words, tRNA over-expression compensated for reduced tRNA thiolation. These results also indicated that reduced tRNA thiolation under heat stress regulates the expression of a specific subset of genes.

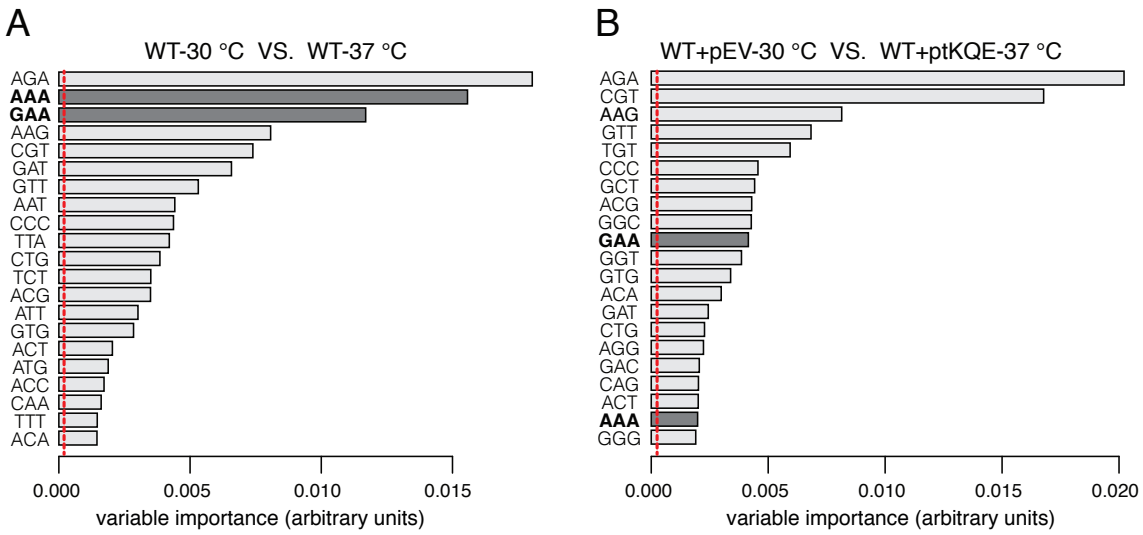

Figure 4.27: tRNA over-expression can compensate for reduced tRNA thiolation. Random forest analysis of up- and down-regulated proteins for codon content bias; for (A) the subset of the 30 °C vs. 37 °C dataset also seen in the tRNA over-expression experiment and (B) for the proteins from the tRNA over-expression experiment also seen in the 30 °C vs. 37 °C experiment. Red dashed line represents absolute value of the lowest predictor.

Table 4.3 shows the proteins that were no longer significantly down-regulated after the over-expression of tRNAs and whose corresponding genes were among the top 10% in the frequency of at least one of the codons AAA, CAA and GAA. This list is rich in the proteins that are either physical components of ribosomes or involved in their synthesis and also includes components of the mitochondrial F1F0 ATP synthase. This suggests that tRNA thiolation contributes to the response to heat stress by affecting the expression of genes involved in translation and respiration.

Table 4.3: Proteins rescued by tRNA over-expression. List of proteins that were significantly down-regulated in the normal 30 °C vs. 37 °C analysis, but not after the over-expression of tRNAs tK^{UUU}, tE^{UUC} and tQ^{UUG}. Highlighted in yellow are the proteins that have roles in translation and in blue are the subunits of F1F0 ATP synthase.

Systematic Name	Standard Name	Description
YAL025C	MAK16	Essential nuclear protein, constituent of 66S pre-ribosomal particles; required for maturation of 25S and 5.8S rRNAs; required for maintenance of M1 satellite double-stranded RNA of the L-A virus
YBL007C	SLA1	Cytoskeletal protein binding protein required for assembly of the cortical actin cytoskeleton; interacts with proteins regulating actin dynamics and proteins required for endocytosis; found in the nucleus and cell cortex; has 3 SH3 domains
YBL099W	ATP1	Alpha subunit of the F1 sector of mitochondrial F1F0 ATP synthase, which is a large, evolutionarily conserved enzyme complex required for ATP synthesis; phosphorylated
YBR245C	ISW1	Member of the imitation-switch (ISWI) class of ATP-dependent chromatin remodelling complexes; ATPase that forms a complex with Ioc2p and Ioc4p to regulate transcription elongation, and a complex with Ioc3p to repress transcription initiation
YCR077C	PAT1	Topoisomerase II-associated deadenylation-dependent mRNA-decapping factor; also required for faithful chromosome transmission, maintenance of rDNA locus stability, and protection of mRNA 3'-UTRs from trimming; functionally linked to Pab1p
YDL148C	NOP14	Nucleolar protein, forms a complex with Noc4p that mediates maturation and nuclear export of 40S ribosomal subunits; also present in the small subunit processome complex, which is required for processing of pre-18S rRNA
YDL153C	SAS10	Essential subunit of U3-containing Small Subunit (SSU) processome complex involved in production of 18S rRNA and assembly of small ribosomal subunit; disrupts silencing when overproduced; mutant has increased aneuploidy tolerance
YDR060W	MAK21	Constituent of 66S pre-ribosomal particles, required for large (60S) ribosomal subunit biogenesis; involved in nuclear export of pre-ribosomes; required for maintenance of dsRNA virus; homolog of human CAATT-binding protein
YDR279W	RNH202	Ribonuclease H2 subunit, required for RNase H2 activity; related to human AGS2 that causes Aicardi-Goutieres syndrome
YDR292C	SRP101	Signal recognition particle (SRP) receptor alpha subunit; contain GTPase domains; involved in SRP-dependent protein targeting; interacts with the beta subunit, Srp102p
YFL045C	SEC53	Phosphomannomutase, involved in synthesis of GDP-mannose and dolichol-phosphate-mannose; required for folding and glycosylation of secretory proteins in the ER lumen
YGL076C	RPL7A	Protein component of the large (60S) ribosomal subunit, nearly identical to Rpl7Bp and has similarity to E. coli L30 and rat L7 ribosomal proteins; contains a conserved C-terminal Nucleic acid Binding Domain (NDB2)
YHL015W	RPS20	Protein component of the small (40S) ribosomal subunit; overproduction suppresses mutations affecting RNA polymerase III-dependent transcription; has similarity to E. coli S10 and rat S20 ribosomal proteins
YHR027C	RPN1	Non-ATPase base subunit of the 19S regulatory particle of the 26S proteasome; may participate in the recognition of several ligands of the proteasome; contains a leucine-rich repeat (LRR) domain, a site for protein-protein interactions

Systematic Name	Standard Name	Description
YJL148W	RPA34	RNA polymerase I subunit A34.5
YJR007W	SUI2	Alpha subunit of the translation initiation factor eIF2, involved in the identification of the start codon; phosphorylation of Ser51 is required for regulation of translation by inhibiting the exchange of GDP for GTP
YJR121W	ATP2	Beta subunit of the F1 sector of mitochondrial F1F0 ATP synthase, which is a large, evolutionarily conserved enzyme complex required for ATP synthesis; phosphorylated
YKL009W	MRT4	Protein involved in mRNA turnover and ribosome assembly, localizes to the nucleolus
YKR006C	MRPL13	Mitochondrial ribosomal protein of the large subunit, not essential for mitochondrial translation
YKR016W	FCJ1	Mitochondrial inner membrane protein involved in formation and molecular structure of cristae junctions; impairs oligomerization of F1F0-ATP synthase; null shows altered mitochondrial morphology and abnormal mitochondrial genome maintenance
YNL016W	PUB1	Poly (A)+ RNA-binding protein, abundant mRNP-component protein that binds mRNA and is required for stability of many mRNAs; component of glucose deprivation induced stress granules, involved in P-body-dependent granule assembly
YNL251C	NRD1	RNA-binding protein, subunit of Nrd1 complex (Nrd1p-Nab3p-Sen1p); complex mediates termination of snoRNAs and cryptic unstable transcripts (CUTs); interacts with the C-terminal domain of the RNA polymerase II large subunit (Rpo21p), preferentially at phosphorylated Ser5; H3K4 trimethylation of transcribed regions by Set1p enhances recruitment of Nrd1p to those sites; required for 3' end maturation of nonpolyadenylated RNAs
YNL302C	RPS19B	Protein component of the small (40S) ribosomal subunit, required for assembly and maturation of pre-40 S particles; mutations in human RPS19 are associated with Diamond Blackfan anemia; nearly identical to Rps19Ap
YOL077C	BRX1	Nucleolar protein, constituent of 66S pre-ribosomal particles; depletion leads to defects in rRNA processing and a block in the assembly of large ribosomal subunits; possesses a sigma(70)-like RNA-binding motif
YOL080C	REX4	Putative RNA exonuclease possibly involved in pre-rRNA processing and ribosome assembly
YOR206W	NOC2	Protein that forms a nucleolar complex with Mak21p that binds to 90S and 66S pre-ribosomes, as well as a nuclear complex with Noc3p that binds to 66S pre-ribosomes; both complexes mediate intranuclear transport of ribosomal precursors
YPL004C	LSP1	Primary component of eisosomes, which are large immobile patch structures at the cell cortex associated with endocytosis, along with Pil1p and Sur7p; null mutants show activation of Pkc1p/Ypk1p stress resistance pathways; member of the BAR domain family
YPL199C	YPL199C	Putative protein of unknown function, predicted to be palmitoylated
YPL210C	SRP72	Core component of the signal recognition particle (SRP) ribonucleoprotein (RNP) complex that functions in targeting nascent secretory proteins to the endoplasmic reticulum (ER) membrane
YPR072W	NOT5	Subunit of the CCR4-NOT complex, which is a global transcriptional regulator with roles in transcription initiation and elongation and in mRNA degradation

4.3 Discussion

4.3.1 Response to prolonged heat stress

Heat is one of the most fundamental stresses with even a slight change in ambient temperature capable of altering the chemical environment of a cell. Therefore, cells adjust their metabolic processes in order to survive and repair the damage caused by changes in the extracellular temperature. In *S. cerevisiae*, a short exposure to a stress, like heat shock, causes transient changes in the expression of several genes that subside as the cells adapt to new growth conditions (Causton et al. 2001; Gasch et al. 2000). In the present study, proteomics analysis showed that even after a prolonged exposure to heat, cells continued to regulate the expression of several genes that are known to play important roles in response to heat and other shocks. For instance, cellular levels of HSPs and chaperones were significantly up-regulated. Since a temperature of 37 °C is considered a mild challenge under which no substantial protein denaturation occurs (Nathan, Vos, and Lindquist 1997; Verghese et al. 2012), up-regulation of HSPs and chaperones might seem unnecessary. However, exposure to a mild heat stress is known to confer tolerance to a second, more severe exposure and the elevated levels of protective proteins could help in coping with the cellular damage. The exact mechanism behind this acquired heat tolerance is not known, except that Hsp104p activity is required (Sanchez and Lindquist 1990; Elliott, Haltiwanger, and Futcher 1996). Hsp104p is a disaggregase that works in conjunction with other chaperones and co-chaperones from the Hsp70 and Hsp40 families respectively (Verghese et al. 2012). Additionally, several proteins require assistance from chaperones for their proper folding and translocation to various organelles even under standard conditions. As the free energy of folding depends on the temperature (Baldwin

1986; Scalley and Baker 1997; Cooper 1999), the chances of a partially folded protein getting stuck in a local minimum of the protein folding energy landscape increase with increasing temperature, making chaperone assisted *de novo* protein folding even more crucial under heat stress.

Along the same lines, many of the proteins that were found to be significantly down-regulated in cells growing at 37 °C have roles in the process of protein synthesis. Protein synthesis is a very energy expensive process (more than 50% of transcription initiation events involving RNA polymerase-II are triggered on genes coding for ribosomal protein (Warner 1999)). The synthesis of RNA components of the translational machinery also requires large amounts of ATP. Therefore, cells prefer to slow down translation to preserve energy under stressful conditions (Gasch and Werner-Washburne 2002; Gasch 2002). Additionally, a reduced rate of translation could give newly translated proteins more time to fold and repair potential stress induced damage. Collectively, up-regulation of protective factors and down-regulation of protein translation at 37 °C should enhance the survival against not only the damage caused by the present stress, but also against a more severe future heat-shock.

Accumulation of trehalose is another important factor for acquired tolerance. Trehalose suppresses aggregation of unfolded proteins and stabilises partially folded proteins (Singer and Lindquist 1998b; Singer and Lindquist 1998a). Interestingly, our proteomics analysis showed concurrent up-regulation of enzymes involved in, both, trehalose synthesis and degradation. The seemingly puzzling mechanism behind trehalose accumulation can be understood by considering the effect of temperature on the kinetics of the trehalose cycle enzymes (Fonseca, Chen, and Voit 2012; Neves and François 1992). Tps1p

and Tps2p, enzymes involved in trehalose biosynthesis, have optimal activity between 35-40 °C. On the other hand, the trehalase activity of Nth1p is optimal at around 30 °C. This allows trehalose synthesis and degradation to rapidly respond to changing temperature. Expectedly, thermotolerance induced by trehalose accumulation is transient as cells degrade this sugar once the stress subsides (Gross and Watson 1998; De Virgilio et al. 1994).

Another aspect of acquired tolerance is the cross protection against other kinds of insults (Verghese et al. 2012). For example, many studies have found that a mild heat shock confers protection against subsequent oxidative stress ((Berry and Gasch 2008; Verghese et al. 2012) and references therein). In fact, heat stress itself is known to cause a secondary oxidative stress in a process that is linked to the electron-transport chain (Davidson et al. 1996; Davidson and Schiestl 2001). In this study, cells growing at 37 °C were found to up-regulate glycolysis and gluconeogenesis, and down-regulate energy production by oxidative phosphorylation. This switch is consistent with the requirement for faster energy production during stress and also for the increased synthesis of protective molecules like trehalose and glycerol. We also found increased activity through the pentose phosphate shunt pathway (PPP) that provides the vital NADPH to defend against the oxidative stress caused by elevated temperatures (Gasch 2002; Morano, Grant, and Moye-Rowley 2012). Furthermore, reducing the activity of the electron transport chain and oxidative phosphorylation could help diminish reactive oxygen species (ROS) (M. P. Murphy 2009). However, *S. cerevisiae* is a Crabtree positive organism that ferments glucose even in the presence of oxygen. Therefore, the actual purpose of this switch in energy production remains to be established.

Consistent with the acquisition of cross protection, proteins involved in the biosynthesis of glycerol were also found to be up-regulated. Accumulation of glycerol plays an important role in osmoprotection (Nevoigt and Stahl 2006), its synthesis is known to be induced under oxidative stress (Pahlman et al. 2001) and yeast cells unable to synthesise glycerol are temperature sensitive (Siderius et al. 2000). Overall, results from the proteomics analysis suggest that cells growing at 37 °C continue to balance their cellular-processes to manage the challenges posed by the present stress and, more importantly, are prepared to defend against a future insult.

4.3.2 Reduced thiolation contributes to the heat stress response

Micro-array based analyses have been instrumental in understanding the regulation of gene expression in the HSR (Gasch et al. 2000). However, transcriptomics studies alone can not gauge the involvement of protein synthesis, modification and degradation. In this study, by directly measuring protein abundance changes in yeast cells grown at an elevated temperature, we discovered that the *URM1*-pathway activity is post-translationally regulated to reduce tRNA thiolation and consequently, the levels of $mcm^5s^2U_{34}$. In the previous chapter, the absence of tRNA thiolation caused by the disruption of the URM1-pathway was found to result in the reduced translation of genes biased in the content of AAA, CAA and GAA codons. Several of these genes code for the proteins that have important roles in the process of protein synthesis. Overall, it also resulted in the up-regulation of stress response pathways and down-regulation of growth. Consistent with these observations, in this chapter we have shown that, the over-expression of tRNAs tK^{UUU}, tQ^{UUG} and tE^{UUC} in

cells exposed to heat stress demonstrated that the diminished URM1-pathway activity leads to the reduced translation of some ribosomal proteins and proteins involved in their synthesis and assembly. Unexpectedly, our unbiased analysis also identified the down-regulation of genes rich in the AGA codon. Since the levels of the mcm^5 modification were unaffected in tR^{UCU}, one likely explanation is that the AGA codon rich genes are transcriptionally down-regulated under heat stress. Remarkably, we found that unlike in yeast, tR^{UCU} from human cells is thiolated, which means that differential thiolation of tRNAs could potentially affect the expression of genes rich in codons AAA, CAA, GAA and AGA in humans. It is tempting to speculate that thiolation on tR^{UCU} could have evolved to attain better control on the translational capacity of the cells.

In addition to heat stress, starvation for sulfur amino acids also caused a reduction in the levels of tRNA thiolation. Interestingly, yeast cells growing in an all-amino acid rich media induce autophagy when shifted to a medium lacking sulfur amino acids (Sutter et al. 2013). This form of autophagy is termed as non-nitrogen starvation induced (NNS) autophagy as it is induced even in the presence of nitrogen sources in the growth medium (X. Wu and Tu 2011). Autophagy involves the mobilisation of resources by degrading cellular components during the period of nutrient limitation and can be triggered in response to several kinds of stresses (Kroemer, Mariño, and Levine 2010). Micro-array analyses have shown that the stress response triggered by amino acid starvation and nitrogen depletion includes down-regulation of the protein synthesis machinery (Gasch et al. 2000). Additionally, mature ribosomes are degraded (ribophagy) during autophagy to not only reduce the energy expensive process of protein synthesis, but also to free up amino acids and

nucleic acids for other cellular processes (Kraft et al. 2008; Beau, Esclatine, and Codogno 2008). This way, autophagy and reduced translational capacity contribute towards the management of stress induced by amino acid starvation (Lempiäinen and Shore 2009). We have not measured the protein abundance changes caused by starvation for sulfur amino acids in this study. However, we speculate that reduced tRNA thiolation should play a similar role in the defense against sulfur amino acid limitation like it does under heat stress by reducing translation and upregulating stress response pathways. Interestingly, ribose methylation is one of the two main post-transcriptional modifications found on rRNA. AdoMet, a metabolite of the sulfur amino acid metabolism pathway, is the principal methyl donor involved in the transmethylation reactions occurring inside a cell. Therefore, reduced availability of AdoMet could be one of the reasons to down-regulate ribosome biogenesis and up-regulate autophagy.

In conclusion, our results indicate that the down-regulation of $mcm^5s^2U_{34}$ contributes to the management of environmental stress by reducing protein synthesis rates and cellular growth, thereby helping to conserve energy and nutrients, allowing additional time for proteins to reach a fully folded native state and assisting in the maintenance of proteome homeostasis - that is, an improved ability to survive stress. Consistent with this notion, *URM1*-pathway mutant strains were recently found to maintain viability in stationary phase for longer than wild-type cells (Laxman et al. 2013).

4.3.3 Multiple mechanisms regulate tRNA thiolation

In vivo thiolation of wobble uridines of the eukaryotic cytoplasmic tRNAs tK^{UUU}, tQ^{UUG} and tE^{UUC} requires the presence of at least four active proteins from the *URM1*-pathway. Namely, Uba4p, Urm1p, Ncs2p and Ncs6p, as the absence of either of these proteins leads to the complete loss of s^2 modification. Our results in addition to those from Laxman et al. (2013) indicate that depending on the nature of stress, cells use different mechanisms to reduce the extent of wobble uridine modification. Interestingly, conjugation of Urm1p to the Lys residues of target proteins (urmylation) has been reported in yeast cells treated with oxidising agents (Van der Veen et al. 2011). This suggests that URM1-pathway might play a role in response to stress via multiple protein and RNA modifications. It will be interesting to understand the functional relevance of urmylation and to figure out if and how it is connected to tRNA thiolation. We did not observe a reduction in the functionally similar mcm^5 modification, but concurrent loss of the mcm^5 and s^2 modifications is lethal in yeast (Bjork et al. 2007; Leidel et al. 2009). Therefore, simultaneous reduction in the levels of both modifications might be undesirable. Nevertheless, it is worth noting that the phosphorylation of Elp1p can modulate the activity of the *ELP*-complex (Fichtner et al. 2003; Mehlgarten et al. 2009), suggesting that the biosynthesis of mcm^5 and ncm^5 modifications can also be regulated.

Remarkably, we found that the high temperature growth causative variant of *NCS2* (*ncs2_A212T*) (Sinha et al. 2008) caused de-coupling of tRNA thiolation levels from heat stress. Even though the presence of Ncs2p is essential for tRNA thiolation, its exact role in the URM1-pathway is not known. Ncs2p shares some sequence motives with Ncs6p, but lacks the residues typically required to

form a PP-loop motif (SGGxDS) (Leidel et al. 2009). Therefore, it is not likely to have the catalytic ability of a PP-loop ATPase. However, Ncs2p and Ncs6p have been suggested to form a complex that activates the target tRNAs for thiolation (Leidel et al. 2009; Dewez et al. 2008; Y. Nakai, Nakai, and Hayashi 2008). Since proteasomal activity was required for the down-regulation of tRNA thiolation, it is possible that the variant form of Ncs2p somehow stabilises the Ncs2p-Ncs6p complex and prevents its degradation. Alternatively, it could enhance the catalytic activity of Ncs6p because of which even reduced amounts of the proteins might be sufficient to maintain tRNA thiolation. Identification of the exact role of Ncs2p and mechanism behind the observed deregulation will require further analysis. Similarly, systematic analyses will be needed to unearth the molecular factors involved in the signalling pathways that impinge upon the *URM1*-pathway activity to down-regulate tRNA thiolation. In this study, we identified the involvement of proteasome in mediating tRNA hypothiolation by using two temperature sensitive mutants. Similarly, yeast gene deletion and temperature sensitive collections can be screened to identify the proteins whose activity is required for the regulation of tRNA thiolation.

5. Conclusions and Outlook

The presence of mcm^5 and s^2 modified U_{34} in the eukaryotic cytoplasmic tRNAs was discovered decades ago (Baczynskyj, Biemann, and Hall 1968; Yoshida, Takeishi, and Ukita 1971; Madison, Boguslawski, and Teetor 1972). Since then, the biosynthetic pathways as well as the phenotypes associated with these modifications have been identified (Esberg et al. 2006; Johansson et al. 2008; Leidel et al. 2009; Pedrioli, Leidel, and Hofmann 2008). However their biological relevance has remained elusive. Several biophysical and *in vitro* ribosomal binding and translation studies had investigated the effect of these modifications on the decoding properties of tRNAs (Yarian et al. 2000; Sekiya, Takeishi, and Ukita 1969; Agris et al. 1992; Sen and Ghosh 1976). However, *in vivo* translation is a complex multifactorial process and experiments conducted in isolated systems can not fully recapitulate the biological role of RNA nucleotide modifications. Additionally, it was not known whether the levels of these modifications were modulated with changes in the physiological conditions. This was the state of research before the start of my presented doctoral work.

We conducted comprehensive proteomics analyses of yeast mutants unable to synthesise $mcm^5s^2U_{34}$. Interestingly, the majority of the proteome was not differentially affected by the absence of this doubly modified uridine. Furthermore, even the differentially expressed fraction of the proteome showed only small changes in abundance. These changes could only be significantly detected through the development and application of a robust statistical quantitative proteomics workflow. Using an unbiased data-driven approach, we found that, *in vivo* and under normal conditions, the translation of mRNAs strongly biased in the content of codons AAA, CAA , and GAA is reduced in the mutant cells unable to synthesise $mcm^5s^2U_{34}$. Importantly, we also identified

that the absence of $mcm^5s^2U_{34}$ leads to down-regulation of protein synthesis and growth and to up-regulation of proteolysis and stress response pathways. These results prompted us to carry out an in-depth proteomics analysis of the heat stress response in budding yeast, which had previously been extensively studied by transcriptomics analyses (Gasch et al. 2000; Causton et al. 2001). We discovered that in response to prolonged heat stress the *URM1*-pathway activity is modulated and tRNA thiolation is reduced. We also found a similar reduction in response to starvation for sulfur containing amino acids. Interestingly, the response to these stress sources was controlled by independent mechanisms. Using an unbiased data-driven approach, we found that under heat stress, modulation of tRNA thiolation is used to regulate the cellular translational capacity during unfavourable growth conditions. In conclusion, we showed that $mcm^5s^2U_{34}$ promotes efficient translation of a proteome subset to maximise cellular growth under standard conditions. Whereas, during stress, cells modulate the level of $mcm^5s^2U_{34}$ to balance growth with repair and maintain proteome homeostasis.

The homologs of the *ELP*- and *URM1*-pathway members have been conserved throughout evolution. So far, $mcm^5s^2U_{34}$ has been detected in tRNAs of several higher eukaryotes like plants, worms, rats and humans (Mehlgarten et al. 2010, C. Chen et al 2009, J. C. Chan et al. 1982, Durant et al. 2005). Moreover, mutations in the *ELP*- or *URM1*-pathway genes have been reported to cause physiological defects in these organisms (Dewez et al. 2008; C. Chen et al 2009; Veen 2011; Y.-T. Chen et al. 2009; Walker et al. 2011; Singh et al. 2010). Importantly, mutations in the *ELP*-genes in humans are associated with complex neurological disorders (Torres et al 2014) and mice with disruption in

the *URM1*- or *ELP*-pathways fail to generate offsprings (Veen 2011; Y.-T. Chen et al. 2009). Given the conservation of ribosomes and other translation components among eukaryotes, the consequence of the absence of $mcm^5s^2U_{34}$ at the molecular level are also likely to be similar. However, the same can not be assumed for their effect on cellular processes. For instance, the sequence of mature tRNAs is known for only 19 out of 49 tRNA isoacceptors in humans (Yacoubi, Bailly, and de Crécy-Lagard 2012). We have shown here that tR^{UCU} from a human cell line is thiolated. Additionally, mcm^5U was not detectable in worms (C. Chen, Tuck, and Byström 2009), suggesting that wobble uridine modification pattern differs slightly in different organisms. Therefore, to understand the role of the *ELP*- and *URM1*-pathway mutations in humans, it is essential to first determine which tRNAs are modified by the two pathways. Purification of individual tRNAs and analysis of modified nucleosides by mass spectrometry, like we have demonstrated in this study, is one way of doing it. However, humans and other higher eukaryotes code multiple isodecoders for a tRNA (having the same anticodon but with variations in the rest of tRNA) that could have differential expression and/or modification levels in different tissues or during different developmental stages (Goodenbour and Pan 2006). Therefore, a workflow is needed that can be used to measure the levels of modified/unmodified pools of tRNAs from multiple samples in a high throughput manner. It is also important to stress that the *ELP*- and *URM1*-pathways have been associated with modification of several targets in addition to tRNAs. In yeast, several studies, including this one, have used biochemical approaches such as tRNA over-expression to prove that the phenotypes associated with mutations in the *ELP*- and *URM1*-pathways are caused by the loss of their tRNA modifying activity. Similar experiments are needed in mammalian cells to

prove that the tRNA hypomodification is causative of diseases. Additionally, the consequences of differential translation caused by loss of the *ELP-* and *URM1-* pathway activity on the cellular processes needs to be investigated in mammalian models in connection with the pathophysiology of the associated physiological defects.

Our results connect tRNA thiolation with the pathways involved in protein turnover and cellular growth, which in humans are implicated in age related diseases such as Alzheimer's and Parkinson's diseases (Powers et al. 2009; Hartl, Bracher, and Hayer-Hartl 2011) and cancer (Liu and Ye 2011; Niforou, Cheimonidou, and Trougakos 2014; U. Begley et al. 2013), respectively. Interestingly, the human *TRM9* like gene (yeast *TRM9* is required for the biosynthesis of the mcm^5 modification) is silenced in several cancers and its re-expression was found to suppress tumourigenecity (U. Begley et al. 2013). Therefore, investigation of the regulation of the mcm^5 and s^2U modifications in response to extracellular cues in higher eukaryotes should also be of considerable interest. Along the same lines, the levels of several tRNA modifications have been reported to change after treatment with oxidative stress inducing chemicals (C. T. Y. Chan et al. 2010). We have also found that the levels of several other proteins involved in post-transcriptional modifications of RNAs were changing in response to heat stress, suggesting that RNA nucleotide modifications have wider regulatory roles. Nearly all RNA types are known to be post-transcriptionally modified. With more functions of the non-coding RNAs being continuously discovered, investigation of the role and regulation of RNA nucleotide modifications has become all the more interesting and important. This thesis presents the first comprehensive system level study

of the functional importance of a post-transcriptionally modified tRNA nucleotide. The discussed experimental and analytical approaches should be useful in designing future experiments to study nucleotide modifications in not just tRNAs, but also in other RNAs.

Mass spectrometry is a fast evolving field. Even during the relatively short duration of my PhD, novel workflows have been introduced, which we have adapted. From using the latest mass spectrometer, uHPLC and long columns for improved separation, addition of DMSO to improve ionisation and sample preparation with the FASP methodology, to using multiple peptide search engines and data analysis with the TPP, we implemented most of the current developments in the field and that allowed us to identify and quantify thousands of proteins in a high throughput fashion. Additionally, this dissertation showcases the various computational tools that were developed in our own group, such as a MySQL based relational database called Prometheus that stores data from proteomics, phenotypic, bioinformatics and various other analyses and makes it possible to correlate the results from different studies. We also developed several R-scripts for the visualisation of data by using packages like ggplot2 and the implementation of LIMMA and other packages that were originally developed for the statistical analysis of transcriptomics data. Lastly, the use of a label switch filter that exploits the labelling information of peptides and removes the erroneously quantified peptides. The vast amount of data generated by high-throughput technologies, such as mass spectrometry, can not be interrogated in a meaningful manner without the use of such tools. Therefore, the tools and approaches used during this project should prove to be a significant contribution towards the field of proteomics in general and should

be useful for other proteomics studies (for example, (Ritorto et al. 2013; Baron et al. 2014)).

6. References

Aebersold, Ruedi, and Matthias Mann. 2003. “Mass Spectrometry-Based Proteomics.” *Nature* 422 (6928): 198–207. doi:10.1038/nature01511.

Agris, Paul F. 2004. “Decoding the Genome: a Modified View..” *Nucleic Acids Research* 32 (1): 223–38. doi:10.1093/nar/gkh185.

Agris, Paul, Hanna Sierzputowska-Gracz, Wanda Smith, A Malkiewicz, Elzbieta Sochacka, and Barbara Nawrot. 1992. “Thiolation of Uridine Carbon-2 Restricts the Motional Dynamics of the Transfer RNA Wobble Position Nucleoside.” *Journal of the American Chemical Society* 114 (7): 2652–56. doi:10.1021/ja00033a044.

Anderson, S L, R Coli, I W Daly, E A Kichula, M J Rork, S A Volpi, J Ekstein, and B Y Rubin. 2001. “Familial Dysautonomia Is Caused by Mutations of the IKAP Gene..” *American Journal of Human Genetics* 68 (3): 753–58. doi:10.1086/318808.

Arias, Patricia, Sonia Díez-Muñiz, Raúl García, César Nombela, José M Rodríguez-Peña, and Javier Arroyo. 1997. “Genome-Wide Survey of Yeast Mutations Leading to Activation of the Yeast Cell Integrity MAPK Pathway: Novel Insights Into Diverse MAPK Outcomes.” *Yeast (Chichester, England)* 13 (11): 1065–75. doi:10.1002/(SICI)1097-0061(19970915)13:11<1065::AID-YEA159>3.0.CO;2-K.

Ashraf, S, E Sochacka, R Cain, R Guenther, A Malkiewicz, and P Agris. 1999. “Single Atom Modification (O-->S) of tRNA Confers Ribosome Binding.” *RNA (New York, NY)* 5 (2): 188–94.

Back, Sung Hoon, Martin Schröder, Kyungho Lee, Kezhong Zhang, and Randal J Kaufman. 2005. “ER Stress Signaling by Regulated Splicing: IRE1/HAC1/XBP1.” *Methods (San Diego, Calif)* 35 (4): 395–416. doi:10.1016/j.ymeth.2005.03.001.

Baczynskyj, L, K Biemann, and R H Hall. 1968. “Sulfur-Containing Nucleoside From Yeast Transfer Ribonucleic Acid: 2-Thio-5(or 6)-Uridine Acetic Acid Methyl Ester..” *Science (New York, NY)* 159 (3822): 1481–83.

Baldwin, R L. 1986. “Temperature Dependence of the Hydrophobic Interaction in Protein Folding..” *Proceedings of the National Academy of Sciences of the United States of America* 83 (21): 8069–72.

Baron, Yorann, Patrick G Pedrioli, kshitiz Tyagi, Clare Johnson, Nicola T Wood, Daniel Fountaine, Melanie Wightman, and Gabriela Alexandru. 2014. “VAPB/ALS8 Interacts with FFAT-Like Proteins Including the P97 Cofactor FAF1 and the ASNA1 ATPase.” *BMC Biology* 12 (1). BioMed Central Ltd: 39. doi:10.1074/jbc.C700106200.

Beau, Isabelle, Audrey Esclatine, and Patrice Codogno. 2008. “Lost to Translation: When Autophagy Targets Mature Ribosomes..” *Trends Cell Biol.* 18 (7): 311–14. doi:10.1016/j.tcb.2008.05.001.

Begley, Ulrike, Maria Soledad Sosa, Alvaro Avivar-Valderas, Ashish Patil, Lauren Endres, Yeriel Estrada, Clement T Y Chan, et al. 2013. “A Human tRNA Methyltransferase 9-Like Protein Prevents Tumour Growth by Regulating LIN9 and HIF1-A.” *EMBO Molecular Medicine*, February. doi: 10.1002/emmm.201201161.

Berry, David B, and Audrey P Gasch. 2008. “Stress-Activated Genomic Expression Changes Serve a Preparative Role for Impending Stress in Yeast..” *Molecular Biology of the Cell* 19 (11): 4580–87. doi:10.1091/mbc.E07-07-0680.

Beuning, P J, and K Musier-Forsyth. 1999. “Transfer RNA Recognition by Aminoacyl-tRNA Synthetases..” *Biopolymers* 52 (1): 1–28. doi:10.1002/(SICI)1097-0282(1999)52:1<1::AID-BIP1>3.0.CO;2-W.

Bjork, G, B Huang, O Persson, and A Bystrom. 2007. “A Conserved Modified Wobble Nucleoside (mcm5s2U) in Lysyl-tRNA Is Required for Viability in Yeast.” *RNA (New York, NY)* 13: 1245–55.

Breci, Linda, Emily Hattrup, Matthew Keeler, Jessica Letarte, Roxanne Johnson, and Paul A Haynes. 2005. “Comprehensive Proteomics in Yeast Using Chromatographic Fractionation, Gas Phase Fractionation, Protein Gel Electrophoresis, and Isoelectric Focusing..” *Proteomics* 5 (8): 2018–28. doi:10.1002/pmic.200401103.

Bullinger, Dino, Richard Fux, Graeme Nicholson, Stefan Plontke, Claus Belka, Stefan Laufer, Christoph H Gleiter, and Bernd Kammerer. 2008. “Identification of Urinary Modified Nucleosides and Ribosylated Metabolites in Humans via Combined ESI-FTICR MS and ESI-IT MS Analysis..” *Journal of the American Society for Mass Spectrometry* 19 (10): 1500–1513. doi:10.1016/j.jasms.2008.06.015.

Burroughs, A Maxwell, S Balaji, Lakshminarayan M Iyer, and Aravind L. 2007. “Small but Versatile: the Extraordinary Functional and Structural Diversity of the B-Grasp Fold.” *Biology Direct* 2 (1). BioMed Central Ltd: 18. doi: 10.1186/1745-6150-2-18.

Cantara, W A, P F Crain, J Rozenski, J A McCloskey, K A Harris, X Zhang, F A P Vendeix, D Fabris, and P F Agris. 2010. “The RNA Modification Database, RNAMDB: 2011 Update.” *Nucleic Acids Research* 39 (Database): D195–D201. doi:10.1093/nar/gkq1028.

Causton, H C, B Ren, S S Koh, C T Harbison, E Kanin, E G Jennings, T I Lee, H L True, E S Lander, and R A Young. 2001. “Remodeling of Yeast

Genome Expression in Response to Environmental Changes..” *Molecular Biology of the Cell* 12 (2): 323–37.

Chan, Clement T Y, Madhu Dyavaiah, Michael S DeMott, Koli Taghizadeh, Peter C Dedon, and Thomas J Begley. 2010. “A Quantitative Systems Approach Reveals Dynamic Control of tRNA Modifications During Cellular Stress..” *PLoS Genetics* 6 (12): e1001247–. doi:10.1371/journal.pgen.1001247.

Chan, J C, J A Yang, M J Dunn, P F Agris, and T W Wong. 1982. “The Nucleotide Sequence of a Glutamate tRNA From Rat Liver..” *Nucleic Acids Research* 10 (15): 4605–8.

Chen, Changchun, Bo Huang, James T Anderson, and Anders S Byström. 2011. “Unexpected Accumulation of Ncm(5)U and Ncm(5)S(2) (U) in a Trm9 Mutant Suggests an Additional Step in the Synthesis of Mcm(5)U and Mcm(5)S(2)U.” *PLoS ONE* 6 (6): e20783. doi:10.1371/journal.pone.0020783.

Chen, Changchun, Bo Huang, Mattias Eliasson, Patrik Rydén, and Anders S Byström. 2011. “Elongator Complex Influences Telomeric Gene Silencing and DNA Damage Response by Its Role in Wobble Uridine tRNA Modification.” *PLoS Genetics* 7 (9). Public Library of Science: e1002258. doi:10.1371/journal.pgen.1002258.

Chen, Changchun, Simon Tuck, and Anders S Byström. 2009. “Defects in tRNA Modification Associated with Neurological and Developmental Dysfunctions in Caenorhabditis Elegans Elongator Mutants..” *PLoS Genetics* 5 (7): e1000561. doi:10.1371/journal.pgen.1000561.

Chen, Xi, and Hemant Ishwaran. 2012. “Random Forests for Genomic Data Analysis.” *Genomics* 99 (6): 323–29. doi:10.1016/j.ygeno.2012.04.003.

Chen, Yei-Tsung, Matthew M Hims, Ranjit S Shetty, James Mull, Lijuan Liu, Maire Leyne, and Susan A Slaugenhaupt. 2009. “Loss of Mouse Ikbkap, a Subunit of Elongator, Leads to Transcriptional Deficits and Embryonic Lethality That Can Be Rescued by Human IKBKAP..” *Molecular and Cellular Biology* 29 (3): 736–44. doi:10.1128/MCB.01313-08.

Chenau, Jérôme, Sylvie Michelland, Jonathan Sidibe, and Michel Seve. 2008. “Peptides OFFGEL Electrophoresis: a Suitable Pre-Analytical Step for Complex Eukaryotic Samples Fractionation Compatible with Quantitative iTRAQ Labeling.” *Proteome Science* 6: 9. doi:10.1186/1477-5956-6-9.

Choi, Hyungwon, and Alexey I Nesvizhskii. 2008. “False Discovery Rates and Related Statistical Concepts in Mass Spectrometry-Based Proteomics.” *Journal of Proteome Research* 7 (1): 47–50. doi:10.1021/pr700747q.

Close, Pierre, Nicola Hawkes, Isabelle Cornez, Catherine Creppe, Charles A Lambert, Bernard Rogister, Ulrich Siebenlist, et al. 2006. “Transcription

Impairment and Cell Migration Defects in Elongator-Depleted Cells: Implication for Familial Dysautonomia..” *Molecular Cell* 22 (4): 521–31. doi:10.1016/j.molcel.2006.04.017.

Cohn, Waldo E. 1960. “Pseudouridine, a Carbon-Carbon Linked Ribonucleoside in Ribonucleic Acids: Isolation, Structure, and Chemical Characteristics.” *The Journal of Biological Chemistry* 235 (5). ASBMB: 1488–98.

Cohn, Waldo E, and Elliot Volkin. 1951. “Nucleoside-5′-Phosphates From Ribonucleic Acid.” *Nature* 167 (March). Nature Publishing Group: 483–84. doi:10.1038/167483a0.

Cooper, A. 1999. “Thermodynamics of Protein Folding and Stability.” Edited by Allen G Stamford 2: 217–70.

Craig, R, and R Beavis. 2004. “TANDEM: Matching Proteins with Tandem Mass Spectra.” *Bioinformatics (Oxford, England)* 20: 1466–67.

Crain, P F, and J A McCloskey. 1997. “The RNA Modification Database.” *Nucleic Acids Research* 25 (1): 126–27. doi:10.1093/nar/25.1.126.

Crick, F. 1966. “Codon--Anticodon Pairing: the Wobble Hypothesis.” *J Mol Biol* 19 (2): 548–55.

Davidson, J F, and R H Schiestl. 2001. “Mitochondrial Respiratory Electron Carriers Are Involved in Oxidative Stress During Heat Stress in Saccharomyces Cerevisiae..” *Molecular and Cellular Biology* 21 (24): 8483–89. doi:10.1128/MCB.21.24.8483-8489.2001.

Davidson, J F, B Whyte, P H Bissinger, and R H Schiestl. 1996. “Oxidative Stress Is Involved in Heat-Induced Cell Death in Saccharomyces Cerevisiae..” *Proceedings of the National Academy of Sciences of the United States of America* 93 (10): 5116–21.

De Virgilio, C, T Hottiger, J Dominguez, T Boller, and A Wiemken. 1994. “The Role of Trehalose Synthesis for the Acquisition of Thermotolerance in Yeast. I. Genetic Evidence That Trehalose Is a Thermoprotectant..” *European Journal of Biochemistry* 219 (1-2): 179–86.

Dedon, Peter C, and Thomas J Begley. 2014. “A System of RNA Modifications and Biased Codon Use Controls Cellular Stress Response at the Level of Translation.” *Chemical Research in Toxicology* 27 (3). American Chemical Society: 330–37. doi:10.1021/tx400438d.

Deutsch, Eric W, Luis Mendoza, David Shteynberg, Terry Farrah, Henry Lam, Natalie Tasman, Zhi Sun, et al. 2010. “A Guided Tour of the Trans-Proteomic Pipeline..” *Proteomics* 10 (6): 1150–59. doi:10.1002/pmic.200900375.

Dewez, Monique, Fanélie Bauer, Marc Dieu, Martine Raes, Jean Vandenhaute, and Damien Hermand. 2008. “The Conserved Wobble Uridine tRNA

Thiolase Ctu1-Ctu2 Is Required to Maintain Genome Integrity..” *Proceedings of the National Academy of Sciences* 105 (14): 5459–64. doi:10.1073/pnas.0709404105.

DiMauro, Salvatore, and Michio Hirano. 2009. “Merrf.” In *GeneReviews® [Internet]*, edited by Roberta A Pagon, Margaret P Adam, Holly H Ardinger, Thomas D Bird, Cynthia R Dolan, Chin-To Fong, Richard JH Smith, and Karen Stephens. Seattle (WA): University of Washington, Seattle. http://www.ncbi.nlm.nih.gov/books/NBK1520/.

Di Santo, Rachael, Susanne Bandau, and Michael J R Stark. 2014. “A Conserved and Essential Basic Region Mediates tRNA Binding to the Elp1 Subunit of the Saccharomyces Cerevisiae Elongator Complex..” *Molecular Microbiology* 92 (6): 1227–42. doi:10.1111/mmi.12624.

Domitrovic, Tatiana, Fernando L Palhano, Christina Barja-Fidalgo, Martha DeFreitas, Marcos T D Orlando, and Patricia M B Fernandes. 2003. “Role of Nitric Oxide in the Response of Saccharomyces Cerevisiae Cells to Heat Shock and High Hydrostatic Pressure..” *FEMS Yeast Research* 3 (4): 341–46.

Elliott, B, R S Haltiwanger, and B Futcher. 1996. “Synergy Between Trehalose and Hsp104 for Thermotolerance in Saccharomyces Cerevisiae..” *Genetics* 144 (3): 923–33.

Eng, Jimmy K, Ashley L McCormack, and John R Yates. 1994. “An Approach to Correlate Tandem Mass Spectral Data of Peptides with Amino Acid Sequences in a Protein Database.” *Journal of the American Society for Mass Spectrometry* 5 (11): 976–89. doi:10.1016/1044-0305(94)80016-2.

Eng, Jimmy K, Tahmina A Jahan, and Michael R Hoopmann. 2012. “Comet: an Open-Source MS/MS Sequence Database Search Tool.” *Proteomics* 13 (1): 22–24. doi:10.1002/pmic.201200439.

Esberg, Anders, Bo Huang, Marcus J O Johansson, and Anders S Byström. 2006. “Elevated Levels of Two tRNA Species Bypass the Requirement for Elongator Complex in Transcription and Exocytosis.” *Molecular Cell* 24 (1): 139–48. doi:10.1016/j.molcel.2006.07.031.

Fernández-Vázquez, Jorge, Itzel Vargas-Pérez, Miriam Sansó, Karin Buhne, Mercè Carmona, Esther Paulo, Damien Hermand, et al. 2013. “Modification of tRNA(Lys) UUU by Elongator Is Essential for Efficient Translation of Stress mRNAs..” *PLoS Genetics* 9 (7): e1003647. doi:10.1371/journal.pgen.1003647.

Fichtner, Lars, Daniel Jablonowski, Angelika Schierhorn, Hiroko K Kitamoto, Michael J R Stark, and Raffael Schaffrath. 2003. “Elongator's Toxin-Target (TOT) Function Is Nuclear Localization Sequence Dependent and

Suppressed by Post-Translational Modification..” *Molecular Microbiology* 49 (5): 1297–1307.

Flick K, and Kaiser P. 2012. “Protein Degradation and the Stress Response.” *Seminars in Cell & Developmental Biology*.

Fonseca, Luis L, Po-Wei Chen, and Eberhard O Voit. 2012. “Canonical Modeling of the Multi-Scale Regulation of the Heat Stress Response in Yeast..” *Metabolites* 2 (1): 221–41. doi:10.3390/metabo2010221.

Furukawa, K, N Mizushima, T Noda, and Y Ohsumi. 2000. “A Protein Conjugation System in Yeast with Homology to Biosynthetic Enzyme Reaction of Prokaryotes..” *The Journal of Biological Chemistry* 275 (11): 7462–65.

Gasch, A P, P T Spellman, C M Kao, O Carmel-Harel, M B Eisen, G Storz, D Botstein, and P O Brown. 2000. “Genomic Expression Programs in the Response of Yeast Cells to Environmental Changes.” *Molecular Biology of the Cell* 11 (12): 4241–57.

Gasch, Audrey P. 2002. “The Environmental Stress Response: a Common Yeast Response to Diverse Environmental Stresses.” In *Yeast Stress Responses*, 1:11–70. Topics in Current Genetics. Berlin, Heidelberg: Springer Berlin Heidelberg. doi:10.1007/3-540-45611-2_2.

Gasch, Audrey P, and Margaret Werner-Washburne. 2002. “The Genomics of Yeast Responses to Environmental Stress and Starvation.” *Functional & Integrative Genomics* 2 (4-5). Springer-Verlag: 181–92. doi:10.1007/s10142-002-0058-2.

Geer, Lewis Y, Sanford P Markey, Jeffrey A Kowalak, Lukas Wagner, Ming Xu, Dawn M Maynard, Xiaoyu Yang, Wenyao Shi, and Stephen H Bryant. 2004. “Open Mass Spectrometry Search Algorithm.” *Journal of Proteome Research* 3 (5). American Chemical Society : 958–64. doi:10.1021/pr0499491.

Ghaemmaghami, Sina, Won-Ki Huh, Kiowa Bower, Russell W Howson, Archana Belle, Noah Dephoure, Erin K O'Shea, and Jonathan S Weissman. 2003. “Global Analysis of Protein Expression in Yeast.” *Nature Cell Biology* 425 (6959): 737–41. doi:10.1038/nature02046.

Ghislain, Michel, Andor Udvardy, and Carl Mann. 1993. “S. Cerevisiae 26S Protease Mutants Arrest Cell Division in G2/Metaphase.” *Nature* 366 (6453): 358–62. doi:10.1038/366358a0.

Glatt, Sebastian, and Christoph W Müller. 2013. “Structural Insights Into Elongator Function.” *Current Opinion in Structural Biology* 23 (2): 235–42. doi:10.1016/j.sbi.2013.02.009.

Glatt, Sebastian, Juliette Létoquart, Céline Faux, Nicholas M I Taylor, Bertrand Séraphin, and Christoph W Müller. 2012. “The Elongator Subcomplex

Elp456 Is a Hexameric RecA-Like ATPase..” *Nature Structural & Molecular Biology* 19 (3): 314–20. doi:10.1038/nsmb.2234.

Goehring, A, D Rivers, and G Sprague. 2003. “Attachment of the Ubiquitin-Related Protein Urm1p to the Antioxidant Protein Ahp1p.” *Eukaryot. Cell* 2: 930–36.

Goodenbour, J M, and T Pan. 2006. “Diversity of tRNA Genes in Eukaryotes.” *Nucleic Acids Research* 34 (21). Oxford University Press: 6137–46. doi:10.1093/nar/gkl725.

Grosjean, H, J Edqvist, K Straby, and R Giege. 1996. “Enzymatic Formation of Modified Nucleosides in tRNA: Dependence on tRNA Architecture.” *J Mol Biol* 255 (1): 67–85. doi:S0022-2836(96)90007-8 [pii] 10.1006/jmbi.1996.0007.

Grosjean, Henri. 2005. “Modification and Editing of RNA: Historical Overview and Important Facts to Remember.” Springer, 1–22. doi:10.1007/b106848.

Gross, C, and K Watson. 1998. “Transcriptional and Translational Regulation of Major Heat Shock Proteins and Patterns of Trehalose Mobilization During Hyperthermic Recovery in Repressed and Derepressed Saccharomyces Cerevisiae..” *Canadian Journal of Microbiology* 44 (4): 341–50.

Hagervall, Tord G, Steven C Pomerantz, and James A McCloskey. 1998. “Reduced Misreading of Asparagine Codons by Escherichia Coli tRNALys with Hypomodified Derivatives of 5-Methylaminomethyl-2-Thiouridine in the Wobble Position.” *Journal of Molecular Biology* 284 (1): 33–42. doi:10.1006/jmbi.1998.2162.

Hahne, Hannes, Fiona Pachl, Benjamin Ruprecht, Stefan K Maier, Susan Klaeger, Dominic Helm, Guillaume Médard, Matthias Wilm, Simone Lemeer, and Bernhard Kuster. 2013. “DMSO Enhances Electrospray Response, Boosting Sensitivity of Proteomic Experiments.” *Nature Methods* 10 (10). Nature Publishing Group: 989–91. doi:10.1038/nmeth.2610.

Han, D K, J Eng, H Zhou, and R Aebersold. 2001. “Quantitative Profiling of Differentiation-Induced Microsomal Proteins Using Isotope-Coded Affinity Tags and Mass Spectrometry.” *Nature Biotechnology* 19 (10): 946–51. doi:10.1038/nbt1001-946.

Hartl, F Ulrich, Andreas Bracher, and Manajit Hayer-Hartl. 2011. “Molecular Chaperones in Protein Folding and Proteostasis.” *Nature* 475 (7356). Nature Publishing Group: 324–32. doi:10.1038/nature10317.

Harvey, Stephen, and M Prabhakaran. 1986. “Ribose Puckering: Structure, Dynamics, Energetics, and the Pseudorotation Cycle.” *Journal of the*

American Chemical Society 108 (20): 6128–36. doi:10.1021/ja00280a004.

Helm, M. 2006. “Post-Transcriptional Nucleotide Modification and Alternative Folding of RNA.” *Nucleic Acids Research* 34 (2): 721–33. doi:34/2/721 [pii] 10.1093/nar/gkj471.

Hinnebusch, Alan G. 2005. “Translational Regulation of GCN4 and the General Amino Acid Control of Yeast.” *Annual Review of Microbiology* 59: 407–50. doi:10.1146/annurev.micro.59.031805.133833.

Hiraoka, Yasushi, Kenichi Kawamata, Tokuko Haraguchi, and Yuji Chikashige. 2009. “Codon Usage Bias Is Correlated with Gene Expression Levels in the Fission Yeast Schizosaccharomyces Pombe..” *Genes to Cells : Devoted to Molecular & Cellular Mechanisms* 14 (4): 499–509. doi:10.1111/j.1365-2443.2009.01284.x.

Hopper, Anita K, and Eric M Phizicky. 2003. “tRNA Transfers to the Limelight..” *Genes & Development* 17 (2): 162–80. doi:10.1101/gad.1049103.

Huang, B, J Lu, and A S Byström. 2008. “A Genome-Wide Screen Identifies Genes Required for Formation of the Wobble Nucleoside 5-Methoxycarbonylmethyl-2-Thiouridine in Saccharomyces Cerevisiae.” *RNA (New York, NY)* 14 (10): 2183–94. doi:10.1261/rna.1184108.

Huang, Bo, Marcus J O Johansson, and Anders S Byström. 2005. “An Early Step in Wobble Uridine tRNA Modification Requires the Elongator Complex..” *RNA (New York, NY)* 11 (4): 424–36. doi:10.1261/rna.7247705.

Igloi, G. 1988. “Interaction of tRNAs and of Phosphorothioate-Substituted Nucleic Acids with an Organomercurial. Probing the Chemical Environment of Thiolated Residues by Affinity Electrophoresis.” *Biochemistry* 27: 3842–49.

Jackman, Jane E, and Juan D Alfonzo. 2012. “Transfer RNA Modifications: Nature's Combinatorial Chemistry Playground.” *Wiley Interdisciplinary Reviews: RNA* 4 (1). NIH Public Access: 35–48. doi:10.1002/wrna.1144.

Johansson, M, A Esberg, B Huang, G Bjork, and A Bystrom. 2008. “Eukaryotic Wobble Uridine Modifications Promote a Functionally Redundant Decoding System.” *Molecular and Cellular Biology* 28 (10): 3301–12. doi:MCB.01542-07 [pii] 10.1128/MCB.01542-07.

Johansson, Marcus JO, and Anders S Byström. 2005. “Transfer RNA Modifications and Modifying Enzymes in Saccharomyces Cerevisiae.” Springer, 87–120. doi:10.1007/b105814.

Kaiser, Peter, Ning-Yuan Su, James L Yen, Ikram Ouni, and Karin Flick. 2006. “The Yeast Ubiquitin Ligase SCFMet30: Connecting Environmental and

Intracellular Conditions to Cell Division..” *Cell Division* 1: 16. doi: 10.1186/1747-1028-1-16.

Kaufman, R J. 1999. “Stress Signaling From the Lumen of the Endoplasmic Reticulum: Coordination of Gene Transcriptional and Translational Controls..” *Genes & Development* 13 (10): 1211–33.

Keith, G. 1984. “The Primary Structures of Two Arginine tRNAs (Anticodons C-C-U and mcm5a2U-C-Psi) and of Glutamine tRNA (Anticodon C-U-G) From Bovine Liver..” *Nucleic Acids Research* 12 (5): 2543–47.

Keller, A, A Nesvizhskii, E Kolker, and R Aebersold. 2002. “Empirical Statistical Model to Estimate the Accuracy of Peptide Identifications Made by MS/MS and Database Search.” *Analytical Chemistry* 74: 5383–92.

Keller, Andrew, Jimmy Eng, Ning Zhang, Xiao-Jun Li, and Ruedi Aebersold. 2005. “A Uniform Proteomics MS/MS Analysis Platform Utilizing Open XML File Formats.” *Molecular Systems Biology* 1: 2005.0017. doi: 10.1038/msb4100024.

King, Nichole L, Eric W Deutsch, Jeffrey A Ranish, Alexey I Nesvizhskii, James S Eddes, Parag Mallick, Jimmy Eng, et al. 2006. “Analysis of the Saccharomyces Cerevisiae Proteome with PeptideAtlas..” *Genome Biology* 7 (11): R106. doi:10.1186/gb-2006-7-11-r106.

Kitagaki, Hiroshi, and Hiroshi Takagi. 2014. “Mitochondrial Metabolism and Stress Response of Yeast: Applications in Fermentation Technologies..” *Journal of Bioscience and Bioengineering* 117 (4): 383–93. doi:10.1016/j.jbiosc.2013.09.011.

Kobayashi, N, and K McEntee. 1990. “Evidence for a Heat Shock Transcription Factor-Independent Mechanism for Heat Shock Induction of Transcription in Saccharomyces Cerevisiae..” *Proceedings of the National Academy of Sciences of the United States of America* 87 (17): 6550–54.

Kraft, Claudine, Anna Deplazes, Marc Sohrmann, and Matthias Peter. 2008. “Mature Ribosomes Are Selectively Degraded Upon Starvation by an Autophagy Pathway Requiring the Ubp3p/Bre5p Ubiquitin Protease.” *Nature Cell Biology* 10 (5): 602–10. doi:10.1038/ncb1723.

Kroemer, Guido, Guillermo Mariño, and Beth Levine. 2010. “Autophagy and the Integrated Stress Response..” *Molecular Cell* 40 (2): 280–93. doi: 10.1016/j.molcel.2010.09.023.

Krüger, M K, S Pedersen, T G Hagervall, and M A Sørensen. 1998. “The Modification of the Wobble Base of tRNAGlu Modulates the Translation Rate of Glutamic Acid Codons in Vivo..” *J Mol Biol* 284 (3): 621–31. doi: 10.1006/jmbi.1998.2196.

Kudla, Grzegorz, Andrew W Murray, David Tollervey, and Joshua B Plotkin. 2009. “Coding-Sequence Determinants of Gene Expression in Escherichia Coli..” *Science (New York, NY)* 324 (5924): 255–58. doi: 10.1126/science.1170160.

Kuhn, K M, J L DeRisi, P O Brown, and P Sarnow. 2001. “Global and Specific Translational Regulation in the Genomic Response of Saccharomyces Cerevisiae to a Rapid Transfer From a Fermentable to a Nonfermentable Carbon Source.” *Molecular and Cellular Biology* 21 (3): 916–27. doi: 10.1128/MCB.21.3.916-927.2001.

Kuranda, Klaudia, Veronique Leberre, Serguei Sokol, Grazyna Palamarczyk, and Jean François. 2006. “Investigating the Caffeine Effects in the Yeast Saccharomyces Cerevisiae Brings New Insights Into the Connection Between TOR, PKC and Ras/cAMP Signalling Pathways..” *Molecular Microbiology* 61 (5): 1147–66. doi:10.1111/j.1365-2958.2006.05300.x.

Laxman, Sunil, Benjamin M Sutter, Xi Wu, Sujai Kumar, Xiaofeng Guo, David C Trudgian, Hamid Mirzaei, and Benjamin P Tu. 2013. “Sulfur Amino Acids Regulate Translational Capacity and Metabolic Homeostasis Through Modulation of tRNA Thiolation.” *Cell* 154 (2). Elsevier: 416–29. doi: 10.1016/j.cell.2013.06.043.

Leach, Michelle D, and Alistair J P Brown. 2012. “Posttranslational Modifications of Proteins in the Pathobiology of Medically Relevant Fungi..” *Eukaryotic Cell* 11 (2): 98–108. doi:10.1128/EC.05238-11.

Leidel, Sebastian, Patrick G A Pedrioli, Tamara Bucher, Renée Brost, Michael Costanzo, Alexander Schmidt, Ruedi Aebersold, Charles Boone, Kay Hofmann, and Matthias Peter. 2009. “Ubiquitin-Related Modifier Urm1 Acts as a Sulphur Carrier in Thiolation of Eukaryotic Transfer RNA.” *Nature* 458 (7235). Nature Publishing Group: 228–32. doi:10.1038/nature07643.

Lempiäinen, Harri, and David Shore. 2009. “Growth Control and Ribosome Biogenesis.” *Current Opinion in Cell Biology* 21 (6): 855–63. doi:10.1016/j.ceb.2009.09.002.

Lewis, J G, R P Learmonth, and K Watson. 1995. “Induction of Heat, Freezing and Salt Tolerance by Heat and Salt Shock in Saccharomyces Cerevisiae..” *Microbiology* 141 (Pt 3) (March): 687–94.

Liu, Yanfen, and Yihong Ye. 2011. “Proteostasis Regulation at the Endoplasmic Reticulum: a New Perturbation Site for Targeted Cancer Therapy.” *Cell Research* 21 (6). Nature Publishing Group: 867–83. doi:10.1038/cr.2011.75.

Machnicka, M A, K Milanowska, O Osman Oglou, E Purta, M Kurkowska, A Olchowik, W Januszewski, et al. 2012. “MODOMICS: a Database of

RNA Modification Pathways--2013 Update." *Nucleic Acids Research* 41 (D1): D262–67. doi:10.1093/nar/gks1007.

MacLean, B, J Eng, R Beavis, and M McIntosh. 2006. "General Framework for Developing and Evaluating Database Scoring Algorithms Using the TANDEM Search Engine." *Bioinformatics (Oxford, England)* 22: 2830–32.

Madison, J T, S J Boguslawski, and G H Teetor. 1972. "Nucleotide Sequence of a Lysine Transfer Ribonucleic Acid From Bakers' Yeast.." *Science (New York, NY)* 176 (4035): 687–89. doi:10.1126/science.176.4035.687.

Madore, E, C Florentz, R Giege, S Sekine, S Yokoyama, and J Lapointe. 1999. "Effect of Modified Nucleotides on Escherichia Coli tRNAGlu Structure and on Its Aminoacylation by Glutamyl-tRNA Synthetase. Predominant and Distinct Roles of the Mnm5 and S2 Modifications of U34.." *European Journal of Biochemistry* 266 (3): 1128–35.

Mann M, R C Hendrickson, and A Pandey. 2001. "Analysis of Proteins and Proteomes by Mass Spectrometry.." *Annual Review of Biochemistry* 70: 437–73. doi:10.1146/annurev.biochem.70.1.437.

Mann, Matthias. 2006. "Functional and Quantitative Proteomics Using SILAC." *Nature Reviews Molecular Cell Biology* 7 (12): 952–58. doi:10.1038/nrm2067.

Marck, Christian, and Henri Grosjean. 2002. "tRNomics: Analysis of tRNA Genes From 50 Genomes of Eukarya, Archaea, and Bacteria Reveals Anticodon-Sparing Strategies and Domain-Specific Features.." *RNA (New York, NY)* 8 (10): 1189–1232.

Mayer, Christine, and Ingrid Grummt. 2005. "Cellular Stress and Nucleolar Function.." *Cell Cycle (Georgetown, Tex.)* 4 (8): 1036–38.

Mehlgarten, Constance, Daniel Jablonowski, Karin D Breunig, Michael J R Stark, and Raffael Schaffrath. 2009. "Elongator Function Depends on Antagonistic Regulation by Casein Kinase Hrr25 and Protein Phosphatase Sit4." *Molecular Microbiology* 73 (5): 869–81. doi:10.1111/j.1365-2958.2009.06811.x.

Mehlgarten, Constance, Daniel Jablonowski, Uta Wrackmeyer, Susan Tschitschmann, David Sondermann, Gunilla Jäger, Zhizhong Gong, Anders S Byström, Raffael Schaffrath, and Karin D Breunig. 2010. "Elongator Function in tRNA Wobble Uridine Modification Is Conserved Between Yeast and Plants.." *Molecular Microbiology* 76 (5): 1082–94. doi:10.1111/j.1365-2958.2010.07163.x.

Mewes, Hans-Werner, Sabine Dietmann, Dmitrij Frishman, Richard Gregory, Gertrud Mannhaupt, Klaus FX Mayer, Martin Münsterkötter, Andreas Ruepp, Manuel Spannagl, and Volker Stümpflen. 2008. "MIPS: Analysis

and Annotation of Genome Information in 2007." *Nucleic Acids Research* 36 (suppl 1). Oxford Univ Press: D196–D201.

Meyer, Jesse G, and Elizabeth A Komives. 2012. "Charge State Coalescence During Electrospray Ionization Improves Peptide Identification by Tandem Mass Spectrometry." *Journal of the American Society for Mass Spectrometry* 23 (8): 1390–99. doi:10.1007/s13361-012-0404-0.

Meyuhas, Oded. 2008. "Physiological Roles of Ribosomal Protein S6: One of Its Kind.." *International Review of Cell and Molecular Biology* 268: 1–37. doi:10.1016/S1937-6448(08)00801-0.

Milon, Pohl, Andrey L Konevega, Claudio O Gualerzi, and Marina V Rodnina. 2008. "Kinetic Checkpoint at a Late Step in Translation Initiation.." *Molecular Cell* 30 (6): 712–20. doi:10.1016/j.molcel.2008.04.014.

Morano, Kevin A, Chris M Grant, and W Scott Moye-Rowley. 2012. "The Response to Heat Shock and Oxidative Stress in Saccharomyces Cerevisiae.." *Genetics* 190 (4): 1157–95. doi:10.1534/genetics.111.128033.

Mueller, Lukas N, Mi-Youn Brusniak, D R Mani, and Ruedi Aebersold. 2008. "An Assessment of Software Solutions for the Analysis of Mass Spectrometry Based Quantitative Proteomics Data.." *Journal of Proteome Research* 7 (1): 51–61. doi:10.1021/pr700758r.

Murphy, Frank V, Venki Ramakrishnan, Andrzej Malkiewicz, and Paul F Agris. 2004. "The Role of Modifications in Codon Discrimination by tRNALysUUU." *Nature Structural & Molecular Biology* 11 (12): 1186–91. doi:10.1038/nsmb861.

Murphy, Michael P. 2009. "How Mitochondria Produce Reactive Oxygen Species.." *The Biochemical Journal* 417 (1): 1–13. doi:10.1042/BJ20081386.

Nagaraj, Nagarjuna, Nils Alexander Kulak, Juergen Cox, Nadin Neuhauser, Korbinian Mayr, Ole Hoerning, Ole Vorm, and Matthias Mann. 2012. "System-Wide Perturbation Analysis with Nearly Complete Coverage of the Yeast Proteome by Single-Shot Ultra HPLC Runs on a Bench Top Orbitrap.." *Molecular & Cellular Proteomics : MCP* 11 (3): M111.013722. doi:10.1074/mcp.M111.013722.

Nakai, Y, M Nakai, and H Hayashi. 2008. "Thio-Modification of Yeast Cytosolic tRNA Requires a Ubiquitin-Related System That Resembles Bacterial Sulfur Transfer Systems." *The Journal of Biological Chemistry* 283 (41): 27469–76. doi:M804043200 [pii] 10.1074/jbc.M804043200.

Nakamura, Tatsuji, Junro Kuromitsu, and Yoshiya Oda. 2008. "Evaluation of Comprehensive Multidimensional Separations Using Reversed-Phase, Reversed-Phase Liquid Chromatography/Mass Spectrometry for

Shotgun Proteomics..” *Journal of Proteome Research* 7 (3): 1007–11. doi:10.1021/pr7005878.

Nathan, D F, M H Vos, and S Lindquist. 1997. “In Vivo Functions of the Saccharomyces Cerevisiae Hsp90 Chaperone..” *Proceedings of the National Academy of Sciences of the United States of America* 94 (24): 12949–56.

Nelissen, Hilde, Delphine Fleury, Leonardo Bruno, Pedro Robles, Lieven De Veylder, Jan Traas, José Luis Micol, Marc Van Montagu, Dirk Inzé, and Mieke Van Lijsebettens. 2005. “The Elongata Mutants Identify a Functional Elongator Complex in Plants with a Role in Cell Proliferation During Organ Growth..” *Proceedings of the National Academy of Sciences of the United States of America* 102 (21): 7754–59. doi: 10.1073/pnas.0502600102.

Nesvizhskii, A, A Keller, E Kolker, and R Aebersold. 2003. “A Statistical Model for Identifying Proteins by Tandem Mass Spectrometry.” *Analytical Chemistry* 75: 4646–58.

Neves, Maria-Jose, and Jean François. 1992. “On the Mechanism by Which a Heat Shock Induces Trehalose Accumulation in Saccharomyces Cerevisiae..” *The Biochemical Journal* 288: 859–64.

Nevoigt, Elke, and Ulf Stahl. 2006. “Osmoregulation and Glycerol Metabolism in the Yeast Saccharomyces Cerevisiae.” *FEMS Microbiology Reviews* 21 (3): 231–41. doi:10.1111/j.1574-6976.1997.tb00352.x.

Nguyen, Laurent, Sandrine Humbert, Frédéric Saudou, and Alain Chariot. 2010. “Elongator - an Emerging Role in Neurological Disorders..” *Trends in Molecular Medicine* 16 (1): 1–6. doi:10.1016/j.molmed.2009.11.002.

Niforou, Katerina, Christina Cheimonidou, and Ioannis P Trougakos. 2014. “Molecular Chaperones and Proteostasis Regulation During Redox Imbalance.” *Redox Biology* 2: 323–32. doi:10.1016/j.redox.2014.01.017.

Nishimura, Akira, Nobuhiro Kawahara, and Hiroshi Takagi. 2013. “The Flavoprotein Tah18-Dependent NO Synthesis Confers High-Temperature Stress Tolerance on Yeast Cells..” *Biochem. Biophys. Res. Commun.* 430 (1): 137–43. doi:10.1016/j.bbrc.2012.11.023.

Nishimura, Akira, Tetsuya Kotani, Yu Sasano, and Hiroshi Takagi. 2010. “An Antioxidative Mechanism Mediated by the Yeast N-Acetyltransferase Mpr1: Oxidative Stress-Induced Arginine Synthesis and Its Physiological Role..” *FEMS Yeast Research* 10 (6): 687–98. doi:10.1111/j. 1567-1364.2010.00650.x.

Nobles, Kelly N, Connie S Yarian, Guihua Liu, Richard H Guenther, and Paul F Agris. 2002. “Highly Conserved Modified Nucleosides Influence Mg2+-Dependent tRNA Folding..” *Nucleic Acids Research* 30 (21): 4751–60.

Noma, A, Y Sakaguchi, and T Suzuki. 2009. “Mechanistic Characterization of the Sulfur-Relay System for Eukaryotic 2-Thiouridine Biogenesis at tRNA Wobble Positions.” *Nucleic Acids Research* 37 (4): 1335–52. doi:gkn1023 [pii] 10.1093/nar/gkn1023.

Novoa, Eva Maria, Mariana Pavon-Eternod, Tao Pan, and Lluís Ribas de Pouplana. 2012. “A Role for tRNA Modifications in Genome Structure and Codon Usage.” *Cell* 149 (1). Elsevier Inc.: 202–13. doi:10.1016/j.cell.2012.01.050.

Ogle, J M, D E Brodersen, W M Clemons, M J Tarry, A P Carter, and V Ramakrishnan. 2001. “Recognition of Cognate Transfer RNA by the 30S Ribosomal Subunit..” *Science (New York, NY)* 292 (5518): 897–902. doi:10.1126/science.1060612.

Olsen, J V, J C Schwartz, J Griep-Raming, M L Nielsen, E Damoc, E Denisov, O Lange, et al. 2009. “A Dual Pressure Linear Ion Trap Orbitrap Instrument with Very High Sequencing Speed.” *Molecular & Cellular Proteomics : MCP* 8 (12). American Society for Biochemistry and Molecular Biology: 2759–69. doi:10.1074/mcp.M900375-MCP200.

Ong, Shao-En, and Matthias Mann. 2005. “Mass Spectrometry–Based Proteomics Turns Quantitative.” *Nature Chemical Biology* 1 (5). Nature Publishing Group: 252–62. doi:10.1038/nchembio736.

Pahlman, A K, K Granath, R Ansell, S Hohmann, and L Adler. 2001. “The Yeast Glycerol 3-Phosphatases Gpp1p and Gpp2p Are Required for Glycerol Biosynthesis and Differentially Involved in the Cellular Responses to Osmotic, Anaerobic, and Oxidative Stress..” *The Journal of Biological Chemistry* 276 (5): 3555–63. doi:10.1074/jbc.M007164200.

Pape, T, W Wintermeyer, and M V Rodnina. 1998. “Complete Kinetic Mechanism of Elongation Factor Tu-Dependent Binding of Aminoacyl-tRNA to the a Site of the E. Coli Ribosome..” *The EMBO Journal* 17 (24): 7490–97. doi:10.1093/emboj/17.24.7490.

Park, Sung-Soo, Wells W Wu, Yu Zhou, Rong-Fong Shen, Bronwen Martin, and Stuart Maudsley. 2012. “Effective Correction of Experimental Errors in Quantitative Proteomics Using Stable Isotope Labeling by Amino Acids in Cell Culture (SILAC)..” *Journal of Proteomics* 75 (12): 3720–32. doi:10.1016/j.jprot.2012.04.035.

Patil, Ashish, Clement T Y Chan, Madhu Dyavaiah, John P Rooney, Peter C Dedon, and Thomas J Begley. 2012. “Translational Infidelity-Induced Protein Stress Results From a Deficiency in Trm9-Catalyzed tRNA Modifications..” *RNA Biology* 9 (7): 990–1001. doi:10.4161/rna.20531.

Pedrioli, Patrick G A. 2010. “Trans-Proteomic Pipeline: a Pipeline for Proteomic Analysis..” *Methods in Molecular Biology (Clifton, N.J.)* 604 (Chapter 15). Totowa, NJ: 213–38. doi:10.1007/978-1-60761-444-9_15.

Pedrioli, Patrick G A, Jimmy K Eng, Robert Hubley, Mathijs Vogelzang, Eric W Deutsch, Brian Raught, Brian Pratt, et al. 2004. “A Common Open Representation of Mass Spectrometry Data and Its Application to Proteomics Research..” *Nature Biotechnology* 22 (11): 1459–66. doi: 10.1038/nbt1031.

Pedrioli, Patrick G A, Sebastian Leidel, and Kay Hofmann. 2008. “Urm1 at the Crossroad of Modifications. ‘Protein Modifications: Beyond the Usual Suspects’ Review Series..” *EMBO Reports* 9 (12): 1196–1202. doi: 10.1038/embor.2008.209.

Phelps, S, A Malkiewicz, P Agris, and S Joseph. 2004. “Modified Nucleotides in tRNA(Lys) and tRNA(Val) Are Important for Translocation.” *J Mol Biol* 338 (3): 439–44. doi:10.1016/j.jmb.2004.02.070 S0022283604002803 [pii].

Phizicky, Eric M, and Anita K Hopper. 2010. “tRNA Biology Charges to the Front..” *Genes & Development* 24 (17): 1832–60. doi:10.1101/gad. 1956510.

Powers, Evan T, Richard I Morimoto, Andrew Dillin, Jeffery W Kelly, and William E Balch. 2009. “Biological and Chemical Approaches to Diseases of Proteostasis Deficiency..” *Annual Review of Biochemistry* 78: 959–91. doi:10.1146/annurev.biochem.052308.114844.

Ramakrishnan, V. 2002. “Ribosome Structure and the Mechanism of Translation.” *Cell* 108 (4): 557–72. doi:10.1016/S0092-8674(02)00619-0.

Rezgui, Vanessa Anissa Nathalie, kshitiz Tyagi, Namit Ranjan, Andrey L Konevega, Joerg Mittelstaet, Marina V Rodnina, Matthias Peter, and Patrick G A Pedrioli. 2013. “tRNA tKUUU, tQUUG, and tEUUC Wobble Position Modifications Fine-Tune Protein Translation by Promoting Ribosome a-Site Binding..” *Proceedings of the National Academy of Sciences* 110 (30): 12289–94. doi:10.1073/pnas.1300781110.

Ritorto, Maria Stella, Ken Cook, kshitiz Tyagi, Patrick G A Pedrioli, and Matthias Trost. 2013. “Hydrophilic Strong Anion Exchange (hSAX) Chromatography for Highly Orthogonal Peptide Separation of Complex Proteomes..” *Journal of Proteome Research* 12 (6): 2449–57. doi: 10.1021/pr301011r.

Robinson, Mark D, Jörg Grigull, Naveed Mohammad, and Timothy R Hughes. 2002. “FunSpec: a Web-Based Cluster Interpreter for Yeast..” *Bmc Bioinformatics* 3 (November): 35.

Rodnina, M V, and W Wintermeyer. 2001. “Fidelity of Aminoacyl-tRNA Selection on the Ribosome: Kinetic and Structural Mechanisms..” *Annual Review of Biochemistry* 70: 415–35. doi:10.1146/annurev.biochem.70.1.415.

Rodriguez-Hernandez, Annia, Jessica L Spears, Kirk W Gaston, Patrick A Limbach, Howard Gamper, Ya-Ming Hou, Rob Kaiser, Paul F Agris, and John J Perona. 2013. “Structural and Mechanistic Basis for Enhanced Translational Efficiency by 2-Thiouridine at the tRNA Anticodon Wobble Position..” *J Mol Biol* 425 (20): 3888–3906. doi:10.1016/j.jmb.2013.05.018.

Roncero, C, M H Valdivieso, J C Ribas, and A Durán. 1988. “Isolation and Characterization of Saccharomyces Cerevisiae Mutants Resistant to Calcofluor White..” *Journal of Bacteriology* 170 (4): 1950–54.

Ros, Alexandra, Michel Faupel, Hervé Mees, Jan van Oostrum, Rosaria Ferrigno, Frédéric Reymond, Philippe Michel, Joël S Rossier, and Hubert H Girault. 2002. “Protein Purification by Off-Gel Electrophoresis..” *Proteomics* 2 (2): 151–56.

Ruvinsky, I, and O Meyuhas. 2006. “Ribosomal Protein S6 Phosphorylation: From Protein Synthesis to Cell Size.” *Trends in Biochemical Sciences*.

Sanchez, Y, and S L Lindquist. 1990. “HSP104 Required for Induced Thermotolerance..” *Science (New York, NY)* 248 (4959): 1112–15.

Santos, dos, S C, and I Sa-Correia. 2011. “A Genome-Wide Screen Identifies Yeast Genes Required for Protection Against or Enhanced Cytotoxicity of the Antimalarial Drug Quinine - Springer.” *Molecular Genetics and Genomics*.

Scalley, M L, and D Baker. 1997. “Protein Folding Kinetics Exhibit an Arrhenius Temperature Dependence When Corrected for the Temperature Dependence of Protein Stability..” *Proceedings of the National Academy of Sciences of the United States of America* 94 (20): 10636–40.

Schlieker, Christian D, Annemarthe G Van der Veen, Jadyn R Damon, Eric Spooner, and Hidde L Ploegh. 2008. “A Functional Proteomics Approach Links the Ubiquitin-Related Modifier Urm1 to a tRNA Modification Pathway..” *Proceedings of the National Academy of Sciences* 105 (47): 18255–60. doi:10.1073/pnas.0808756105.

Schmitz, Jennifer, Mita Mullick Chowdhury, Petra Hänzelmann, Manfred Nimtz, Eun-Young Lee, Hermann Schindelin, and Silke Leimkühler. 2008. “The Sulfurtransferase Activity of Uba4 Presents a Link Between Ubiquitin-Like Protein Conjugation and Activation of Sulfur Carrier Proteins..” *Biochemistry* 47 (24): 6479–89. doi:10.1021/bi800477u.

Searle, Brian C, Mark Turner, and Alexey I Nesvizhskii. 2008. “Improving Sensitivity by Probabilistically Combining Results From Multiple MS/MS

Search Methodologies." *Journal of Proteome Research* 7 (1). American Chemical Society : 245–53. doi:10.1021/pr070540w.

Sekiya, Takao, Keiichi Takeishi, and Tyunosin Ukita. 1969. "Specificity of Yeast Glutamic Acid Transfer RNA for Codon Recognition." *Biochimica Et Biophysica Acta (BBA)-Nucleic Acids and Protein Synthesis* 182 (2). Elsevier: 411–26.

Sen, G C, and H P Ghosh. 1976. "Role of Modified Nucleosides in tRNA: Effect of Modification of the 2-Thiouridine Derivative Located at the 5'-End of the Anticodon of Yeast Transfer RNA Lys2.." *Nucleic Acids Research* 3 (3): 523–35.

Shah, Premal, Yang Ding, Malwina Niemczyk, Grzegorz Kudla, and Joshua B Plotkin. 2013. "Rate-Limiting Steps in Yeast Protein Translation." *Cell* 153 (7). Elsevier: 1589–1601. doi:10.1016/j.cell.2013.05.049.

Shohat, Mordechai, and Gabrielle J Halpern. 2010. "Familial Dysautonomia." In *GeneReviews® [Internet]*, edited by Roberta A Pagon, Margaret P Adam, Holly H Ardinger, Thomas D Bird, Cynthia R Dolan, Chin-To Fong, Richard JH Smith, and Karen Stephens. Seattle (WA): University of Washington, Seattle. http://www.ncbi.nlm.nih.gov/books/NBK1180/.

Shteynberg, David, Eric W Deutsch, Henry Lam, Jimmy K Eng, Zhi Sun, Natalie Tasman, Luis Mendoza, Robert L Moritz, Ruedi Aebersold, and Alexey I Nesvizhskii. 2011. "iProphet: Multi-Level Integrative Analysis of Shotgun Proteomic Data Improves Peptide and Protein Identification Rates and Error Estimates.." *Molecular & Cellular Proteomics : MCP* 10 (12): M111.007690. doi:10.1074/mcp.M111.007690.

Siderius, M, O Van Wuytswinkel, K A Reijenga, M Kelders, and W H Mager. 2000. "The Control of Intracellular Glycerol in Saccharomyces Cerevisiae Influences Osmotic Stress Response and Resistance to Increased Temperature.." *Molecular Microbiology* 36 (6): 1381–90.

Simpson, Claire L, Robin Lemmens, Katarzyna Miskiewicz, Wendy J Broom, Valerie K Hansen, Paul W J van Vught, John E Landers, et al. 2009. "Variants of the Elongator Protein 3 (ELP3) Gene Are Associated with Motor Neuron Degeneration.." *Human Molecular Genetics* 18 (3): 472–81. doi:10.1093/hmg/ddn375.

Singer, M A, and S Lindquist. 1998a. "Multiple Effects of Trehalose on Protein Folding in Vitro and in Vivo.." *Molecular Cell* 1 (5): 639–48.

Singer, Mike A, and Susan Lindquist. 1998b. "Thermotolerance in Saccharomyces Cerevisiae: the Yin and Yang of Trehalose." *Trends in Biotechnology* 16 (11): 460–68. doi:10.1016/S0167-7799(98)01251-7.

Singh, Neetu, Meridith T Lorbeck, Ashley Zervos, John Zimmerman, and Felice Elefant. 2010. "The Histone Acetyltransferase Elp3 Plays in Active Role

in the Control of Synaptic Bouton Expansion and Sleep in Drosophila.." *Journal of Neurochemistry* 115 (2): 493–504. doi:10.1111/j.1471-4159.2010.06892.x.

Sinha, Himanshu, Lior David, Renata C Pascon, Sandra Clauder-Münster, Sujatha Krishnakumar, Michelle Nguyen, Getao Shi, et al. 2008. "Sequential Elimination of Major-Effect Contributors Identifies Additional Quantitative Trait Loci Conditioning High-Temperature Growth in Yeast.." *Genetics* 180 (3): 1661–70. doi:10.1534/genetics.108.092932.

Slaugenhaupt, S A, A Blumenfeld, S P Gill, M Leyne, J Mull, M P Cuajungco, C B Liebert, et al. 2001. "Tissue-Specific Expression of a Splicing Mutation in the IKBKAP Gene Causes Familial Dysautonomia.." *American Journal of Human Genetics* 68 (3): 598–605.

Slaugenhaupt, Susan A, and James F Gusella. 2002. "Familial Dysautonomia." *Current Opinion in Genetics & Development* 12 (3): 307–11. doi:10.1016/S0959-437X(02)00303-9.

Slebos, Robbert J C, Jonathan W C Brock, Nancy F Winters, Sarah R Stuart, Misti A Martinez, Ming Li, Mathew C Chambers, et al. 2008. "Evaluation of Strong Cation Exchange Versus Isoelectric Focusing of Peptides for Multidimensional Liquid Chromatography-Tandem Mass Spectrometry.." *Journal of Proteome Research* 7 (12): 5286–94. doi:10.1021/pr8004666.

Smyth, G K. 2005. "Limma: Linear Models for Microarray Data." In *Bioinformatics and Computational Biology Solutions Using R and Bioconductor*

, edited by R Gentleman, V Carey, S Dudoit, R Irizarry, and W Huber, 397–420. Statistics for Biology and Health. New York: Springer. doi:10.1007/0-387-29362-0_23.

Smyth, Gordon K. 2004. "Linear Models and Empirical Bayes Methods for Assessing Differential Expression in Microarray Experiments.." *Statistical Applications in Genetics and Molecular Biology* 3: Article3. doi:10.2202/1544-6115.1027.

Solé, Carme, Mariona Nadal-Ribelles, Claudine Kraft, Matthias Peter, Francesc Posas, and Eulàlia de Nadal. 2011. "Control of Ubp3 Ubiquitin Protease Activity by the Hog1 SAPK Modulates Transcription Upon Osmostress.." *The EMBO Journal* 30 (16): 3274–84. doi:10.1038/emboj.2011.227.

Soroka, Joanna, Sebastian K Wandinger, Nina Mäusbacher, Thiemo Schreiber, Klaus Richter, Henrik Daub, and Johannes Buchner. 2012. "Conformational Switching of the Molecular Chaperone Hsp90 via Regulated Phosphorylation." *Molecular Cell* 45 (4): 517–28. doi:10.1016/j.molcel.2011.12.031.

Strug, Lisa J, Tara Clarke, Theodore Chiang, Minchen Chien, Zeynep Baskurt, Weili Li, Ruslan Dorfman, et al. 2009. “Centrotemporal Sharp Wave EEG Trait in Rolandic Epilepsy Maps to Elongator Protein Complex 4 (ELP4)..” *European Journal of Human Genetics : EJHG* 17 (9): 1171–81. doi:10.1038/ejhg.2008.267.

Sutter, Benjamin M, Xi Wu, Sunil Laxman, and Benjamin P Tu. 2013. “Methionine Inhibits Autophagy and Promotes Growth by Inducing the SAM-Responsive Methylation of PP2A.” *Cell* 154 (2): 403–15. doi: 10.1016/j.cell.2013.06.041.

Sylvers, L, K Rogers, M Shimizu, E Ohtsuka, and D Soll. 1993. “A 2-Thiouridine Derivative in tRNAGlu Is a Positive Determinant for Aminoacylation by Escherichia Coli Glutamyl-tRNA Synthetase.” *Biochemistry* 32 (15): 3836–41.

Takai, K, and S Yokoyama. 2003. “Roles of 5-Substituents of tRNA Wobble Uridines in the Recognition of Purine-Ending Codons.” *Nucleic Acids Research* 31 (22): 6383–91.

Takeoka, S, M Unoki, Y Onouchi, S Doi, H Fujiwara, A Miyatake, K Fujita, I Inoue, Y Nakamura, and M Tamari. 2001. “Amino-Acid Substitutions in the IKAP Gene Product Significantly Increase Risk for Bronchial Asthma in Children..” *Journal of Human Genetics* 46 (2): 57–63. doi:10.1007/s100380170109.

Team, R Development Core. 2009. *R: a Language and Environment for Statistical Computing*. *Book*. R Foundation for Statistical Computing. http://www.R-project.org/.

Thakur, Suman S, Tamar Geiger, Bhaswati Chatterjee, Peter Bandilla, Florian Fröhlich, Juergen Cox, and Matthias Mann. 2011. “Deep and Highly Sensitive Proteome Coverage by LC-MS/MS Without Prefractionation.” *Molecular & Cellular Proteomics : MCP* 10 (8): M110.003699. doi: 10.1074/mcp.M110.003699.

The Gene Ontology Consortium. 2007. “The Gene Ontology Project in 2008.” *Nucleic Acids Research* 36 (Database): D440–44. doi:10.1093/nar/gkm883.

Ting, Lily, Mark J Cowley, Seah Lay Hoon, Michael Guilhaus, Mark J Raftery, and Ricardo Cavicchioli. 2009. “Normalization and Statistical Analysis of Quantitative Proteomics Data Generated by Metabolic Labeling..” *Molecular & Cellular Proteomics : MCP* 8 (10): 2227–42. doi:10.1074/mcp.M800462-MCP200.

Torres, Adrian Gabriel, Eduard Batlle, and Lluis Ribas de Pouplana. 2014. “Role of tRNA Modifications in Human Diseases..” *Trends in Molecular Medicine*, February. doi:10.1016/j.molmed.2014.01.008.

Touw, Wouter G, Jumamurat R Bayjanov, Lex Overmars, Lennart Backus, Jos Boekhorst, Michiel Wels, and Sacha AFT van Hijum. 2012. “Data Mining in the Life Sciences with Random Forest: a Walk in the Park or Lost in the Jungle?.” *Briefings in Bioinformatics*. Oxford Univ Press, bbs034.

Van der Veen, Annemarthe G, Kenji Schorpp, Christian Schlieker, Ludovico Buti, Jadyn R Damon, Eric Spooner, Hidde L Ploegh, and Stefan Jentsch. 2011. “Role of the Ubiquitin-Like Protein Urm1 as a Noncanonical Lysine-Directed Protein Modifier..” *Proceedings of the National Academy of Sciences* 108 (5): 1763–70. doi:10.1073/pnas.1014402108.

Veen, A G van der. 2011. “Urm1 in tRNA Thiolation and Protein Modification.” *Utrecht University*.

Vendeix, Franck A P, Frank V Murphy, William A Cantara, Grażyna Leszczyńska, Estella M Gustilo, Brian Sproat, Andrzej Malkiewicz, and Paul F Agris. 2012. “Human tRNA(Lys3)(UUU) Is Pre-Structured by Natural Modifications for Cognate and Wobble Codon Binding Through Keto-Enol Tautomerism..” *J Mol Biol* 416 (4): 467–85. doi:10.1016/j.jmb.2011.12.048.

Verghese, Jacob, Jennifer Abrams, Yanyu Wang, and Kevin A Morano. 2012. “Biology of the Heat Shock Response and Protein Chaperones: Budding Yeast (Saccharomyces Cerevisiae) as a Model System..” *Microbiology and Molecular Biology Reviews : MMBR* 76 (2): 115–58. doi:10.1128/MMBR.05018-11.

Walker, Jane, So Yeon Kwon, Paul Badenhorst, Phil East, Helen McNeill, and Jesper Q Svejstrup. 2011. “Role of Elongator Subunit Elp3 in Drosophila Melanogaster Larval Development and Immunity..” *Genetics* 187 (4): 1067–75. doi:10.1534/genetics.110.123893.

Wandinger, Sebastian K, Michael H Suhre, Harald Wegele, and Johannes Buchner. 2006. “The Phosphatase Ppt1 Is a Dedicated Regulator of the Molecular Chaperone Hsp90.” *The EMBO Journal* 25 (2). European Molecular Biology Organization: 367–76. doi:10.1038/sj.emboj.7600930.

Wang, Y Karen, Zhixiang Ma, Douglas F Quinn, and Emil W Fu. 2001. “Inverse 18O Labeling Mass Spectrometry for the Rapid Identification of Marker/Target Proteins.” *Analytical Chemistry* 73 (15). American Chemical Society : 3742–50. doi:10.1021/ac010043d.

Warner, J R. 1999. “The Economics of Ribosome Biosynthesis in Yeast..” *Trends Biochem. Sci.* 24 (11): 437–40.

Webb, Michael E, Andrée Marquet, Ralf R Mendel, Fabrice Rébeillé, and Alison G Smith. 2007. “Elucidating Biosynthetic Pathways for Vitamins and

Cofactors..” *Natural Product Reports* 24 (5): 988–1008. doi:10.1039/b703105j.

Werner-Washburne, M, J Becker, J Kosic-Smithers, and E A Craig. 1989. “Yeast Hsp70 RNA Levels Vary in Response to the Physiological Status of the Cell..” *Journal of Bacteriology* 171 (5): 2680–88.

Wieser, R, G Adam, A Wagner, C Schüller, G Marchler, H Ruis, Z Krawiec, and T Bilinski. 1991. “Heat Shock Factor-Independent Heat Control of Transcription of the CTT1 Gene Encoding the Cytosolic Catalase T of Saccharomyces Cerevisiae..” *The Journal of Biological Chemistry* 266 (19): 12406–11.

Wiśniewski, Jacek R, Alexandre Zougman, Nagarjuna Nagaraj, and Matthias Mann. 2009. “Universal Sample Preparation Method for Proteome Analysis.” *Nature Methods* 6 (5): 359–62. doi:10.1038/nmeth.1322.

Wittschieben, B O, G Otero, T de Bizemont, J Fellows, H Erdjument-Bromage, R Ohba, Y Li, C D Allis, P Tempst, and J Q Svejstrup. 1999. “A Novel Histone Acetyltransferase Is an Integral Subunit of Elongating RNA Polymerase II Holoenzyme..” *Molecular Cell* 4 (1): 123–28.

Woodward, W R, and E Herbert. 1972. “Coding Properties of Reticulocyte Lysine Transfer RNA's in Hemoglobin Synthesis.” *Science (New York, NY)* 177 (4055): 1197–99. doi:10.1126/science.177.4055.1197.

Wu, Chang-Yi, Sanja Roje, Francisco J Sandoval, Amanda J Bird, Dennis R Winge, and David J Eide. 2009. “Repression of Sulfate Assimilation Is an Adaptive Response of Yeast to the Oxidative Stress of Zinc Deficiency..” *Journal of Biological Chemistry* 284 (40): 27544–56. doi:10.1074/jbc.M109.042036.

Wu, Xi, and Benjamin P Tu. 2011. “Selective Regulation of Autophagy by the Iml1-Npr2-Npr3 Complex in the Absence of Nitrogen Starvation..” *Molecular Biology of the Cell* 22 (21): 4124–33. doi:10.1091/mbc.E11-06-0525.

Xi, J, Y Ge, C Kinsland, F W McLafferty, and T P Begley. 2001. “Biosynthesis of the Thiazole Moiety of Thiamin in Escherichia Coli: Identification of an Acyldisulfide-Linked Protein--Protein Conjugate That Is Functionally Analogous to the Ubiquitin/E1 Complex..” *Proceedings of the National Academy of Sciences of the United States of America* 98 (15): 8513–18. doi:10.1073/pnas.141226698.

Xu, Junjie, Jiahai Zhang, Li Wang, Jie Zhou, Hongda Huang, Jihui Wu, Yang Zhong, and Yunyu Shi. 2006. “Solution Structure of Urm1 and Its Implications for the Origin of Protein Modifiers..” *Proceedings of the National Academy of Sciences of the United States of America* 103 (31): 11625–30. doi:10.1073/pnas.0604876103.

Yacoubi, El, Basma, Marc Bailly, and Valérie de Crécy-Lagard. 2012. “Biosynthesis and Function of Posttranscriptional Modifications of Transfer RNAs..” *Annu. Rev. Genet.* 46: 69–95. doi:10.1146/annurev-genet-110711-155641.

Yarian, Connie, Hannah Townsend, Wojciech Czestkowski, Elzbieta Sochacka, Andrzej J Malkiewicz, Richard Guenther, Agnieszka Miskiewicz, and Paul F Agris. 2002. “Accurate Translation of the Genetic Code Depends on tRNA Modified Nucleosides..” *The Journal of Biological Chemistry* 277 (19): 16391–95. doi:10.1074/jbc.M200253200.

Yarian, Connie, Michal Marszalek, Elzbieta Sochacka, Andrzej Malkiewicz, Richard Guenther, Agnieszka Miskiewicz, and Paul F Agris. 2000. “Modified Nucleoside Dependent Watson–Crick and Wobble Codon Binding by tRNA LysUUUSpecies †.” *Biochemistry* 39 (44). American Chemical Society : 13390–95. doi:10.1021/bi001302g.

Yasukawa, T, T Suzuki, N Ishii, T Ueda, S Ohta, and K Watanabe. 2000. “Defect in Modification at the Anticodon Wobble Nucleotide of Mitochondrial tRNA(Lys) with the MERRF Encephalomyopathy Pathogenic Mutation..” *FEBS Letters* 467 (2-3): 175–78.

Yokoyama, S, T Watanabe, K Murao, H Ishikura, Z Yamaizumi, S Nishimura, and T Miyazawa. 1985. “Molecular Mechanism of Codon Recognition by tRNA Species with Modified Uridine in the First Position of the Anticodon..” *Proceedings of the National Academy of Sciences of the United States of America* 82 (15): 4905–9.

Yoshida, M, K Takeishi, and T Ukita. 1971. “Structural Studies on a Yeast Glutamic Acid tRNA Specific to GAA Codon..” *Biochim Biophys Acta* 228 (1): 153–66.

Zinshteyn, Boris, and Wendy V Gilbert. 2013. “Loss of a Conserved tRNA Anticodon Modification Perturbs Cellular Signaling..” *PLoS Genetics* 9 (8): e1003675. doi:10.1371/journal.pgen.1003675.

Appendix I: Supplementary to chapter 3

Table A1.1: Differentially expressed proteins in *urm1Δ*.
List of proteins that were found to have significantly altered expression in *urm1Δ* cells compared to wild-type cells. Protein ratios were obtained using the SILAC based quantitative proteomics from six biological replicates and were median normalised prior to statistical analysis by Bayes moderated *t*-test . An adjusted *p*-value of 0.05 (that corresponds to 5% FDR) was chosen as the threshold for statistical significance. List is sorted by $\log_2$(wt/*urm1Δ*) in the ascending order (up-regulated to down-regulated)

Systematic name	log2(wt/*urm1Δ*)	adj.P.Val	Protein name
YCR042C	-3.70	0.000	TAF2
YJR005W	-2.22	0.049	APL1
YMR303C	-1.90	0.021	ADH2
YHR216W	-1.79	0.001	IMD2
YJL200C	-1.38	0.000	ACO2
YDL113C	-1.20	0.031	ATG20
YML131W	-1.11	0.049	YML131W
YBR195C	-1.07	0.044	MSI1
YOR374W	-0.99	0.000	ALD4
YHR137W	-0.92	0.001	ARO9
YOL147C	-0.86	0.024	PEX11
YLR364W	-0.85	0.015	GRX8
YER073W	-0.82	0.006	ALD5
YML004C	-0.76	0.001	GLO1
YDR234W	-0.73	0.006	LYS4
YMR318C	-0.73	0.001	ADH6
YPL015C	-0.72	0.048	HST2
YJR103W	-0.70	0.001	URA8
YKR080W	-0.69	0.002	MTD1
YMR062C	-0.68	0.001	ARG7
YCR036W	-0.68	0.006	RBK1
YKL006C-A	-0.68	0.049	SFT1
YBL058W	-0.65	0.001	SHP1
YMR226C	-0.64	0.001	YMR226C
YHR029C	-0.64	0.004	YHI9
YNR074C	-0.63	0.006	AIF1
YML058W	-0.63	0.005	SML1
YDL125C	-0.63	0.002	HNT1
YDR394W	-0.63	0.001	RPT3
YKL206C	-0.62	0.002	ADD66

Systematic name	log2(wt/*urm1Δ*)	adj.P.Val	Protein name
YNL155W	-0.61	0.042	YNL155W
YEL060C	-0.60	0.002	PRB1
YDR380W	-0.60	0.039	ARO10
YDL131W	-0.60	0.048	LYS21
YDL007W	-0.60	0.001	RPT2
YJR109C	-0.59	0.017	CPA2
YER004W	-0.58	0.030	FMP52
YOL151W	-0.57	0.009	GRE2
YJL001W	-0.57	0.001	PRE3
YMR236W	-0.56	0.006	TAF9
YDL182W	-0.55	0.015	LYS20
YMR276W	-0.54	0.005	DSK2
YPR145W	-0.54	0.007	ASN1
YKL210W	-0.54	0.008	UBA1
YLR225C	-0.54	0.024	YLR225C
YOL143C	-0.53	0.034	RIB4
YDL189W	-0.53	0.012	RBS1
YCR073W-A	-0.53	0.001	SOL2
YMR002W	-0.53	0.023	MIC17
YML067C	-0.52	0.025	ERV41
YGR063C	-0.52	0.003	SPT4
YDR487C	-0.52	0.005	RIB3
YER090W	-0.52	0.004	TRP2
YBL022C	-0.51	0.001	PIM1
YHR076W	-0.51	0.011	PTC7
YNL312W	-0.51	0.002	RFA2
YJR096W	-0.51	0.013	YJR096W
YGR270W	-0.50	0.018	YTA7
YOR298C-A	-0.50	0.007	MBF1
YHR027C	-0.50	0.005	RPN1
YNR046W	-0.50	0.002	TRM112
YJR104C	-0.50	0.015	SOD1
YOR251C	-0.50	0.006	TUM1
YOR362C	-0.49	0.002	PRE10
YFL044C	-0.49	0.021	OTU1
YEL032W	-0.48	0.001	MCM3
YIL079C	-0.48	0.041	AIR1
YHR012W	-0.47	0.003	VPS29
YMR152W	-0.47	0.045	YIM1

Systematic name	log2(wt/*urm1Δ*)	adj.P.Val	Protein name
YDL006W	-0.47	0.004	PTC1
YER055C	-0.46	0.006	HIS1
YCL034W	-0.46	0.009	LSB5
YCL011C	-0.45	0.002	GBP2
YOR197W	-0.45	0.017	MCA1
YHR179W	-0.45	0.006	OYE2
YPR069C	-0.45	0.001	SPE3
YPL273W	-0.44	0.012	SAM4
YHR041C	-0.44	0.004	SRB2
YKR048C	-0.44	0.021	NAP1
YPL111W	-0.44	0.025	CAR1
YKL145W	-0.44	0.009	RPT1
YER074W-A	-0.44	0.037	YOS1
YPR062W	-0.44	0.004	FCY1
YEL056W	-0.43	0.008	HAT2
YCL033C	-0.43	0.003	MXR2
YIL108W	-0.43	0.019	YIL108W
YCL043C	-0.42	0.002	PDI1
YER042W	-0.42	0.013	MXR1
YOR007C	-0.42	0.005	SGT2
YOL149W	-0.42	0.014	DCP1
YIL035C	-0.42	0.032	CKA1
YOR259C	-0.42	0.004	RPT4
YOL098C	-0.41	0.040	YOL098C
YKL214C	-0.41	0.040	YRA2
YDR135C	-0.41	0.041	YCF1
YGL026C	-0.41	0.002	TRP5
YOR117W	-0.41	0.001	RPT5
YKL126W	-0.40	0.026	YPK1
YBR125C	-0.40	0.038	PTC4
YDR365C	-0.40	0.022	ESF1
YKL190W	-0.40	0.013	CNB1
YER094C	-0.40	0.009	PUP3
YLR244C	-0.39	0.002	MAP1
YGL100W	-0.39	0.037	SEH1
YDR211W	-0.39	0.014	GCD6
YLR257W	-0.38	0.021	YLR257W
YBR177C	-0.38	0.007	EHT1
YMR009W	-0.38	0.035	ADI1

Systematic name	log2(wt/*urm1Δ*)	adj.P.Val	Protein name
YPR127W	-0.38	0.035	YPR127W
YOR074C	-0.38	0.013	CDC21
YBR256C	-0.38	0.009	RIB5
YNL287W	-0.38	0.006	SEC21
YOR021C	-0.38	0.007	YOR021C
YDR143C	-0.38	0.018	SAN1
YIL065C	-0.38	0.007	FIS1
YNL084C	-0.37	0.003	END3
YDL120W	-0.37	0.008	YFH1
YAR014C	-0.37	0.009	BUD14
YNL241C	-0.37	0.003	ZWF1
YKR018C	-0.37	0.041	YKR018C
YPL170W	-0.37	0.005	DAP1
YPR016C	-0.37	0.002	TIF6
YIL041W	-0.37	0.002	GVP36
YML092C	-0.37	0.006	PRE8
YER012W	-0.37	0.002	PRE1
YGL242C	-0.37	0.038	YGL242C
YFR006W	-0.36	0.042	YFR006W
YHR200W	-0.36	0.036	RPN10
YKR066C	-0.36	0.010	CCP1
YLR351C	-0.36	0.007	NIT3
YCL057W	-0.36	0.008	PRD1
YOL070C	-0.36	0.035	NBA1
YGR124W	-0.36	0.025	ASN2
YHL011C	-0.35	0.005	PRS3
YGL234W	-0.35	0.002	ADE5,7
YMR214W	-0.35	0.009	SCJ1
YPL117C	-0.35	0.005	IDI1
YNR001C	-0.35	0.024	CIT1
YKL117W	-0.35	0.004	SBA1
YER143W	-0.35	0.005	DDI1
YAL042W	-0.35	0.015	ERV46
YLR055C	-0.35	0.046	SPT8
YHR190W	-0.35	0.013	ERG9
YGL238W	-0.34	0.041	CSE1
YGR001C	-0.34	0.013	YGR001C
YDR129C	-0.34	0.011	SAC6
YBL047C	-0.34	0.009	EDE1

Systematic name	log2(wt/*urm1Δ*)	adj.P.Val	Protein name
YNL220W	-0.34	0.017	ADE12
YNL035C	-0.34	0.009	YNL035C
YIR012W	-0.34	0.012	SQT1
YKR068C	-0.34	0.012	BET3
YGL106W	-0.33	0.006	MLC1
YOR286W	-0.33	0.036	RDL2
YPL004C	-0.33	0.045	LSP1
YFL016C	-0.33	0.008	MDJ1
YKL040C	-0.33	0.050	NFU1
YKL007W	-0.33	0.005	CAP1
YMR178W	-0.33	0.046	YMR178W
YOR155C	-0.32	0.012	ISN1
YLR147C	-0.32	0.034	SMD3
YML125C	-0.32	0.018	PGA3
YIL051C	-0.32	0.004	MMF1
YPL169C	-0.32	0.025	MEX67
YNL166C	-0.32	0.018	BNI5
YLR025W	-0.32	0.020	SNF7
YHR158C	-0.32	0.040	KEL1
YOR115C	-0.32	0.043	TRS33
YHL039W	-0.32	0.039	EFM1
YEL058W	-0.31	0.031	PCM1
YLR209C	-0.31	0.004	PNP1
YOR168W	-0.31	0.007	GLN4
YOR243C	-0.31	0.012	PUS7
YNL104C	-0.31	0.013	LEU4
YLR285W	-0.31	0.016	NNT1
YDL168W	-0.31	0.031	SFA1
YML101C	-0.31	0.012	CUE4
YFR004W	-0.31	0.012	RPN11
YDL235C	-0.31	0.016	YPD1
YDL173W	-0.31	0.012	PAR32
YNL108C	-0.30	0.011	YNL108C
YOR176W	-0.30	0.006	HEM15
YGR232W	-0.30	0.014	NAS6
YGR189C	-0.30	0.030	CRH1
YER122C	-0.30	0.012	GLO3
YGR086C	-0.30	0.007	PIL1
YOR157C	-0.30	0.043	PUP1

Systematic name	log2(wt/*urm1Δ*)	adj.P.Val	Protein name
YKL142W	-0.30	0.018	MRP8
YFR024C-A	-0.30	0.050	LSB3
YDL126C	-0.29	0.005	CDC48
YKR074W	-0.29	0.006	AIM29
YJL173C	-0.29	0.016	RFA3
YPR173C	-0.29	0.007	VPS4
YBR164C	-0.29	0.039	ARL1
YNR015W	-0.28	0.017	SMM1
YKL186C	-0.28	0.004	MTR2
YGR132C	-0.28	0.015	PHB1
YDR363W-A	-0.28	0.030	SEM1
YGL020C	-0.28	0.013	GET1
YHR138C	-0.27	0.042	YHR138C
YOL016C	-0.27	0.041	CMK2
YFR044C	-0.27	0.013	DUG1
YPL061W	-0.27	0.014	ALD6
YLR300W	-0.27	0.009	EXG1
YLR420W	-0.27	0.019	URA4
YNL064C	-0.27	0.033	YDJ1
YOR027W	-0.27	0.012	STI1
YNL330C	-0.27	0.021	RPD3
YMR091C	-0.26	0.015	NPL6
YGL105W	-0.26	0.005	ARC1
YEL036C	-0.26	0.030	ANP1
YDR411C	-0.26	0.038	DFM1
YGR253C	-0.26	0.008	PUP2
YLR212C	-0.26	0.046	TUB4
YIL034C	-0.26	0.007	CAP2
YBL045C	-0.26	0.034	COR1
YLR447C	-0.26	0.005	VMA6
YHR065C	-0.26	0.029	RRP3
YHR122W	-0.26	0.016	YHR122W
YNL232W	-0.26	0.007	CSL4
YGL048C	-0.26	0.005	RPT6
YLR413W	-0.25	0.050	YLR413W
YML036W	-0.25	0.026	CGI121
YML069W	-0.25	0.012	POB3
YGL246C	-0.25	0.039	RAI1
YDL065C	-0.25	0.038	PEX19

Systematic name	log2(wt/*urm1Δ*)	adj.P.Val	Protein name
YGR135W	-0.25	0.012	PRE9
YDR500C	-0.24	0.031	RPL37B
YDR167W	-0.24	0.018	TAF10
YPL188W	-0.24	0.014	POS5
YHL030W	-0.24	0.041	ECM29
YAL044C	-0.24	0.031	GCV3
YJL041W	-0.23	0.022	NSP1
YML105C	-0.23	0.007	SEC65
YDR035W	-0.23	0.035	ARO3
YML078W	-0.23	0.011	CPR3
YLR259C	-0.23	0.009	HSP60
YPR034W	-0.23	0.012	ARP7
YFR052W	-0.23	0.045	RPN12
YER021W	-0.23	0.031	RPN3
YOR323C	-0.23	0.010	PRO2
YML124C	-0.22	0.031	TUB3
YER078C	-0.22	0.043	ICP55
YKR043C	-0.22	0.022	SHB17
YKL077W	-0.22	0.010	YKL077W
YDR071C	-0.22	0.007	PAA1
YGR244C	-0.21	0.037	LSC2
YFR010W	-0.21	0.049	UBP6
YFR050C	-0.21	0.048	PRE4
YDL226C	-0.21	0.043	GCS1
YCL009C	-0.21	0.033	ILV6
YDR212W	-0.21	0.037	TCP1
YLR421C	-0.21	0.034	RPN13
YDL066W	-0.21	0.041	IDP1
YDR368W	-0.20	0.015	YPR1
YMR038C	-0.20	0.043	CCS1
YAL016W	-0.20	0.025	TPD3
YMR222C	-0.20	0.029	FSH2
YGR095C	-0.20	0.049	RRP46
YMR314W	-0.19	0.015	PRE5
YDR032C	-0.19	0.009	PST2
YOR046C	-0.19	0.018	DBP5
YGL221C	-0.19	0.017	NIF3
YFL018C	-0.19	0.013	LPD1
YJL014W	-0.19	0.014	CCT3

Systematic name	log2(wt/*urm1Δ*)	adj.P.Val	Protein name
YDL100C	-0.19	0.011	GET3
YLR231C	-0.19	0.049	BNA5
YOR057W	-0.19	0.037	SGT1
YFL028C	-0.19	0.016	CAF16
YER048W-A	-0.19	0.035	ISD11
YIR003W	-0.19	0.046	AIM21
YGR207C	-0.19	0.020	CIR1
YNL037C	-0.18	0.018	IDH1
YPL028W	-0.18	0.020	ERG10
YJR065C	-0.18	0.026	ARP3
YMR186W	-0.18	0.029	HSC82
YGL202W	-0.18	0.030	ARO8
YPR041W	-0.18	0.015	TIF5
YFR009W	-0.17	0.028	GCN20
YGR245C	-0.17	0.050	SDA1
YDL086W	-0.17	0.029	YDL086W
YJR045C	-0.17	0.041	SSC1
YKL029C	-0.17	0.030	MAE1
YPL218W	-0.16	0.038	SAR1
YDR092W	-0.15	0.046	UBC13
YLR325C	-0.15	0.040	RPL38
YCL028W	-0.12	0.049	RNQ1
YNL247W	0.14	0.039	YNL247W
YKL056C	0.15	0.050	TMA19
YDL185W	0.15	0.031	VMA1
YER165W	0.15	0.027	PAB1
YOR212W	0.16	0.046	STE4
YNL071W	0.16	0.030	LAT1
YBR048W	0.16	0.040	RPS11B
YDR025W	0.16	0.040	RPS11A
YJR105W	0.17	0.031	ADO1
YCR002C	0.17	0.040	CDC10
YDR429C	0.18	0.028	TIF35
YOR361C	0.18	0.031	PRT1
YGR159C	0.18	0.042	NSR1
YOL111C	0.19	0.046	MDY2
YMR309C	0.19	0.037	NIP1
YMR146C	0.20	0.021	TIF34
YNL307C	0.20	0.028	MCK1

Systematic name	log2(wt/*urm1Δ*)	adj.P.Val	Protein name
YHR127W	0.20	0.037	YHR127W
YCR012W	0.20	0.009	PGK1
YBR162C	0.20	0.041	TOS1
YPR183W	0.20	0.025	DPM1
YDR214W	0.20	0.012	AHA1
YDL103C	0.20	0.040	QRI1
YMR131C	0.21	0.012	RRB1
YBR094W	0.21	0.050	PBY1
YNL010W	0.21	0.026	YNL010W
YCR090C	0.21	0.044	YCR090C
YGR208W	0.21	0.030	SER2
YNL185C	0.21	0.044	MRPL19
YNL209W	0.22	0.007	SSB2
YBR154C	0.22	0.030	RPB5
YLR378C	0.22	0.042	SEC61
YHL004W	0.22	0.048	MRP4
YPL105C	0.22	0.007	SYH1
YNL208W	0.23	0.017	YNL208W
YKR001C	0.23	0.037	VPS1
YLR153C	0.23	0.021	ACS2
YDL161W	0.24	0.035	ENT1
YNL147W	0.24	0.047	LSM7
YDL055C	0.24	0.018	PSA1
YOR042W	0.24	0.009	CUE5
YGL157W	0.24	0.006	ARI1
YOR123C	0.24	0.032	LEO1
YNL007C	0.24	0.026	SIS1
YOR310C	0.24	0.031	NOP58
YDR060W	0.25	0.022	MAK21
YAR015W	0.25	0.039	ADE1
YGR155W	0.25	0.004	CYS4
YGR185C	0.26	0.004	TYS1
YOL059W	0.26	0.007	GPD2
YGR083C	0.26	0.025	GCD2
YMR220W	0.27	0.026	ERG8
YGR279C	0.27	0.017	SCW4
YOR051C	0.27	0.007	ETT1
YIL083C	0.27	0.015	CAB2
YMR124W	0.28	0.021	YMR124W

Systematic name	log2(wt/*urm1Δ*)	adj.P.Val	Protein name
YIL022W	0.28	0.013	TIM44
YMR072W	0.28	0.004	ABF2
YLR372W	0.28	0.030	SUR4
YGR218W	0.28	0.033	CRM1
YBL032W	0.28	0.003	HEK2
YDR385W	0.28	0.005	EFT2
YOR133W	0.28	0.005	EFT1
YER110C	0.28	0.004	KAP123
YNL197C	0.29	0.030	WHI3
YHR183W	0.29	0.007	GND1
YBR227C	0.29	0.029	MCX1
YOL077C	0.29	0.014	BRX1
YPL263C	0.29	0.028	KEL3
YGR180C	0.30	0.034	RNR4
YJR069C	0.30	0.005	HAM1
YMR109W	0.30	0.017	MYO5
YDR408C	0.30	0.010	ADE8
YNR026C	0.30	0.048	SEC12
YGR229C	0.30	0.013	SMI1
YBR159W	0.30	0.046	IFA38
YML025C	0.31	0.046	YML6
YCR084C	0.31	0.012	TUP1
YJR014W	0.31	0.002	TMA22
YBL091C	0.32	0.002	MAP2
YER112W	0.32	0.004	LSM4
YPL127C	0.32	0.016	HHO1
YPL243W	0.32	0.035	SRP68
YMR012W	0.32	0.033	CLU1
YAR042W	0.32	0.024	SWH1
YBR146W	0.32	0.027	MRPS9
YBR139W	0.32	0.040	YBR139W
YDL099W	0.32	0.022	BUG1
YMR296C	0.32	0.014	LCB1
YPL212C	0.33	0.016	PUS1
YER068W	0.33	0.044	MOT2
YDR023W	0.33	0.002	SES1
YKR095W-A	0.33	0.011	PCC1
YBR160W	0.33	0.016	CDC28
YML017W	0.33	0.014	PSP2

Systematic name	log2(wt/*urm1Δ*)	adj.P.Val	Protein name
YLR295C	0.33	0.021	ATP14
YDR533C	0.33	0.013	HSP31
YHR049W	0.33	0.039	FSH1
YDR518W	0.33	0.047	EUG1
YKR014C	0.34	0.034	YPT52
YLR033W	0.34	0.037	RSC58
YKL140W	0.34	0.021	TGL1
YBR118W	0.34	0.025	TEF2
YPR080W	0.34	0.025	TEF1
YGL049C	0.34	0.046	TIF4632
YNL168C	0.34	0.040	FMP41
YKL013C	0.34	0.025	ARC19
YJL080C	0.34	0.015	SCP160
YER048C	0.35	0.021	CAJ1
YEL071W	0.35	0.013	DLD3
YOL057W	0.35	0.019	YOL057W
YER025W	0.36	0.044	GCD11
YDL002C	0.36	0.020	NHP10
YPL195W	0.36	0.027	APL5
YGR156W	0.36	0.014	PTI1
YGR152C	0.36	0.013	RSR1
YHR020W	0.36	0.003	YHR020W
YLR418C	0.37	0.020	CDC73
YNL239W	0.37	0.006	LAP3
YNL141W	0.37	0.047	AAH1
YFL008W	0.38	0.019	SMC1
YLR309C	0.38	0.022	IMH1
YCR030C	0.38	0.010	SYP1
YCL059C	0.38	0.046	KRR1
YMR307W	0.39	0.028	GAS1
YHR121W	0.39	0.005	LSM12
YIL123W	0.40	0.011	SIM1
YEL042W	0.40	0.010	GDA1
YPR073C	0.40	0.007	LTP1
YGR082W	0.40	0.039	TOM20
YOR375C	0.40	0.021	GDH1
YGL253W	0.40	0.006	HXK2
YOR207C	0.40	0.041	RET1
YML094W	0.40	0.016	GIM5

Systematic name	log2(wt/*urm1Δ*)	adj.P.Val	Protein name
YCR093W	0.40	0.013	CDC39
YKL054C	0.41	0.054	DEF1
YPL231W	0.41	0.004	FAS2
YNL110C	0.41	0.010	NOP15
YDL208W	0.41	0.011	NHP2
YLR249W	0.42	0.002	YEF3
YKL122C	0.42	0.004	SRP21
YER082C	0.42	0.023	UTP7
YJR010W	0.42	0.009	MET3
YPR148C	0.43	0.003	YPR148C
YBL015W	0.43	0.021	ACH1
YJL033W	0.43	0.038	HCA4
YDR144C	0.43	0.014	MKC7
YGL206C	0.43	0.046	CHC1
YGL095C	0.43	0.046	VPS45
YOL109W	0.43	0.004	ZEO1
YFL045C	0.43	0.002	SEC53
YPR133C	0.43	0.014	SPN1
YKL065C	0.43	0.039	YET1
YKL082C	0.44	0.003	RRP14
YJL158C	0.44	0.030	CIS3
YML106W	0.44	0.022	URA5
YGL009C	0.44	0.007	LEU1
YLR229C	0.44	0.018	CDC42
YDR251W	0.45	0.043	PAM1
YGL173C	0.46	0.014	XRN1
YJL026W	0.46	0.003	RNR2
YNL182C	0.46	0.004	IPI3
YAL021C	0.46	0.036	CCR4
YLR449W	0.46	0.030	FPR4
YNR016C	0.47	0.036	ACC1
YBR133C	0.47	0.039	HSL7
YDR279W	0.48	0.028	RNH202
YDR170C	0.48	0.020	SEC7
YDL147W	0.48	0.017	RPN5
YDL124W	0.49	0.010	YDL124W
YMR235C	0.49	0.001	RNA1
YHR019C	0.49	0.009	DED81
YCR016W	0.49	0.007	YCR016W

Systematic name	log2(wt/*urm1Δ*)	adj.P.Val	Protein name
YLR248W	0.49	0.007	RCK2
YML072C	0.50	0.036	TCB3
YJL124C	0.50	0.008	LSM1
YDL165W	0.51	0.002	CDC36
YMR173W	0.51	0.002	DDR48
YGR019W	0.51	0.032	UGA1
YFR041C	0.52	0.010	ERJ5
YDR292C	0.52	0.025	SRP101
YPL019C	0.53	0.045	VTC3
YGL232W	0.53	0.003	TAN1
YHR135C	0.53	0.007	YCK1
YER043C	0.53	0.002	SAH1
YGL125W	0.53	0.001	MET13
YDL171C	0.53	0.020	GLT1
YLR175W	0.54	0.001	CBF5
YKL001C	0.54	0.034	MET14
YMR128W	0.54	0.008	ECM16
YMR099C	0.56	0.003	YMR099C
YGR009C	0.56	0.002	SEC9
YJR132W	0.56	0.007	NMD5
YMR043W	0.56	0.008	MCM1
YLR206W	0.56	0.025	ENT2
YDR502C	0.57	0.001	SAM2
YOR198C	0.57	0.005	BFR1
YMR205C	0.57	0.023	PFK2
YJR007W	0.57	0.002	SUI2
YFR001W	0.57	0.003	LOC1
YPL146C	0.57	0.007	NOP53
YNL231C	0.57	0.005	PDR16
YHR107C	0.57	0.002	CDC12
YBR216C	0.57	0.036	YBP1
YLL013C	0.58	0.019	PUF3
YOL140W	0.58	0.017	ARG8
YNL015W	0.59	0.007	PBI2
YKL129C	0.59	0.017	MYO3
YDR233C	0.59	0.001	RTN1
YER091C	0.59	0.001	MET6
YKL148C	0.60	0.003	SDH1
YDR091C	0.60	0.004	RLI1

Systematic name	log2(wt/*urm1Δ*)	adj.P.Val	Protein name
YFL034C-A	0.61	0.003	RPL22B
YOL012C	0.61	0.006	HTZ1
YGL111W	0.63	0.001	NSA1
YLR069C	0.64	0.002	MEF1
YKL184W	0.64	0.036	SPE1
YNL088W	0.65	0.014	TOP2
YDL201W	0.65	0.001	TRM8
YLR354C	0.66	0.012	TAL1
YHR113W	0.66	0.007	APE4
YOL082W	0.66	0.036	ATG19
YOR163W	0.67	0.028	DDP1
YKL057C	0.68	0.043	NUP120
YOR206W	0.69	0.008	NOC2
YBR169C	0.70	0.011	SSE2
YPL084W	0.71	0.042	BRO1
YIL063C	0.73	0.001	YRB2
YBR233W	0.74	0.026	PBP2
YGL196W	0.77	0.048	DSD1
YNL167C	0.78	0.044	SKO1
YOL103W-B	0.78	0.007	YOL103W-B
YKL157W	0.79	0.002	APE2
YOL031C	0.79	0.015	SIL1
YDL213C	0.79	0.000	NOP6
YDR150W	0.81	0.034	NUM1
YKL105C	0.81	0.036	YKL105C
YPL081W	0.83	0.001	RPS9A
YBL005W-B	0.84	0.007	YBL005W-B
YKR095W	0.84	0.024	MLP1
YOR120W	0.85	0.007	GCY1
YPR072W	0.85	0.001	NOT5
YMR045C	0.86	0.031	YMR045C
YHR201C	0.87	0.010	PPX1
YPL199C	0.87	0.002	YPL199C
YKR016W	0.93	0.003	FCJ1
YJL088W	0.98	0.007	ARG3
YDL021W	0.99	0.008	GPM2
YBR053C	0.99	0.017	YBR053C
YLR003C	1.01	0.005	CMS1
YGR177C	1.09	0.022	ATF2

Systematic name	log2(wt/*urm1Δ*)	adj.P.Val	Protein name
YBR072W	1.09	0.049	HSP26
YCR005C	1.12	0.002	CIT2
YDR538W	1.14	0.034	PAD1
YDR033W	1.30	0.010	MRH1
YKL120W	1.38	0.041	OAC1
YJL052W	1.40	0.001	TDH1
YOR289W	1.41	0.028	YOR289W
YNL160W	1.65	0.001	YGP1
YDL045W-A	1.95	0.015	MRP10
YOL154W	2.04	0.007	ZPS1
YJL153C	3.25	0.004	INO1
YKL166C	3.52	0.014	TPK3
YIL008W	3.85	0.005	URM1
YOR137C	6.58	0.002	SIA1
YGR109W-B	8.42	0.017	YGR109W-B
YIL080W	8.42	0.017	YIL080W
YIL082W-A	8.42	0.017	YIL082W-A

Table A1.2: GO BP and MIPS functional classes up-regulated in *urm1Δ*.
Significantly down-regulated proteins in *urm1Δ* cells were tested for the enrichment of gene ontology terms for biological processes and MIPS functional classes using the web based FunSpec tool. Shown here are the different GO or MIPS categories with their respective p-values. f = total number of proteins in the yeast proteome belonging to a category, and k = total number of proteins in the input cluster that can be associated to that category. Also see figure 3.9A.

GO Biological Process				
Category	**p-value**	**In category from cluster**	**k**	**f**
proteasomal ubiquitin-dependent protein catabolic process	0.0000	Shp1 Sem1 Pre1 Pup3 Rpn11 Pre4 Rpt6 Pre9 Pup2 Pre3 Pre8 Pre5 Pup1 Pre10	14	32
proteasomal ubiquitin-independent protein catabolic process	0.0000	Pre1 Pup3 Pre4 Pre9 Pup2 Pre3 Pre8 Pre5 Pup1 Pre10	10	14
ubiquitin-dependent protein catabolic process	0.0000	Rpt2 Cdc48 Sem1 Rpt3 Rpn3 Ddi1 Ubp6 Rpn12 Pre9 Pup2 Rpn1 Rpn10 Rpt1 Rpn13 Pre8 Pre5 Rpt5 Pre10	18	69
proteolysis involved in cellular protein catabolic process	0.0000	Pre1 Pup3 Pre4 Pre9 Pup2 Pre3 Pre8 Pre5 Pup1 Pre10	10	18
oxidation-reduction process	0.0000	Mxr2 Idp1 Yfh1 Sfa1 Pst2 Ypr1 Mxr1 Ald5 Lpd1 Oye2 Erg9 Imd2 Yjr096W Sod1 Mae1 Ccp1 Mtd1 Pga3 Yml131W Adi1 Ccs1 Yim1 Ymr226C Adh2 Adh6 Idh1 Zwf1 Smm1 Aif1 Gre2 Pro2 Ald4 Ald6 Ypr127W	34	272
proteasome regulatory particle assembly	0.0000	Rpt2 Rpt3 Rpt6 Nas6 Rpt1 Rpt5 Rpt4	7	10
metabolic process	0.0000	Ilv6 Hnt1 Lys21 Sfa1 Lys20 Aro3 Paa1 Lys4 Fmp52 Ald5 Dug1 Trp5 Ade5,7 Crh1 Lsc2 Ptc7 Oye2 Erg9 Imd2 Aco2 Cpa2 Mae1 Uba1 Mtd1 Bna5 Exg1 Yml131W Arg7 Yim1 Ymr226C Adh2 Adh6 Idh1 Leu4 Zwf1 Smm1 Gre2 Pro2 Ald4 Erg10 Ald6 Pos5 Fcy1	43	425
positive regulation of RNA polymerase II transcriptional preinitiation complex assembly	0.0000	Rpt3 Rpt6 Rpt1 Pob3 Rpt5 Rpt4	6	10
cellular amino acid biosynthetic process	0.0000	Ilv6 Lys21 Lys20 Aro3 Lys4 His1 Trp2 Trp5 Asn2 Cpa2 Adi1 Arg7 Leu4 Pro2 Sam4 Asn1	16	98
de novo' protein folding	0.0000	Mdj1 Hsp60 Hsc82 Ydj1	4	6
response to heat	0.0001	Get3 Mdj1 Pil1 Ydj1 Sgt2 Lsp1	6	17
proteolysis	0.0001	Pim1 Cor1 Prd1 Prb1 Icp55 Ddi1 Yfr006W Rpn12 Nas6 Map1 Yol098C Mca1	12	74
acetate biosynthetic process	0.0001	Ald5 Ald4 Ald6	3	3
protein catabolic process	0.0001	Rpt2 Rpt3 Rpt6 Rpt1 Rpt5 Rpt4	6	19

GO Biological Process				
Category	**p-value**	**In category from cluster**	**k**	**f**
protein folding	0.0002	Pdi1 Tcp1 Mdj1 Phb1 Cct3 Ssc1 Sba1 Hsp60 Cpr3 Hsc82 Scj1 Ydj1 Sti1	13	96
proteasome assembly	0.0003	Sem1 Pre4 Ecm29 Add66 Hsc82	5	15
protein refolding	0.0004	Mdj1 Ssc1 Hsp60 Hsc82 Ydj1	5	16
ER-associated protein catabolic process	0.0009	Shp1 Cdc48 Dfm1 Add66 Scj1 Dsk2 Ydj1 Rpt4	8	48
biosynthetic process	0.0014	Aro3 Gcd6 Trp2 Aro8 Yhi9 Aro9 Erg9	7	40
furaldehyde metabolic process	0.0019	Sfa1 Adh6	2	2
mature ribosome assembly	0.0019	Tif6 Tif5	2	2
aromatic amino acid family metabolic process	0.0019	Aro8 Aro9	2	2
actin filament capping	0.0019	Cap2 Cap1	2	2
positive regulation of sequence-specific DNA binding transcription factor activity	0.0019	Rpt6 Sod1	2	2
apoptosis	0.0021	Oye2 Fis1 Cpr3 Aif1 Mca1	5	22
NADPH regeneration	0.0025	Zwf1 Ald4 Ald6	3	7
cellular process	0.0025	Icp55 Yfr006W Map1	3	7
protein stabilization	0.0025	Pex19 Icp55 Hsp60	3	7
peroxisome fission	0.0025	Rpn11 Fis1 Pex11	3	7
riboflavin biosynthetic process	0.0025	Rib5 Rib3 Rib4	3	7
carboxylic acid metabolic process	0.0038	Lys21 Lys20 Leu4	3	8
lysine biosynthetic process	0.0038	Lys21 Lys20 Lys4	3	8
lysine biosynthetic process via aminoadipic acid	0.0038	Lys21 Lys20 Lys4	3	8
pyruvate metabolic process	0.0038	Lpd1 Mae1 Ald4	3	8
cGMP biosynthetic process	0.0054	Bet3 Trs33	2	3
leucine catabolic process	0.0054	Aro10 Lpd1	2	3
asparagine biosynthetic process	0.0054	Asn2 Asn1	2	3
pyrimidine base biosynthetic process	0.0054	Ura8 Ura4	2	3
glycine catabolic process	0.0054	Gcv3 Lpd1	2	3
misfolded or incompletely synthesized protein catabolic process	0.0056	Pim1 Mdj1 Mca1	3	9
retrograde vesicle-mediated transport, Golgi to ER	0.0064	Get3 Gcs1 Glo3 Get1 Sec21	5	28

GO Biological Process				
Category	**p-value**	**In category from cluster**	**k**	**f**
purine nucleotide biosynthetic process	0.0065	Ade5,7 Imd2 Mtd1 Ade12	4	18
tricarboxylic acid cycle	0.0086	Idp1 Lsc2 Aco2 Idh1 Cit1	5	30

MIPS Functional Classification				
Category	**p-value**	**In category from cluster**	**k**	**f**
protein processing (proteolytic)	0.0000	Rpt2 Rpt3 Pre1 Pup3 Rpn11 Pre4 Rpn12 Rpt6 Pre9 Pup2 Rpn1 Rpn10 Pre3 Rpt1 Map1 Rpn13 Pre8 Pre5 Rpt5 Pup1 Rpt4 Pre10	22	63
proteasomal degradation (ubiquitin/proteasomal pathway)	0.0000	Shp1 Rpt2 Cdc48 Ubc13 San1 Sem1 Rpt3 Pre1 Rpn3 Pup3 Ddi1 Otu1 Rpn11 Pre4 Rpn12 Rpt6 Pre9 Pup2 Rpn1 Rpn10 Pre3 Rpt1 Uba1 Pre8 Pre5 Sgt1 Rpt5 Pup1 Rpt4 Pre10	30	128
protein folding and stabilization	0.0000	Pdi1 Tcp1 Mdj1 Cct3 Ssc1 Sba1 Hsp60 Cpr3 Ccs1 Hsc82 Scj1 Ydj1 Sti1 Sgt1	14	93
ATP binding	0.0001	Pim1 Rbk1 Rpt2 Get3 Cdc48 San1 Rpt3 Mcm3 Caf16 Gcn20 Rpt6 Ade5,7 Lsc2 Yta7 Rrp3 Ssc1 Rpt1 Uba1 Rpt5 Rpt4 Vps4	21	191
C-2 compound and organic acid catabolism	0.0004	Ald5 Adh2 Ald4 Ald6	4	9
oxidative stress response	0.0005	Mxr2 Yfh1 Pst2 Mxr1 Sod1 Ccp1 Aif1 Gre2 Pos5	9	55
heat shock response	0.0013	Pim1 Get3 Pil1 Gre2 Lsp1	5	20
tricarboxylic-acid pathway (citrate cycle, Krebs cycle, TCA cycle)	0.0018	Idp1 Lpd1 Lsc2 Aco2 Idh1 Cit1	6	31
metabolism of alkaloids	0.0019	Aro8 Aro9	2	2
ER to Golgi transport	0.0030	Erv46 Gcs1 Yos1 Glo3 Bet3 Erv41 Sec21 Trs33 Sar1	9	70
endocytosis	0.0036	Ede1 Lsb5 Sac6 Mlc1 Cap2 Cap1 Ypk1 End3	8	59
protein/peptide degradation	0.0038	Pim1 Icp55 Mdj1 Yfr006W Phb1 Ecm29 Rpn13	7	47
metabolism of tryptophan	0.0038	Aro8 Aro9 Bna5	3	8
aminoadipic acid pathway	0.0056	Lys21 Lys20 Lys4	3	9
purine nucleotide/ nucleoside/nucleobase anabolism	0.0074	Ade5,7 Prs3 Imd2 Mtd1 Ade12	5	29
temperature perception and response	0.0080	Pim1 Get3 Pil1 Lsp1	4	19

Table A1.3: GO BP and MIPS functional classes down-regulated in *urm1Δ*. Significantly down-regulated proteins in *urm1Δ* cells were tested for the enrichment of gene ontology terms for biological processes and MIPS functional classes using the web based FunSpec tool. Shown here are the different GO or MIPS categories with their respective p-values. f = total number of proteins in the yeast proteome belonging to a category, and k = total number of proteins in the input cluster that can be associated to that category. Also see figure figure 3.9B.

GO Biological Process				
Category	***p*-value**	**In category from cluster**	**k**	**f**
translational initiation	0.0000	Rli1 Tif35 Gcd11 Tif4632 Gcd2 Sui2 Tma22 Clu1 Tif34 Nip1 Sis1 Prt1	12	43
translation	0.0000	Rps11B Tef2 Mrps9 Ses1 Rps11A Rli1 Eft2 Tif35 Gcd11 Rpl22B Tif4632 Gcd2 Tys1 Mrp4 Ded81 Yhr020W Sui2 Tma19 Mef1 Yef3 Yml6 Tif34 Nip1 Mrpl19 Ssb2 Ynl247W Brx1 Eft1 Prt1 Rps9A Tef1	31	318
nuclear-transcribed mRNA poly(A) tail shortening	0.0000	Ccr4 Cdc39 Cdc36 Mot2 Not5	5	8
ribosome biogenesis	0.0000	Krr1 Nhp2 Nop6 Mak21 Rli1 Utp7 Loc1 Nsa1 Hca4 Rrp14 Cbf5 Ecm16 Rrb1 Nop15 Ipi3 Brx1 Noc2 Nop58 Rps9A Nop53	20	170
rRNA processing	0.0000	Krr1 Nhp2 Nop6 Rli1 Utp7 Lsm4 Nsa1 Kem1 Nsr1 Hca4 Rrp14 Cbf5 Ecm16 Rrb1 Nop15 Lsm7 Ipi3 Ssb2 Nop58 Rps9A Nop53	21	195
GTP catabolic process	0.0000	Tef2 Eft2 Gcd11 Rsr1 Vps1 Mef1 Eft1 Tef1	8	33
nuclear-transcribed mRNA catabolic process, deadenylation-dependent decay	0.0001	Ccr4 Cdc39 Cdc36 Lsm1 Puf3	5	12
nuclear-transcribed mRNA catabolic process	0.0001	Pby1 Lsm4 Kem1 Puf3 Lsm7	5	14
methionine metabolic process	0.0001	Sam2 Sah1 Met13 Met3 Met14	5	14
translational elongation	0.0002	Tef2 Eft2 Mef1 Yef3 Eft1 Tef1	6	22
transcription elongation from RNA polymerase II promoter	0.0002	Ccr4 Cdc39 Cdc36 Mot2 Rsc58 Cdc73 Leo1 Not5 Spn1	9	54
snRNA pseudouridine synthesis	0.0011	Nhp2 Cbf5 Pus1	3	6
ribosomal subunit export from nucleus	0.0013	Rli1 Rna1 Ssb2 Noc2	4	13
protein import into nucleus	0.0014	Rtn1 Kap123 Nmd5 Mlp1 Rna1 Acc1	6	32
deoxyribonucleoside diphosphate metabolic process	0.0016	Rnr4 Rnr2	2	2
actin cortical patch assembly	0.0017	Syp1 Ent1 Arc19 Ent2	4	14

GO Biological Process				
Category	***p*-value**	**In category from cluster**	**k**	**f**
intracellular mRNA localization	0.0017	Hek2 Loc1 Scp160 Puf3	4	14
protein targeting to ER	0.0023	Srp101 Sec53 Srp21 Srp68	4	15
glycolysis	0.0043	Pgk1 Gpm2 Hxk2 Tdh1 Pfk2	5	28
response to pheromone involved in conjugation with cellular fusion	0.0045	Cdc39 Cdc36	2	3
fatty acid elongation	0.0045	Ifa38 Sur4	2	3
rRNA pseudouridine synthesis	0.0045	Nhp2 Cbf5	2	3
endocytosis	0.0048	Swh1 Ent1 Chc1 Yck1 Myo3 Vps1 Ypt52 Ent2 Myo5	9	82
bipolar cellular bud site selection	0.0051	Cdc10 Rsr1 Cdc12 Myo3 Myo5	5	29
conjugation with cellular fusion	0.0070	Cdc10 Mot2 Scw4 Cdc12	4	20
fatty acid biosynthetic process	0.0099	Ifa38 Sur4 Acc1 Fas2	4	22

MIPS Functional Classification				
Category	***p*-value**	**In Category from Cluster**	**k**	**f**
translation initiation	0.0000	Rli1 Tif35 Gcd11 Tif4632 Gcd2 Sui2 Clu1 Tif34 Nip1 Sis1 Prt1	11	40
RNA processing	0.0000	Ccr4 Hek2 Cdc39 Cdc36 Mot2 Loc1 Puf3 Not5	8	31
ribosome biogenesis	0.0000	Krr1 Loc1 Nsa1 Crm1 Tma19 Ecm16 Rrb1 Rna1 Nop15 Noc2 Nop53	11	64
translation elongation	0.0001	Tef2 Eft2 Mef1 Yef3 Eft1 Tef1	6	21
RNA binding	0.0002	Hek2 Nhp2 Rnh202 Utp7 Pab1 Loc1 Tan1 Pti1 Nsr1 Mrp4 Lsm12 Scp160 Lsm1 Tma22 Puf3 Lsm7 Whi3 Brx1 Bfr1	19	189
RNA degradation	0.0002	Ccr4 Cdc39 Cdc36 Mot2 Kem1 Lsm1 Puf3 Lsm7 Not5	9	52
BIOGENESIS OF CELLULAR COMPONENTS	0.0006	Mak21 Rrb1 Noc2	3	5
budding, cell polarity and filament formation	0.0013	Hsl7 Cdc28 Cdc10 Cdc39 Ent1 Pam1 Vps45 Kem1 Sec9 Rsr1 Cdc12 Yck1 Cis3 Arc19 Rrp14 Myo3 Tpk3 Ent2 Cdc42 Sur4 Myo5 Whi3 Bfr1 Ste4	24	312
protein targeting, sorting and translocation	0.0016	Srp101 Kap123 Sec53 Vps45 Chc1 Tom20 Crm1 Tim44 Yrb2 Nmd5 Nup120 Srp21 Vps1 Ypt52 Mlp1 Imh1 Sec61 Rna1 Acc1 Sil1 Atg19 Srp68	22	281
NAD/NADP binding	0.0026	Ydl124W Met13 Gnd1 Ino1 Gpd2 Gdh1	6	36

MIPS Functional Classification				
Category	***p*-value**	**In Category from Cluster**	**k**	**f**
rRNA processing	0.0027	Krr1 Nhp2 Nop6 Utp7 Lsm4 Kem1 Nsr1 Hca4 Lsm1 Cbf5 Ecm16 Rna1 Ipi3 Nop58 Nop53	15	169
metabolism of cyclic and unusual nucleotides	0.0038	Ppx1 Met3 Cbf5 Pus1	4	17
sugar, glucoside, polyol and carboxylate catabolism	0.0044	Pgk1 Gpm2 Psa1 Sec53 Scw4 Tdh1 Sdh1 Tal1 Pfk2	9	81
nuclear transport	0.0056	Kap123 Crm1 Yrb2 Nmd5 Nup120 Mlp1 Rna1 Acc1 Noc2	9	84
pyrimidine nucleotide/ nucleoside/nucleobase metabolism	0.0068	Qri1 Gda1 Cbf5 Ura5 Pus1	5	31
metabolism of methionine	0.0084	Sam2 Sah1 Met13 Met3	4	21
protein transport	0.0097	Srp101 Kap123 Sec53 Tom20 Crm1 Tim44 Yrb2 Nmd5 Nup120 Srp21 Sec61 Srp68	12	141

Figure A1.1: Volcano plots of the codon biased genes from the WT vs. *urm1Δ* dataset.

Volcano plots showing the protein abundance ratios, measured by SILAC-based quantitative proteomics, with statistical significance, computed using Bayes moderated *t* test, of the top 1% yeast genes with the highest frequency of the indicated codons. The dotted red line indicates the 5% FDR, threshold for statistically significant changes in protein abundance. The grey dotted line indicates a wild-type/*urm1Δ* of 1.

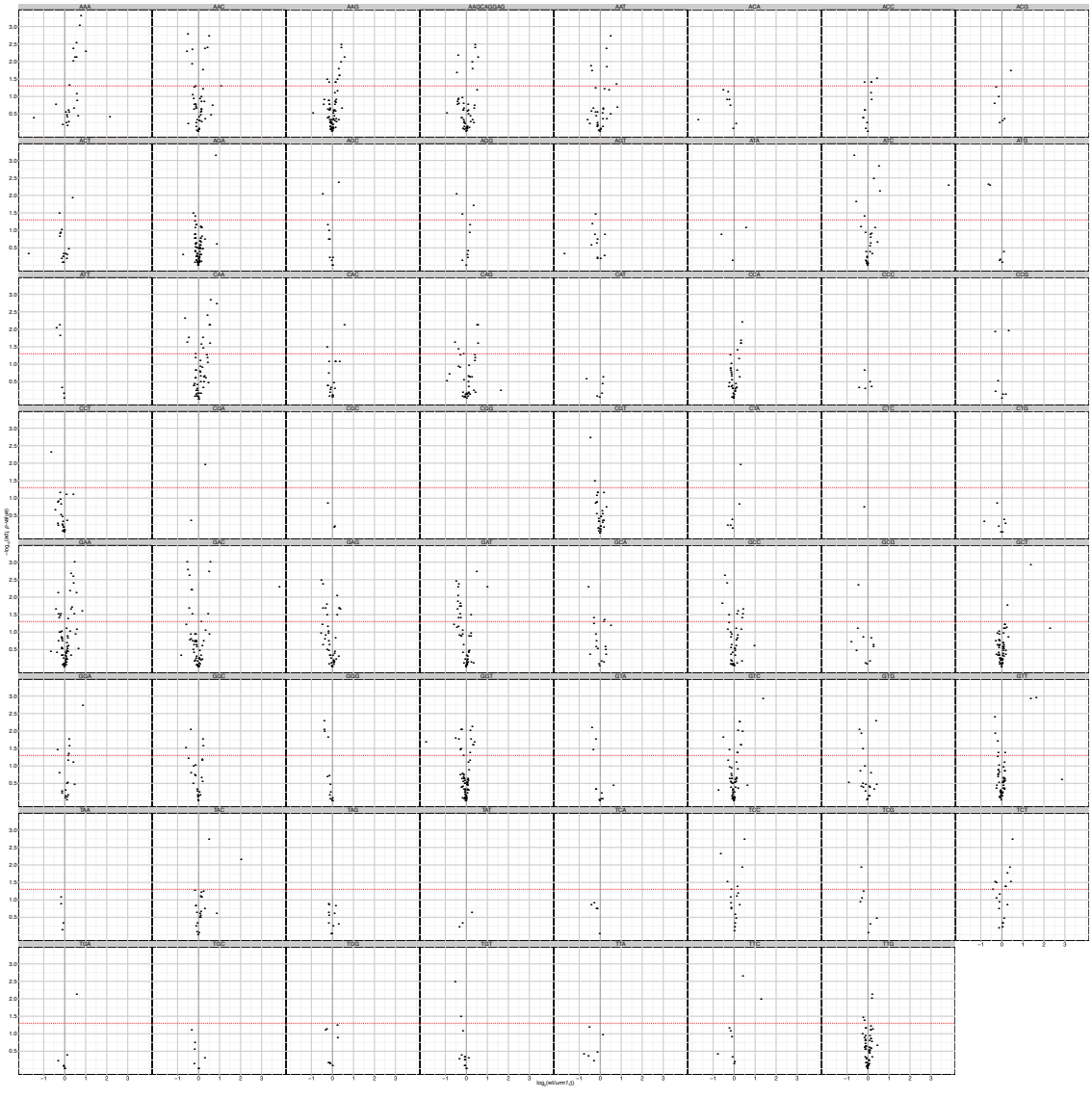

Appendix II: Supplementary to chapter 4

Table A2.1: Differentially expressed proteins at 37 °C.
List of proteins that were found to have significantly altered abundance in the cells grown at 37 °C compared to the cells grown at 30 °C. Protein ratios were obtained using the SILAC based quantitative proteomics from three biological replicates and were filtered and median normalised prior to statistical analysis by Bayes moderated *t*-test. An adjusted *p*-value of 0.01 (that corresponds to 1% FDR) was chosen as the threshold for statistical significance. List is sorted by $\log_2$(30 °C/37 °C) in the ascending order (that is, from the most up-regulated to the most down-regulated).

Systematic name	$\log_2$(30 ℃/37 ℃)	adj.P.Val	Protein name
YJR078W	-3.75	0.000	BNA2
YBR054W	-2.85	0.001	YRO2
YOR303W	-2.82	0.000	CPA1
YGR032W	-2.70	0.000	GSC2
YLR142W	-2.10	0.001	PUT1
YOL140W	-2.01	0.000	ARG8
YPL240C	-2.01	0.000	HSP82
YDL021W	-1.85	0.002	GPM2
YDR214W	-1.84	0.000	AHA1
YGL121C	-1.81	0.000	GPG1
YJL088W	-1.77	0.000	ARG3
YGR256W	-1.67	0.001	GND2
YBR072W	-1.65	0.000	HSP26
YOR020C	-1.65	0.000	HSP10
YDR258C	-1.64	0.000	HSP78
YER069W	-1.63	0.000	ARG5,6
YNL077W	-1.59	0.000	APJ1
YER103W	-1.45	0.000	SSA4
YNL281W	-1.45	0.000	HCH1
YAL005C	-1.40	0.000	SSA1
YLL026W	-1.37	0.000	HSP104
YBR085W	-1.33	0.001	AAC3
YLR178C	-1.27	0.000	TFS1
YOL055C	-1.25	0.000	THI20
YOL032W	-1.25	0.000	OPI10
YBL064C	-1.24	0.000	PRX1
YGR248W	-1.23	0.000	SOL4
YLR259C	-1.23	0.000	HSP60
YER137C	-1.21	0.000	YER137C
YAL060W	-1.21	0.000	BDH1
YOR374W	-1.20	0.000	ALD4

Systematic name	log_2(30 ℃/37 ℃)	adj.P.Val	Protein name
YOR027W	-1.19	0.000	STI1
YGR043C	-1.18	0.000	NQM1
YPL017C	-1.18	0.000	IRC15
YLR216C	-1.17	0.000	CPR6
YHR179W	-1.17	0.000	OYE2
YDR171W	-1.16	0.000	HSP42
YNL160W	-1.15	0.007	YGP1
YEL066W	-1.15	0.000	HPA3
YJR096W	-1.14	0.000	YJR096W
YPL214C	-1.13	0.000	THI6
YLR251W	-1.12	0.000	SYM1
YOL052C	-1.11	0.000	SPE2
YNL194C	-1.10	0.001	YNL194C
YHR199C	-1.10	0.001	AIM46
YOL058W	-1.10	0.000	ARG1
YAL061W	-1.09	0.000	BDH2
YPL092W	-1.06	0.002	SSU1
YPL111W	-1.05	0.000	CAR1
YFL016C	-1.05	0.000	MDJ1
YMR264W	-1.05	0.000	CUE1
YCR048W	-1.00	0.001	ARE1
YMR008C	-0.99	0.000	PLB1
YHR112C	-0.99	0.000	YHR112C
YGR177C	-0.98	0.000	ATF2
YML059C	-0.98	0.001	NTE1
YJR103W	-0.98	0.000	URA8
YBL075C	-0.97	0.001	SSA3
YJL082W	-0.96	0.001	IML2
YKL024C	-0.95	0.000	URA6
YDR173C	-0.95	0.001	ARG82
YJR047C	-0.95	0.000	ANB1
YJL052W	-0.95	0.000	TDH1
YMR083W	-0.94	0.000	ADH3
YPL071C	-0.94	0.000	YPL071C
YHR104W	-0.94	0.000	GRE3
YGL037C	-0.93	0.000	PNC1
YCL004W	-0.93	0.001	PGS1
YKR080W	-0.93	0.000	MTD1
YKL151C	-0.93	0.000	YKL151C
YCR008W	-0.92	0.001	SAT4
YDR239C	-0.92	0.004	YDR239C

Systematic name	log_2(30 ℃/37 ℃)	adj.P.Val	Protein name
YOR137C	-0.91	0.004	SIA1
YCR005C	-0.91	0.001	CIT2
YLR258W	-0.90	0.000	GSY2
YMR104C	-0.90	0.001	YPK2
YJL137C	-0.90	0.007	GLG2
YLR179C	-0.89	0.000	YLR179C
YPL119C	-0.89	0.001	DBP1
YPR127W	-0.89	0.001	YPR127W
YKL218C	-0.89	0.001	SRY1
YCR083W	-0.88	0.001	TRX3
YCL047C	-0.88	0.001	POF1
YDR493W	-0.87	0.000	MZM1
YDR511W	-0.87	0.001	ACN9
YFR053C	-0.85	0.000	HXK1
YBL057C	-0.85	0.000	PTH2
YGR012W	-0.85	0.000	YGR012W
YLR063W	-0.84	0.000	YLR063W
YNR034W-A	-0.84	0.002	YNR034W-A
YKR009C	-0.84	0.002	FOX2
YHR047C	-0.84	0.000	AAP1
YIL156W-B	-0.83	0.001	YIL156W-B
YMR022W	-0.83	0.002	UBC7
YFR021W	-0.82	0.000	ATG18
YIL094C	-0.81	0.001	LYS12
YHR030C	-0.81	0.001	SLT2
YJL066C	-0.81	0.000	MPM1
YIL007C	-0.81	0.000	NAS2
YOR057W	-0.79	0.001	SGT1
YKR046C	-0.79	0.000	PET10
YPR002W	-0.79	0.001	PDH1
YBR092C	-0.79	0.001	PHO3
YOR148C	-0.78	0.002	SPP2
YPL152W	-0.78	0.001	RRD2
YJL159W	-0.78	0.002	HSP150
YDR453C	-0.78	0.001	TSA2
YBR169C	-0.78	0.001	SSE2
YFR007W	-0.77	0.001	YFH7
YGR049W	-0.77	0.002	SCM4
YMR262W	-0.77	0.001	YMR262W
YDL119C	-0.77	0.000	YDL119C
YLR326W	-0.76	0.002	YLR326W

Systematic name	log_2(30 ℃/37 ℃)	adj.P.Val	Protein name
YAL058W	-0.76	0.000	CNE1
YLR177W	-0.76	0.001	YLR177W
YCR068W	-0.76	0.002	ATG15
YMR186W	-0.76	0.001	HSC82
YBR006W	-0.76	0.001	UGA2
YGR180C	-0.76	0.000	RNR4
YBR101C	-0.75	0.001	FES1
YGL108C	-0.75	0.002	YGL108C
YER044C	-0.75	0.000	ERG28
YPR172W	-0.74	0.001	YPR172W
YMR303C	-0.74	0.001	ADH2
YDL131W	-0.74	0.001	LYS21
YJL034W	-0.73	0.001	KAR2
YPR026W	-0.73	0.001	ATH1
YNL310C	-0.73	0.003	ZIM17
YOR305W	-0.72	0.001	RRG7
YER061C	-0.72	0.001	CEM1
YBR230C	-0.72	0.001	OM14
YJR148W	-0.72	0.001	BAT2
YOL011W	-0.71	0.001	PLB3
YOR130C	-0.71	0.002	ORT1
YDL168W	-0.71	0.002	SFA1
YEL047C	-0.71	0.001	YEL047C
YDL175C	-0.71	0.002	AIR2
YHR029C	-0.71	0.001	YHI9
YBL098W	-0.71	0.001	BNA4
YLR137W	-0.71	0.001	RKM5
YER073W	-0.71	0.001	ALD5
YNL111C	-0.70	0.006	CYB5
YNR040W	-0.70	0.001	YNR040W
YOL133W	-0.70	0.001	HRT1
YKL142W	-0.70	0.001	MRP8
YNL200C	-0.69	0.001	YNL200C
YNL007C	-0.69	0.001	SIS1
YOR230W	-0.69	0.001	WTM1
YNR034W	-0.69	0.001	SOL1
YGR149W	-0.69	0.007	YGR149W
YPL196W	-0.69	0.001	OXR1
YDL022W	-0.68	0.001	GPD1
YJR135C	-0.68	0.001	MCM22
YIL065C	-0.68	0.001	FIS1

Systematic name	log_2(30 ℃/37 ℃)	adj.P.Val	Protein name
YKL120W	-0.68	0.008	OAC1
YER053C	-0.68	0.004	PIC2
YBR126C	-0.68	0.001	TPS1
YGL221C	-0.67	0.001	NIF3
YEL060C	-0.67	0.001	PRB1
YJR008W	-0.67	0.001	YJR008W
YML100W	-0.67	0.001	TSL1
YML130C	-0.67	0.001	ERO1
YOR089C	-0.66	0.001	VPS21
YOR147W	-0.66	0.005	MDM32
YDR381C-A	-0.66	0.001	YDR381C-A
YPL245W	-0.66	0.001	YPL245W
YPR042C	-0.65	0.001	PUF2
YPL097W	-0.65	0.004	MSY1
YHR207C	-0.65	0.001	SET5
YGR254W	-0.65	0.006	ENO1
YHR034C	-0.65	0.001	PIH1
YLR356W	-0.65	0.002	ATG33
YJL046W	-0.65	0.001	AIM22
YHR017W	-0.64	0.001	YSC83
YDL052C	-0.63	0.001	SLC1
YOL025W	-0.63	0.002	LAG2
YPL106C	-0.63	0.002	SSE1
YGR199W	-0.63	0.001	PMT6
YIL051C	-0.63	0.001	MMF1
YDR032C	-0.63	0.001	PST2
YGR250C	-0.63	0.001	YGR250C
YDR019C	-0.62	0.002	GCV1
YNL020C	-0.62	0.004	ARK1
YDL230W	-0.62	0.001	PTP1
YLR324W	-0.62	0.001	PEX30
YKL129C	-0.62	0.001	MYO3
YOR007C	-0.62	0.001	SGT2
YJL071W	-0.62	0.002	ARG2
YOR357C	-0.62	0.001	SNX3
YLR347C	-0.62	0.001	KAP95
YMR278W	-0.61	0.001	PGM3
YJL172W	-0.61	0.001	CPS1
YNR019W	-0.61	0.004	ARE2
YDR313C	-0.61	0.001	PIB1
YIL108W	-0.61	0.001	YIL108W

Systematic name	log_2(30 ℃/37 ℃)	adj.P.Val	Protein name
YKL103C	-0.61	0.001	LAP4
YMR087W	-0.61	0.001	YMR087W
YIR002C	-0.61	0.002	MPH1
YOR347C	-0.61	0.001	PYK2
YBL078C	-0.60	0.001	ATG8
YDR409W	-0.60	0.002	SIZ1
YMR170C	-0.60	0.002	ALD2
YNL064C	-0.60	0.001	YDJ1
YIL107C	-0.60	0.005	PFK26
YOL016C	-0.60	0.003	CMK2
YAL010C	-0.59	0.003	MDM10
YGL185C	-0.59	0.002	YGL185C
YOL107W	-0.59	0.002	YOL107W
YGR136W	-0.59	0.005	LSB1
YJR091C	-0.59	0.002	JSN1
YDR186C	-0.59	0.002	YDR186C
YMR214W	-0.59	0.001	SCJ1
YCR073W-A	-0.59	0.001	SOL2
YOR166C	-0.59	0.001	SWT1
YJL068C	-0.59	0.001	YJL068C
YBR022W	-0.59	0.001	POA1
YBR222C	-0.58	0.001	PCS60
YHL024W	-0.58	0.004	RIM4
YJR133W	-0.58	0.001	XPT1
YHR111W	-0.58	0.001	UBA4
YGR284C	-0.58	0.001	ERV29
YPL191C	-0.58	0.003	YPL191C
YDL217C	-0.57	0.004	TIM22
YBL060W	-0.57	0.001	YEL1
YCL040W	-0.57	0.002	GLK1
YDL135C	-0.57	0.001	RDI1
YBR256C	-0.57	0.003	RIB5
YGL212W	-0.57	0.008	VAM7
YDR533C	-0.57	0.003	HSP31
YDL125C	-0.56	0.001	HNT1
YJL057C	-0.56	0.001	IKS1
YJL055W	-0.56	0.002	YJL055W
YDR513W	-0.56	0.002	GRX2
YGL169W	-0.56	0.008	SUA5
YOL113W	-0.56	0.006	SKM1
YJL026W	-0.56	0.002	RNR2

Systematic name	log_2(30 ℃/37 ℃)	adj.P.Val	Protein name
YJL133W	-0.56	0.001	MRS3
YML014W	-0.56	0.001	TRM9
YKR066C	-0.55	0.003	CCP1
YIR035C	-0.55	0.002	YIR035C
YAL030W	-0.55	0.004	SNC1
YLR050C	-0.55	0.006	YLR050C
YJR025C	-0.55	0.002	BNA1
YOR054C	-0.55	0.004	VHS3
YOR094W	-0.55	0.001	ARF3
YMR105C	-0.55	0.001	PGM2
YFL014W	-0.54	0.004	HSP12
YOR349W	-0.54	0.002	CIN1
YDR204W	-0.54	0.002	COQ4
YCR076C	-0.54	0.008	YCR076C
YOR222W	-0.54	0.001	ODC2
YOR288C	-0.54	0.001	MPD1
YOR120W	-0.53	0.004	GCY1
YDR515W	-0.53	0.006	SLF1
YAL049C	-0.53	0.001	AIM2
YPL140C	-0.52	0.008	MKK2
YAL051W	-0.52	0.001	OAF1
YGL056C	-0.52	0.002	SDS23
YDR231C	-0.52	0.005	COX20
YNR030W	-0.52	0.003	ALG12
YHR123W	-0.52	0.003	EPT1
YBR160W	-0.52	0.003	CDC28
YER143W	-0.52	0.001	DDI1
YHR046C	-0.52	0.002	INM1
YJL073W	-0.52	0.002	JEM1
YOR112W	-0.52	0.002	CEX1
YJL141C	-0.51	0.002	YAK1
YIR037W	-0.51	0.003	HYR1
YDR228C	-0.51	0.002	PCF11
YOL009C	-0.51	0.002	MDM12
YDL177C	-0.51	0.004	YDL177C
YPR160W	-0.50	0.001	GPH1
YKR067W	-0.50	0.006	GPT2
YGL010W	-0.50	0.002	YGL010W
YGL087C	-0.50	0.003	MMS2
YCL043C	-0.50	0.002	PDI1
YGL045W	-0.50	0.009	RIM8

Systematic name	log_2(30 ℃/37 ℃)	adj.P.Val	Protein name
YDL100C	-0.49	0.002	GET3
YKL186C	-0.49	0.003	MTR2
YDL223C	-0.49	0.005	HBT1
YJR072C	-0.49	0.003	NPA3
YMR121C	-0.49	0.002	RPL15B
YLL024C	-0.49	0.002	SSA2
YDR177W	-0.48	0.005	UBC1
YDR400W	-0.48	0.008	URH1
YGR129W	-0.48	0.006	SYF2
YGL073W	-0.48	0.004	HSF1
YHR198C	-0.48	0.002	AIM18
YDR001C	-0.48	0.003	NTH1
YHR040W	-0.48	0.008	BCD1
YHR161C	-0.48	0.003	YAP1801
YNR006W	-0.47	0.007	VPS27
YHR043C	-0.47	0.007	DOG2
YDL006W	-0.47	0.002	PTC1
YDL182W	-0.47	0.006	LYS20
YDR234W	-0.47	0.008	LYS4
YER048W-A	-0.47	0.003	ISD11
YNL037C	-0.47	0.002	IDH1
YLR099W-A	-0.47	0.003	YLR099W-A
YOR220W	-0.47	0.004	RCN2
YEL017W	-0.47	0.003	GTT3
YIL097W	-0.47	0.002	FYV10
YML017W	-0.47	0.002	PSP2
YMR111C	-0.47	0.007	YMR111C
YGR038W	-0.47	0.002	ORM1
YDL144C	-0.46	0.004	YDL144C
YOL086C	-0.46	0.002	ADH1
YKL130C	-0.46	0.003	SHE2
YLR268W	-0.46	0.002	SEC22
YER062C	-0.46	0.004	HOR2
YBR176W	-0.46	0.002	ECM31
YNR047W	-0.46	0.003	FPK1
YPR049C	-0.46	0.008	ATG11
YGL040C	-0.45	0.003	HEM2
YIR007W	-0.45	0.007	YIR007W
YKL096W	-0.45	0.005	CWP1
YBL013W	-0.45	0.006	FMT1
YGR268C	-0.45	0.008	HUA1

Systematic name	log_2(30 ℃/37 ℃)	adj.P.Val	Protein name
YAL014C	-0.45	0.009	SYN8
YLR025W	-0.45	0.007	SNF7
YNL045W	-0.45	0.004	LAP2
YGL080W	-0.44	0.008	FMP37
YNL274C	-0.44	0.003	GOR1
YOR077W	-0.44	0.005	RTS2
YDR121W	-0.44	0.002	DPB4
YHR049W	-0.44	0.003	FSH1
YOR275C	-0.44	0.004	RIM20
YLR134W	-0.44	0.002	PDC5
YMR157C	-0.44	0.003	AIM36
YPL225W	-0.44	0.004	YPL225W
YAR042W	-0.44	0.002	SWH1
YAL041W	-0.44	0.002	CDC24
YNL191W	-0.44	0.003	DUG3
YDL146W	-0.44	0.002	LDB17
YGL141W	-0.44	0.002	HUL5
YGR019W	-0.43	0.002	UGA1
YHR192W	-0.43	0.003	YHR192W
YAL047C	-0.43	0.003	SPC72
YGR189C	-0.43	0.002	CRH1
YFR029W	-0.43	0.009	PTR3
YKL054C	-0.43	0.002	DEF1
YCL017C	-0.43	0.002	NFS1
YJR009C	-0.43	0.006	TDH2
YMR258C	-0.43	0.004	ROY1
YHL021C	-0.43	0.003	AIM17
YGR072W	-0.43	0.002	UPF3
YJR060W	-0.42	0.002	CBF1
YKL094W	-0.42	0.002	YJU3
YDR293C	-0.42	0.002	SSD1
YGR277C	-0.42	0.008	CAB4
YDR323C	-0.42	0.004	PEP7
YKR089C	-0.42	0.009	TGL4
YCR066W	-0.42	0.004	RAD18
YDL113C	-0.42	0.008	ATG20
YDL215C	-0.42	0.002	GDH2
YLR387C	-0.42	0.007	REH1
YLR256W	-0.41	0.005	HAP1
YDR516C	-0.41	0.003	EMI2
YBR082C	-0.41	0.006	UBC4

Systematic name	log_2(30 ℃/37 ℃)	adj.P.Val	Protein name
YMR222C	-0.41	0.004	FSH2
YLR270W	-0.41	0.004	DCS1
YGR111W	-0.41	0.003	YGR111W
YBR011C	-0.41	0.004	IPP1
YGL017W	-0.41	0.003	ATE1
YOR271C	-0.41	0.006	FSF1
YCL008C	-0.41	0.004	STP22
YMR020W	-0.40	0.003	FMS1
YNR035C	-0.40	0.004	ARC35
YCR012W	-0.40	0.005	PGK1
YKL149C	-0.40	0.004	DBR1
YNL130C	-0.40	0.007	CPT1
YHR025W	-0.40	0.003	THR1
YPR069C	-0.40	0.007	SPE3
YHL031C	-0.40	0.005	GOS1
YER141W	-0.40	0.007	COX15
YDR088C	-0.40	0.006	SLU7
YJL149W	-0.40	0.004	DAS1
YMR071C	-0.40	0.006	TVP18
YNR001C	-0.40	0.004	CIT1
YBR139W	-0.40	0.003	YBR139W
YDL064W	-0.40	0.005	UBC9
YOR273C	-0.39	0.009	TPO4
YHR008C	-0.39	0.004	SOD2
YER064C	-0.39	0.003	YER064C
YML020W	-0.39	0.005	YML020W
YER099C	-0.39	0.006	PRS2
YNL164C	-0.39	0.005	IBD2
YJR045C	-0.39	0.006	SSC1
YGL043W	-0.39	0.004	DST1
YLR116W	-0.39	0.003	MSL5
YMR062C	-0.39	0.003	ARG7
YOR238W	-0.39	0.004	YOR238W
YPL002C	-0.39	0.008	SNF8
YDR294C	-0.38	0.004	DPL1
YDL086W	-0.38	0.004	YDL086W
YOL059W	-0.38	0.004	GPD2
YOL088C	-0.38	0.004	MPD2
YMR102C	-0.38	0.004	YMR102C
YMR019W	-0.38	0.005	STB4
YCR086W	-0.38	0.009	CSM1

Systematic name	log_2(30 ℃/37 ℃)	adj.P.Val	Protein name
YJR074W	-0.37	0.009	MOG1
YGL050W	-0.37	0.008	TYW3
YJL099W	-0.37	0.006	CHS6
YAL036C	-0.37	0.007	RBG1
YLR072W	-0.37	0.005	YLR072W
YPL112C	-0.37	0.004	PEX25
YFL046W	-0.37	0.006	FMP32
YNL067W	-0.37	0.004	RPL9B
YFL042C	-0.37	0.005	YFL042C
YGR263C	-0.36	0.009	SAY1
YOR125C	-0.36	0.005	CAT5
YPR081C	-0.36	0.005	GRS2
YPL151C	-0.36	0.005	PRP46
YPL098C	-0.36	0.006	MGR2
YKL027W	-0.36	0.008	YKL027W
YGL224C	-0.36	0.006	SDT1
YPR025C	-0.36	0.005	CCL1
YGR080W	-0.36	0.008	TWF1
YPL144W	-0.36	0.004	POC4
YER042W	-0.36	0.005	MXR1
YBR234C	-0.36	0.004	ARC40
YML125C	-0.36	0.007	PGA3
YPL169C	-0.36	0.006	MEX67
YMR241W	-0.36	0.005	YHM2
YDR430C	-0.35	0.005	CYM1
YDR034C	-0.35	0.006	LYS14
YPR028W	-0.35	0.006	YOP1
YNL155W	-0.35	0.007	YNL155W
YDR002W	-0.35	0.005	YRB1
YNL035C	-0.35	0.006	YNL035C
YGL047W	-0.35	0.009	ALG13
YBR025C	-0.35	0.005	OLA1
YDR335W	-0.35	0.006	MSN5
YHR012W	-0.34	0.009	VPS29
YLR351C	-0.34	0.005	NIT3
YER087W	-0.34	0.009	AIM10
YHL029C	-0.34	0.004	OCA5
YJR032W	-0.34	0.007	CPR7
YDR481C	-0.34	0.005	PHO8
YKL073W	-0.34	0.009	LHS1
YBR065C	-0.34	0.005	ECM2

Systematic name	log_2(30 ℃/37 ℃)	adj.P.Val	Protein name
YFL038C	-0.34	0.009	YPT1
YKL144C	-0.34	0.005	RPC25
YIR021W	-0.33	0.009	MRS1
YNL055C	-0.33	0.006	POR1
YMR165C	-0.33	0.008	PAH1
YDR376W	-0.33	0.009	ARH1
YEL038W	-0.33	0.006	UTR4
YHR169W	-0.33	0.008	DBP8
YLL006W	-0.33	0.008	MMM1
YMR099C	-0.33	0.006	YMR099C
YER094C	-0.32	0.007	PUP3
YOR138C	-0.32	0.008	RUP1
YOR267C	-0.32	0.007	HRK1
YJR102C	-0.32	0.009	VPS25
YNL076W	-0.32	0.007	MKS1
YGL001C	-0.32	0.010	ERG26
YLR407W	-0.32	0.007	YLR407W
YNL026W	-0.31	0.006	SAM50
YIR036C	-0.31	0.006	IRC24
YIL104C	-0.31	0.008	SHQ1
YLR044C	-0.31	0.007	PDC1
YOR280C	-0.31	0.006	FSH3
YLR451W	-0.31	0.007	LEU3
YPR040W	-0.31	0.010	TIP41
YDR243C	-0.31	0.007	PRP28
YCR054C	-0.31	0.006	CTR86
YDL180W	-0.31	0.007	YDL180W
YNL068C	-0.31	0.009	FKH2
YDR517W	-0.30	0.007	GRH1
YJL201W	-0.30	0.007	ECM25
YMR196W	-0.30	0.009	YMR196W
YDR470C	-0.30	0.009	UGO1
YOR002W	-0.30	0.009	ALG6
YFR047C	-0.30	0.009	BNA6
YPL048W	-0.30	0.008	CAM1
YML013W	-0.30	0.008	UBX2
YLR186W	-0.29	0.007	EMG1
YNR049C	-0.29	0.009	MSO1
YER120W	-0.29	0.008	SCS2
YER019W	-0.29	0.009	ISC1
YKR049C	-0.29	0.009	FMP46

Systematic name	log_2(30 ℃/37 ℃)	adj.P.Val	Protein name
YLL018C	-0.29	0.009	DPS1
YIL136W	-0.28	0.009	OM45
YPR175W	-0.28	0.009	DPB2
YOR362C	-0.28	0.009	PRE10
YLR433C	-0.28	0.009	CNA1
YJL019W	-0.28	0.010	MPS3
YER074W	0.27	0.010	RPS24A
YIL069C	0.27	0.010	RPS24B
YHL015W	0.28	0.010	RPS20
YNL330C	0.28	0.010	RPD3
YOR371C	0.28	0.009	GPB1
YGL135W	0.28	0.009	RPL1B
YPL220W	0.28	0.009	RPL1A
YHR019C	0.28	0.009	DED81
YPR118W	0.28	0.009	MRI1
YNL251C	0.29	0.008	NRD1
YER148W	0.29	0.009	SPT15
YIL137C	0.29	0.009	TMA108
YGL103W	0.29	0.008	RPL28
YGL027C	0.29	0.008	CWH41
YGL133W	0.29	0.009	ITC1
YPL210C	0.30	0.009	SRP72
YOR184W	0.30	0.007	SER1
YDL083C	0.30	0.009	RPS16B
YMR143W	0.30	0.009	RPS16A
YDL153C	0.30	0.007	SAS10
YHR027C	0.30	0.008	RPN1
YDR440W	0.31	0.008	DOT1
YDL148C	0.31	0.008	NOP14
YPL228W	0.31	0.009	CET1
YPL243W	0.31	0.009	SRP68
YOR206W	0.31	0.009	NOC2
YDR292C	0.31	0.007	SRP101
YML075C	0.31	0.009	HMG1
YDR101C	0.31	0.007	ARX1
YAL025C	0.31	0.009	MAK16
YDR036C	0.31	0.008	EHD3
YJL111W	0.31	0.006	CCT7
YGR010W	0.31	0.009	NMA2
YER095W	0.31	0.007	RAD51

Systematic name	log_2(30 ℃/37 ℃)	adj.P.Val	Protein name
YBL024W	0.31	0.006	NCL1
YDR389W	0.31	0.007	SAC7
YOR043W	0.32	0.008	WHI2
YPR072W	0.32	0.009	NOT5
YOL070C	0.32	0.006	NBA1
YPR018W	0.32	0.006	RLF2
YPL184C	0.32	0.006	MRN1
YGL030W	0.32	0.009	RPL30
YBL091C	0.33	0.007	MAP2
YGL150C	0.33	0.009	INO80
YKL002W	0.33	0.009	DID4
YJR138W	0.33	0.005	IML1
YPL199C	0.33	0.009	YPL199C
YOR310C	0.33	0.006	NOP58
YER165W	0.33	0.005	PAB1
YNL016W	0.33	0.006	PUB1
YBR245C	0.34	0.008	ISW1
YBR015C	0.34	0.006	MNN2
YML067C	0.34	0.007	ERV41
YCL011C	0.34	0.009	GBP2
YAL042W	0.34	0.005	ERV46
YKR016W	0.34	0.004	FCJ1
YNL075W	0.34	0.006	IMP4
YHR201C	0.34	0.008	PPX1
YOR151C	0.35	0.007	RPB2
YOR142W	0.35	0.007	LSC1
YBR106W	0.35	0.006	PHO88
YDL055C	0.35	0.005	PSA1
YER002W	0.35	0.009	NOP16
YDR060W	0.35	0.005	MAK21
YGR118W	0.35	0.006	RPS23A
YPR132W	0.35	0.006	RPS23B
YNL291C	0.35	0.006	MID1
YGR267C	0.35	0.005	FOL2
YDR507C	0.35	0.005	GIN4
YGL055W	0.35	0.005	OLE1
YHR088W	0.35	0.007	RPF1
YER070W	0.35	0.004	RNR1
YLR197W	0.35	0.004	NOP56
YPL212C	0.36	0.004	PUS1
YGL206C	0.36	0.006	CHC1

Systematic name	log_2(30 ℃/37 ℃)	adj.P.Val	Protein name
YNL096C	0.36	0.004	RPS7B
YOR201C	0.36	0.006	MRM1
YKL081W	0.36	0.009	TEF4
YBL007C	0.36	0.009	SLA1
YOL077C	0.36	0.005	BRX1
YNL192W	0.36	0.008	CHS1
YGR237C	0.36	0.009	YGR237C
YDR035W	0.36	0.007	ARO3
YKL009W	0.36	0.004	MRT4
YJR007W	0.36	0.004	SUI2
YNR053C	0.36	0.004	NOG2
YOR322C	0.36	0.006	LDB19
YBR191W	0.36	0.007	RPL21A
YOR001W	0.36	0.004	RRP6
YKR006C	0.36	0.004	MRPL13
YNL197C	0.36	0.008	WHI3
YMR060C	0.36	0.006	SAM37
YDR148C	0.36	0.004	KGD2
YPL143W	0.36	0.004	RPL33A
YOL065C	0.36	0.007	INP54
YJL186W	0.37	0.004	MNN5
YIL074C	0.37	0.005	SER33
YNL307C	0.37	0.005	MCK1
YOL057W	0.37	0.004	YOL057W
YNL256W	0.37	0.004	FOL1
YGR056W	0.37	0.009	RSC1
YDR117C	0.37	0.005	TMA64
YGL184C	0.37	0.005	STR3
YJL098W	0.37	0.004	SAP185
YDR075W	0.37	0.008	PPH3
YJL044C	0.37	0.004	GYP6
YPL004C	0.37	0.008	LSP1
YOL004W	0.38	0.006	SIN3
YBL035C	0.38	0.004	POL12
YGL076C	0.38	0.004	RPL7A
YPL115C	0.38	0.007	BEM3
YBR009C	0.38	0.006	HHF1
YNL030W	0.38	0.006	HHF2
YOL031C	0.38	0.009	SIL1
YJL148W	0.38	0.004	RPA34
YLR249W	0.39	0.005	YEF3

Systematic name	log_2(30 ℃/37 ℃)	adj.P.Val	Protein name
YFL002C	0.39	0.004	SPB4
YHR082C	0.39	0.008	KSP1
YPL093W	0.39	0.006	NOG1
YDL019C	0.39	0.004	OSH2
YFL008W	0.39	0.004	SMC1
YLR009W	0.39	0.005	RLP24
YCR077C	0.39	0.007	PAT1
YMR131C	0.39	0.009	RRB1
YHR089C	0.39	0.005	GAR1
YHR168W	0.39	0.008	MTG2
YDL066W	0.39	0.003	IDP1
YBR079C	0.39	0.003	RPG1
YLR406C	0.39	0.005	RPL31B
YMR125W	0.39	0.004	STO1
YDL208W	0.39	0.009	NHP2
YGL031C	0.39	0.009	RPL24A
YBR058C-A	0.39	0.006	TSC3
YFL047W	0.40	0.005	RGD2
YAL039C	0.40	0.005	CYC3
YML011C	0.40	0.008	RAD33
YGR055W	0.40	0.004	MUP1
YER089C	0.40	0.003	PTC2
YDL040C	0.40	0.003	NAT1
YMR215W	0.40	0.006	GAS3
YML073C	0.40	0.003	RPL6A
YKL092C	0.40	0.004	BUD2
YLR439W	0.40	0.004	MRPL4
YMR309C	0.40	0.003	NIP1
YOR150W	0.40	0.005	MRPL23
YDR238C	0.40	0.004	SEC26
YER001W	0.40	0.006	MNN1
YNL175C	0.41	0.004	NOP13
YKL134C	0.41	0.003	Oct-01
YDR385W	0.41	0.003	EFT2
YOR133W	0.41	0.003	EFT1
YBR177C	0.41	0.003	EHT1
YOL080C	0.41	0.003	REX4
YDR502C	0.41	0.004	SAM2
YER088C	0.41	0.009	DOT6
YKL182W	0.41	0.005	FAS1
YDL140C	0.41	0.006	RPO21

Systematic name	log_2(30 ℃/37 ℃)	adj.P.Val	Protein name
YER025W	0.41	0.003	GCD11
YML080W	0.41	0.008	DUS1
YKL122C	0.41	0.004	SRP21
YER006W	0.41	0.002	NUG1
YBR086C	0.41	0.008	IST2
YGR270W	0.42	0.004	YTA7
YML046W	0.42	0.005	PRP39
YNL271C	0.42	0.007	BNI1
YER004W	0.42	0.003	FMP52
YBL076C	0.42	0.004	ILS1
YGL057C	0.42	0.004	GEP7
YPL015C	0.42	0.003	HST2
YDR091C	0.42	0.004	RLI1
YIL078W	0.43	0.002	THS1
YDR296W	0.43	0.008	MHR1
YGR123C	0.43	0.003	PPT1
YJR140C	0.43	0.003	HIR3
YHR084W	0.43	0.003	STE12
YJR142W	0.43	0.009	YJR142W
YJL063C	0.43	0.005	MRPL8
YML010W	0.43	0.002	SPT5
YPL231W	0.43	0.004	FAS2
YNL085W	0.43	0.002	MKT1
YGL203C	0.43	0.003	KEX1
YJR121W	0.43	0.007	ATP2
YDL204W	0.43	0.004	RTN2
YOR051C	0.43	0.003	ETT1
YCR037C	0.43	0.007	PHO87
YHL033C	0.43	0.006	RPL8A
YLR310C	0.43	0.002	CDC25
YIL126W	0.44	0.003	STH1
YFL004W	0.44	0.005	VTC2
YBR220C	0.44	0.008	YBR220C
YJL060W	0.44	0.007	BNA3
YGL006W	0.44	0.006	PMC1
YEL055C	0.44	0.003	POL5
YGL094C	0.44	0.003	PAN2
YNL262W	0.44	0.004	POL2
YLR248W	0.44	0.002	RCK2
YBR205W	0.44	0.002	KTR3
YBR242W	0.44	0.003	YBR242W

Systematic name	log_2(30 ℃/37 ℃)	adj.P.Val	Protein name
YOR171C	0.44	0.005	LCB4
YMR015C	0.44	0.004	ERG5
YOR090C	0.45	0.003	PTC5
YBL046W	0.45	0.002	PSY4
YJL012C	0.45	0.003	VTC4
YKL138C	0.45	0.004	MRPL31
YPL160W	0.45	0.006	CDC60
YOR017W	0.45	0.002	PET127
YNL049C	0.45	0.004	SFB2
YLL058W	0.46	0.006	YLL058W
YMR128W	0.46	0.002	ECM16
YNL088W	0.46	0.004	TOP2
YHL027W	0.46	0.003	RIM101
YDR147W	0.46	0.009	EKI1
YKL150W	0.46	0.003	MCR1
YER142C	0.46	0.007	MAG1
YFR018C	0.46	0.004	YFR018C
YJL092W	0.46	0.004	SRS2
YLR175W	0.46	0.002	CBF5
YLR048W	0.47	0.010	RPS0B
YNL277W	0.47	0.008	MET2
YGL110C	0.47	0.004	CUE3
YCR016W	0.47	0.004	YCR016W
YCR019W	0.48	0.003	MAK32
YDR128W	0.48	0.003	MTC5
YML111W	0.48	0.003	BUL2
YKL216W	0.48	0.002	URA1
YBR218C	0.48	0.003	PYC2
YJL002C	0.48	0.003	OST1
YMR229C	0.48	0.008	RRP5
YJL050W	0.48	0.002	MTR4
YDR309C	0.48	0.007	GIC2
YFR032C-A	0.48	0.005	RPL29
YLR228C	0.49	0.006	ECM22
YDR337W	0.49	0.009	MRPS28
YKL172W	0.49	0.002	EBP2
YBL099W	0.49	0.002	ATP1
YGR194C	0.49	0.002	XKS1
YDR429C	0.49	0.003	TIF35
YJL096W	0.49	0.009	MRPL49
YHR110W	0.49	0.003	ERP5

Systematic name	log_2(30 ℃/37 ℃)	adj.P.Val	Protein name
YKL032C	0.50	0.006	IXR1
YGR157W	0.50	0.002	CHO2
YPL043W	0.50	0.002	NOP4
YAL026C	0.50	0.006	DRS2
YER126C	0.50	0.002	NSA2
YDR182W	0.50	0.002	CDC1
YLR143W	0.50	0.002	YLR143W
YHR052W	0.50	0.002	CIC1
YBR039W	0.50	0.001	ATP3
YPR189W	0.50	0.006	SKI3
YDR452W	0.50	0.002	PPN1
YIL116W	0.51	0.002	HIS5
YNL129W	0.51	0.001	NRK1
YDL025C	0.51	0.001	RTK1
YGR103W	0.51	0.002	NOP7
YJL124C	0.51	0.004	LSM1
YDR170C	0.51	0.002	SEC7
YBR163W	0.51	0.007	EXO5
YMR146C	0.52	0.001	TIF34
YOL126C	0.52	0.002	MDH2
YJL074C	0.52	0.001	SMC3
YKL045W	0.52	0.002	PRI2
YFL045C	0.52	0.001	SEC53
YDR279W	0.52	0.002	RNH202
YNL047C	0.53	0.002	SLM2
YKL087C	0.53	0.002	CYT2
YIL125W	0.53	0.001	KGD1
YKR028W	0.53	0.001	SAP190
YOR095C	0.53	0.002	RKI1
YBR023C	0.53	0.006	CHS3
YNL112W	0.53	0.001	DBP2
YML054C	0.53	0.005	CYB2
YOR099W	0.53	0.002	KTR1
YNL102W	0.54	0.004	POL1
YOL083W	0.54	0.005	ATG34
YDR497C	0.54	0.006	ITR1
YNL110C	0.54	0.002	NOP15
YGR124W	0.55	0.001	ASN2
YPL146C	0.55	0.001	NOP53
YFR038W	0.55	0.002	IRC5
YPL103C	0.55	0.002	FMP30

Systematic name	log_2(30 ℃/37 ℃)	adj.P.Val	Protein name
YOL089C	0.55	0.003	HAL9
YGR085C	0.55	0.008	RPL11B
YPR102C	0.55	0.008	RPL11A
YDL003W	0.55	0.002	MCD1
YOR252W	0.55	0.010	TMA16
YKL006W	0.56	0.001	RPL14A
YMR090W	0.56	0.003	YMR090W
YIL009W	0.56	0.002	FAA3
YGL147C	0.56	0.001	RPL9A
YLR413W	0.56	0.003	YLR413W
YML072C	0.56	0.003	TCB3
YDL198C	0.56	0.001	GGC1
YBR034C	0.57	0.001	HMT1
YOR048C	0.57	0.001	RAT1
YEL053C	0.57	0.003	MAK10
YOR101W	0.57	0.002	RAS1
YMR238W	0.57	0.002	DFG5
YJR066W	0.57	0.004	TOR1
YPL134C	0.57	0.004	ODC1
YOR335C	0.58	0.002	ALA1
YNL072W	0.58	0.002	RNH201
YNL095C	0.58	0.004	YNL095C
YER043C	0.58	0.001	SAH1
YMR116C	0.58	0.004	ASC1
YDR224C	0.58	0.004	HTB1
YHR086W	0.58	0.002	NAM8
YGL167C	0.58	0.001	PMR1
YJL198W	0.59	0.003	PHO90
YBL018C	0.59	0.004	POP8
YNL201C	0.59	0.002	PSY2
YFR041C	0.59	0.001	ERJ5
YNR074C	0.59	0.001	AIF1
YFL041W	0.59	0.001	FET5
YMR145C	0.59	0.001	NDE1
YER164W	0.59	0.002	CHD1
YOL068C	0.59	0.001	HST1
YPL083C	0.60	0.008	SEN54
YMR158W	0.60	0.001	MRPS8
YLL062C	0.60	0.004	MHT1
YKL113C	0.60	0.001	RAD27
YNL078W	0.61	0.006	NIS1

Systematic name	log_2(30 ℃/37 ℃)	adj.P.Val	Protein name
YMR031C	0.61	0.001	EIS1
YHR147C	0.61	0.001	MRPL6
YMR096W	0.61	0.001	SNZ1
YDR150W	0.62	0.005	NUM1
YGL038C	0.62	0.006	OCH1
YGR116W	0.62	0.001	SPT6
YOR219C	0.62	0.001	STE13
YEL024W	0.62	0.004	RIP1
YOR176W	0.62	0.001	HEM15
YNL306W	0.62	0.001	MRPS18
YEL046C	0.62	0.001	GLY1
YMR307W	0.62	0.001	GAS1
YOR161C	0.63	0.005	PNS1
YJL122W	0.63	0.002	ALB1
YNL005C	0.63	0.001	MRP7
YOR191W	0.63	0.004	ULS1
YHR028C	0.63	0.002	DAP2
YER092W	0.63	0.005	IES5
YLR420W	0.64	0.002	URA4
YBR014C	0.64	0.001	GRX7
YPL006W	0.64	0.001	NCR1
YNL302C	0.64	0.002	RPS19B
YDR399W	0.64	0.001	HPT1
YLR325C	0.65	0.003	RPL38
YDR391C	0.65	0.001	YDR391C
YEL050C	0.65	0.002	RML2
YGR084C	0.65	0.004	MRP13
YGR246C	0.65	0.001	BRF1
YMR282C	0.66	0.001	AEP2
YDL205C	0.66	0.001	HEM3
YBL054W	0.66	0.001	TOD6
YKL170W	0.66	0.004	MRPL38
YMR193W	0.66	0.001	MRPL24
YOR236W	0.67	0.001	DFR1
YGR061C	0.67	0.001	ADE6
YGR130C	0.68	0.001	YGR130C
YMR012W	0.68	0.001	CLU1
YHR149C	0.68	0.001	SKG6
YDR483W	0.68	0.001	KRE2
YBR057C	0.69	0.004	MUM2
YFL001W	0.69	0.001	DEG1

Systematic name	log_2(30 ℃/37 ℃)	adj.P.Val	Protein name
YNL119W	0.69	0.002	NCS2
YML088W	0.69	0.003	UFO1
YNL292W	0.69	0.001	PUS4
YBR282W	0.69	0.004	MRPL27
YDR365C	0.69	0.001	ESF1
YIR026C	0.70	0.002	YVH1
YGL226C-A	0.70	0.002	OST5
YDR405W	0.70	0.001	MRP20
YHR155W	0.70	0.005	YSP1
YEL042W	0.70	0.001	GDA1
YKL176C	0.71	0.001	LST4
YER156C	0.71	0.001	YER156C
YPR166C	0.71	0.002	MRP2
YCL057W	0.71	0.000	PRD1
YNL284C	0.71	0.002	MRPL10
YLR359W	0.72	0.001	ADE13
YBR179C	0.72	0.002	FZO1
YPL208W	0.72	0.001	RKM1
YGL257C	0.72	0.002	MNT2
YBL028C	0.73	0.005	YBL028C
YDR237W	0.73	0.001	MRPL7
YDR326C	0.74	0.001	YSP2
YPL173W	0.74	0.000	MRPL40
YGR162W	0.74	0.001	TIF4631
YER057C	0.74	0.001	HMF1
YMR210W	0.74	0.005	YMR210W
YDR047W	0.75	0.001	HEM12
YAR015W	0.75	0.000	ADE1
YIL119C	0.76	0.003	RPI1
YNL134C	0.76	0.001	YNL134C
YHL023C	0.76	0.002	NPR3
YPL118W	0.76	0.001	MRP51
YML081C-A	0.77	0.001	ATP18
YDR462W	0.77	0.001	MRPL28
YGR159C	0.77	0.002	NSR1
YJR144W	0.77	0.001	MGM101
YGR165W	0.77	0.000	MRPS35
YPL207W	0.78	0.003	TYW1
YER081W	0.78	0.001	SER3
YDR322W	0.78	0.000	MRPL35
YDL174C	0.78	0.000	DLD1

Systematic name	log_2(30 ℃/37 ℃)	adj.P.Val	Protein name
YGR245C	0.78	0.000	SDA1
YAL056W	0.78	0.007	GPB2
YIL147C	0.78	0.001	SLN1
YIL016W	0.79	0.000	SNL1
YEL032W	0.79	0.000	MCM3
YNL137C	0.80	0.004	NAM9
YER078C	0.80	0.001	ICP55
YPL053C	0.81	0.001	KTR6
YNL169C	0.81	0.001	PSD1
YDR267C	0.82	0.007	CIA1
YER174C	0.82	0.001	GRX4
YMR171C	0.82	0.006	EAR1
YJR113C	0.83	0.000	RSM7
YDR041W	0.83	0.002	RSM10
YCR069W	0.83	0.000	CPR4
YGL140C	0.83	0.001	YGL140C
YBR028C	0.84	0.001	YPK3
YDL076C	0.85	0.003	RXT3
YPL181W	0.86	0.001	CTI6
YLR019W	0.86	0.004	PSR2
YLR180W	0.86	0.000	SAM1
YDR083W	0.86	0.000	RRP8
YPR020W	0.86	0.001	ATP20
YOR065W	0.86	0.000	CYT1
YNL249C	0.86	0.000	MPA43
YGR170W	0.86	0.003	PSD2
YBR140C	0.87	0.001	IRA1
YLR342W	0.87	0.001	FKS1
YDR541C	0.88	0.002	YDR541C
YMR054W	0.88	0.000	STV1
YDR116C	0.90	0.007	MRPL1
YNL252C	0.90	0.000	MRPL17
YDR298C	0.90	0.000	ATP5
YFR015C	0.90	0.001	GSY1
YDR072C	0.91	0.000	IPT1
YBL106C	0.91	0.002	SRO77
YOL077W-A	0.92	0.001	ATP19
YMR266W	0.92	0.001	RSN1
YPL078C	0.93	0.001	ATP4
YKL184W	0.93	0.001	SPE1
YMR272C	0.94	0.001	SCS7

Systematic name	log_2(30 ℃/37 ℃)	adj.P.Val	Protein name
YEL003W	0.94	0.008	GIM4
YLR303W	0.94	0.000	MET17
YOR158W	0.95	0.000	PET123
YMR188C	0.95	0.001	MRPS17
YOL019W	0.95	0.002	YOL019W
YKL016C	0.95	0.000	ATP7
YKL001C	0.95	0.002	MET14
YMR172W	0.95	0.000	HOT1
YDR175C	0.96	0.000	RSM24
YKL185W	0.96	0.001	ASH1
YDR380W	0.96	0.001	ARO10
YER091C	0.97	0.000	MET6
YGL255W	0.97	0.001	ZRT1
YDR222W	0.98	0.002	YDR222W
YPL013C	0.98	0.003	MRPS16
YGL173C	0.99	0.000	XRN1
Q0085	1.00	0.001	ATP6
YGR065C	1.00	0.002	VHT1
YDR322C-A	1.00	0.001	TIM11
YGL129C	1.01	0.000	RSM23
YGL101W	1.01	0.000	YGL101W
YLR107W	1.02	0.002	REX3
YLR300W	1.03	0.001	EXG1
YBR265W	1.03	0.003	TSC10
YDL227C	1.04	0.001	HO
YBR251W	1.04	0.000	MRPS5
Q0140	1.06	0.001	VAR1
YKR042W	1.06	0.002	UTH1
YMR120C	1.08	0.000	ADE17
YBR146W	1.08	0.000	MRPS9
YJL101C	1.08	0.000	GSH1
YOR243C	1.08	0.000	PUS7
YIL140W	1.08	0.000	AXL2
YDR377W	1.10	0.001	ATP17
YPR052C	1.10	0.001	NHP6A
YPL127C	1.11	0.000	HHO1
YHR001W-A	1.11	0.000	QCR10
YDR530C	1.13	0.001	APA2
YDL070W	1.13	0.001	BDF2
YML004C	1.13	0.000	GLO1
YIL015W	1.13	0.001	BAR1

Systematic name	log_2(30 ℃/37 ℃)	adj.P.Val	Protein name
YGL187C	1.13	0.000	COX4
YBR208C	1.14	0.000	DUR1,2
YKR056W	1.14	0.000	TRM2
YBR244W	1.15	0.001	GPX2
YKR031C	1.16	0.001	SPO14
YDR529C	1.17	0.001	QCR7
YCL030C	1.20	0.000	HIS4
YML060W	1.20	0.001	OGG1
YIL005W	1.21	0.000	EPS1
YJL166W	1.23	0.002	QCR8
YDR465C	1.23	0.000	RMT2
YBR141C	1.29	0.003	YBR141C
YOR367W	1.34	0.000	SCP1
YDR494W	1.37	0.001	RSM28
YLR247C	1.41	0.000	IRC20
YGL191W	1.48	0.001	COX13
YJL157C	1.49	0.001	FAR1
YJR010W	1.50	0.000	MET3
YDR111C	1.51	0.000	ALT2
YGR143W	1.71	0.000	SKN1
YIL123W	1.77	0.002	SIM1
YOR215C	1.83	0.000	AIM41
YGR276C	1.83	0.000	RNH70
YJL212C	1.91	0.000	OPT1
YJR137C	2.00	0.000	MET5
YGL211W	2.01	0.000	NCS6
YNL052W	2.04	0.000	COX5A
YGR234W	2.15	0.000	YHB1
YFR030W	2.21	0.000	MET10
YLR108C	2.21	0.000	YLR108C
YLR452C	2.40	0.000	SST2
Q0250	2.40	0.000	COX2
YHR033W	2.51	0.000	YHR033W
YOL154W	2.78	0.000	ZPS1

Table A2.2: GO BP and MIPS functional classes up-regulated at 37 °C.
Over-represented GO terms for Biological Processes and MIPS Functional Classes, identified by analysing the significantly up-regulated proteins at 37°C with FunSpec. Shown here is the cluster of input proteins and the enrichment of different GO or MIPS categories with their respective *p*-values. f = total number of proteins in the yeast proteome belonging to a category, and k = total number of proteins in the input cluster that can be associated to that category. Highlighted in the red colour are the categories that were also over-represented in the significantly up-regulated proteins in the *urm1Δ* cells (presented in (Rezgui et al. 2013)). Also see figure 4.11.

GO Biological Process				
Category	**p-value**	**In category from cluster**	**k**	**f**
metabolic process [GO:0008152]	0.0000	BDH1 BDH2 BNA4 UGA2 PCS60 PGS1 NFS1 GPM2 GPD1 SLC1 HNT1 LYS21 YDL144C SFA1 LYS20 GDH2 NTH1 LYS4 ARH1 URH1 PHO8 UTR4 HPA3 CEM1 HOR2 ARG5,6 ALD5 BNA6 HXK1 ERG26 PNC1 HEM2 YGL185C SDT1 YGR012W NQM1 CRH1 GND2 DOG2 UBA4 EPT1 OYE2 YIR007W YIR035C IRC24 TDH1 CPS1 TDH2 BNA1 BAT2 YKL027W SRY1 FOX2 GPT2 MTD1 TGL4 PDC1 PDC5 GSY2 TRM9 NTE1 PLB1 ARG7 ADH3 ALD2 YMR196W ADH2 IDH1 LAP2 DUG3 GOR1 PLB3 GPD2 ALD4 THI6 ATH1	76	425
protein folding [GO:0006457]	0.0000	SSA1 CNE1 SSA3 HSP26 SSE2 PDI1 AHA1 SSA4 MDJ1 PIH1 JEM1 CPR7 SSC1 SSA2 CPR6 HSP60 ERO1 HSC82 SCJ1 SIS1 YDJ1 APJ1 HCH1 ZIM17 MPD2 HSP10 STI1 MPD1 CIN1 SSE1 HSP82	31	96
protein refolding [GO:0042026]	0.0000	SSA1 SSE2 HSP78 MDJ1 CPR7 SSC1 CPR6 HSP60 HSC82 YDJ1 HSP10 SSE1 HSP82	13	16
oxidation-reduction process [GO:0055114]	0.0000	BDH1 BDH2 PRX1 BNA4 UGA2 GPD1 YDL144C SFA1 GDH2 PST2 ARH1 TSA2 YEL047C MXR1 ARG5,6 ALD5 ERG26 YGL185C RNR4 GND2 AIM17 SOD2 GRE3 OYE2 LYS12 YIR035C IRC24 HYR1 RNR2 TDH1 TDH2 BNA1 BNA2 YJR096W FOX2 FMP46 CCP1 MTD1 PUT1 PGA3 ERO1 FMS1 ADH3 ALD2 ADH2 IDH1 GOR1 GPD2 ADH1 GCY1 CAT5 ALD4 IRC15 YPR127W	54	272
response to stress [GO:0006950]	0.0000	SSA1 SSA3 HSP26 UBC4 TPS1 SSE2 PTC1 GPD1 NTH1 HSP42 UBC1 AHA1 HSP78 HSP31 HOR2 SSA4 HSP12 MDJ1 HSF1 GRE3 KAR2 HSP150 CPR7 SSC1 SSA2 HSP104 HSP60 TRM9 TSL1 HSC82 YDJ1 HCH1 STI1 SSE1 HSP82 ATH1	36	152
arginine biosynthetic process [GO:0006526]	0.0000	ARG5,6 ARG2 ARG3 ARG7 ARG1 ARG8 ORT1 CPA1	8	10

GO Biological Process				
Category	**p-value**	**In category from cluster**	**k**	**f**
de novo' protein folding [GO:0006458]	0.0000	MDJ1 HSP60 HSC82 YDJ1 HSP82	5	6
ornithine biosynthetic process [GO:0006592]	0.0000	ARG5,6 ARG2 ARG7 ARG8	4	4
cellular amino acid biosynthetic process [GO:0008652]	0.0001	CTR86 LYS21 LYS20 LYS14 LYS4 UTR4 ARG5,6 YGR012W THR1 LYS12 ARG2 ARG3 BAT2 LEU3 ARG7 ARG1 ARG8 ORT1 CPA1	19	98
lysine biosynthetic process [GO:0009085]	0.0001	LYS21 LYS20 LYS14 LYS4 LYS12	5	8
glycolysis [GO:0006096]	0.0001	GLK1 PGK1 GPM2 EMI2 HXK1 ENO1 TDH1 TDH2 PYK2	9	28
ER-associated protein catabolic process [GO:0030433]	0.0001	CNE1 UBC1 URH1 HUL5 DOG2 KAR2 JEM1 UBX2 UBC7 SCJ1 CUE1 YDJ1	12	48
de novo NAD biosynthetic process from tryptophan [GO:0034354]	0.0001	BNA4 BNA6 BNA1 BNA2	4	5
carbohydrate metabolic process [GO:0005975]	0.0001	GLK1 SOL2 GPD1 EMI2 HXK1 ALG13 NQM1 CRH1 SOL4 YIR007W YMR099C PGM2 PGM3 SOL1 GPD2 CAT5 ATH1 GPH1	18	94
glucose metabolic process [GO:0006006]	0.0002	GLK1 HXK1 DOG2 TDH1 TDH2 PGM2 PGM3 CAT5	8	23
cell redox homeostasis [GO:0045454]	0.0003	PRX1 PDI1 TRX3 TSA2 GRX2 POR1 MPD2 MPD1 IRC15	9	31
cellular response to oxidative stress [GO:0034599]	0.0003	PRX1 UGA2 TRX3 TSA2 GRX2 MXR1 HSP12 GRE3 UBA4 HYR1 YJR096W CCP1 GCY1 OXR1	14	67
amino acid catabolic process to alcohol via Ehrlich pathway [GO:0000947]	0.0004	SFA1 ADH3 ADH2 ADH1	4	6
NADH oxidation [GO:0006116]	0.0004	GPD1 ADH3 ADH2 GPD2 ADH1	5	10
SRP-dependent cotranslational protein targeting to membrane, translocation [GO:0006616]	0.0004	SSA1 SSA3 SSA4 KAR2 SSA2	5	10
protein unfolding [GO:0043335]	0.0004	HSP78 SSC1 HSP104	3	3
protein metabolic process [GO:0019538]	0.0004	MXR1 HSP104 CAT5	3	3

GO Biological Process				
Category	**p-value**	**In category from cluster**	**k**	**f**
post-translational protein modification [GO:0043687]	0.0004	UBC4 STP22 UBC9 UBC1 MMS2 UBC7	6	15
response to unfolded protein [GO:0006986]	0.0007	ORM1 KAR2 LHS1 SCJ1 ZIM17	5	11
protein stabilization [GO:0050821]	0.0009	ARG82 HSP78 HSP60 ZIM17	4	7
phospholipid biosynthetic process [GO:0008654]	0.0012	PGS1 SLC1 SCS2 EPT1 URA8 GPT2 PAH1 CPT1 OPI10	9	37
gluconeogenesis [GO:0006094]	0.0014	PGK1 ACN9 ENO1 TDH1 TDH2 CAT5	6	18
arabinose catabolic process [GO:0019568]	0.0015	GRE3 YJR096W GCY1	3	4
ethanol metabolic process [GO:0006067]	0.0015	SYM1 ADH2 ALD4	3	4
glucose 6-phosphate metabolic process [GO:0051156]	0.0015	GLK1 EMI2 PGM2	3	4
D-xylose catabolic process [GO:0042843]	0.0015	GRE3 YJR096W GCY1	3	4
pantothenate biosynthetic process [GO:0015940]	0.0016	ECM31 FMS1 SPE2 SPE3	4	8
lysine biosynthetic process via aminoadipic acid [GO:0019878]	0.0016	LYS21 LYS20 LYS14 LYS4	4	8
pyruvate metabolic process [GO:0006090]	0.0016	PDC1 PDC5 PYK2 ALD4	4	8
protein import into mitochondrial outer membrane [GO:0045040]	0.0016	MDM10 MMM1 SAM50 MDM12	4	8
pentose-phosphate shunt [GO:0006098]	0.0025	SOL2 NQM1 SOL4 GND2 SOL1	5	14
pyridine nucleotide biosynthetic process [GO:0019363]	0.0028	BNA4 BNA6 PNC1 BNA1	4	9
ubiquitin-dependent protein catabolic process via the multivesicular body sorting pathway [GO:0043162]	0.0035	UBC4 STP22 VPS25 SNF7 SNF8	5	15

GO Biological Process				
Category	**p-value**	**In category from cluster**	**k**	**f**
glycerol ether metabolic process [GO:0006662]	0.0036	PDI1 TRX3 MPD1	3	5
phosphorylation [GO:0016310]	0.0048	CDC28 GLK1 SAT4 PGK1 ARG82 EMI2 ARG5,6 PRS2 YFH7 HXK1 THR1 SLT2 PFK26 IKS1 YAK1 URA6 YPK2 ARK1 FPK1 CMK2 THI20 SKM1 HRK1 PYK2 MKK2 THI6	26	206
formaldehyde catabolic process [GO:0046294]	0.0055	SFA1 YJL068C	2	2
deoxyribonucleoside diphosphate metabolic process [GO:0009186]	0.0055	RNR4 RNR2	2	2
glycerol-3-phosphate catabolic process [GO:0046168]	0.0055	GPD1 GPD2	2	2
positive regulation of mitotic cell cycle [GO:0045931]	0.0055	CDC28 IRC15	2	2
spermidine biosynthetic process [GO:0008295]	0.0055	SPE2 SPE3	2	2
cellular modified amino acid biosynthetic process [GO:0042398]	0.0055	AIM18 AIM46	2	2
cellular membrane fusion [GO:0006944]	0.0055	ATG8 MSO1	2	2
response to heat [GO:0009408]	0.0063	GET3 MDJ1 HSF1 YDJ1 SGT2	5	17
cellular carbohydrate metabolic process [GO:0044262]	0.0063	TPS1 CIT2 HOR2 YMR099C CIT1	5	17
fermentation [GO:0006113]	0.0068	ADH3 ADH2 ADH1	3	6

MIPS Functional Classification				
Category	**p-value**	**In Category from Cluster**	**k**	**f**
protein folding and stabilization [14.01]	0.0000	SSA1 SSA3 HSP26 SSE2 PDI1 HSP42 AHA1 HSP78 SSA4 MDJ1 PIH1 KAR2 JEM1 CPR7 SSC1 LHS1 SSA2 HSP104 CPR6 HSP60 ERO1 HSC82 SCJ1 YDJ1 APJ1 HCH1 MPD2 HSP10 STI1 SGT1 MPD1 CIN1 SSE1 HSP82	34	93

MIPS Functional Classification				
Category	**p-value**	**In Category from Cluster**	**k**	**f**
C-compound and carbohydrate metabolism [01.05]	0.0000	BDH1 BDH2 PHO3 GLK1 CIT2 GPD1 LYS21 SFA1 LYS20 CYM1 ACN9 EMI2 YEL047C CEM1 HOR2 SCS2 HSP12 HXK1 ALG13 UGA1 ATF2 PMT6 ENO1 GND2 DOG2 INM1 IRC24 XPT1 PDC1 PDC5 FMS1 ADH3 ALD2 PGM3 LAP2 GOR1 ALG12 GPD2 ADH1 ALG6 GCY1 IRC15 PDH1	43	223
unfolded protein response (e.g. ER quality control) [32.01.07]	0.0000	SSA1 HSP26 HSP42 COX20 HSP78 HSP31 SSA4 MDJ1 ORM1 KAR2 JEM1 CPR7 LHS1 CPR6 HSC82 SCJ1 SIS1 APJ1 HSP10 STI1 SSE1	21	69
biosynthesis of arginine [01.01.03.05.01]	0.0000	ARG5,6 ARG2 ARG3 PUT1 ARG7 ARG1 ARG8 ORT1 CPA1	9	13
secondary metabolism [01.20]	0.0000	YDL086W COQ4 GRE3 YJR096W ARG1 GCY1 CAT5	7	12
metabolism of nonprotein amino acids [01.20.17.01]	0.0000	ARG5,6 ARG2 ARG3 ARG7 ALD2 ARG8	6	10
protein binding [16.01]	0.0000	SSA1 ATG8 HSP26 UBC4 STP22 RAD18 YRB1 SLU7 HSP42 UBC1 PCF11 COX20 HSP78 PIB1 MSN5 HSP31 SSA4 SCS2 DDI1 MDJ1 MMS2 HUL5 TWF1 YAP1801 KAR2 JEM1 CPR7 NPA3 MOG1 MCM22 LHS1 MTR2 HSP104 CPR6 UBC7 HSC82 SCJ1 CUE1 SIS1 APJ1 VPS27 HRT1 HSP10 STI1 SGT1 RUP1 CIN1 SNX3 SSE1 MEX67 YOP1	51	391
stress response [32.01]	0.0001	SSA3 YRO2 UBC4 TPS1 SSE2 SAT4 NTH1 AHA1 SSD1 DDI1 SLT2 DOG2 HSP150 SSC1 HSP104 HSP60 TRM9 TSL1 UBC7 YDJ1 YGP1 HCH1 VHS3 MKK2 HSP82 ATH1	26	162
oxidative stress response [32.01.01]	0.0001	PRX1 UGA2 TRX3 PST2 TSA2 GRX2 MXR1 HSP12 SOD2 HYR1 FMP46 CCP1 OXR1	13	55
alcohol fermentation [02.16.01]	0.0002	PDC1 PDC5 ADH3 ADH2 ADH1 ALD4	6	13
aminoadipic acid pathway [01.01.06.06.01.03]	0.0002	LYS21 LYS20 LYS14 LYS4 LYS12	5	9
sugar, glucoside, polyol and carboxylate catabolism [01.05.02.07]	0.0002	TPS1 PGK1 GPM2 NTH1 NQM1 ENO1 GRE3 PFK26 TDH1 TDH2 YJR096W PGM2 IDH1 CIT1 PYK2 ATH1	16	81
protein targeting, sorting and translocation [14.04]	0.0004	SSA1 SYN8 SSA3 ATG8 STP22 ATG20 TIM22 YRB1 HSP78 PEP7 MSN5 CYM1 SSA4 SCS2 ATG18 GOS1 VPS29 KAR2 SSC1 MOG1 VPS25 LHS1 SSA2 SNF7 HSP60 KAP95 UBX2 SCJ1 CUE1 SAM50 YDJ1 VPS27 HSP10 VPS21 SNX3 SNF8 ATG11	37	281

MIPS Functional Classification				
Category	**p-value**	**In Category from Cluster**	**k**	**f**
biosynthesis of vitamins, cofactors, and prosthetic groups [01.07.01]	0.0004	BNA4 ECM31 RIB5 COQ4 ARH1 COX15 BNA6 HEM2 CAB4 BNA1 BNA2 YKL027W FMS1 FSH2 SPE2 THI20 VHS3 THI6 SPE3	19	110
pentose-phosphate pathway [02.07]	0.0010	SOL2 PRS2 NQM1 SOL4 GND2 PGM2 SOL1	7	23
proteasomal degradation (ubiquitin/proteasomal pathway) [14.13.01.01]	0.0010	CNE1 UBC4 RAD18 UBC9 YRB1 UBC1 PIB1 PUP3 DDI1 ATE1 MMS2 HUL5 NAS2 DEF1 UBX2 UBC7 CUE1 HRT1 SGT1 PRE10	20	128
metabolism of energy reserves (e.g. glycogen, trehalose) [02.19]	0.0023	TPS1 NTH1 GSC2 AAP1 GLG2 GSY2 TSL1 PGM2 HSP82 ATH1 GPH1	11	56
glycolysis and gluconeogenesis [02.01]	0.0025	GLK1 PGK1 GPM2 ACN9 ENO1 TDH1 TDH2 PGM2 PYK2	9	41
C-2 compound and organic acid catabolism [01.05.06.07]	0.0028	ALD5 SYM1 ADH2 ALD4	4	9
mitochondrial transport [20.09.04]	0.0038	AAC3 YDL119C TIM22 HSP78 UGO1 MRS3 SSC1 OAC1 SSA2 HSP60 YHM2 SAM50 POR1 YDJ1 ORT1 ODC2	16	104
metabolism of urea (urea cycle) [01.01.05.03]	0.0068	ARG3 ARG1 CAR1	3	6
phosphate metabolism [01.04]	0.0077	SSA1 SSA3 IPP1 POA1 PHO3 CDC28 GLK1 SAT4 PGK1 PTC1 GET3 PTP1 ARG82 HSP78 PHO8 HOR2 ARG5,6 PRS2 HXK1 THR1 SLT2 DOG2 INM1 EPT1 PFK26 KAR2 YAK1 SSC1 URA6 HSP104 CNA1 YMR087W YPK2 ARK1 FPK1 CMK2 THI20 SKM1 HRK1 PYK2 MKK2 THI6 HSP82	43	401
lipid, fatty acid and isoprenoid metabolism [01.06]	0.0087	SWH1 PCS60 ATG15 GPD1 SLC1 DPL1 PIB1 ARH1 ISC1 HSP12 ATF2 YIR035C YJL068C FOX2 TGL4 LAP2 CYB5 GPD2	18	133

Table A2.3: GO BP and MIPS functional classes down-regulated at 37 °C.

Over-represented GO terms for Biological Processes and MIPS Functional Classes, identified by analysing the significantly down-regulated proteins at 37°C with FunSpec. Shown here is the cluster of input proteins and the enrichment of different GO or MIPS categories with their respective *p*-values. f = total number of proteins in the yeast proteome belonging to a category, and k = total number of proteins in the input cluster that can be associated to that category. Highlighted in the red colour are the categories that were also over-represented in the significantly down-regulated proteins in *urm1Δ* cells (presented in (Rezgui et al. 2013)). Also see figure 4.11.

GO Biological Process				
Category	**p-value**	**In Category from Cluster**	**k**	**f**
mitochondrial translation [GO:0032543]	0.0000	VAR1 MRPS9 MRPS5 MRPL27 RSM10 MRPL1 RSM24 MRPL7 MRPL35 MRPS28 MRP20 MRPL28 RSM23 MRP13 MRPS35 MRPL6 MRPL8 MRPL49 RSM7 MRPL31 MRPL38 MRPL13 MRPL4 MRPS8 MRPS17 MRPL24 MRP7 NAM9 MRPL17 MRPL10 MRPS18 MRPL23 PET123 MRPS16 MRP51 MRPL40 MRP2	37	88
translation [GO:0006412]	0.0000	VAR1 MAK16 ILS1 RPG1 MRPS9 RPL21A MRPS5 RPS16B RSM10 RLI1 MRPL1 MRPL7 MRPS28 EFT2 MRP20 TIF35 RSM28 RML2 GCD11 RPS24A RPL29 RPL30 RPL24A RPL7A RPL28 RPL1B RPL9A RPL11B RPS23A TIF4631 RPS20 RPL8A DED81 RPF1 MRPL6 MTG2 RPS24B THS1 MRPL8 MRPL49 SUI2 RSM7 RPL14A TEF4 MRPL38 RLP24 RPS0B YEF3 RPL38 RPL31B MRPL4 RPL6A RPS16A TIF34 MRPS8 MRPS17 MRPL24 NIP1 MRP7 IMP4 RPS7B MRPL10 RPS19B MRPS18 BRX1 EFT1 MRPL23 AIM41 ALA1 MRPS16 RPL33A CDC60 MRPL40 RPL1A RPL11A RPS23B MRP2	77	318
ribosome biogenesis [GO:0042254]	0.0000	NOP14 SAS10 NHP2 MAK21 RLI1 ESF1 NOP16 NUG1 NSA2 SPB4 NOP7 SDA1 RNH70 RPL8A CIC1 RPF1 GAR1 TMA108 ALB1 TOR1 MRT4 EBP2 RLP24 RPS0B CBF5 NOP56 ECM16 RRB1 RRP5 IMP4 RPS7B NOP15 DBP2 NOG2 BRX1 NOC2 PUS7 NOP58 NOP4 NOG1 NOP53	41	170
ATP synthesis coupled proton transport [GO:0015986]	0.0000	ATP6 ATP1 ATP3 ATP5 TIM11 ATP17 ATP2 ATP7 ATP18 ATP19 ATP4 ATP20	12	17
rRNA processing [GO:0006364]	0.0000	POP8 NOP14 SAS10 NHP2 RRP8 RLI1 ESF1 NOP16 NUG1 NSA2 SPB4 RPL30 KEM1 NOP7 NSR1 RNH70 RPF1 GAR1 MTR4 MRT4 EBP2 RPS0B REX3 CBF5 NOP56 ECM16 RRB1 RRP5 IMP4 RPS7B NOP15 DBP2 REX4 RRP6 RAT1 PUS7 NOP58 NOP4 NOG1 NOP53	40	195
ATP biosynthetic process [GO:0006754]	0.0000	ATP6 DRS2 ATP1 ATP3 ATP5 TIM11 ATP17 PMC1 PMR1 ATP2 ATP7 ATP18 ATP19 ATP20	14	31
ribosomal large subunit biogenesis [GO:0042273]	0.0000	MAK16 RLI1 ARX1 NOP16 NSA2 NOP7 TIF4631 SDA1 CIC1 ALB1 MRT4 RLP24 NOP15 NOG1	14	37

GO Biological Process				
Category	**p-value**	**In Category from Cluster**	**k**	**f**
proton transport [GO:0015992]	0.0000	ATP6 ATP1 ATP3 ATP5 TIM11 ATP17 ATP2 ATP7 ATP18 STV1 ATP19 ATP4 ATP20	13	41
methionine biosynthetic process [GO:0009086]	0.0000	MET6 MET10 STR3 MET3 MET5 MET14 YLL058W MHT1 MET17 MET2 MRI1	11	31
RNA processing [GO:0006396]	0.0000	MRPL1 RPL1B CIC1 TRM2 CBF5 PRP39 RRP5 PUS4 RRP6 RAT1 MRM1 RPL1A	12	37
snRNA pseudouridine synthesis [GO:0031120]	0.0000	NHP2 GAR1 CBF5 PUS7 PUS1	5	6
protein glycosylation [GO:0006486]	0.0000	MNN2 KTR3 PSA1 KRE2 GDA1 MNN1 MNT2 OST1 MNN5 KTR1 KTR6	11	35
translational initiation [GO:0006413]	0.0001	RPG1 RLI1 TMA64 TIF35 RSM28 GCD11 TIF4631 BRF1 SUI2 CLU1 TIF34 NIP1	12	43
N-glycan processing [GO:0006491]	0.0002	KTR3 KRE2 MNN1 KTR1	4	5
cellular amino acid biosynthetic process [GO:0008652]	0.0002	HIS4 ARO3 SER3 MET6 MET10 STR3 ASN2 YHR033W SER33 HIS5 MET3 MET5 MET14 YLL058W MHT1 MET17 MET2 SER1 MRI1	19	98
methionine metabolic process [GO:0006555]	0.0004	SAM2 SAH1 MET3 MET14 SAM1 MET17	6	14
negative regulation of DNA damage checkpoint [GO:2000002]	0.0005	PSY4 PPH3 PSY2	3	3
DNA synthesis involved in DNA repair [GO:0000731]	0.0005	PRI2 POL1 POL2	3	3
ribosomal large subunit assembly [GO:0000027]	0.0005	MAK21 SPB4 RPL11B RPF1 YVH1 MRT4 RPL6A BRX1 REX4 RPL11A	10	38
RNA modification [GO:0009451]	0.0005	DEG1 CBF5 PUS4 PUS7 PUS1	5	10
pseudouridine synthesis [GO:0001522]	0.0005	DEG1 CBF5 PUS4 PUS7 PUS1	5	10
mitochondrial electron transport, ubiquinol to cytochrome c [GO:0006122]	0.0009	QCR7 RIP1 QCR10 QCR8 CYT1	5	11
nucleobase, nucleoside, nucleotide and nucleic acid metabolic process [GO:0006139]	0.0014	POL5 KEM1 SPT6 POL1 POL2 RRP6 RAT1	7	23
cysteine biosynthetic process [GO:0019344]	0.0015	MET10 MET3 MET5 MET14 MET17	5	12

GO Biological Process				
Category	**p-value**	**In Category from Cluster**	**k**	**f**
ion transport [GO:0006811]	0.0015	ATP6 ATP1 ATP3 ATP5 TIM11 ATP17 FET5 PMC1 PMR1 ZRT1 ATP2 ATP7 ATP18 STV1 MID1 ATP19 ATP4 ATP20	18	107
serine family amino acid biosynthetic process [GO:0009070]	0.0018	SER3 SER33 SER1	3	4
histone H3-K79 methylation [GO:0034729]	0.0018	HHF1 DOT1 HHF2	3	4
phosphatidylcholine biosynthetic process [GO:0006656]	0.0035	EKI1 CHO2 PSD2 PSD1	4	9
de novo' IMP biosynthetic process [GO:0006189]	0.0035	ADE1 ADE6 ADE13 ADE17	4	9
nucleosome positioning [GO:0016584]	0.0035	ISW1 CHD1 INO80 STH1	4	9
U5 snRNA 3'-end processing [GO:0034476]	0.0035	RNH70 MTR4 REX3 RRP6	4	9
electron transport chain [GO:0022900]	0.0041	COX2 QCR7 RIP1 MET10 OLE1 QCR10 QCR8 CYB2 SCS7 CYT1	10	49
cristae formation [GO:0042407]	0.0043	TIM11 FCJ1 ATP20	3	5
L-serine biosynthetic process [GO:0006564]	0.0043	SER3 SER33 SER1	3	5
glucose mediated signaling pathway [GO:0010255]	0.0043	GPB2 ASC1 GPB1	3	5
protein targeting to ER [GO:0045047]	0.0046	SRP101 SEC53 SRP21 SRP72 SRP68	5	15
metabolic process [GO:0008152]	0.0060	DRS2 DUR1,2 PYC2 YBR242W TSC10 HIS4 ARO3 EHD3 IPT1 KGD2 APA2 YDR541C FMP52 RNR1 SER3 SEC53 GSY1 MET10 PMC1 CWH41 YGL101W PMR1 FOL2 FAA3 SER33 HIS5 KGD1 MRPL49 MET5 FAS1 URA1 SPO14 EXG1 MET17 CYB2 OGG1 DUS1 YMR090W SNZ1 ADE17 DFG5 NRK1 YNL134C FOL1 MDH2 LSC1 SER1 FAS2	48	425
3-keto-sphinganine metabolic process [GO:0006666]	0.0062	TSC3 TSC10	2	2
peptidyl-arginine methylation [GO:0018216]	0.0062	HMT1 RMT2	2	2
interspecies interaction between organisms [GO:0044419]	0.0062	MAK32 MKT1	2	2

GO Biological Process				
Category	**p-value**	**In Category from Cluster**	**k**	**f**
signal transduction involved in meiotic recombination checkpoint [GO:0072462]	0.0062	PPH3 PSY2	2	2
transposon integration [GO:0070893]	0.0062	SPT15 BRF1	2	2
protein oligomerization [GO:0051259]	0.0062	TIM11 ATP20	2	2
glycine biosynthetic process [GO:0006545]	0.0062	GLY1 DFR1	2	2
polyphosphate catabolic process [GO:0006798]	0.0062	PPN1 PPX1	2	2
negative regulation of transcription during meiosis [GO:0051038]	0.0062	RPD3 SIN3	2	2
tetrahydrofolate biosynthetic process [GO:0046654]	0.0062	FOL2 FOL1	2	2
protein O-linked glycosylation [GO:0006493]	0.0062	KTR3 KRE2 MNN1 MNT2 KTR1	5	16
maturation of SSU-rRNA from tricistronic rRNA transcript (SSU-rRNA, 5.8S rRNA, LSU-rRNA) [GO:0000462]	0.0063	RPS16B NOP14 SAS10 RPS24A NOP7 RPS23A RPS20 RPS24B ECM16 RPS16A RPS23B	11	60
chromatin assembly or disassembly [GO:0006333]	0.0073	HHF1 HTB1 CHD1 HHF2 TOP2 ULS1	6	23
ribosomal large subunit export from nucleus [GO:0000055]	0.0073	CIA1 NUG1 SDA1 RPF1 NOG2 NOP53	6	23
oxidation-reduction process [GO:0055114]	0.0076	COX2 GPX2 TSC10 HIS4 IDP1 DLD1 YDR541C RIP1 RNR1 SER3 FET5 MET10 OLE1 YHB1 SER33 KGD1 MET5 MCR1 FAS1 URA1 CYB2 HMG1 DUS1 ERG5 NDE1 SCS7 COX5A YNL134C AIF1 MDH2 DFR1 TYW1 FAS2	33	272
sulfate assimilation [GO:0000103]	0.0080	MET10 MET3 MET5 MET14	4	11
fungal-type cell wall biogenesis [GO:0009272]	0.0080	CWH41 RIM101 UTH1 DFG5	4	11

GO Biological Process				
Category	**p-value**	**In Category from Cluster**	**k**	**f**
SRP-dependent cotranslational protein targeting to membrane, signal sequence recognition [GO:0006617]	0.0081	SRP21 SRP72 SRP68	3	6
negative regulation of transcription from RNA polymerase I promoter [GO:0016479]	0.0081	RXT3 RPD3 SIN3	3	6
RNA polymerase III transcriptional preinitiation complex assembly [GO:0070898]	0.0081	SPT15 BRF1 NHP6A	3	6
negative regulation of Ras protein signal transduction [GO:0046580]	0.0081	GPB2 IRA1 GPB1	3	6
traversing start control point of mitotic cell cycle [GO:0007089]	0.0081	KEM1 SDA1 CDC25	3	6
filamentous growth [GO:0030447]	0.0082	DOT6 KEM1 KSP1 BUD2 GAS1	5	17
tRNA processing [GO:0008033]	0.0090	POP8 NCL1 DEG1 NCS6 RNH70 TRM2 DUS1 NCS2 PUS4 PUS7 SEN54 TYW1 PUS1	13	80

MIPS Functional Classification				
Category	**p-value**	**In Category from Cluster**	**k**	**f**
ribosomal proteins [12.01.01]	0.0000	VAR1 MRPS9 RPL21A MRPS5 MRPL27 RPS16B RSM10 MAK21 RLI1 MRPL1 RSM24 MRPL7 MRPL35 MRPS28 MRP20 MRPL28 RSM28 RML2 RPS24A SPB4 RPL29 RPL30 RPL24A RPL7A RPL28 RSM23 RPL1B RPL9A MRP13 RPL11B RPS23A NSR1 MRPS35 RPS20 RPL8A RPF1 MRPL6 RPS24B MRPL8 MRPL49 RSM7 RPL14A MRPL31 MRPL38 MRPL13 RPS0B RPL38 RPL31B MRPL4 RPL6A RPS16A MRPS8 MRPS17 MRPL24 MRP7 RPS7B NAM9 MRPL17 MRPL10 RPS19B MRPS18 BRX1 MRPL23 PET123 MRPS16 MRP51 RPL33A MRPL40 RPL1A RPL11A RPS23B MRP2	72	246
mitochondrion [42.16]	0.0000	VAR1 MRPS9 FZO1 MRPS5 MRPL27 DLD1 GGC1 RSM10 MRPL1 RSM24 MRPL7 MRPL35 MRPS28 MRP20 MRPL28 RML2 RSM23 MRP13 MRPS35 MRPL6 MRPL8 MRPL49 RSM7 MRPL31 MRPL38 MRPL13 UTH1 MRPL4 CYB2 CLU1 SAM37 NDE1 MRPS8 MRPS17 MRPL24 MRP7 NAM9 MRPL17 MRPL10 MRPS18 MRPL23 PET123 MRPS16 MRP51 MRPL40 MRP2	46	170

MIPS Functional Classification				
Category	**p-value**	**In Category from Cluster**	**k**	**f**
electron transport and membrane-associated energy conservation [02.11]	0.0000	ATP6 COX2 ATP1 ATP3 ATP5 TIM11 ATP17 QCR7 RIP1 COX4 COX13 QCR10 QCR8 ATP2 ATP7 MCR1 CYB2 ATP18 NDE1 COX5A ATP19 ATP4 ATP20	23	58
energy generation (e.g. ATP synthase) [02.45.15]	0.0000	ATP6 ATP1 ATP3 ATP5 TIM11 ATP17 ATP2 ATP7 ATP18 ATP19 CYT1 ATP4 ATP20	13	21
ribosome biogenesis [12.01]	0.0000	MAK16 NOP14 ARX1 NOP16 NUG1 NSA2 NOP7 SDA1 MTG2 TOR1 MRT4 RLP24 ASC1 ECM16 RRB1 NOP15 NCS2 NOG2 REX4 NOC2 NOG1 NOP53	22	64
electron transport [20.01.15]	0.0000	ATP6 COX2 ATP1 ATP3 ATP5 TIM11 ATP17 GRX4 COX4 COX13 ATP2 ATP7 MCR1 URA1 ATP18 STV1 NDE1 COX5A ATP19 CYT1 ATP4 ATP20	22	83
respiration [02.13]	0.0000	ATP6 ATP1 ATP3 ATP5 TIM11 ATP17 MAK10 ATP2 ATP7 MCR1 FCJ1 RCK2 CYB2 ATP18 AEP2 ATP19 ATP4 ATP20	18	59
rRNA processing [11.04.01]	0.0000	DRS2 POP8 NOP14 SAS10 NHP2 RRP8 ESF1 NUG1 SPB4 RPL30 KEM1 NOP7 NSR1 RPF1 GAR1 MTR4 LSM1 MRT4 EBP2 CBF5 NOP56 ECM16 RRP5 IMP4 DBP2 REX4 RRP6 RAT1 MRM1 NOP58 NOP4 NOP53	32	169
metabolism of secondary products derived from glycine, L-serine and L-alanine [01.20.19]	0.0000	GLY1 CHO2 PSD2 PSD1	4	4
metabolism of porphyrins [01.20.19.01]	0.0001	CYC3 GGC1 HEM3 HEM12 FET5 CYT2 HEM15	7	15
metabolism of cyclic and unusual nucleotides [01.03.10]	0.0002	APA2 DEG1 PPX1 MET3 CBF5 PUS4 PUS1	7	17
translation initiation [12.04.01]	0.0002	RPG1 RLI1 TIF35 RSM28 GCD11 TIF4631 SUI2 CLU1 TIF34 NIP1 MRP51	11	40
cation transport (H+, Na+, K+, Ca2+ , NH4+, etc.) [20.01.01.01]	0.0002	ATP6 DRS2 ATP1 ATP3 ATP5 ATP17 PMC1 VHT1 ATP2 ATP7 ATP18 STV1 MID1 ATP19 ATP4	15	68
rRNA modification [11.06.01]	0.0003	NHP2 GAR1 CBF5 NOP56 IMP4 MRM1 NOP58	7	18
biosynthesis of methionine [01.01.06.05.01]	0.0005	MET6 MET14 MET2 MRI1	4	6
RNA binding [16.03.03]	0.0008	GBP2 NOP14 SAS10 NHP2 TMA64 RNH202 MRPS28 ESF1 PAB1 RPL24A RPL28 NSR1 NAM8 RPF1 GAR1 LSM1 RPL14A PRP39 RPL6A STO1 RRP5 RNH201 IMP4 NOP13 WHI3 NRD1 BRX1 NOP4	28	189

MIPS Functional Classification				
Category	**p-value**	**In Category from Cluster**	**k**	**f**
aerobic respiration [02.13.03]	0.0008	COX2 DLD1 MRPL1 RSM24 QCR7 RIP1 COX4 COX13 MRPS35 QCR10 QCR8 NDE1 MRPS17 COX5A CYT1	15	77
sulfate assimilation [01.02.03.01]	0.0020	MET10 MET3 MET5 MET14	4	8
transport ATPases [20.03.22]	0.0023	ATP6 DRS2 ATP1 ATP3 ATP5 PMC1 PMR1 ATP2 ATP7 STV1 ATP4	11	53
regulator of G-protein signalling [18.02.05]	0.0032	IRA1 RGD2 CDC25 SST2 BEM3	5	14
BIOGENESIS OF CELLULAR COMPONENTS [42]	0.0043	MAK21 RRB1 NOC2	3	5
metabolism of methionine [01.01.06.05]	0.0045	SAM2 SAH1 MET3 MHT1 SAM1 MET17	6	21
O-directed glycosylation, deglycosylation [14.07.02.01]	0.0046	KTR3 KRE2 MNN1 MNT2 KTR1	5	15
biosynthesis of vitamins, cofactors, and prosthetic groups [01.07.01]	0.0051	HEM3 HEM12 SAH1 NMA2 FOL2 RPI1 BNA3 GSH1 YJR142W SPE1 SNZ1 NRK1 FOL1 HEM15 SER1 DFR1 FAS2	17	110
purine nucleotide/ nucleoside/nucleobase anabolism [01.03.01.03]	0.0060	ADE1 HIS4 HPT1 ADE6 ADE13 ADE17 SER1	7	29
polynucleotide degradation [01.03.16]	0.0073	RNH202 RNH70 THS1 RNH201 MKT1 REX4	6	23
pyrimidine nucleotide/ nucleoside/nucleobase metabolism [01.03.04]	0.0089	APA2 GDA1 DEG1 URA1 CBF5 PUS4 PUS1	7	31

Figure A2.1: RNA MS for mcm^{5}U and mcm^{5}s^{2}U in tE^{UUC}
Levels of mcm^{5}s^{2}U and mcm^{5}U were estimated from the area of their extracted ion chromatograms for the m/z values corresponding to protonated nucleoside (MH^+) and protonated nucleobase (BH^+) of U, mcm^{5}s^{2}U and mcm^{5}U obtained after digestion and dephosphorylation of the tRNA tE^{UUC} purified from wild-type yeast cells either grown in rich medium at 30 °C or rich medium at 37 °C or in absence of sulfur amino acids at 30 °C. (also see figure 4.17 for summary)

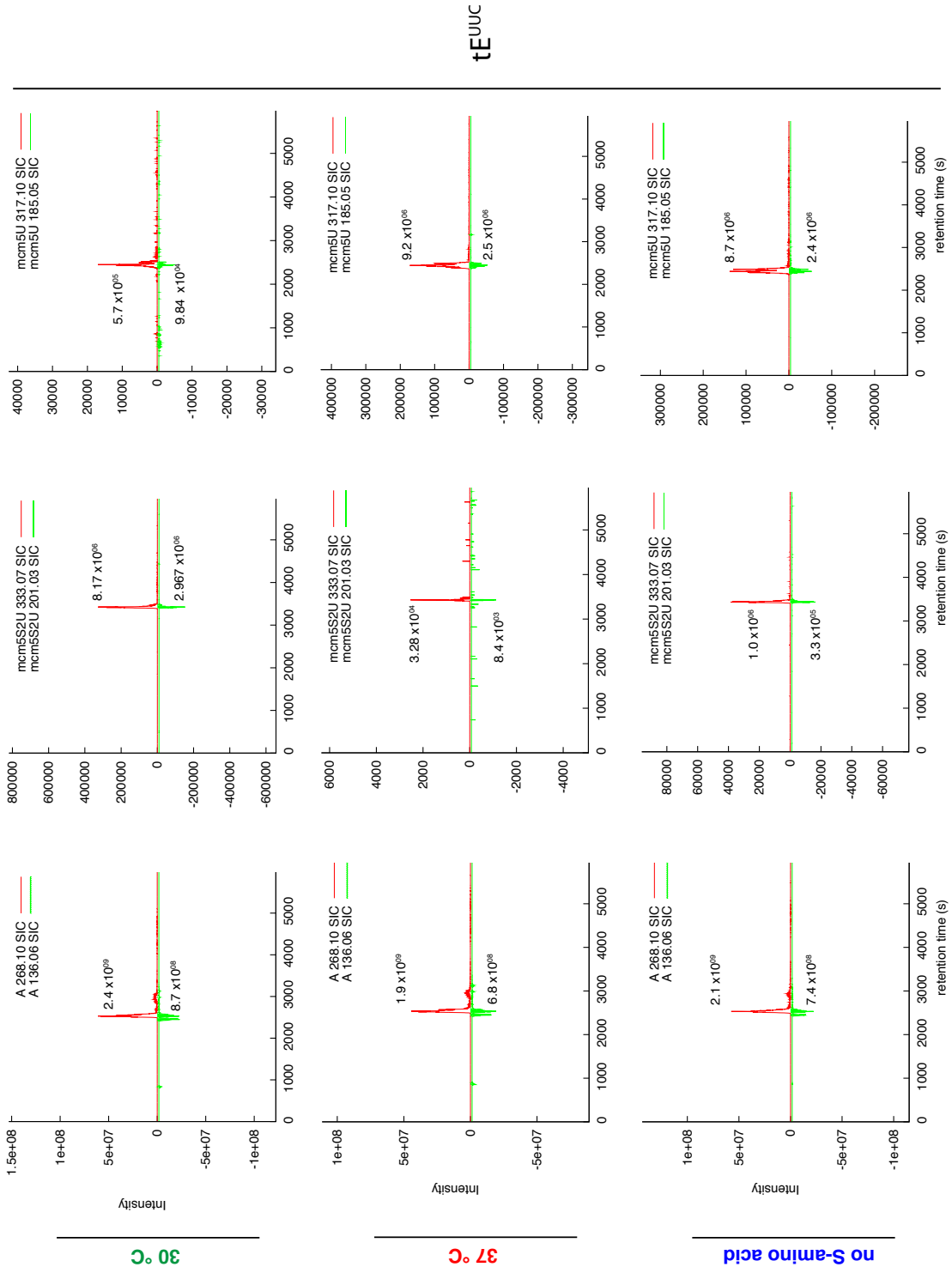

Figure A2.2: RNA MS for mcm^{5}U and mcm^{5}s^{2}U in tQ^{UUG}
Levels of mcm^{5}s^{2}U and mcm^{5}U were estimated from the area of their extracted ion chromatograms for the m/z values corresponding to protonated nucleoside (MH^+) and protonated nucleobase (BH^+) of U, mcm^{5}s^{2}U and mcm^{5}U obtained after digestion and dephosphorylation of the tRNA tQ^{UUG} purified from wild-type yeast cells either grown in rich medium at 30 °C or rich medium at 37 °C or in absence of sulfur amino acids at 30 °C. (also see figure 4.17 for summary)

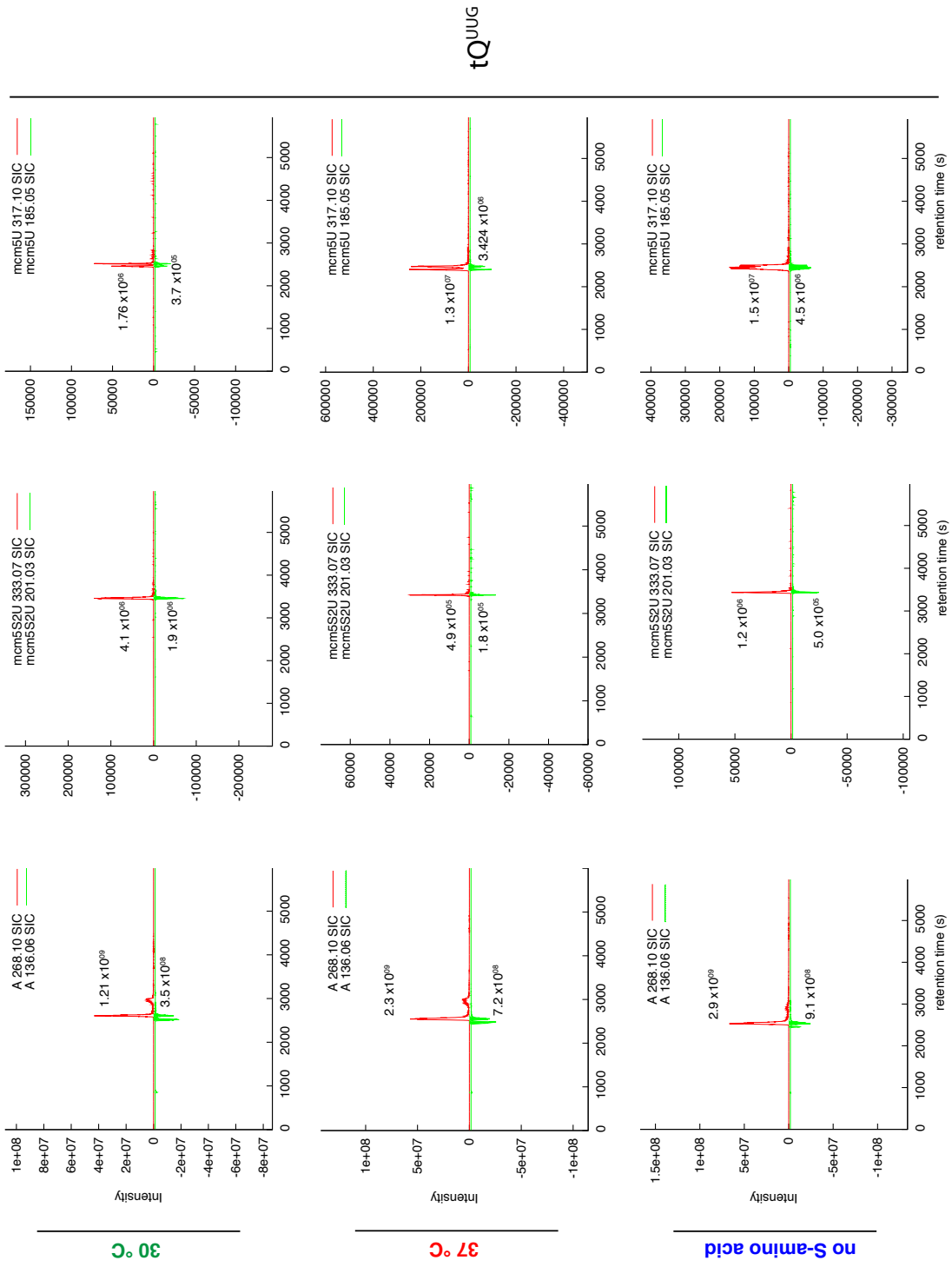

Figure A2.3: RNA MS for mcm^{5}U and mcm^{5}s^{2}U in tR^{UCU}
Levels of mcm^{5}s^{2}U and mcm^{5}U were estimated from the area of their extracted ion chromatograms for the m/z values corresponding to protonated nucleoside (MH^+) and protonated nucleobase (BH^+) of U, mcm^{5}s^{2}U and mcm^{5}U obtained after digestion and dephosphorylation of the tRNA tR^{UCU} purified from wild-type yeast cells either grown in rich medium at 30 °C or rich medium at 37 °C or in absence of sulfur amino acids at 30 °C. (also see figure 4.17 for summary)

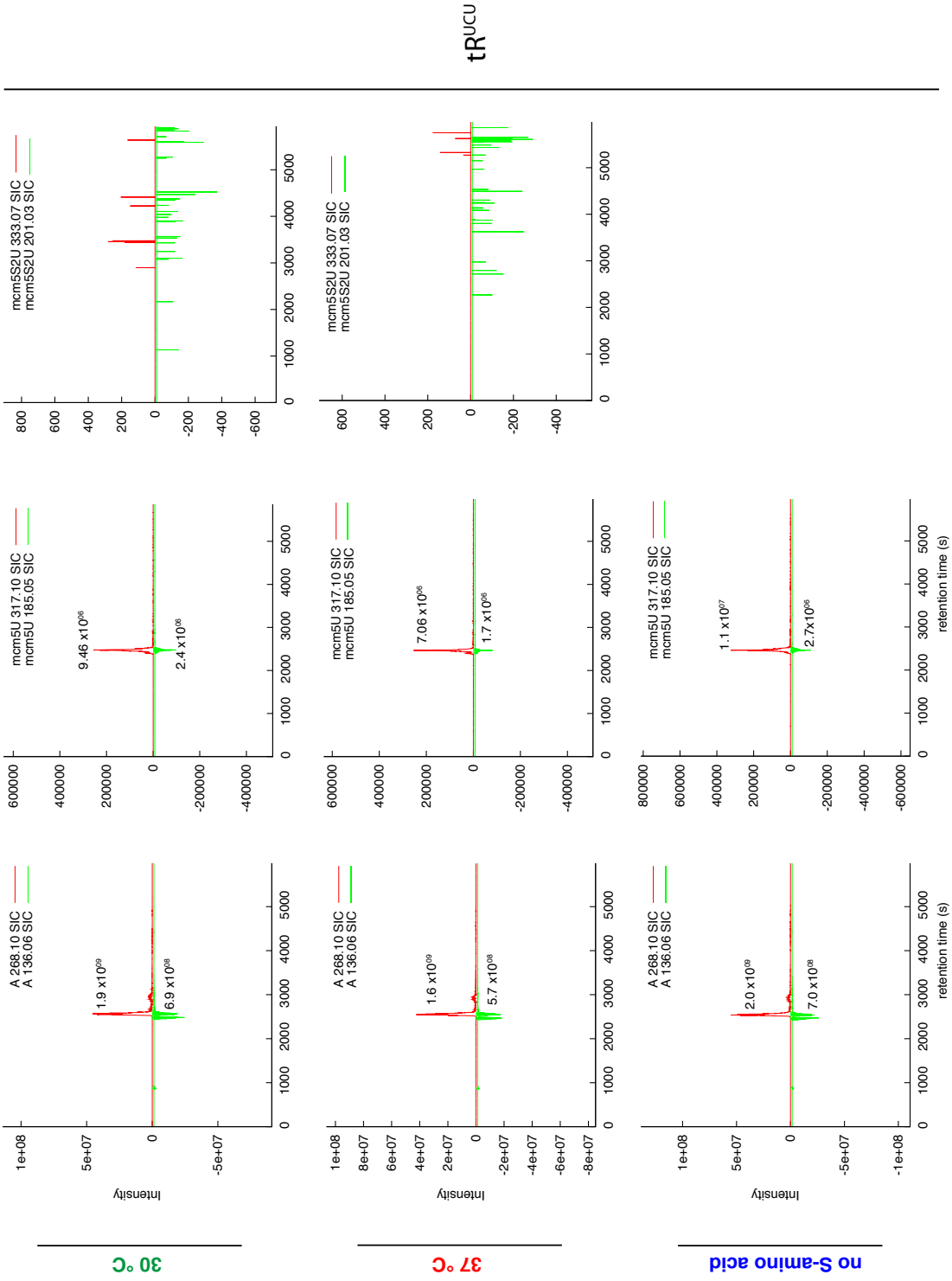

Figure A2.4: Volcano plots of the codon biased genes from the 30 °C vs. 37 °C dataset.

Volcano plots showing the protein abundance ratios, measured by SILAC-based quantitative proteomics, with statistical significance, computed using Bayes moderated *t* test, of the top 1% yeast genes with the highest frequency of the indicated codons. The dotted red line indicates 1% FDR, threshold for statistically significant changes in protein abundance. The grey dotted line indicates a ratio (30 °C/37 °C) of 1.